

**CELLULAR AND ACELLULAR ASSAYS FOR MEASURING
OXIDATIVE STRESS INDUCED BY AMBIENT AND
LABORATORY-GENERATED AEROSOL**

A Dissertation
Presented to
The Academic Faculty

by

Wing Y. Tuet

In Partial Fulfillment
of the Requirements for the Degree
Doctor of Philosophy in the
School of Chemical and Biomolecular Engineering

Georgia Institute of Technology

May 2018

Copyright © Wing Y. Tuet 2018

**CELLULAR AND ACELLULAR ASSAYS FOR MEASURING
OXIDATIVE STRESS INDUCED BY AMBIENT AND
LABORATORY-GENERATED AEROSOL**

Approved by:

Dr. Nga L. Ng, Advisor
School of Chemical and Biomolecular
Engineering
Georgia Institute of Technology

Dr. Hang Lu
School of Chemical and Biomolecular
Engineering
Georgia Institute of Technology

Dr. Julie A. Champion
School of Chemical and Biomolecular
Engineering
Georgia Institute of Technology

Dr. Rodney J. Weber
School of Earth and Atmospheric Sciences
Georgia Institute of Technology

Dr. Anna Grosberg
Department of Biomedical Engineering
University of California at Irvine

Date Approved: March 6, 2018

To my parents

ACKNOWLEDGEMENTS

There are many people I would like to thank for their support over the past five years leading to the completion of this dissertation. First, I would like to thank my advisor, Dr. Sally Ng, for her guidance in both scientific research and professional development. Her generous support provided me with numerous opportunities to present my research, where I learned valuable communication skills and gained helpful insights on my projects. I am grateful for her encouragement throughout these years.

I would also like to thank my committee members for their valuable time and contributions. Their comments and suggestions have greatly improved my research, from offering fresh viewpoints to providing critical input. Dr. Julie Champion, Dr. Anna Grosberg, and Dr. Rodney Weber have also been incredibly generous and supportive regarding the use of their laboratory equipment for collaborations. The knowledge I gained from each exchange has been extremely valuable in the completion of this dissertation. I would also like to thank Dr. Hang Lu for keeping me focused on the bigger picture and providing a broader perspective regarding my research goals. Besides current faculty at Georgia Tech, I would like to especially acknowledge and thank my undergraduate professor, Dr. George Georgiou. His past references and continued support helped tremendously these past few years.

I acknowledge my past and present labmates for their support in my research and their company throughout these past five years. Lu Xu, Chris Boyd, and Javier Sanchez always offered assistance and moral support when problems arose. Yunle Chen provided technical support, company, and snacks during long experiments. Theo Nah gave useful

career advice, Yi Ji and Gamze Eris were great shopping companions, Taekyu Joo gave lots of travelling advice, and Masayuki Takeuchi and Thomas Berkemeier provided interesting conversations in the office. I would also like to thank Weber group, Champion group, and Grosberg group for their assistance. My experiments would not have been completed as smoothly without their help. In particular, I would like to thank Ting Fang for providing her research expertise and being a great friend. I would also like to thank Marlene Tagle Rodriguez for being a wonderful collaborator and tour guide during my time at UC – Irvine.

Finally, I would like to thank my family and friends for their continued support. I would like to thank all of my friends for all the fun times we've shared throughout these years. I would also like to thank Melinda Jue for being a great roommate and helping me with my hobbies these past five years. I would especially like to thank my parents for their unconditional love and belief. They have always been there, listening to my problems, providing encouragement, and celebrating my achievements. Without them, this work would not have been possible.

TABLE OF CONTENTS

ACKNOWLEDGEMENTS	iv
LIST OF TABLES	ix
LIST OF FIGURES	xi
LIST OF SYMBOLS AND ABBREVIATIONS	xx
SUMMARY	xxiii
CHAPTER 1: Introduction	1
1.1 Motivation to study air pollution	1
1.2 Previous assays developed to study PM-induced health effects	2
1.3 PM components associated with adverse health	4
1.4 Motivation to study secondary organic aerosol (SOA) toxicity	6
1.5 Scope and overview	8
CHAPTER 2: Dose-dependent intracellular ROS/RNS production from PM exposure – comparison to oxidative potential and chemical composition	10
2.1 Background	10
2.2 Methods	12
2.2.1 Alveolar macrophage cell line.	12
2.2.2 Ventricular myocyte isolation and culture	13
2.2.3 PM collection and extraction	14
2.2.4 Pure metal solutions	15
2.2.5 Oxidative potential	15
2.2.6 Intracellular ROS/RNS measurement	16
2.2.7 Statistical analysis	18
2.3 Results	19
2.3.1 PM-induced dose-dependent ROS/RNS production	19
2.3.2 ROS/RNS production and oxidative potential	21
2.3.3 ROS/RNS production and PM composition	22
2.3.4 Comparison between MH-S and NRVM	24
2.4 Discussion	25
2.4.1 Cellular ROS/RNS assay optimization	25
2.4.2 Comparison between MH-S and NRVM	28
2.4.3 Associations between ROS/RNS production and oxidative potential	28
2.4.4 PM constituents associated with AUC	30
2.5 Implications	34
CHAPTER 3: Chemical oxidative potential of secondary organic aerosol generated from biogenic and anthropogenic precursors	37
3.1 Background	37

3.2	Methods	41
3.2.1	Chamber experiments	41
3.2.2	Aerosol collection and extraction	45
3.2.3	Oxidative potential	45
3.3	Results and Discussion	46
3.3.1	Laboratory-generated aerosol	46
3.3.2	Effect of SOA precursor and formation condition on oxidative potential	48
3.3.3	Comparison to other types of PM	56
3.4	Implications	60
 CHAPTER 4: Inflammatory responses to secondary organic aerosol generated from biogenic and anthropogenic precursors		 63
4.1	Background	63
4.2	Methods	67
4.2.1	Alveolar macrophage cell line	67
4.2.2	Chamber experiments	68
4.2.3	Aerosol collection and extraction	71
4.2.4	Intracellular ROS/RNS measurement	72
4.2.5	Cytokine measurement	74
4.2.6	Cellular metabolic activity	74
4.2.7	Statistical analysis	75
4.3	Results and Discussion	75
4.3.1	Effect of SOA precursor and formation condition on inflammatory response	75
4.3.2	Relationship between inflammatory responses	86
4.3.3	Comparison with ambient data	88
4.4	Implications	91
 CHAPTER 5: Oxidant production induced by naphthalene secondary organic aerosol: effect of redox-active metals and photochemical aging		 95
5.1	Background	95
5.2	Methods	98
5.2.1	Naphthalene aerosol generation	98
5.2.2	Aerosol collection and extraction	100
5.2.3	Oxidative potential	101
5.2.4	Intracellular ROS/RNS measurement	101
5.2.5	Cellular metabolic activity	103
5.3	Results and Discussion	103
5.3.1	Laboratory-generated aerosol	103
5.3.2	Effect of iron seed on cellular ROS/RNS production	105
5.3.3	Effect of iron seed on OP	111
5.3.4	Relationship between photochemical aging of aerosol and toxicity	114
5.4	Implications	116
 CHAPTER 6: Summary and Future Work		 119
6.1	Summary of major findings	119
6.2	Suggestions for future work	120

APPENDIX A: Supplement for Chapter 2	124
APPENDIX B: Supplement for Chapter 3	136
APPENDIX C: Supplement for Chapter 4	141
APPENDIX D: Supplement for Chapter 5	146
REFERENCES	156

LIST OF TABLES

Table 3-1	Experimental conditions for chamber experiments.	43
Table 4-1	Experimental conditions for photooxidation SOA.	70
Table 5-1	Experimental conditions for naphthalene SOA.	100
Table A-1	Pearson's correlation coefficients for overall linear regressions between dose-response parameters and PM components. Dose-response parameters were obtained from Hill Equation fits and include max response, EC ₅₀ , Hill slope, threshold, and AUC per volume of air sampled. PM components include water-soluble metals, water-soluble organic carbon (WSOC), and brown carbon (BrC). Metals were also grouped by metal sources: Brake/Tire Wear (BTW: Ti, Cu, Zn, Ba), Biomass Burning (BB: K, As, Br, Pb), Secondary Formation (SF: S, Fe, Se), and Mineral Dust (MD: Ca, Mn, Sr). $n = 104$ ambient filters; * indicates significance, $p < 0.05$.	132
Table A-2	Pearson's correlation coefficients for overall linear regressions between dose-response parameters and PM component fractions. Dose-response parameters include max response, EC ₅₀ , Hill slope, threshold, and AUC per mass of PM. PM components include water-soluble metals, water-soluble organic carbon (WSOC), and metals grouped by source: Brake/Tire Wear (BTW: Ti, Cu, Zn, Ba), Biomass Burning (BB: K, As, Br, Pb), Secondary Formation (SF: S, Fe, Se), and Mineral Dust (MD: Ca, Mn, Sr). $n = 104$ ambient filters; * indicates significance, $p < 0.05$.	133
Table A-3	Comparison between assays parameters used in previous studies and this study. Parameters include: ROS/RNS probe, cell density, ROS/RNS probe concentration, sample incubation time, signal normalization scheme, and analysis approach. All parameters were optimized for measuring ROS/RNS production as a result of PM exposure in this study.	134
Table A-4	Root-mean-squared error (RMSE) between observed and fitted area under the curve (AUC) for summer and winter filter samples. Fits are based on a simple linear regression between AUC and the predictor of interest, which include: dithiothreitol (DTT) activity, water-soluble organic carbon (WSOC) concentration, brown carbon (BrC) concentration, and iron (Fe) concentration. $n = 104$ ambient filters (10 spring, 47 summer, 15 autumn, and 32 winter).	135

Table B-1	Hydrocarbon precursor structure and reaction rate constants.	140
Table C-1	SOA precursor structures.	145
Table D-1	Elemental ratios (O:C, H:C, N:C) as determined by AMS.	155

LIST OF FIGURES

Figure 2-1	Cellular assay optimized for measuring ROS/RNS production as a result of PM exposure. Major steps include: (1) pre-treatment of wells, (2) seeding of cells onto wells, (3) incubation of cells with carboxy-H ₂ DCFDA, (4) incubation of probe-treated cells with samples or controls, and (5) detection of carboxy-DCF (proportional to ROS/RNS) using microplate reader.	17
Figure 2-2	Representative dose-response curve of ROS/RNS produced as a result of ambient PM exposure (filter ID: YRK 07/10/12). ROS/RNS production is expressed as fold increase over control, defined as probe-treated cells incubated with stimulant-free media. Dose is expressed as either (a) mass in extract (μg) or (b) volume of air sampled (m ³). Data shown are means ± SE of exposure experiments performed in triplicate. Hill equation (HE) parameters shown include: max response, Hill slope (rate at which max response is attained), EC ₅₀ (dose at which 50% of max response is attained), threshold (dose at which response is 10% above baseline), and AUC (area under the dose-response curve).	20
Figure 2-3	AUC per volume of air sampled (a) and per mass of PM (b) as determined by Hill equation fits to ROS/RNS dose-response data for ambient samples spanning a wide range of (a) extrinsic and (b) intrinsic DTT activity. Each data point represents a single ambient filter for which a dose-response was obtained (10 dilutions performed in triplicate). Data points are colored by season as determined by solstice and equinox dates between June 2012 and October 2013. Linear regressions and Pearson's correlation coefficients are shown for summer and winter filter samples. <i>n</i> = 104 ambient filters (10 spring, 47 summer, 15 autumn, and 32 winter); * indicates significance, <i>p</i> < 0.05.	22
Figure 2-4	AUC per volume of air sampled for ambient samples spanning a wide range of (a) water-soluble organic carbon (WSOC), (b) brown carbon (BrC), (c) titanium (Ti), and (d) iron (Fe). Each data point represents a single ambient filter for which a dose-response was obtained (10 dilutions performed in triplicate) and fitted using the Hill equation. Data points are colored by season as determined by solstice and equinox dates between June 2012 and October 2013. Linear regressions and Pearson's correlation coefficients are shown for summer and winter filter samples. <i>n</i> = 104 ambient filters (10 spring, 47 summer, 15 autumn, and 32 winter); * indicates significance, <i>p</i> < 0.05. Removal of the sample with	24

high WSOC introduces a slight slope (0.03) in the winter correlation, which is still relatively flat (panel a).

- Figure 2-5 AUC per mass of PM for MH-S and NRVN. Each data point represents a single filter dose-response obtained from 10 dilutions (1x to 0.00125x) performed in triplicate. An orthogonal regression and the corresponding Pearson's coefficient is shown. A 1:1 line is shown for reference. $n = 18$ ambient filters; * indicates significance, $p < 0.05$. 25
- Figure 3-1 Typical reaction profile for a chamber experiment under $\text{RO}_2 + \text{NO}$ dominant conditions. NO and NO_2 concentrations were monitored by CAPS NO_2 and chemiluminescence NO_x monitors, respectively. Hydrocarbon decay was monitored using GC-FID, while initial hydrocarbon (naphthalene) concentrations were determined using the chamber volume and mass of hydrocarbon injected. Aerosol mass concentrations were determined using volume concentrations obtained from SMPS and assuming an aerosol density of 1 g cm^{-3} . While typical SOA density is about 1.4 g cm^{-3} , it varies with hydrocarbon precursor identity and reaction conditions, and a density between $\sim 1.0\text{--}1.6 \text{ g cm}^{-3}$ has been reported in previous studies (Ng et al., 2007a; Ng et al., 2007b; Chan et al., 2009; Tasoglou and Pandis, 2015; Bahreini et al., 2005; Ng et al., 2006). The use of a density of 1 g cm^{-3} is to facilitate easier comparisons with past and future studies. Results from future studies can be scaled accordingly for comparison with the current work. Mass concentrations have been corrected for particle wall loss (Nah et al., 2017). 47
- Figure 3-2 Intrinsic DTT activities for SOA generated from various hydrocarbon precursors (ISO: isoprene, AP: α -pinene, BCAR: β -caryophyllene, PD: pentadecane, MX: *m*-xylene, and NAPH: naphthalene) under various conditions (red circles: dry, $\text{RO}_2 + \text{HO}_2$; blue squares: humid, $\text{RO}_2 + \text{HO}_2$; and black triangles: dry, $\text{RO}_2 + \text{NO}$). Dry, $\text{RO}_2 + \text{HO}_2$ experiments were repeated to ensure reproducibility in SOA generation and collection. Error bars represent a 15% coefficient of variation (Fang et al., 2015c). 49
- Figure 3-3 van Krevelen plot for various SOA systems. Data points are colored by SOA system (red: isoprene, yellow: α -pinene, green: β -caryophyllene, light blue: pentadecane, blue: *m*-xylene, and purple: naphthalene), shaped according to reaction conditions (circle: dry, $\text{RO}_2 + \text{HO}_2$; square: humid, $\text{RO}_2 + \text{HO}_2$; and triangle: dry, $\text{RO}_2 + \text{NO}$), and sized by intrinsic DTT activity. OA factors resolved from PMF analysis of ambient AMS data are shown as black markers, also sized by intrinsic DTT activity. Hydrocarbon precursors are shown as stars, colored by SOA system. Specifics 55

on site locations and factor resolution methods are described elsewhere. COA: cooking OA, BBOA: biomass burning OA, Isoprene-OA: isoprene-derived OA, MO-OOA: more-oxidized oxygenated OA (Verma et al., 2015a; Xu et al., 2015a; Xu et al., 2015b).

- Figure 3-4 Intrinsic DTT activities for chamber SOA, various PM subtypes resolved from ambient data, and diesel exhaust particles. It should be noted that the DTT activity for isoprene SOA in Kramer et al. (2016) was determined using a different DTT method and may not be directly comparable. All other studies shown used the method outlined in Cho et al. (2005). DTT activities obtained in this study are shaped by reaction condition (circle: dry, RO₂ + HO₂; square: humid, RO₂ + HO₂; triangle: dry, RO₂ + NO). Specifics on site locations and factor resolution methods are described elsewhere. DTT activities for Beijing and Atlanta are averages obtained across multiple seasons. Isoprene-OA: isoprene-derived OA, MO-OOA: more-oxidized oxygenated OA, BBOA: biomass burning OA, COA: cooking OA, LDGV: light-duty gasoline vehicles, HDDV: heavy-duty diesel vehicles, BURN: biomass burning, DEP: diesel exhaust particles (Kramer et al., 2016; McWhinney et al., 2013b; Verma et al., 2015a; Bates et al., 2015; McWhinney et al., 2013a; Xu et al., 2015a; Xu et al., 2015b; Lu et al., 2014; Fang et al., 2015c). 57
- Figure 4-1 Representative dose-response curve of ROS/RNS produced as a result of filter exposure (naphthalene SOA formed under dry, RO₂ + NO dominant conditions). ROS/RNS is expressed as a fold increase over control cells, defined as probe-treated cells incubated with stimulant-free media. Dose is expressed as mass in extract (μg). Data shown are means ± standard error of triplicate exposure experiments. The Hill equation was used to fit the dose-response curve and the area under the dose-response curve (AUC) is shown. 73
- Figure 4-2 Area under the dose-response curve for various inflammatory responses induced as a result of SOA exposure: ROS/RNS, IL-6, and TNF-α. SOA were generated from various precursors (ISO: isoprene, AP: α-pinene, BCAR: β-caryophyllene, PD: pentadecane, MX: *m*-xylene, and NAPH: naphthalene) under various conditions (circles: dry, RO₂ + HO₂; squares: humid, RO₂ + HO₂; and triangles: dry, RO₂ + NO). Lines connecting the same inflammatory response for SOA generated from the same precursor under different formation conditions are also shown. 77
- Figure 4-3 van Krevelen plot for various SOA systems sized by ROS/RNS levels (panel A) and correlation between ROS/RNS levels and 79

average carbon oxidation state (panel B). Data points are colored by SOA system (red: isoprene, yellow: α -pinene, green: β -caryophyllene, light blue: pentadecane, blue: *m*-xylene, and purple: naphthalene), shaped according to formation conditions (circle: dry, RO₂ + HO₂; square: humid, RO₂ + HO₂; and triangle: dry, RO₂ + NO). SOA precursors are shown as stars, colored by SOA system. * indicates significance, $p < 0.05$.

- Figure 4-4 Area under the dose-response curve per mass of SOA for various inflammatory responses induced as a result of SOA exposure. Data points are sized according to ROS/RNS level. SOA were generated from various SOA precursors (red: isoprene, yellow: α -pinene, green: β -caryophyllene, light blue: pentadecane, blue: *m*-xylene, and purple: naphthalene) under various conditions (circles: dry, RO₂ + HO₂; squares: humid, RO₂ + HO₂; and triangles: dry, RO₂ + NO). A fitted curve excluding naphthalene data is shown as a guide. Shaded regions for each system, colored by SOA precursor, are also shown to show the extent of clustering and provide a visualization for the different patterns observed. 88
- Figure 4-5 ROS/RNS production and intrinsic DTT activities for chamber SOA and ambient samples collected around the greater Atlanta area. All samples were analyzed using the method outlined in Cho et al. (2005) and Tuet et al. (2016). Ambient samples are colored by season as determined by solstice and equinox dates between June 2012 and October 2013 (Tuet et al., 2016). A fitted curve for laboratory-generated samples is shown as a guide. 89
- Figure 5-1 ROS/RNS produced as a result of naphthalene SOA exposure and corresponding ROS/RNS response from pure iron sulfate seed. ROS/RNS are expressed as the area under the dose-response curve (AUC). SOA were generated from the photooxidation of naphthalene in the presence of different seed particles (ammonium sulfate or iron sulfate), OH• radical precursor (H₂O₂), and NO. Data from previous studies, where SOA were generated in the presence of ammonium sulfate seed, were included for comparison. Initial hydrocarbon concentrations for other experiments are as follows: dry, RO₂ + HO₂ (178 ppb); humid, RO₂ + HO₂ (431 ppb); and dry, RO₂ + NO (146 ppb) (Tuet et al., 2017b). 106
- Figure 5-2 Exponential trend between ROS/RNS levels and average carbon oxidation state (\overline{OS}_c) for naphthalene photooxidation SOA generated in the presence of different seed particles (ammonium sulfate or iron sulfate), OH• radical precursor (H₂O₂), and NO. ROS/RNS production are expressed as the area under the dose-response curve (AUC). Error bars were determined using the 109

methodology outlined in Tuet et al. (2016). Data from previous studies were included for comparison (Tuet et al., 2017b). \overline{OS}_c ranges for less oxidized oxygenated organic aerosol (LO-OOA) and more oxidized OOA (MO-OOA) are shaded for context (Kroll et al., 2011).

- Figure 5-3 Intrinsic OP and ROS/RNS levels for naphthalene photooxidation SOA collected over the course of a single experiment (Expt. 5). Time series for AMS m/z 77 and 91, which are likely phenyl and benzyl ions, are also shown. SOA was generated in a humid chamber in the presence of ammonium sulfate, OH• radical precursor (H₂O₂), and NO. Error bars represent a 15% coefficient of variation for OP (Fang et al., 2015c). ROS/RNS levels are expressed as the area under the dose-response curve (AUC) with error bars calculated following the methodology described in Tuet et al. (2016). 110
- Figure 5-4 Intrinsic OP for SOA generated from the photooxidation of naphthalene under various conditions and pure iron sulfate seed. SOA from this study was generated in a humid chamber in the presence of different seed particles (ammonium sulfate or iron sulfate), OH• radical precursor (H₂O₂), and NO. Data from previous studies, where SOA were generated in the presence of ammonium sulfate seed, were included for comparison. Initial hydrocarbon concentrations for other experiments are as follows: dry, RO₂ + HO₂ (178 ppb); humid, RO₂ + HO₂ (431 ppb); and dry, RO₂ + NO (146 ppb) (Tuet et al., 2017b). 112
- Figure A-1 Ambient sampling sites for the Southeastern Center for Air Pollution and Epidemiology (SCAPE) study. Sites include: JST (located on Jefferson Street, representative of urban Atlanta), RS (located near Interstate Highways I-75/I-85, representative of traffic emissions), GT (located on the roof of the Ford Environmental Science and Technology building at Georgia Tech, representative of near-road emissions), and YRK (located in Yorkville, representative of rural background). 124
- Figure A-2 ROS/RNS production as a result of treatment with positive controls over various sample incubation times. Data shown are means \pm SE of experiments performed in triplicate. ROS/RNS production is expressed as fold increase over probe-treated cells incubated with stimulant-free media (control cells). At 24 hrs, the normalized positive response is highest for both cell types. 125
- Figure A-3 Dose-response behaviors observed in this study: (1) maximum response not attained, (2) decreased response at higher doses, and (3) no response above baseline at all doses. Data shown are means 126

\pm SE of experiments performed in triplicate. ROS/RNS production is expressed as fold increase over probe-treated cells incubated with stimulant-free media (control cells).

- Figure A-4 Dose-response parameters for ambient filters spanning a wide range of extrinsic DTT activity. Each data point represents a single dose-response obtained from 10 dilutions (1x to 0.00125x) performed in triplicate. Solid markers represent MH-S data; open markers represent NRVM data. Linear regressions and corresponding Pearson's coefficients are given for each parameter. $n = 104$ ambient filters; * indicates significance, $p < 0.05$. 127
- Figure A-5 AUC per mass of PM for ambient samples containing various fractions of (a) titanium (Ti) and (b) chromium (Cr). Each data point represents a single ambient filter for which a dose-response was obtained (10 dilutions performed in triplicate) and fitted to the Hill equation. Data points are colored by season with cut-off dates determined by solstice and equinox dates. Linear regressions and Pearson's correlation coefficients are shown for summer and winter filter samples. $n = 104$ ambient filters (10 spring, 47 summer, 15 autumn, and 32 winter); * indicates significance, $p < 0.05$. 128
- Figure A-6 AUCs for spring and autumn filter samples spanning a range of (a) extrinsic and (b) intrinsic DTT activity. Each data point represents a single ambient filter for which a dose-response was obtained (10 dilutions performed in triplicate) and fitted to the Hill equation. Linear regressions with corresponding confidence (dashed) and prediction (shaded) intervals are shown for summer and winter filter samples. $n = 104$ ambient filters (10 spring, 47 summer, 15 autumn, and 32 winter). 129
- Figure A-7 Maximum ROS/RNS production and corresponding EC_{50} for ambient filters investigated. Each data point represents a single dose-response obtained from 10 dilutions (1x to 0.00125x) performed in triplicate. Solid markers represent MH-S data; open markers represent NRVM data. A simple linear regression and corresponding Pearson's coefficient are given. $n = 104$ ambient filters; * indicates significance, $p < 0.05$. 130
- Figure A-8 ROS/RNS production as a result of exposure to 6 pure metal salt solutions and corresponding dose-response curves. Concentrations span the water soluble metal concentrations observed in ambient samples. ROS/RNS production is expressed 131

as fold increase over control, probe-treated cells not exposed to stimulant. Data shown are means \pm SE of triplicate experiments.

- Figure B-1 Aerosol mass spectra of SOA formed from the photooxidation of various hydrocarbon precursors (ISO: isoprene, AP: α -pinene, BCAR: β -caryophyllene, PD: pentadecane, MX: *m*-xylene, and NAPH: naphthalene) under various conditions (red bars: dry, RO₂ + HO₂; blue squares: humid, RO₂ + HO₂; and black triangles: dry, RO₂ + NO). Characteristic fragments for each system are labeled. 136
- Figure B-2 Comparison between mass spectra of SOA formed from the photooxidation of various hydrocarbon precursors (ISO: isoprene, AP: α -pinene, BCAR: β -caryophyllene, PD: pentadecane, MX: *m*-xylene, and NAPH: naphthalene) under various conditions (blue: humid, RO₂ + HO₂; and black: dry, RO₂ + NO). A 1:1 line is shown in red for reference. 137
- Figure B-3 Intrinsic DTT activities (per μ g) for various SOA systems spanning a wide range of N:C. Data points are colored by SOA system (red: isoprene, yellow: α -pinene, green: β -caryophyllene, light blue: pentadecane, blue: *m*-xylene, and purple: naphthalene). 138
- Figure C-1 ROS/RNS produced as a result of exposure to background filters (OH precursor and seed only). ROS/RNS is expressed as a fold increase over probe-treated control cells incubated with stimulant-free media. Data shown are means \pm standard error of triplicate exposure experiments. 141
- Figure C-2 Post filter exposure cellular metabolic activity as measured by the MTT assay (filter: naphthalene SOA formed under dry, RO₂ + NO dominant conditions). Cellular metabolic activity is normalized to cells exposed to stimulant-free media. Data shown are means \pm standard error of triplicate exposure experiments. All filter exposures produced similar results. 142
- Figure C-3 van Krevelen plot for various SOA systems. Data points are colored by SOA system (red: isoprene, yellow: α -pinene, green: β -caryophyllene, light blue: pentadecane, blue: *m*-xylene, and purple: naphthalene), shaped according to formation conditions (circle: dry, RO₂ + HO₂; square: humid, RO₂ + HO₂; and triangle: dry, RO₂ + NO), and sized by TNF- α and IL-6 levels. SOA precursors are shown as stars, colored by SOA system. 143
- Figure C-4 ROS/RNS, TNF- α , and IL-6 (represented as AUC per μ g) for various SOA systems spanning a wide range of N:C ratios. Data points are colored by SOA system (red: isoprene, yellow: α - 144

pinene, green: β -caryophyllene, light blue: pentadecane, blue: *m*-xylene, and purple: naphthalene).

- Figure D-1 Representative dose-response curve of ROS/RNS produced as a result of filter exposure (Expt. 7). ROS/RNS is expressed as a fold increase over control (probe-treated cells incubated with stimulant-free media); dose is expressed as mass in the filter extract (μg). Data shown are means \pm standard error of experiments performed in triplicate. The dose-response curve was fitted using the Hill equation and the area under the curve (AUC) is shown. 146
- Figure D-2 Typical reaction profile for a chamber experiment under humid conditions in the presence of NO using A) ammonium sulfate seed particles (Expt. 3) and B) iron sulfate seed particles (Expt. 4). Naphthalene and NO concentrations were monitored using a GC-FID and chemiluminescence NO_x monitor, respectively. Aerosol mass concentrations were determined using SMPS volume concentration and assuming an aerosol density of 1 g cm^{-3} . It should be noted that aerosol mass concentrations have not been corrected for particle wall loss. 147
- Figure D-3 Aerosol mass spectra of SOA formed from the photooxidation of naphthalene under humid conditions in the presence of NO using various seed (red bars: ammonium sulfate; blue markers: iron sulfate). Each row represents a different initial naphthalene concentration (30, 75, 150, and 300 ppb). Characteristics fragments are labeled. Ions greater than m/z 120 are shown in the inset of each mass spectrum. 148
- Figure D-4 Comparison between mass spectra of SOA formed from the photooxidation of naphthalene under humid conditions in the presence of NO using various seeds. A 1:1 line is shown for reference. 149
- Figure D-5 Difference (FS seeded SOA – AS seeded SOA) between normalized mass spectra of SOA formed from the photooxidation of naphthalene under humid conditions in the presence of NO using various seeds. 150
- Figure D-6 Average carbon oxidation state ($\overline{\text{OS}}_c$) for naphthalene SOA spanning a range of organic mass loading (ΔM_o). SOA from this study was generated in a humid chamber in the presence of different seed particles (ammonium sulfate or iron sulfate), OH radical precursor (H_2O_2), and NO. 151

Figure D-7	ROS/RNS produced as a result of exposure to FeSO ₄ (red: aerosolized into the chamber at experimental concentration, collected onto a filter, and extracted into media; blue: aqueous seed solution diluted in media). ROS/RNS is expressed as a fold increase over probe-treated control cells incubated with stimulant-free media. Data shown are means \pm standard error of triplicate exposure experiments.	152
Figure D-8	Method for estimating the mass of seed collected onto each filter (Expt. 6). A double exponential was used to characterize seed particle wall loss (using seed concentrations obtained from the SMPS as a function of time). The fitted seed concentration as a function of time was then integrated over the filter collection period (shown as the shaded region). To obtain the total mass of seed collected, the integral ($40.78 \mu\text{g m}^{-3}$) was multiplied by the volumetric flow rate ($1.72 \text{ m}^3 \text{ hr}^{-1}$, for an estimated total seed mass of $70.14 \mu\text{g}$ on the filter for this experiment).	153
Figure D-9	Intrinsic OP for naphthalene SOA spanning a range of average carbon oxidation states ($\overline{\text{OS}}_c$). SOA from this study was generated in a humid chamber in the presence of different seed particles (ammonium sulfate or iron sulfate), OH radical precursor (H ₂ O ₂), and NO. Error bars represent a 15% coefficient of variation (Fang et al., 2015c). Data from previous studies were included for comparison (Tuet et al., 2017b).	154

LIST OF SYMBOLS AND ABBREVIATIONS

AA	Ascorbic acid
AP	α -pinene
AS	Ammonium sulfate
AUC	Area under the dose-response curve
BBOA	Biomass burning organic aerosol
BCAR	β -caryophyllene
BME	β -mercaptoethanol
BrC	Brown carbon
CAPS	Cavity attenuated phase shift
carboxy-DCFH	carboxy-2',7'-dichlorodihydrofluorescein
carboxy-DCF	carboxy-2',7'-dichlorofluorescein
carboxy-H ₂ DCFDA	carboxy-2',7'-dichlorodihydrofluorescein diacetate
CO ₂	Carbon dioxide
DCFH-DA	2',7'-dichlorofluorescein diacetate
DI	Deionized
DMSO	Dimethyl sulfoxide
DTNB	5,5'-dithiobis-(2-nitrobenzoic acid)
DTT	Dithiothreitol
EC ₅₀	Dose at which 50% of the response is attained
ELISA	Enzyme-linked immunosorbent assay
FBS	Fetal bovine serum
FN	Fibronectin

FS	Iron (II) sulfate
GC-FID	Gas chromatograph flame ionization detector
GFP	Green fluorescent protein
GTEC	Georgia Tech Environmental Chamber
H ₂ O ₂	Hydrogen peroxide
H:C	Hydrogen to carbon ratio
HEPES	4-(2-hydroxyethyl)-1-piperazineethanesulfonic acid
HO ₂	Hydroperoxyl radical
HONO	Nitrous acid
HR-ToF-AMS	High resolution time-of-flight aerosol mass spectrometer
IEPOX	Isoprene epoxydiol
IL-6	Interleukin-6
ISO	Isoprene
LPS	Lipopolysaccharide
MAE	Methacrylic acid epoxide
MEM	Minimum essential medium
MTT	3-(4,5-dimethylthiazol-2-yl)-2,5-diphenyltetrazolium bromide
MS	Magnesium sulfate
MX	<i>m</i> -xylene
NAPH	Naphthalene
N:C	Nitrogen to carbon ratio
NO ₂	Nitrogen dioxide
NO _x	Nitrogen oxides
NAD(P)H	Nicotinamide adenine dinucleotide (phosphate)
NFκB	Nuclear factor kappa-light-chain-enhancer of activated B cells

NRVM	Neonatal rat ventricular myocyte
OA	Organic aerosol
O:C	Oxygen to carbon ratio
O ₃	Ozone
OH•	Hydroxyl radical
$\overline{\text{OS}}_{\text{c}}$	Average carbon oxidation state
PAH	Polycyclic aromatic hydrocarbon
PBS	Phosphate buffered saline
PD	Pentadecane
PDMS	Polydimethylsiloxane
PM	Particulate matter
POA	Primary organic aerosol
RH	Relative humidity
RO ₂	Peroxyl radical
ROS/RNS	Reactive oxygen and nitrogen species
SA	Sulfuric acid
SCAPE	Southeastern Center for Air Pollution and Epidemiology
SMPS	Scanning mobility particle sizer
SOA	Secondary organic aerosol
TNB	2-nitro-5-mercaptobenzoic acid
TNF- α	Tumor necrosis factor- α
VOC	Volatile organic compound
WSOC	Water-soluble organic carbon

SUMMARY

Many studies have established associations between exposure to air pollution, or atmospheric particulate matter (PM) and adverse health effects. An increasing array of studies have suggested oxidative stress as a possible mechanism by which PM-induced health effects arise, and many chemical and cellular assays have been developed to study PM-induced oxidant production. While significant progress has been made in recent years, there are still many gaps in this area of research that have not been addressed. Many prior studies have focused on aerosol of primary origin (e.g., aerosol emitted from combustion engines) even though aerosol formed from the oxidation of volatile species, secondary organic aerosol (SOA), have been shown to dominate even in urban areas. Current SOA health studies are limited and as such, the health effects of SOA are poorly characterized and there is a lack of perspective in terms of the relative toxicities of different SOA systems. Additionally, while chemical assays have elucidated constituents associated with adverse health endpoints, the applicability of these results to cellular responses has not been well established.

The overall objective of this study was to better understand the oxidative properties of different types and components of PM mixtures (especially SOA) through systematic laboratory chamber experiments and ambient field studies. Ambient PM samples were collected from urban and rural sites in the greater Atlanta area as part of the Southeastern Center for Air Pollution and Epidemiology (SCAPE) study, and the concentrations of water-soluble species (e.g., water-soluble organic carbon (WSOC), brown carbon (BrC), metals) were characterized using a variety of instruments. Laboratory studies were

conducted in the Georgia Tech Environmental Chamber (GTEC) facility to generate SOA under well-controlled photooxidation conditions. Precursors of biogenic (isoprene, α -pinene, β -caryophyllene) and anthropogenic (pentadecane, *m*-xylene, naphthalene) origin were oxidized under various formation conditions (dry vs. humid, NO_x, ammonium sulfate vs. iron sulfate seed particles) to produce SOA of differing chemical composition and mass loading. A suite of instruments were utilized to monitor gas- and particle-phase species.

For all aerosol samples, chemical oxidative potentials were determined for water-soluble extracts using a semi-automated dithiothreitol (DTT) assay system. To investigate cellular effects post-exposure, we optimized an assay to measure reactive oxygen and nitrogen species (ROS/RNS) produced as a result of exposure to PM extracts. Optimized parameters include cell density (2×10^4 cells well⁻¹ for murine alveolar macrophages and 3.33×10^4 cells well⁻¹ for neonatal rat ventricular myocytes), probe concentration (10 μ M), and sample incubation time (24 hrs). Results from both ambient and laboratory-generated aerosol demonstrate that ROS/RNS production was highly dose-dependent and non-linear with respect to PM dose. Of the dose-response metrics investigated in this study (maximum response, threshold, EC₅₀, Hill slope, and area under the dose-response curve (AUC)), we found that the AUC was the most robust parameter whose informativeness did not depend on dose range.

For the ambient study, a positive, significant correlation was observed between ROS/RNS production as represented by AUC and chemical oxidative potential as measured by DTT for summer samples. Conversely, a relatively constant AUC was observed for winter ambient samples regardless of the corresponding DTT activity. We also identified several PM constituents (WSOC, BrC, Fe, and Ti) which were significantly

correlated with AUC for summer samples. Although few metal correlations were observed, exposure to laboratory-prepared metal solutions induced ROS/RNS production, indicating that a lack of correlation does not necessarily translate to a lack of response. Collectively, these results suggest that complex interactions may occur between PM species. Furthermore, the strong correlation between organic species and ROS/RNS response highlights a need to understand the contribution of organic aerosol, especially photochemically driven SOA, to PM-induced health effects.

In terms of laboratory-generated aerosol, precursor identity influenced oxidative potentials significantly, with isoprene and naphthalene SOA having the lowest and highest DTT activities, respectively. Both precursor identity and formation condition significantly influenced inflammatory responses induced by SOA exposure, and several response patterns were identified for SOA precursors whose photooxidation products share similar carbon chain length and functionalities. The presence of iron sulfate seed particles did not have an apparent effect on oxidative potentials, however, a higher level of ROS/RNS production was observed for all SOA formed in the presence of iron sulfate compared to ammonium sulfate. This effect was primarily attributed to differences in aerosol carbon oxidation state (\overline{OS}_c). In the presence of iron, radical concentrations are elevated via iron redox cycling, resulting in more oxidized species. An exponential trend was also observed between ROS/RNS and \overline{OS}_c for all naphthalene SOA, regardless of seed type or aerosol formation condition. This may have important implications as aerosol have an atmospheric lifetime of a week, over which \overline{OS}_c increases due to continued photochemical aging, potentially resulting in more toxic aerosol. Finally, in the context of ambient samples, laboratory-generated SOA induced comparable or higher levels of ROS/RNS. Oxidative

potentials for all laboratory SOA systems, with the exception of naphthalene which was higher, were all comparable with oxidative potentials observed in ambient samples. These results suggest that the health effects of SOA are important considerations for understanding the health implications of ambient aerosol.

CHAPTER 1: INTRODUCTION

1.1 Motivation to study air pollution

Exposure to particulate matter (PM), defined as liquid or solid particles suspended in the air, is a leading global human health risk (Lim et al., 2012; Gakidou et al., 2017). Over the past few decades, there have been multiple epidemiological studies reporting associations between elevated PM concentrations and increased incidences of cardiopulmonary morbidity and mortality (Li et al., 2008; Pope III and Dockery, 2006; Brunekreef and Holgate, 2002; Dockery et al., 1993; Hoek et al., 2013; Anderson et al., 2011; Pope et al., 2002; Lim et al., 2012). A recent commission by The Lancet on air pollution and health also makes the assertion that “[air] pollution is the largest environmental cause of disease and premature death in the world today” (Landrigan et al., 2017), indicating the growing importance of understanding aerosol induced health effects.

More recent studies have also found significant associations between cardiopulmonary health effects and particle oxidative potential (Bates et al., 2015; Fang et al., 2016; Yang et al., 2016; Weichenthal et al., 2016). Furthermore, findings from toxicological studies suggest that PM-induced oxidant production, including reactive oxygen and nitrogen species (ROS/RNS), may be a possible mechanism for PM-induced health effects (Li et al., 2003a; Tao et al., 2003; Castro and Freeman, 2001; Gurgueira et al., 2002). Other potential mechanisms have also emerged from recent studies, including alteration of the brain’s innate immune response (Calderón-Garcidueñas et al., 2008) and activation of vascular responses via blood DNA hypomethylation (Bellavia et al., 2013). Nevertheless, despite these additional possible mechanisms, PM-induced oxidative stress

remains the current paradigm for PM-induced health effects (Li et al., 2003a). Specifically, oxidative species generated as a result of PM exposure can initiate cellular inflammatory cascades, and prolonged stimulation of these cascades can lead to oxidative stress, cellular damage (e.g., lipid peroxidation, protein oxidation, and nucleic acid alteration), and chronic inflammation for which there is an established link to cancer (Wiseman and Halliwell, 1996; Hensley et al., 2000; Philip et al., 2004). Collectively, these findings suggest that a possible link exists between PM exposure and observed health endpoints.

1.2 Previous assays developed to study PM-induced health effects

Multiple chemical and cellular assays have been developed to measure PM-induced oxidant production and elucidate constituents responsible for oxidant production (Kumagai et al., 2002; Cho et al., 2005; Fang et al., 2015c; Landreman et al., 2008). In biological systems, ROS/RNS are formed by mitochondria (Murphy, 2009) or the reaction between oxygen and reducing agents present in the cell, such as NADPH and NADH (Frei, 1994). PM species can react with these reducing agents to initiate a series of redox reactions that ultimately produce superoxide anions, which can further react to produce hydrogen peroxides (e.g., Rattanavaraha et al., 2011).

The reaction between oxygen and reducing agent is the basis of cell-free chemical assays, where an anti-oxidant surrogate (e.g., dithiothreitol, DTT; ascorbic acid, AA; or other species present in the respiratory tract lining fluid) is used to simulate biologically relevant redox reactions. In the presence of redox-active species in the PM sample, an electron is transferred between the surrogate anti-oxidant (e.g., DTT) and molecular oxygen. This reaction consumes DTT and produces a superoxide anion (Kumagai et al.,

2002; Cho et al., 2005). Consumption of DTT (or other anti-oxidant surrogate) then provides a measure of the concentration of redox-active species in a sample (Fang et al., 2015c; Cho et al., 2005; Kumagai et al., 2002). These chemical assays are generally performed in buffered solutions (pH ~ 7.4) at 37 °C to simulate biologically relevant conditions (Fang et al., 2015c).

In principle, the superoxide anion produced in these cell-free chemical assays can react further to produce other ROS/RNS species, including hydrogen peroxide (H₂O₂) or the hydroxyl radical (OH•) (Kumagai et al., 2002). As a result, oxidative potentials measured using these assays, particularly DTT activities, have frequently been used to represent ROS/RNS production. However, a study comparing the consumption of DTT and the generation of ROS, specifically OH• and H₂O₂, has recently shown that DTT consumption and actual ROS generation are not equivalent (Xiong et al., 2017). In fact, metal species known to be highly active in DTT oxidation (i.e., Cu) produced negligible ROS, while other metals known to be largely inactive in DTT oxidation (i.e., Fe) contributed significantly to ROS production in mixtures with other aerosol components (Xiong et al., 2017).

Cellular assays, on the other hand, utilize a non-fluorescent probe that reacts with ROS/RNS and produces a fluorescent compound post-reaction. The measured fluorescence is proportional to the concentration of ROS/RNS produced as a result of PM exposure (Landreman et al., 2008). In cellular systems, cells may also generate ROS/RNS as a signaling molecule and/or upregulate antioxidant defenses in response to stimuli (Wiseman and Halliwell, 1996), which affect the measured ROS/RNS production. The cellular assay utilized in this study measures ROS/RNS produced by the cell in response to PM exposure.

Redox-active species in the aerosol, the concentration of which is measured by chemical assays, can induce cellular ROS/RNS production and may hence be measured by the cellular assay as well. Furthermore, it may be possible for particle-bound ROS/RNS to diffuse across the cell membrane and react with the ROS/RNS probe. This is the basis of another acellular chemical assay, which has been used previously to study the oxidative properties of PM (Møller et al., 2009). Therefore, there exists some overlap between the types of ROS/RNS measured by both chemical and cellular assays.

1.3 PM components associated with adverse health

Epidemiological studies and various assays have associated numerous PM components with adverse health effects. The potential contributions of metals have been explored extensively as many metals are redox-active and hence may produce ROS/RNS via Fenton-like reactions (Frei, 1994; Chevion, 1988). Many studies report findings that support the adverse influence of metals on PM-induced health effects. Epidemiological studies have found strong associations between metals, namely Fe, Ni, and Zn, and mortality (Burnett et al., 2001). These observations are supported by toxicological studies, where various oxidative properties (e.g., cytotoxicity, inflammatory cytokine release) were found to be most significant in metal-containing samples (Akhtar et al., 2010; Pardo et al., 2015). Strong correlations between oxidative properties (e.g., neutrophil influx and oxidative potential) and water-soluble metals have also been reported (Huang et al., 2003; Charrier and Anastasio, 2012; Charrier et al., 2015; Verma et al., 2010).

Similarly, organic carbon constituents have been found to be toxicologically relevant. Verma et al. (2009) found that DTT activity was strongly associated with water-

soluble organic carbon (WSOC), and a subsequent study on the relative contributions of water-soluble and water-insoluble PM fractions to oxidative potentials further suggested the importance of hydrophobic organic compounds, such as humic-like substances (HULIS) (Verma et al., 2012). These findings led to the development of a novel technique to isolate various fractions of HULIS and the observation that highly DTT-active HULIS components were polar in nature (Verma et al., 2015b). The importance of HULIS and polycyclic aromatic hydrocarbons (PAH) to particle redox potential have been implicated in additional studies as well (Dou et al., 2015; Saffari et al., 2014b; Antinolo et al., 2015; Li et al., 2003b). Another study comparing the relative oxidative potentials of various organic aerosol subtypes reported DTT activities on par or higher than that of ambient PM, further implicating the importance of organic species to PM-induced health effects (Verma et al., 2015a).

Besides investigations utilizing chemical oxidative potential, inhalation and exposure studies have found that organic carbon constituents may play a significant role in PM-induced adverse effects (Kleinman et al., 2005; Hamad et al., 2015). Kleinman et al. (2005) exposed ovalbumin-sensitized BALB/c mice to PM collected downwind of a freeway in Los Angeles and observed significant correlations between enhanced inflammatory and allergic responses and organic and elemental carbon constituents. Similarly, an *in vitro* study utilizing a macrophage-based assay to assess oxidative stress found an association between WSOC from biomass burning and ROS production (Hamad et al., 2015). Despite these findings, many inhalation and exposure studies involved limited data sets and low-throughput methods, while the applicability of chemical oxidative potentials to cellular responses have not been established.

1.4 Motivation to study secondary organic aerosol (SOA) toxicity

Ambient PM consists of a complex mixture of hundreds to thousands of species. Organic aerosol constitute a significant portion of PM and can be further divided into primary organic aerosol (POA) and secondary organic aerosol (SOA) (Kanakidou et al., 2005; Jimenez et al., 2009). POA are directly emitted as PM from a variety of sources, such as vegetation, fossil fuel combustion, and power plant operation. SOA, on the other hand, are formed from the oxidation of volatile species followed by gas-particle partitioning (Hallquist et al., 2009; Kroll and Seinfeld, 2008). Currently, many pollution control strategies and policies are focused on primary emissions. Field studies, however, have shown that SOA mass loadings often dominate over POA, even in urban environments (Zhang et al., 2007; Jimenez et al., 2009; Ng et al., 2010). In the past, many health studies focused on primary emissions, such as PM emitted from diesel and gasoline exhaust (Bai et al., 2001; Kumagai et al., 2002; McWhinney et al., 2013a; Turner et al., 2015), or were conducted on particles that were not representative of ambient exposures (Koike and Kobayashi, 2006).

More recent studies explored the potential health implications of SOA (McWhinney et al., 2013b; Rattanavaraha et al., 2011; Kramer et al., 2016; Lund et al., 2013; McDonald et al., 2010; McDonald et al., 2012; Baltensperger et al., 2008; Arashiro et al., 2016; Platt et al., 2014). The oxidative potentials and cellular responses measured in these studies demonstrated that pure SOA could indeed contribute to PM-induced health effects. McWhinney et al. (2013b) and Kramer et al. (2016) measured the oxidative potentials of naphthalene and isoprene SOA, respectively. Both SOA systems were found to be redox active, however, there was a lack of perspective due to the large range of

oxidative potentials that remained unexplored. The oxidative potentials of additional particle systems, including aged diesel exhaust particles and SOA generated in the presence of a simulated urban environment, were also explored in a study by Rattanavaraha et al. (2011), although a lack of perspective still exists regarding the relative toxicities of different SOA systems.

Results from cellular exposure studies also included different measures of response (e.g., ROS/RNS, gene expression, inflammatory markers) and were inconclusive, with some studies reporting significant response as a result of SOA exposure and others observing little to no response (Arashiro et al., 2016; Lund et al., 2013; McDonald et al., 2010; McDonald et al., 2012; Baltensperger et al., 2008). Mice and rats exposed to α -pinene and toluene SOA exhibited negligible pulmonary inflammation and a mild cardiovascular response (McDonald et al., 2010; McDonald et al., 2012). A subsequent exposure study investigating the cardiovascular effects of α -pinene and toluene SOA formed in the presence of different gaseous components also reported limited biological responses, however, significant differences in SOA-mediated toxicity were observed depending on the specific chemistry under which the SOA was formed (Lund et al., 2013). In contrast to these observations, significant and distinct responses were reported for multiple pulmonary cell culture systems exposed to SOA in another study (Baltensperger et al., 2008). *In vitro* exposures to isoprene SOA also induced significant cellular responses, such as increased expression of inflammation-related genes (Arashiro et al., 2016; Lin et al., 2017; Lin et al., 2016). These differences in cellular responses may, in part, be due to the different exposure doses and different cellular endpoints explored in each study, resulting in difficult direct comparisons between studies. Consequently, there is a lack of perspective in terms of the

relative toxicities of individual SOA systems formed from various precursors, and it is unclear whether responses resulting from SOA exposure are indeed toxic compared to other sources and subtypes of PM.

Finally, the potential health implications arising from organic aerosol formed in the presence of redox-active metals have also not been explored, even though this formation condition can be atmospherically relevant as these metals are readily emitted via combustion and various mechanical processes (Charrier and Anastasio, 2012; Fang et al., 2015a). Moreover, both components (metals and organics) have been shown to have considerable health effects in previous studies (Akhtar et al., 2010; Pardo et al., 2015; Burnett et al., 2001; Huang et al., 2003; Kleinman et al., 2005; Hamad et al., 2015; Verma et al., 2015b; Li et al., 2003b; McWhinney et al., 2013b; Antinolo et al., 2015). This formation of organic aerosol in the presence of metals may therefore produce aerosol that is highly detrimental to health. Furthermore, organic aerosol have a lifetime of approximately one week, over which continued photochemical aging can alter their physical and chemical properties (Seinfeld and Pandis, 2016). These changes have potential health implications that have not been explored.

1.5 Scope and overview

This dissertation covers several important gaps in the area of aerosol toxicity, with a specific focus on providing perspective on SOA toxicity and comparing aerosol toxicity results from different assays. Chapter 2 focuses on the development and optimization of a cellular assay for measuring ROS/RNS produced as a result of aerosol exposure. The optimized assay was then used to analyze a large set of ambient samples to evaluate

whether results from chemical assays are representative of cellular responses. In chapters 3 and 4, chemical oxidative potentials and cellular ROS/RNS productions were evaluated for various laboratory SOA systems generated from different precursors under different formation conditions. Additional cellular responses were also evaluated to provide further insight. Chapter 5 then discusses the effect of aerosol age and redox-active metals on aerosol toxicity. Finally, chapter 6 summarizes the main findings of this dissertation and provides recommendations for future work.

CHAPTER 2: DOSE-DEPENDENT INTRACELLULAR ROS/RNS PRODUCTION FROM PM EXPOSURE – COMPARISON TO OXIDATIVE POTENTIAL AND CHEMICAL COMPOSITION

2.1 Background

Adverse health effects resulting from particulate matter (PM) exposure have received considerable attention with increasing epidemiological studies associating elevated PM concentrations with increases in cardiopulmonary hospitalizations and mortality, specifically increases in lung cancer, asthma, chronic obstructive pulmonary disease, arrhythmia, and ischemic heart disease (Li et al., 2008; Pope III and Dockery, 2006; Brunekreef and Holgate, 2002; Dockery et al., 1993; Hoek et al., 2013; Anderson et al., 2011; Pope et al., 2002). Contributions from PM-associated deaths worldwide also rank among the top 10 global risks (Lim et al., 2012), and in 2013, the World Health Organization classified PM as a Group I carcinogen (Loomis et al., 2013). Toxicology studies suggest that PM-induced oxidative stress may play a role in initiating these adverse effects (Li et al., 2003a; Tao et al., 2003; Castro and Freeman, 2001; Gurgueira et al., 2002). Specifically, PM-induced reactive oxygen/nitrogen species (ROS/RNS) production can initiate inflammatory cascades, and prolonged stimulation of these cascades can lead to oxidative stress and cellular damage, including lipid peroxidation, protein oxidation, and DNA/RNA alteration (Wiseman and Halliwell, 1996; Hensley et al., 2000). Additionally, there is a well-established link between chronic inflammation and cancer (Philip et al., 2004). A possible link between PM exposure and observed health endpoints therefore exists as PM can generate ROS/RNS via redox reactions and by inducing cellular pathways that produce ROS/RNS (Rattanavaraha et al., 2011; Becker et al., 2005).

Despite these associations, the specific mechanisms and components responsible for PM-induced oxidative stress have not been fully explored. Metals have received considerable attention in this regard as many are redox active and can produce ROS/RNS via Fenton-like reactions (Frei, 1994; Chevion, 1988). For instance, studies with standard reference materials and PM samples have found that oxidative potential, cytotoxicity, and inflammatory responses were most significant in metal-containing samples (Akhtar et al., 2010; Pardo et al., 2015). Epidemiological studies have also found that specific metals (Fe, Ni, and Zn) were more strongly associated with mortality than fine particle (PM_{2.5}) mass alone (Burnett et al., 2001). Additionally, Huang et al. (2003) showed that water-soluble metals in concentrated ambient particles were correlated with increased neutrophil influx and blood fibrinogen in humans. Besides metals, organic carbon components were also found to be toxicologically relevant in inhalation and exposure studies (Kleinman et al., 2005; Hamad et al., 2015), and ROS have been linked to quinones, polycyclic aromatic hydrocarbons (PAHs), and other oxygenated aromatics, such as humic-like substances (Verma et al., 2015b; McWhinney et al., 2013b; Li et al., 2003b; Antinolo et al., 2015). Many of these studies, however, involve limited data sets and low-throughput methods.

Chemical assays have been developed and widely used to determine PM oxidative potential. In these assays, an anti-oxidant (e.g. DTT; ascorbic acid, AA; or other species present in the respiratory tract lining fluid) is used to simulate redox reactions that would occur in biological systems (Kumagai et al., 2002; Cho et al., 2005). PM catalyzes electron transfer from the anti-oxidant to oxygen, and anti-oxidant decay provides a measure of redox-active species in the sample. These assays can be automated and high-throughput systems exist for DTT and AA (Fang et al., 2015c). Studies involving oxidative potential

as measured by DTT have shown strong correlations with redox metals (Charrier and Anastasio, 2012; Charrier et al., 2015; Verma et al., 2010), water-soluble organic carbon (WSOC), and PAHs (Verma et al., 2012; Verma et al., 2009; Saffari et al., 2014b). However, the question remains as to whether chemical assays are representative of cellular responses.

In this study, alveolar macrophages and ventricular myocytes were exposed to ambient PM extracts over a wide dilution series to fully capture dose-dependent reactive oxygen and nitrogen species (ROS/RNS) production and obtain dose-response parameters. The PM filters were collected at multiple rural and urban sites in the greater Atlanta area during the Southeastern Center for Air Pollution and Epidemiological (SCAPE) study. Response parameters were then compared with chemical oxidative potential, measured by DTT (Verma et al., 2014), to determine whether results from chemical assays represent cellular responses. Finally, water-soluble PM components were compared with cellular response parameters to elucidate components associated with ROS/RNS production. Spatial and seasonal trends were also investigated for each comparison.

2.2 Methods

2.2.1 Alveolar macrophage cell line.

Alveolar macrophages are closely involved in foreign particle clearance and inflammatory signaling and were thus chosen as cells representing the first line of defense against environmental insults (Oberdörster, 1993; Oberdörster et al., 1992). Immortalized murine alveolar macrophages (MH-S, ATCC®CRL-2019™) were cultured in RPMI-1640 media supplemented with 10% fetal bovine serum (FBS, Quality Biological, Inc.), 1%

penicillin-streptomycin, and 50 μM β -mercaptoethanol (BME) at 37 °C and 5% CO_2 . Prior to sample exposure, MH-S cells were seeded at 2×10^4 cells well⁻¹ onto 96-well plates pre-treated with 10% FBS in phosphate buffered saline (PBS, Cellgro). For seeding and thereon, all culture media was supplemented with 10% FBS without BME addition since BME is a reducing agent that may interfere with ROS/RNS measurement. Seeded plates were then incubated overnight to allow cells to adhere and acclimate.

2.2.2 *Ventricular myocyte isolation and culture*

Primary ventricular myocytes were chosen as an alternate active cell type to investigate, as cardiac health is known to be affected by pollution. Neonatal rat ventricular myocytes (NRVM) were harvested from 2-day-old neonatal Sprague-Dawley rats (Charles River Laboratories) based on pre-established protocol (Grosberg et al., 2012). Isolated cells were resuspended in M199 culture medium supplemented with 10% FBS, 10 mM HEPES, 0.1 mM MEM non-essential amino acids, 3.5 g L⁻¹ glucose, 2 mM L-glutamine, 2 mg L⁻¹ vitamin B12, and 50 U mL⁻¹ penicillin. Prior to seeding, several iterations of pre-plating were performed to increase the cardiomyocyte purity to 90 – 98%. Cells were then seeded onto 96-well plates pre-coated with polydimethylsiloxane (PDMS, Dow Corning Sylgard 184) and fibronectin (FN, Fisher Scientific) at 3.33×10^4 cells well⁻¹. Seeded plates were incubated at 37 °C and 5% CO_2 and cultured for 2 days prior to exposure. Approximately 24 hrs after seeding, cells were washed with PBS to remove dead cells and the media was replaced. From 48 hrs on, 2% FBS was used for culturing and exposure.

2.2.3 *PM collection and extraction*

Ambient PM_{2.5} samples were collected from multiple urban (Jefferson Street, Roadside, Georgia Tech) and rural (Yorkville) sites around the greater Atlanta area (Figure A-1) between June 2012 and October 2013 as part of the Southeastern Center for Air Pollution and Epidemiology (SCAPE) study (Verma et al., 2014; Fang et al., 2015a; Xu et al., 2015a; Xu et al., 2015b). High-volume samplers (ThermoAndersen) were used to collect particles over 23 hrs onto pre-baked quartz filters (Pallflex®Tissuquartz™). Collected samples were wrapped in pre-baked aluminum foil and stored at -20 °C until extraction and analysis (Fang et al., 2015c). For this study, ambient samples were selected to span the range of extrinsic (per volume of air sampled) and intrinsic (per mass of PM) DTT activities observed in SCAPE (Verma et al., 2014).

The concentrations of various water-soluble species in the PM samples were determined and reported in previous studies (Fang et al., 2015a; Fang et al., 2015b). Specifics on PM chemical characterization are described elsewhere (Fang et al., 2015a). Briefly, filter samples were sectioned and extracted in deionized (DI) water for chemical analysis. WSOC and brown carbon (BrC) absorption were then measured using an automated system comprised of an autosampler, a liquid waveguide capillary cell, a spectrophotometer, and a total organic carbon analyzer (Verma et al., 2014). A Xact™ 625 automated multi-metals monitor was used to determine water-soluble metal concentrations using acidified water-soluble extracts (Fang et al., 2015a). Elemental and organic carbon were also determined using a thermal/optical transmittance analyzer on sections of filter samples (Verma et al., 2014).

In this study, collected particles were extracted following the procedure described in Fang et al. (2015a) with modifications for cellular exposure. Briefly, filter samples were sectioned into 1.45 cm²-punches and extracted in cell culture media for measuring cellular ROS/RNS production or DI water for determining oxidative potential. Punches were submerged in extraction medium and sonicated for 30 min using an Ultrasonic Cleanser (VWR International). Extracts were then filtered using 0.45 µm PTFE syringe filters (Fisherbrand™) to remove quartz fibers, which are known to elicit inflammatory responses (Fubini and Hubbard, 2003; Knaapen et al., 2002). Prior to exposure, media extracts were supplemented with FBS and diluted over ten dilutions to obtain a dose-response curve from 1x to 0.00125x, with 1x being the undiluted extract.

2.2.4 Pure metal solutions

Concentrated pure metal solutions were prepared by dissolving metal salts [Cu(II)SO₄, ZnCl₂, C₆K₂O₁₂Ti, Cr(III)Cl₃, Fe(II)SO₄, Mn(II)SO₄] in DI water to a final concentration of 400 mM (Cu, Zn), 200 mM (Ti, Cr, Mn), and 1000 mM (Fe). Prior to exposure, metal solutions were diluted 1000x in FBS-supplemented media to produce the “1x” solution. These concentrations were chosen to span the observed range for these metals in SCAPE (Verma et al., 2014).

2.2.5 Oxidative potential

PM oxidative potential was measured in previous studies using a semi-automated DTT assay system (Fang et al., 2015c). Details of this high-throughput system are described elsewhere (Fang et al., 2015c), and oxidative potential results from SCAPE have been reported and extensively discussed in the context of PM composition and source

apportionment in prior publications (Verma et al., 2014; Fang et al., 2015a; Verma et al., 2015a). Briefly, the method consisted of three main steps: (1) oxidation of DTT by redox-active species, (2) reaction of residual DTT with DTNB to form 2-nitro-5-mercaptobenzoic acid (TNB), repeated at specific time intervals, and (3) measurement of TNB to determine DTT consumption.

2.2.6 Intracellular ROS/RNS measurement

ROS/RNS were detected using 5-(and-6)-carboxy-2',7'-dichlorodihydrofluorescein diacetate (carboxy-H₂DCFDA, Molecular Probes C-400), a cell-permeable compound that becomes deacetylated intracellularly and is better retained than other commonly used probes due to its additional negative charges (Chen et al., 2010; Uchida et al., 2004). The deacetylated ROS/RNS probe (carboxy-DCFH) is subsequently oxidized by cellular ROS/RNS to produce a fluorescent compound (carboxy-DCF). The protocol established by Landreman et al. (2008), which measured ROS production from alveolar macrophages exposed to diesel exhaust particles, was used as a general reference for assay development and optimization in this study. The optimized ROS/RNS assay, shown schematically in Figure 2-1, consisted of the following major steps: (1) pre-treatment of 96-well plates, (2) seeding of cells, (3) treatment of cells with ROS/RNS probe, (4) exposure of probe-treated cells to samples, and (5) detection of ROS/RNS.

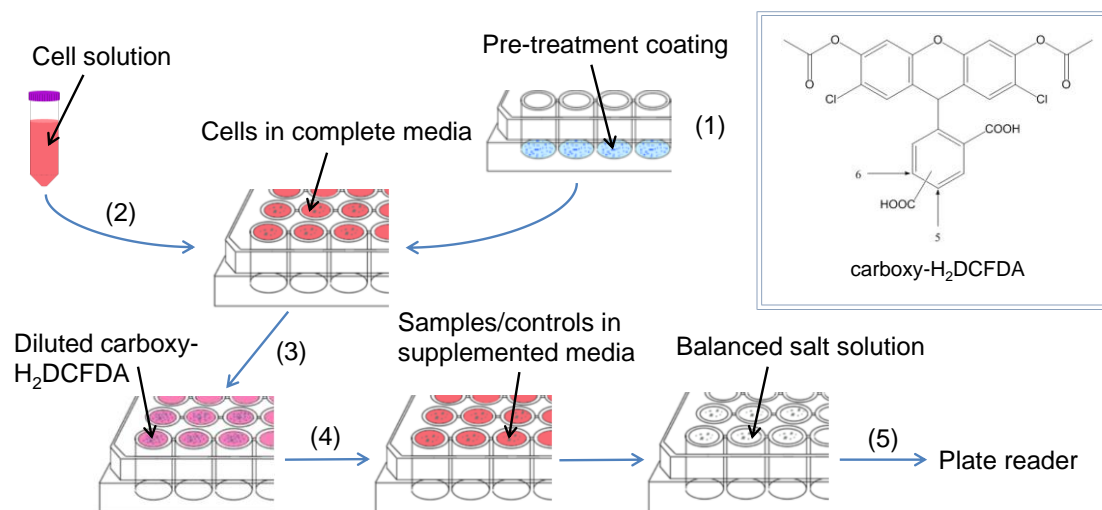


Figure 2-1. Cellular assay optimized for measuring ROS/RNS production as a result of PM exposure. Major steps include: (1) pre-treatment of wells, (2) seeding of cells onto wells, (3) incubation of cells with carboxy-H₂DCFDA, (4) incubation of probe-treated cells with samples or controls, and (5) detection of carboxy-DCF (proportional to ROS/RNS) using microplate reader.

In the first step, 96-well plates were pre-treated to reduce cell aggregation near hydrophobic walls and ensure a uniform cell density throughout the well. Next, wells were seeded at a density optimized for ROS/RNS measurement (MH-S) or predetermined to form a confluent monolayer tissue (NRVM) (Grosberg et al., 2012). MH-S cell density was optimized with the following considerations: (1) too few cells could result in saturation where different PM samples yield the same ROS/RNS signal, and (2) too many cells could result in overcrowding stress and increased background ROS/RNS production.

Approximately 24 hrs after seeding, the cell culture media was removed and cells were washed with PBS. 120 μ L of ROS/RNS probe diluted to a final concentration of 10 μ M was then added to each well and incubated for 40 min at 37 °C and 5% CO₂. After probe treatment, the probe solution was removed and replaced with 120 μ L of PM extract or control solution. All controls were dissolved or extracted in cell culture media

supplemented with FBS. Positive controls included LPS ($1 \mu\text{g mL}^{-1}$), H_2O_2 ($100 \mu\text{M}$), and reference filter extract (10 filter punches mL^{-1} , 1 per filter sample, from various ambient filters collected at the Georgia Tech site). LPS and H_2O_2 have been shown to induce oxidative stress and inflammation in macrophages (Chen et al., 2007; Tang et al., 2007), whereas reference filter extract contains ambient particles that should elicit similar cellular pathways as filter samples of interest. Negative controls include blank filter extract (2 punches mL^{-1}) and control cells (probe-treated cells exposed to media only, no stimulants). After sample/control addition, cells were incubated for 24 hrs. This sample incubation time was chosen to maximize positive and negative response signal separation (Figure A-2). After 24 hrs, samples and controls were removed and replaced with PBS. Fluorescence was then measured (ex/em: 485/525 nm) using a microplate reader (BioTek Synergy H4).

Cellular metabolic activity was determined for selected samples using the MTT (3-(4,5-dimethylthiazol-2-yl)-2,5-diphenyltetrazolium bromide) assay (Biotium). Briefly, samples were removed after exposure and replaced with media containing MTT. Cells were then incubated for 4 hrs, during which the dye was reduced by cellular NAD(P)H to produce an insoluble purple salt. Finally, dimethyl sulfoxide was used to solubilize the salt and absorbance at 570 nm was measured using a microplate reader.

2.2.7 Statistical analysis

Linear regressions between cellular response and oxidative potential or PM composition were evaluated using Pearson's correlation coefficient. Significance was determined using multiple imputation to calculate the total variance associated with the slope of each regression. Details of this method are given in Pan and Shimizu (2009).

Briefly, fit parameters were assumed to be normally distributed and 10 parameter “estimates” were obtained for each parameter using the average and standard deviation determined from the fit. Estimates were then plotted against the component of interest to obtain 10 fits, each with a corresponding slope. The generated slopes and variances were then used to calculate the between and within variance to obtain the total variance. Finally, the student’s *t*-test and a 95% confidence was used to calculate and evaluate the associated *p*-values.

2.3 Results

2.3.1 PM-induced dose-dependent ROS/RNS production

ROS/RNS production, expressed as fold increase in fluorescence over control cells, was measured over 10 dilutions for each PM sample. A representative dose-response curve with three distinguishable regions is shown in Figure 2-2. In the first region, there exists a dose below which there is no observable difference in response compared to control cells. Next, there is a region where response increases with dose. Finally, there exists a dose beyond which there is no further increase in response.

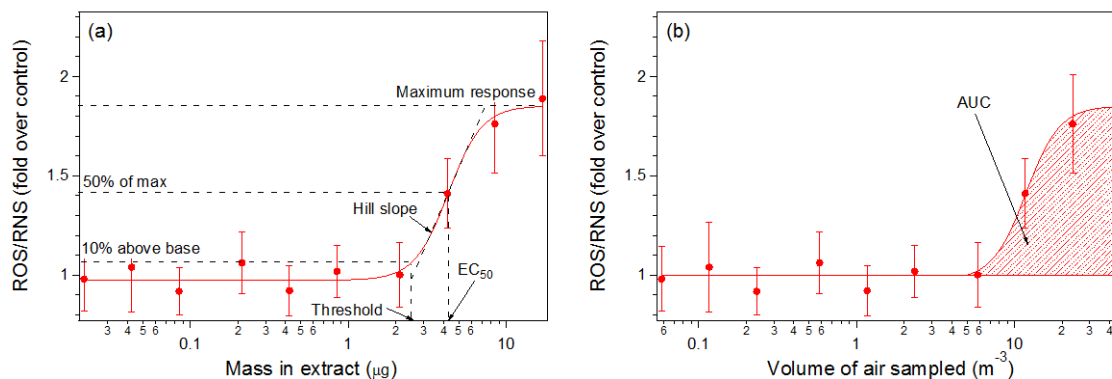


Figure 2-2. Representative dose-response curve of ROS/RNS produced as a result of ambient PM exposure (filter ID: YRK 07/10/12). ROS/RNS production is expressed as fold increase over control, defined as probe-treated cells incubated with stimulant-free media. Dose is expressed as either (a) mass in extract (μg) or (b) volume of air sampled (m^3). Data shown are means \pm SE of exposure experiments performed in triplicate. Hill equation (HE) parameters shown include: max response, Hill slope (rate at which max response is attained), EC_{50} (dose at which 50% of max response is attained), threshold (dose at which response is 10% above baseline), and AUC (area under the dose-response curve).

To characterize each dose-response, the Hill equation, used extensively in pharmacology to determine drug dose-response relationships (Goutelle et al., 2008; Hill, 1910), was applied to each data set to obtain response parameters. These parameters, labeled in Figure 2-2a, include the max response attained as a result of PM exposure, the rate at which the max response is attained once there is response (Hill slope), the dose at which 50% of the max response is attained (EC_{50}), and the dose at which response is 10% above the fitted baseline (threshold).

In addition to the classical dose-response shown in Figure 2-2, some samples exhibited behaviors that required adjustments to analysis methods (Figure A-3):

- (1) **Maximum response not attained:** the Hill equation was applied and the maximum response was estimated from the fit. Fitted parameters in these cases were generally associated with large uncertainties.
- (2) **Decreased response at higher doses:** doses after the initial decrease in response were excluded from the fit. MTT for selected filters showed a decrease in cell viability at the same dose where ROS/RNS production decreased.
- (3) **No response above baseline at all doses:** a maximum response of 1 and a threshold equal to the highest dose investigated was assigned. EC_{50} and Hill slope were not calculated.

The area under the fitted dose-response curve (AUC), labeled in Figure 2-2b, was also considered as a measure of the overall effect of PM exposure across the dose range investigated (Huang and Pang, 2012). Doses (in μg) were converted to volume of air sampled to obtain dose-response curves across the same dose range. Uncertainties associated with AUC determination were approximated by averaging AUCs calculated by fitting dose-response data with each point removed systematically. Max response and Hill slope values did not change with dose conversion. Furthermore, the uncertainties associated with AUC determination were low for all samples investigated, including those with non-classical dose-response behaviors.

2.3.2 *ROS/RNS production and oxidative potential*

AUC per volume of air sampled (AUC_{volume}) and AUC per mass of PM (AUC_{mass}) were compared with extrinsic and intrinsic DTT activity, respectively. Results are shown

in Figure 2-3, colored by season for both cell types. It is noted that the DTT activity results have been reported previously in Verma et al. (2014) For summer filters, AUC_{volume} was significantly correlated with DTT activity ($n = 47$, $R = 0.63$, $p < 0.05$), but a relatively constant AUC_{volume} was observed for winter samples ($n = 32$). A statistically significant correlation between AUC_{mass} and DTT activity (Figure 2-3b) was observed for summer data, while no correlation was observed for winter data. No other dose-response parameter was significantly correlated with DTT activity (Figure A-4) and no spatial trends were observed.

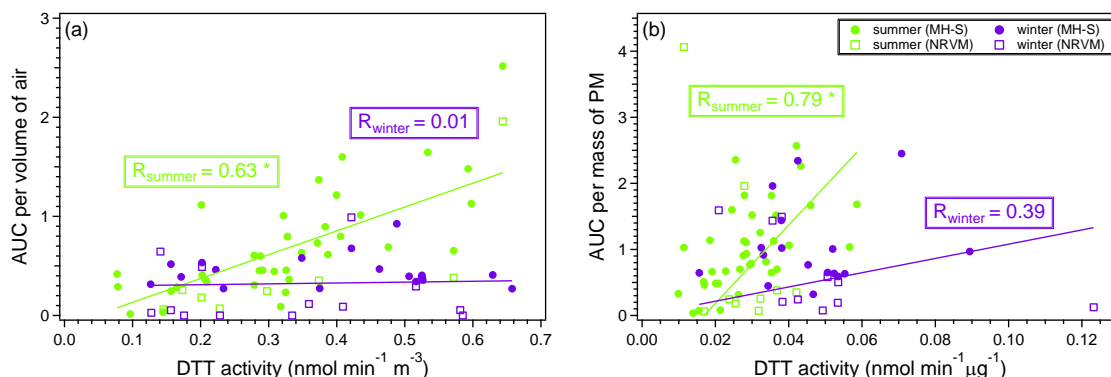


Figure 2-3. AUC per volume of air sampled (a) and per mass of PM (b) as determined by Hill equation fits to ROS/RNS dose-response data for ambient samples spanning a wide range of (a) extrinsic and (b) intrinsic DTT activity. Each data point represents a single ambient filter for which a dose-response was obtained (10 dilutions performed in triplicate). Data points are colored by season as determined by solstice and equinox dates between June 2012 and October 2013. Linear regressions and Pearson's correlation coefficients are shown for summer and winter filter samples. $n = 104$ ambient filters (10 spring, 47 summer, 15 autumn, and 32 winter); * indicates significance, $p < 0.05$

2.3.3 ROS/RNS production and PM composition

Absolute mass concentrations and relative mass fractions of all water-soluble PM components (Fang et al., 2015a) were compared with AUC_{volume} and AUC_{mass} , respectively. Seasonal trends for these correlations are shown in Figure 2-4. For summer filters,

AUC_{volume} was significantly correlated with WSOC ($R = 0.66$), brown carbon absorption (BrC, $R = 0.62$), titanium (Ti, $R = 0.71$), and iron (Fe, $R = 0.65$) (Figure 2-4), while AUC_{mass} was significantly correlated with titanium fraction ($R = 0.66$) and chromium fraction (Cr, $R = 0.79$) (Figure A-5). For winter filters, a relatively constant AUC_{volume} was observed for WSOC, BrC, and Fe, while no statistically significant correlations were observed for AUC_{mass} and water-soluble PM constituents. Other correlations, including metals grouped by source apportionment result (Fang et al., 2015a), were not statistically significant (Table A-1 and Table A-2).

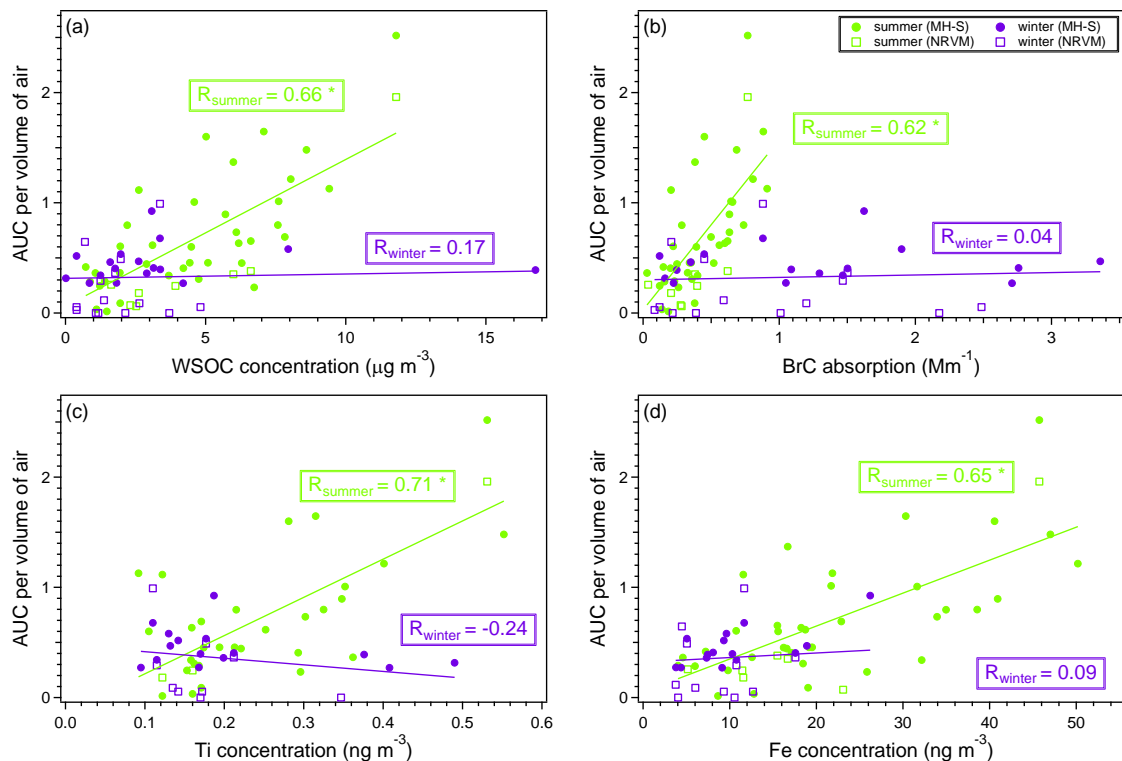


Figure 2-4. AUC per volume of air sampled for ambient samples spanning a wide range of (a) water-soluble organic carbon (WSOC), (b) brown carbon (BrC), (c) titanium (Ti), and (d) iron (Fe). Each data point represents a single ambient filter for which a dose-response was obtained (10 dilutions performed in triplicate) and fitted using the Hill equation. Data points are colored by season as determined by solstice and equinox dates between June 2012 and October 2013. Linear regressions and Pearson's correlation coefficients are shown for summer and winter filter samples. $n = 104$ ambient filters (10 spring, 47 summer, 15 autumn, and 32 winter); * indicates significance, $p < 0.05$. Removal of the sample with high WSOC introduces a slight slope (0.03) in the winter correlation, which is still relatively flat (panel a).

2.3.4 Comparison between MH-S and NRVM

AUC_{mass} data for ambient filters investigated using both cell types are shown in Figure 2-5. A total of 18 filters were analyzed with both cellular assays. AUC_{mass} was significantly correlated between the cell types ($R = 0.80$, $p < 0.05$). No seasonal or spatial trends were observed.

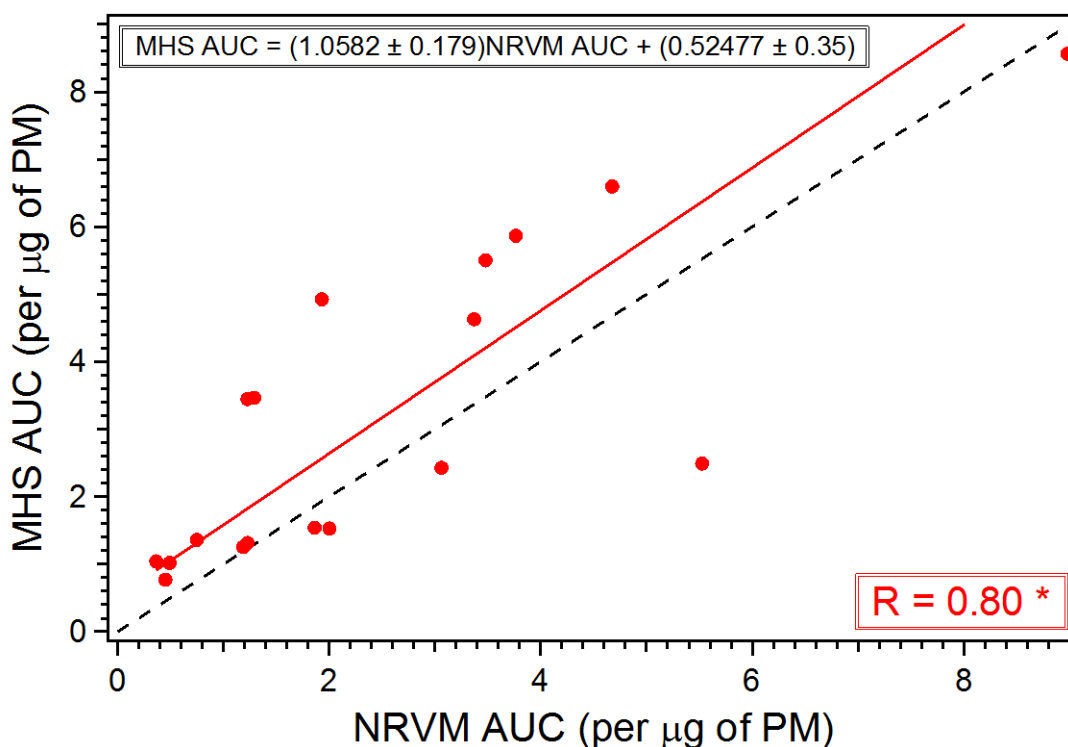


Figure 2-5. AUC per mass of PM for MH-S and NRVM. Each data point represents a single filter dose-response obtained from 10 dilutions (1x to 0.00125x) performed in triplicate. An orthogonal regression and the corresponding Pearson's coefficient is shown. A 1:1 line is shown for reference. $n = 18$ ambient filters; * indicates significance, $p < 0.05$.

2.4 Discussion

2.4.1 Cellular ROS/RNS assay optimization

In the present study, MH-S and NRVM were exposed to PM extracts containing water-soluble components in an assay optimized for measuring ROS/RNS production (Figure 2-1). Previous cellular assays (Saffari et al., 2014a; Landreman et al., 2008) were used as a general guideline for method optimization. For this study, the following parameters were optimized using MH-S and later adapted for NRVM: cell density, ROS/RNS probe concentration, and sample incubation time (Table A-3). Optimization experiments with stimulant-free, probe-treated cells showed that 1×10^5 cells well⁻¹,

commonly used in prior studies (Landreman et al., 2008; Hamad et al., 2015; Saffari et al., 2014a), produced a higher ROS/RNS baseline with greater signal variability. Likewise, studies have shown that cells experienced oxidative stress under crowded conditions (Sung et al., 2006; Murray et al., 2004). A lower cell density, 2×10^4 cells well⁻¹, produced a low baseline and was visually consistent with low-density reference images (ATCC). Further optimization experiments also showed that probe concentrations ≥ 30 μ M resulted in visually enlarged cells and membrane irregularities similar to those observed under crowded conditions. These observations suggest that ROS/RNS productions observed using higher probe concentrations, such as 45 μ M (Saffari et al., 2014a; Daher et al., 2014), may be due to basally stressed cells and may not accurately reflect PM exposure. Finally, a time series experiment (Figure A-2) showed that a significant fold increase in ROS/RNS production was not observed until 8 – 24 hrs. This is much longer than exposure times used in previous cellular assays, typically ~ 2.5 hrs (Hu et al., 2008; Saffari et al., 2014a; Daher et al., 2014), but is in accordance with the LPS peak response time found in other inflammatory assays (Haddad, 2001). The final assay parameters are as follows: 2×10^4 cells well⁻¹ (MH-S), 3.33×10^4 cells well⁻¹ (NRVM), 10 μ M ROS/RNS probe, and 24 hrs sample incubation.

In addition to parameter optimization, a dose-response approach was used in this study. Prior studies using the macrophage assay involved normalizing raw fluorescence measurements to a positive control (e.g., zymosan or H₂O₂) in order to obtain a single value for comparison with DTT activity (Gali et al., 2015; Saffari et al., 2014a). However, studies involving inflammatory stimulants and cellular endpoints, including IL-6, IL-8, NF- κ B, and TNF- α , showed that endpoints generally followed a sigmoidal dose-response curve

(Haddad, 2001; Yoo et al., 2013; Hardin et al., 2008). Here, we demonstrated clearly that ROS/RNS production from PM exposure was non-linear, highly dose-dependent, and could not be represented by a single concentration measurement. Furthermore, the specific dose-response region captured for each filter depended strongly on the dilution range used. A narrow dilution range could only capture the full response behavior for certain filters and may result in overestimates and underestimates for filters of lower and higher potency, respectively. Additionally, in this study, ROS/RNS production was reported as a fold increase over control cells to take into account variability between batches of cells (basal cellular ROS production). This normalization scheme was chosen to reduce uncertainty in ROS/RNS production, since signals were observed to increase with increasing response and were especially variable with positive controls.

Another common scheme used in prior studies involved obtaining a linear slope for macrophage ROS production over a few dilutions (Wang et al., 2013). However, as demonstrated in this study, the dose-response curve (Figure 2-2) is highly non-linear and the slope varies significantly depending on the dose range chosen. Furthermore, large-scale pharmacology studies showed that different dose-response metrics were correlated with different subsets of drugs, highlighting the importance of considering information from multiple dose-response metrics (Fallahi-Sichani et al., 2013). For comparison studies where a single measure was required, the same study demonstrated that AUC was robust whereas other metrics varied in informativeness depending on dose. Another study involving simulation and experimental results also demonstrated that AUC was the most robust metric in classifying and ranking drugs (Huang and Pang, 2012). Conversely, EC_{50} and Hill slope were found to be less reliable and more unstable due to their sensitivity to

dose range, especially in cases where either the base or maximum response are not observed (Beam and Motsinger-Reif, 2014). In the current study, all dose-response metrics were considered to avoid missing important information. Still, AUC was found to be the most robust metric in this study.

2.4.2 Comparison between MH-S and NRVM

To determine whether PM-induced ROS/RNS production varied between cell types that participate in the first line of defense (macrophages) and other active cells that would be exposed to pollution less directly (cardiomyocytes), all response parameters were compared for both cell types. AUC_{mass} was significantly correlated between the cell types ($R = 0.80$, $p < 0.05$) (Figure 2-5). Both macrophages, which participate in the immune response, and ventricular myocytes, which contract to pump blood, are active cells. Thus, the strong correlation suggests that the ROS/RNS response may be similar for different active cell types. However, the response is likely to be different for structural cells that are largely inactive and warrants future studies.

2.4.3 Associations between ROS/RNS production and oxidative potential

To determine whether chemical oxidative potential (i.e. DTT activity) is representative of cellular responses, all response parameters (AUC_{mass} , AUC_{volume} , threshold, Hill slope, EC_{50} , max response) were compared with DTT activity (Figure 2-3 and Figure A-4). Distinct seasonal trends were observed for correlations between AUC_{volume} and extrinsic DTT activity (Figure 2-3a). A strong, statistically significant correlation was observed for summer filters. Conversely, with the same sample variability as measured by root-mean-squared error (Table A-4), a relatively constant AUC_{volume} was

observed regardless of DTT activity for winter filters. Spring and autumn samples in the present study (Figure A-6) do not span the observed DTT range and the sample size is too small ($n = 10$ and 15 , respectively) to determine statistical significance, however, the majority of spring and autumn responses fall within summer and winter prediction intervals. This suggests that spring and autumn samples may exhibit overall trends that fall somewhere between summer and winter trends. AUC_{mass} was also significantly correlated with intrinsic DTT activity for summer samples (Figure 2-3b), however, no statistically significant correlation was observed for winter samples. The observed seasonal differences suggest that a simple correlation does not exist for oxidative potential as measured by DTT and cellular ROS/RNS responses and appear to be dependent on PM composition (section 4.4). However, due to its automation and high throughput, DTT may serve as a useful tool for screening samples for cellular analysis, as low DTT will most likely correspond to a low cellular response.

Other dose-response parameters were not significantly correlated with DTT activity. The lack of correlation with other parameters may be the result of large uncertainties associated with parameter determination for samples that did not attain a maximum response. Indeed, AUC was the most robust measurement with low associated uncertainties and did not require samples to attain maximum response. This is in agreement with other drug studies, where AUC was the most reliable measure for differentiating drug performance (Huang and Pang, 2012; Haibe-Kains et al., 2013). Collectively, these results suggest that DTT activity may not fully represent every aspect of the cellular ROS/RNS response, as each dose-response parameter serves as a different measure of toxicity. Since

DTT was significantly correlated with AUC for summer samples, DTT may be more indicative of the overall effect of PM, which AUC represents.

Although neither EC_{50} nor max response was correlated with DTT activity or composition, a significant positive correlation was found between these parameters for all filters investigated (Figure A-7). This is in contrast to the expected anti-correlation, where a more potent sample (lower EC_{50}) would induce more ROS/RNS production (higher max). Previous studies investigating anti-oxidant activities found a significant correlation between EC_{50} and anti-oxidant concentration (Zhang et al., 2006; Chiang et al., 2015). It is therefore possible that certain species in more potent samples are involved in anti-oxidant production pathways, resulting in neutralization of ROS/RNS species and thus a lower maximal ROS/RNS production. Alternatively, species may induce cellular protective pathways that prevent or reverse oxidative damage, thus reducing cellular damage and possibly enabling cells to produce more ROS/RNS. Studies with pro-inflammatory and anti-inflammatory molecules generally did not include correlations with Hill slope or threshold, however these parameters could potentially better capture other cellular pathways or simply include contributions from a combination of cellular events. Further studies are required to test these hypotheses.

2.4.4 PM constituents associated with AUC

To assess whether a good predictor exists for cellular ROS/RNS production, all cellular response parameters were compared with water-soluble PM constituents, mass fractions of constituents, and constituents grouped by sources (Table A-1 and Table A-2). Distinct seasonal patterns for AUC_{volume} correlations with composition were observed for

WSOC, a surrogate of secondary organic aerosol (SOA), BrC, and to a lesser extent Ti and Fe (Figure 2-4), where a statistically significant correlation with AUC_{volume} was found for summer samples and a relatively flat AUC_{volume} was found for winter samples.

The observed seasonal variability could potentially be explained by chemical composition, as PM collected during different seasons at the sampling sites differ in mass concentration and chemical composition (Fang et al., 2015a; Verma et al., 2014; Verma et al., 2015a; Xu et al., 2015a; Xu et al., 2015b). Similarly, seasonal variability has been observed for sources of organic species. Using positive matrix factorization (PMF) analysis of high-resolution aerosol mass spectrometry (HR-ToF-AMS) data, Xu et al. (2015b) showed that organic aerosol at these sites are dominated by SOA, which can be further deconvolved into different subtypes. With more intense photochemistry in summer, the correlation between AUC_{volume} and WSOC for summer samples may reflect contributions from photochemical SOA and/or aged SOA (Xu et al., 2015b). There may also be significant contributions from less-oxidized and more-oxidized oxygenated organic aerosol (LO-OOA and MO-OOA, respectively), which are present at higher concentrations in summer due to stronger photooxidation and emissions of biogenic volatile organic compounds (Xu et al., 2015b). This further highlights the importance of understanding the contribution of SOA to PM-induced health effects, especially those arising from photochemical oxidation reaction pathways.

Similarly, seasonal variability observed for AUC_{volume} vs. BrC may be the result of different sources of BrC inducing different cellular pathways. Although biomass burning is the predominant source of BrC, especially in winter, BrC may also have non-negligible contributions from aged SOA (Hecobian et al., 2010). Furthermore, while BrC was

observed in both summer and winter during the filter collection period (Verma et al., 2014), biomass burning organic aerosol (BBOA) was not resolved from PMF analysis of HR-ToF-AMS data in summer, suggesting an unknown source of BrC other than biomass burning (Xu et al., 2015b). The cellular ROS/RNS assay may only be sensitive to BrC from the unknown source, rather than BBOA. This is further supported by the low AUCs observed for winter samples even though BBOA was previously found to be highly redox active compared to ambient PM and other sources of organic aerosol (Verma et al., 2015a). Additionally, it is possible that some BrC species may not pass through the cell membrane or that transport through the membrane may be hindered once a certain intracellular concentration is attained, resulting in a consistent response regardless of concentration. This may be especially true for humic-like substances, a source of BrC from biomass burning that includes large molecular weight hydrophobic compounds (Sullivan and Weber, 2006). Transport of large compounds across the cellular membrane could be impeded, which may result in lack of increased response. While size-dependent impedance on cellular transport has been observed for macromolecules (Matsukawa et al., 1997) and nanoparticles (Sheng-Hann et al., 2010), further studies may be needed to establish this for atmospheric aerosol.

Among the metal species, only Fe and Ti were significantly correlated with AUC_{volume} for summer filters. Both are transition metals with positive oxidation states that have been correlated with DTT activity, a measure of the concentration of redox active species, and shown to participate in reactions that generate ROS/RNS (Verma et al., 2009; Fang et al., 2015a; Charrier and Anastasio, 2012; Halliwell and Gutteridge, 1984; Saffari et al., 2013). Furthermore, Fe (II) may produce ROS/RNS via Fenton-like reactions (Sutton

and Winterbourn, 1989), while Ti (IV) may interfere with protein structure by interacting with cysteines or forming other proteins complexes (Tinoco and Valentine, 2005; Conroy and Park, 1968). Titanium dioxide (TiO₂) is also known to induce pulmonary inflammation (Bermudez et al., 2004). No other response parameter was correlated with any metals, and no spatial trends were observed for any species. This is in contrast with previous ROS studies using filter samples collected in California where correlations with Fe, Cu, Cr, Pb, Mn, Zn, As, Ni, and V were observed (Saffari et al., 2014a; Daher et al., 2014; Wang et al., 2013; Hu et al., 2008). However, this is not surprising as previous studies used different metrics (e.g. measurement at single PM dose, linear slope from few PM doses, etc.) to represent ROS production. While Hill slope is similar to the linear slope method used in some of these studies, we found this metric to be strongly influenced by dose range and previous pharmacology studies also found this metric less reliable (Beam and Motsinger-Reif, 2014). Still, correlations between DTT activity and K, Mn, Fe, Cu and Zn were also previously reported in SCAPE studies (Verma et al., 2014). The lack of correlation with other metals, however, does not reflect a lack of response in the present study. Exposure to pure metal salt solutions at concentrations observed in ambient filters induced dose-dependent ROS/RNS production (Figure A-8). These results demonstrate that complex interactions may occur such that a simple sum of individual effects cannot recapitulate observed response. For example, while metals induce ROS/RNS production, complex interactions between species may hinder metal-cell interactions or individual organic species may have a greater contribution that masks metal contributions. Verma et al. (2012) previously showed that certain metals (V, Zn, and Fe) were retained on a C-18 column, which largely removes hydrophobic compounds. This supports the hypothesis that certain

metals may be involved in metal-organic complexes, which may be too large to freely diffuse across the cell membrane and interact with cellular components that promote ROS/RNS production.

Furthermore, the relative WSOC:metal ratio may mediate this effect, where a higher WSOC:metal ratio may exhibit more metal-cell hindrance due to enhanced metal-organic complex formation. In the present study, the WSOC:metal ratio averages from 18 – 23, whereas the ratio ranges from 0.98 – 3 for ambient samples from California (Hu et al., 2008; Daher et al., 2014; Saffari et al., 2014a). This substantial difference could explain the few correlations between cellular response and metal concentrations observed in the present study, where a significant portion of metals may be complexed with organics. However, while metal-organic complexes have been observed in aqueous solutions (Horcajada et al., 2010; Rue and Bruland, 1995), further studies are required to establish this for organics and metals present in PM extracts. Interactions with proteins in FBS, added to PM extracts to prevent cell starvation, may also be possible and could either promote or prevent species-cell interactions depending on whether the protein involved participates in cell interactions or not, respectively (Sarkar, 1989; Thierse et al., 2004). These interactions may be important considerations as proteins, sugars, and lipids are also present in the alveolar fluid, however, further studies are required to establish whether PM species participate in these interactions.

2.5 Implications

PM-induced intracellular reactive oxygen/nitrogen species (ROS/RNS) production from 104 filters collected from the greater Atlanta area was measured using an optimized

alveolar macrophage and ventricular myocyte cellular assay. Results from this study demonstrate that a wide dose range (instead of a single point) should be considered to accurately compare cellular responses between different PM samples. Furthermore, multiple dose-response metrics (i.e., max response, EC₅₀, Hill slope, threshold, AUC) should be examined as each metric may serve as a different measure of toxicity. Overall, AUC was found to be the most robust metric, as its informativeness did not depend on dose range.

Seasonal differences in the correlation between water-soluble DTT activity, a measure of the concentration of redox-active species in the sample, and intracellular ROS/RNS produced as a result of interactions between PM species and cells were also observed in this study, which may be largely driven by PM composition. Nevertheless, DTT may serve as a useful tool to screen samples for cellular analysis. It should be noted that only the water-soluble DTT activity and water-soluble PM components were considered in this study. Results may differ for total DTT activity, where water-insoluble components would also be present.

Thus far, most aerosol health studies have focused on the effects of primary pollutants, though ambient studies have repeatedly shown that SOA dominates ambient fine PM, even in urban centers (Zhang et al., 2007). In this study, the observed correlations between cellular ROS/RNS production and organic species (WSOC, BrC) in summer samples highlight the importance of understanding the contribution of organic aerosol, especially photochemically-driven summertime SOA, to PM-induced health effects. Furthermore, results from the current study also show that PM species cannot be treated as individuals in water-soluble PM extracts. While few water-soluble metals were correlated

with ROS/RNS response, exposure to individual metals induced measureable ROS/RNS production. These results suggest that complex interactions may occur between PM species, resulting in the involvement of multiple cellular pathways such that the overall cellular response cannot be approximated by a simple sum of the individual effects of components. Mixture effects may therefore be an important consideration in future studies. This study highlights the need to systematically investigate ROS/RNS production from different PM mixtures. In particular, generating well-characterized PM mixtures in laboratory experiments and measuring their cellular ROS/RNS response could provide fundamental data to interpret results from ambient mixtures.

CHAPTER 3: CHEMICAL OXIDATIVE POTENTIAL OF SECONDARY ORGANIC AEROSOL GENERATED FROM BIOGENIC AND ANTHROPOGENIC PRECURSORS

3.1 Background

Numerous epidemiological studies have found associations between elevated particulate matter (PM) concentrations and increased incidences of cardiopulmonary disease, including increases in lung cancer, asthma, chronic obstructive pulmonary disease, arrhythmia, and ischemic heart disease (Li et al., 2008; Pope III and Dockery, 2006; Brunekreef and Holgate, 2002; Dockery et al., 1993; Hoek et al., 2013; Anderson et al., 2011; Pope et al., 2002). Furthermore, ambient PM pollution ranked among the top 10 global risk factors in the 2010 Global Burden of Disease Study, with significant contributions from cardiopulmonary diseases and lower respiratory infections (Lim et al., 2012). Recent epidemiological studies have also found an association between particle oxidative potential and various cardiopulmonary health endpoints (Bates et al., 2015; Fang et al., 2016; Yang et al., 2016; Weichenthal et al., 2016), and results from toxicology studies suggest that PM-induced oxidant production, including reactive oxygen and nitrogen species (ROS/RNS), is a possible mechanism by which PM exposure results in adverse health effects (Li et al., 2003a; Tao et al., 2003; Castro and Freeman, 2001; Gurgueira et al., 2002). These species can initiate inflammatory cascades, which may ultimately lead to oxidative stress and cellular damage (Wiseman and Halliwell, 1996; Hensley et al., 2000). Prolonged stimulation of inflammatory cascades may also lead to chronic inflammation, for which there is a well-established link between chronic inflammation and cancer (Philip et al., 2004). Collectively, these findings suggest a

possible link between PM exposure and epidemiologically associated health endpoints as PM can contain ROS/RNS and generate ROS/RNS via redox reactions and by inducing cellular pathways that produce ROS/RNS.

Chemical assays in which an anti-oxidant is used to simulate redox reactions that would occur in biological systems have been developed to study the oxidative potential of PM samples (Kumagai et al., 2002; Cho et al., 2005). In these assays, redox-active species in PM samples catalyze electron transfer from the anti-oxidant (e.g., dithiothreitol, DTT; ascorbic acid, AA; etc.) to oxygen, and anti-oxidant decay provides a measure of the concentration of redox-active species in the sample (Fang et al., 2015c). These assays have been utilized extensively to characterize ambient PM samples and source apportionment regressions have been applied to DTT activity results to identify PM sources that may be detrimental to health (Bates et al., 2015; Fang et al., 2015a; Verma et al., 2015a; Verma et al., 2014). Results from these regressions, as well as inhalation and exposure studies, suggest that organic carbon constituents may play a significant role in PM-induced health effects (Li et al., 2003b; Kleinman et al., 2005; Hamad et al., 2015; Verma et al., 2015b). In particular, humic-like substances (HULIS) and oxygenated polycyclic aromatic hydrocarbons (PAH) have been shown to contribute significantly to the redox activity of water-soluble PM samples (Verma et al., 2012; Verma et al., 2015a; Dou et al., 2015; Verma et al., 2015b; Lin and Yu, 2011). Recently, Tuet et al. (2016) also showed that there is a significant correlation between intracellular ROS/RNS production and organic species (water-soluble organic carbon and brown carbon) for summer ambient samples, which suggests that photochemically-driven secondary organic aerosol (SOA) may be important in PM-induced oxidative stress.

Many prior studies have focused on the health effects of primary emissions, such as PM directly emitted from diesel and gasoline engines (Bai et al., 2001; Kumagai et al., 2002; McWhinney et al., 2013a; Turner et al., 2015). Conversely, few studies have explored the potential health implications of SOA, which are formed from the oxidation of volatile organic compounds (VOCs) (McWhinney et al., 2013b; Rattanavaraha et al., 2011; Kramer et al., 2016; Lund et al., 2013; McDonald et al., 2010; McDonald et al., 2012; Baltensperger et al., 2008; Arashiro et al., 2016; Platt et al., 2014), even though field studies have shown that SOA often dominate over primary aerosol even in urban environments (Zhang et al., 2007; Jimenez et al., 2009; Ng et al., 2010). The few studies that exist focus on SOA generated from a single class of hydrocarbon precursor or on SOA formed in a simulated urban background (Kramer et al., 2016; McWhinney et al., 2013b; Rattanavaraha et al., 2011; Arashiro et al., 2016; McDonald et al., 2012). While studies on oxidative potential have shown that SOA is indeed redox active, the combined range of oxidative potentials observed for individual SOA systems is quite large and remains unexplored (McWhinney et al., 2013b; Kramer et al., 2016). Furthermore, results from cellular exposure studies are inconclusive, with some studies finding significant response from SOA exposure and others finding little to no response. The exposure dose also differed from study to study, which may result in inconclusive results. This also highlights a need to consider dose-response relationships as demonstrated recently in Tuet et al. (2016). Comparisons between the observed cellular endpoints from exposure to SOA formed from individual precursors are also lacking (Baltensperger et al., 2008; Lund et al., 2013; McDonald et al., 2010; McDonald et al., 2012; Arashiro et al., 2016). As such, there is a lack of perspective in terms of different individual SOA systems and their contributions to

PM-induced health effects, making it unclear whether certain responses are indeed toxic for a range of sources and subtypes of PM. However, as cellular assays and animal inhalation experiments are more complex, a systematic study on the oxidative potential of individual SOA systems may be warranted first.

In the present study, the water-soluble oxidative potential of SOA generated from various precursors under different reaction conditions was measured using the DTT assay (henceforth referred to as OP^{WS-DTT}). While numerous cell-free assays have been developed to measure oxidative potential, the DTT assay is well-suited for the purposes of this study due to its proven sensitivity to organic carbon constituents and correlation with organic carbon (Janssen et al., 2014; Visentin et al., 2016). Furthermore, there are many previous studies reporting the DTT activities of laboratory-generated SOA and ambient samples for comparison purposes (Kramer et al., 2016; Bates et al., 2015; McWhinney et al., 2013a; McWhinney et al., 2013b; Verma et al., 2015a; Xu et al., 2015a; Xu et al., 2015b; Fang et al., 2015c; Lu et al., 2014). VOCs were chosen to represent the major classes of compounds known to produce SOA upon oxidation by atmospheric oxidants and to include precursors of both anthropogenic and biogenic origins (Table B-1). Biogenic precursors include isoprene, α -pinene, and β -caryophyllene, while anthropogenic precursors include pentadecane, *m*-xylene, and naphthalene. Isoprene was chosen as it is the most abundant non-methane hydrocarbon, with estimated global emissions around 500 Tg yr⁻¹ (Guenther et al., 2006). α -pinene and β -caryophyllene were chosen as representative, well-studied monoterpenes and sesquiterpenes, respectively. Both classes of compounds contribute significantly to ambient aerosol (Eddingsaas et al., 2012; Hoffmann et al., 1997; Tasoglou and Pandis, 2015; Goldstein and Galbally, 2007). α -pinene emissions (~50 Tg yr⁻¹) are also

on the same order of global anthropogenic emissions ($\sim 110 \text{ Tg yr}^{-1}$) (Guenther et al., 1993; Piccot et al., 1992). Similarly, anthropogenic precursors were chosen to include a long-chain alkane (pentadecane), a single-ring aromatic (*m*-xylene), and a poly-aromatic (naphthalene). These classes of compounds are emitted as products of incomplete combustion (Robinson et al., 2007; Jia and Batterman, 2010; Bruns et al., 2016) and have been shown to have considerable SOA yields (e.g., Chan et al., 2009; Ng et al., 2007b; Lambe et al., 2011). In addition to precursor identity, the effects of humidity (dry vs. humid) and NO_x (differing peroxy radical (RO_2) fates, $\text{RO}_2 + \text{HO}_2$ vs. $\text{RO}_2 + \text{NO}$) on $\text{OP}^{\text{WS-DTT}}$ were investigated, as these conditions have been shown to affect the chemical composition and mass loading of SOA formed (Chhabra et al., 2010; Chhabra et al., 2011; Eddingsaas et al., 2012; Ng et al., 2007b; Loza et al., 2014; Ng et al., 2007a; Chan et al., 2009; Boyd et al., 2015). Finally, intrinsic $\text{OP}^{\text{WS-DTT}}$ was compared with bulk aerosol composition, specifically elemental ratios, to investigate whether there is a link between $\text{OP}^{\text{WS-DTT}}$ and aerosol composition.

3.2 Methods

3.2.1 Chamber experiments

SOA from the photooxidation of biogenic and anthropogenic VOCs were generated in the Georgia Tech Environmental Chamber (GTEC) facility. Details of the facility are described elsewhere (Boyd et al., 2015). Briefly, the facility consists of two 12 m^3 Teflon chambers suspended inside a $6.4 \text{ m} \times 3.7 \text{ m}$ (21 ft x 12 ft) temperature-controlled enclosure, surrounded by black lights (Sylvania 24922) and natural sunlight fluorescent lamps (Sylvania 24477). Multiple sampling ports from each chamber allow for gas- and aerosol-

phase measurements, as well as introduction of reagents. Gas-phase measurements include O_3 , NO_2 , and NO_x concentrations as measured by an O_3 analyzer (Teledyne T400), a cavity attenuated phase shift (CAPS) NO_2 monitor (Aerodyne), and a chemiluminescence NO_x monitor (Teledyne 200EU) respectively. Additionally, a gas chromatography-flame ionization detector (GC-FID, Agilent 7890A) was used to monitor hydrocarbon decay and estimate hydroxyl radical ($OH\bullet$) concentration. In terms of aerosol-phase measurements, aerosol volume concentrations and distributions were measured using a Scanning Mobility Particle Sizer (SMPS, TSI), while bulk aerosol composition was determined using a High Resolution Time-of-Flight Aerosol Mass Spectrometer (HR-ToF-AMS, Aerodyne; henceforth referred to as the AMS) (DeCarlo et al., 2006). HR-ToF-AMS data was analyzed using the data analysis toolkit SQUIRREL (v. 1.57) and PIKA (v. 1.16G). Elemental ratios (O:C, H:C, and N:C) were obtained using the method outlined by Canagaratna et al. (2015), and used to calculate the average carbon oxidation state (\overline{OS}_c) (Kroll et al., 2011). Temperature and relative humidity (RH) were monitored using a hygrometer (Vaisala HMP110).

Experimental conditions, given in Table 3-1, were designed to probe the effects of humidity, RO_2 fate, and precursor hydrocarbon on OP^{WS-DTT} . All experiments were performed at $\sim 25^\circ C$ under dry ($RH < 5\%$) or humid ($RH \sim 45\%$) conditions. Prior to each experiment, the chambers were flushed with pure air for ~ 24 hrs. For humid experiments, the chambers were also humidified by means of a bubbler filled with deionized (DI) water during this time. Seed aerosol was then injected by atomizing a 15 mM $(NH_4)_2SO_4$ seed solution (Sigma Aldrich) until the seed concentration was approximately $20 \mu g m^{-3}$. It is noted that for experiment 7 (isoprene SOA under $RO_2 + HO_2$ dominant, “humid”

conditions), experimental conditions deviated due to extremely low SOA mass yields. For this experiment, an acidic seed solution (8 mM MgSO₄ and 16 mM H₂SO₄) was used under dry conditions to promote SOA formation via the IEPOX uptake pathway, which has a higher SOA mass yield compared to the IEPOX + OH pathway and contributes significantly to ambient OA (Surratt et al., 2010; Lin et al., 2012).

Table 3-1. Experimental conditions for chamber experiments.

Experiment	Compound	OH precursor	Relative humidity (%)	[HC] ₀ (ppb)	[SOA] ^c (μg m ⁻³)
1 ^a	isoprene	H ₂ O ₂	< 5%	97	5.73
2 ^a	α-pinene	H ₂ O ₂	< 5%	191	119
3 ^a	β-caryophyllene	H ₂ O ₂	< 5%	36	221
4 ^a	pentadecane	H ₂ O ₂	< 5%	106	9.71
5 ^a	<i>m</i> -xylene	H ₂ O ₂	< 5%	450	89.3
6 ^a	naphthalene	H ₂ O ₂	< 5%	178	128
7	isoprene	H ₂ O ₂	< 5% ^b	97	17.1
8	α-pinene	H ₂ O ₂	40%	334	154
9	β-caryophyllene	H ₂ O ₂	42%	63	230
10	pentadecane	H ₂ O ₂	45%	106	23.5
11	<i>m</i> -xylene	H ₂ O ₂	45%	450	13.9
12	naphthalene	H ₂ O ₂	44%	431	132
13	isoprene	HONO	< 5%	970	148
14	α-pinene	HONO	< 5%	174	166
15	β-caryophyllene	HONO	< 5%	21	80.8
16	pentadecane	HONO	< 5%	74	35.7
17	<i>m</i> -xylene	HONO	< 5%	431	153
18	naphthalene	HONO	< 5%	145	142

^a These experiments were repeated to establish reproducibility; ^b Acidic seed (8 mM MgSO₄ and 16 mM H₂SO₄) was used instead of 8 mM (NH₄)₂SO₄; ^c Average SOA concentration in the chamber during filter collection

Once the seed concentration stabilized, hydrocarbon was added by injecting a known volume of hydrocarbon solution [isoprene, 99%; α -pinene, $\geq 99\%$; β -caryophyllene, $> 98.5\%$; pentadecane, $\geq 99\%$; *m*-xylene, $\geq 99\%$; naphthalene, 99% (Sigma Aldrich)] into a glass bulb and passing zero air at 5 L min^{-1} over the solution until fully evaporated (~ 10 min). For pentadecane and β -caryophyllene, the glass bulb was gently heated to ensure full evaporation (Tasoglou and Pandis, 2015). Naphthalene was injected by passing pure air over the solid, as outlined in previous studies (Chan et al., 2009). After hydrocarbon injection, OH precursor was added to the chamber. Experiments were conducted under various NO_x conditions where different RO_2 reaction pathways prevailed. For $\text{RO}_2 + \text{HO}_2$ experiments, hydrogen peroxide (H_2O_2) was used as the OH precursor. H_2O_2 (50% aqueous solution, Sigma Aldrich) was injected using the method described for hydrocarbon injection to achieve an H_2O_2 concentration of 3 ppm, which yielded OH concentrations on the order of $10^6 \text{ molec cm}^{-3}$. For $\text{RO}_2 + \text{NO}$ experiments, nitrous acid (HONO), was used as the OH precursor. HONO was prepared by adding 10 mL of 1% wt aqueous NaNO_2 (VWR International) dropwise into 20 mL of 10% wt H_2SO_4 (VWR International) in a glass bulb. Zero air was then passed over the solution to introduce HONO into the chamber (Chan et al., 2009; Kroll et al., 2005). Photolysis of HONO yielded OH concentrations on the order of $10^7 \text{ molec cm}^{-3}$. NO and NO_2 were also formed as byproducts of HONO synthesis. Once all the H_2O_2 evaporated ($\text{RO}_2 + \text{HO}_2$ experiments) or NO_x concentrations stabilized ($\text{RO}_2 + \text{NO}$ experiments), the UV lights were turned on to initiate photooxidation.

3.2.2 Aerosol collection and extraction

Aerosol samples were collected onto 47 mm Teflon™ filters (0.45 µm pore size, Pall Laboratory) for approximately 1.5 hrs at a flow rate of 28 L min⁻¹. For each experiment, two filters (front filter and backing filter) were loaded in series to account for possible sampling artifacts (Conny and Slater, 2002). Total mass collected was determined by integrating the SMPS volume concentration as a function of time over the filter collection period and using the total volume of air collected. Volume concentrations were integrated using time-dependent data. Background filters containing seed and OH precursor (H₂O₂ or HONO) only at experimental conditions were also collected to account for potential H₂O₂ or HONO uptake, which may influence oxidative potential. Collected filter samples were placed in sterile petri dishes, sealed with Parafilm M®, and stored at -20 °C until extraction and analysis (Fang et al., 2015c). Prior to determining OP^{WS-DTT}, collected particles were extracted in DI water by submerging the filter and sonicating for 1 hr using an Ultrasonic Cleanser (VWR International) (Fang et al., 2015a). Sonication steps were performed in 30 min intervals with water replacement after each interval to reduce bath temperature. After sonication, extracts were filtered using 0.45 µm PTFE syringe filters (Fisherbrand™) to remove insoluble material (Fang et al., 2015c). All filter samples were extracted within 1-2 days of collection and analyzed immediately following extraction.

3.2.3 Oxidative potential

The decay of DTT, a chemical species that reacts with redox-active species in a sample via electron transfer reactions, was used as a measure of oxidative potential (Cho et al., 2005; Kumagai et al., 2002). The intrinsic OP^{WS-DTT} of aerosol samples, as well as

method blanks and positive controls (9,10-phenanthraquinone), was determined using a semi-automated DTT system. Specifics of the high-throughput system are detailed in Fang et al. (2015c). Briefly, the method consisted of three main steps: (1) oxidation of DTT by redox-active species in the sample, (2) reaction of residual DTT with DTNB to form 2-nitro-5-mercaptobenzoic acid (TNB), repeated at specific time intervals, and (3) measurement of TNB to determine DTT consumption. After each time interval and between samples, the system was flushed with DI water.

3.3 Results and Discussion

3.3.1 Laboratory-generated aerosol

Over the course of each experiment, gas and aerosol composition was continuously monitored. A typical time series for NO, NO₂, gas-phase hydrocarbon concentration, and aerosol mass concentration is shown in Figure 3-1 for naphthalene photooxidation under RO₂ + NO dominant reaction conditions. Hydrocarbon decay was monitored using GC-FID, while initial gas-phase hydrocarbon concentrations were determined using the chamber volume and mass of hydrocarbon injected. Following irradiation, NO decreased due to reaction with RO₂ from hydrocarbon oxidations. Nevertheless, ozone formation was suppressed owing to the high NO concentration throughout the experiment. Aerosol growth is observed shortly after initiation of photooxidation (i.e., turning on the lights) due to the efficient photolysis of HONO, which produced a high OH concentration on the order of 10⁷ molec cm⁻³. Once HONO was completely consumed, no further decay in the parent hydrocarbon and growth in aerosol mass were observed.

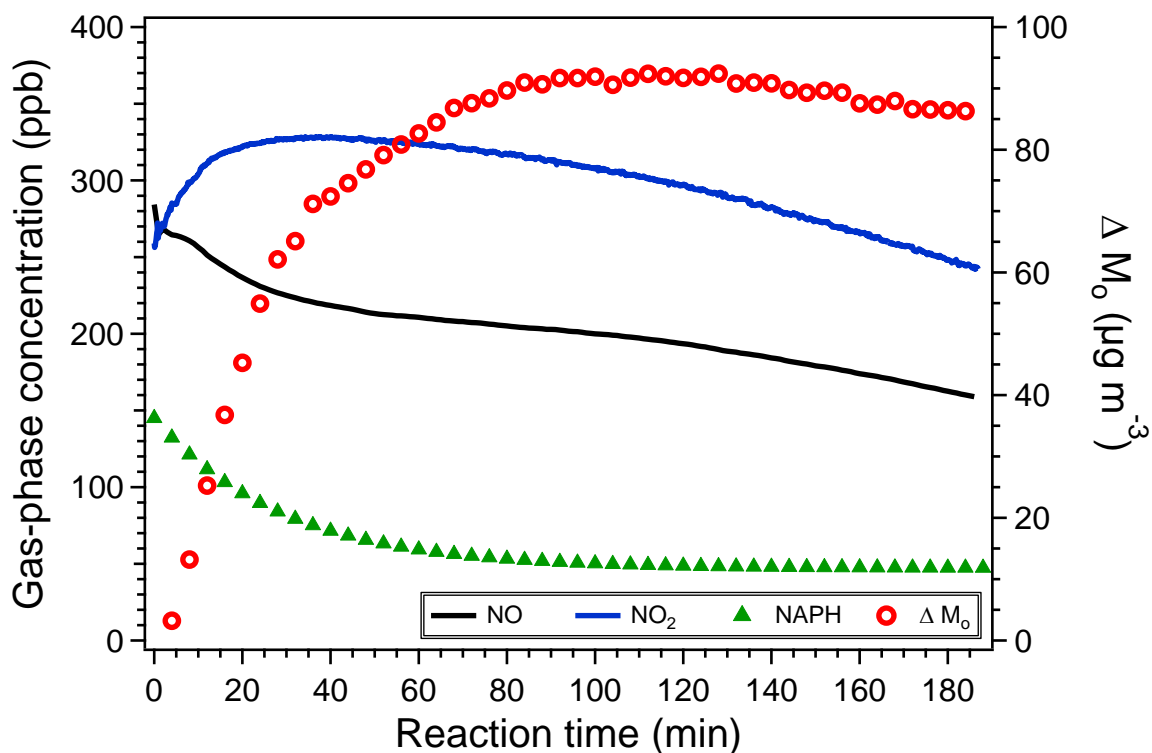


Figure 3-1. Typical reaction profile for a chamber experiment under RO₂ + NO dominant conditions. NO and NO₂ concentrations were monitored by CAPS NO₂ and chemiluminescence NO_x monitors, respectively. Hydrocarbon decay was monitored using GC-FID, while initial hydrocarbon (naphthalene) concentrations were determined using the chamber volume and mass of hydrocarbon injected. Aerosol mass concentrations were determined using volume concentrations obtained from SMPS and assuming an aerosol density of 1 g cm⁻³. While typical SOA density is about 1.4 g cm⁻³, it varies with hydrocarbon precursor identity and reaction conditions, and a density between ~1.0–1.6 g cm⁻³ has been reported in previous studies (Ng et al., 2007a; Ng et al., 2007b; Chan et al., 2009; Tasoglou and Pandis, 2015; Bahreini et al., 2005; Ng et al., 2006). The use of a density of 1 g cm⁻³ is to facilitate easier comparisons with past and future studies. Results from future studies can be scaled accordingly for comparison with the current work. Mass concentrations have been corrected for particle wall loss (Nah et al., 2017).

For each experiment, aerosol chemical composition was also monitored using the AMS. The average AMS mass spectra (Figure B-1) for all VOC systems were consistent with those reported in previous studies (Chhabra et al., 2010; Chhabra et al., 2011). For RO₂ + NO dominant experiments, the NO⁺:NO₂⁺ ratio has been used extensively in previous studies to differentiate between organic and inorganic nitrates (Farmer et al.,

2010; Fry et al., 2009; Boyd et al., 2015; Xu et al., 2015b). The observed $\text{NO}^+:\text{NO}_2^+$ ratio for all $\text{RO}_2 + \text{NO}$ dominant experiments (4.2 – 6.1) was higher than that observed for inorganic (ammonium) nitrates (~2.3), which indicates that these peaks are likely from organic nitrates rather than inorganic nitrates. The observed range is also consistent with values measured in previous organic nitrate studies for similar VOC systems and ambient studies (Bruns et al., 2010; Sato et al., 2010; Xu et al., 2015b). Elemental ratios (O:C, H:C, and N:C) were also obtained for each SOA system using the AMS. The aerosol systems investigated span a wide range of O:C ratios, as observed in previous laboratory and field studies (Chhabra et al., 2011; Lambe et al., 2011; Jimenez et al., 2009; Ng et al., 2010).

3.3.2 *Effect of SOA precursor and formation condition on oxidative potential*

To investigate whether different types of SOA differ in toxicity, the $\text{OP}^{\text{WS-DTT}}$, a measure of the concentration of redox-active species present in a sample, was measured for SOA generated from six VOCs under three conditions (see Table 3-1 for specifics). The blank-corrected $\text{OP}^{\text{WS-DTT}}$, represented on a per mass (μg) basis, are shown in Figure 3-2. Uncertainties associated with $\text{OP}^{\text{WS-DTT}}$ determination were approximated using a 15% coefficient of variation, in accordance with previous studies using the same semi-automated system (Fang et al., 2015c). The $\text{OP}^{\text{WS-DTT}}$ of all backing filters and background filters were also measured and found to be within the uncertainty for blank Teflon filters, which indicates that there were no observable sampling artifacts, gaseous absorption onto Teflon filters, or $\text{H}_2\text{O}_2/\text{HONO}$ uptake onto seed particles.

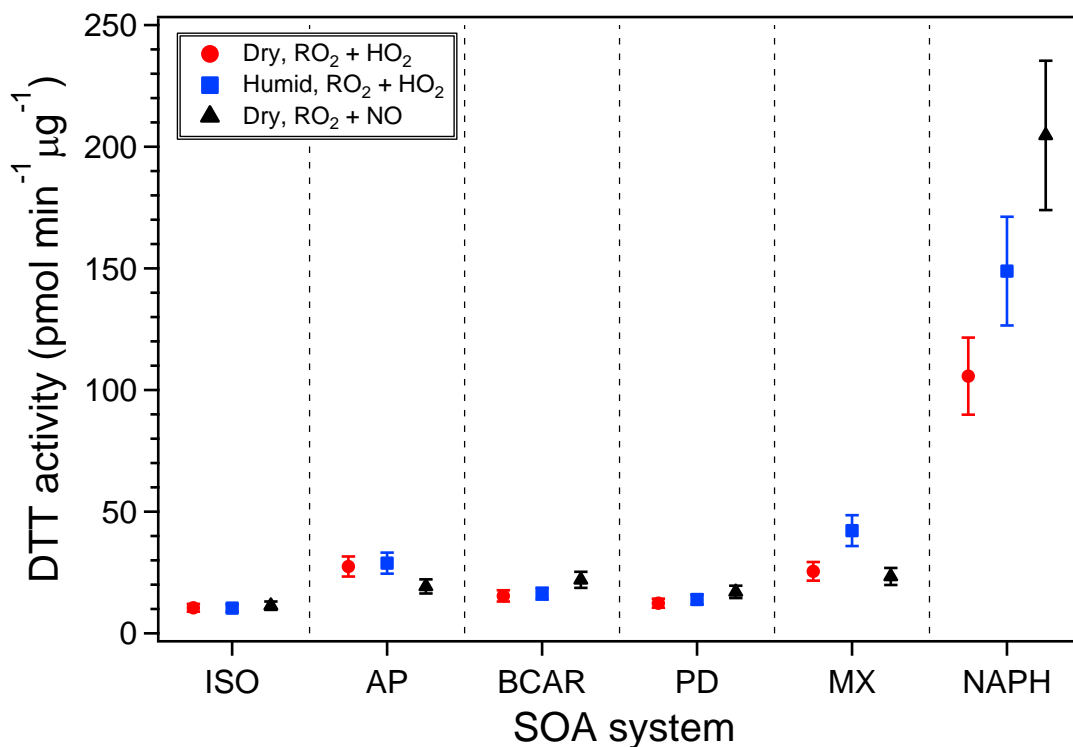


Figure 3-2. Intrinsic DTT activities for SOA generated from various hydrocarbon precursors (ISO: isoprene, AP: α -pinene, BCAR: β -caryophyllene, PD: pentadecane, MX: *m*-xylene, and NAPH: naphthalene) under various conditions (red circles: dry, RO₂ + HO₂; blue squares: humid, RO₂ + HO₂; and black triangles: dry, RO₂ + NO). Dry, RO₂ + HO₂ experiments were repeated to ensure reproducibility in SOA generation and collection. Error bars represent a 15% coefficient of variation (Fang et al., 2015c).

Overall, it is clear that the hydrocarbon precursor identity influenced OP^{WS-DTT}, with naphthalene having the highest intrinsic DTT activity (Figure 3-2). All other hydrocarbon precursors investigated produced SOA with relatively low intrinsic OP^{WS-DTT} (~9 – 45 pmol min⁻¹ μg⁻¹). For isoprene, the SOA in this study was generated through different reaction pathways, including isoprene photooxidation under different RO₂ fates and IEPOX reactive uptake to acidic seed particles. Although these different conditions produced different products and SOA compositions (Xu et al., 2014; Surratt et al., 2010; Chan et al., 2010), the OP^{WS-DTT} is very similar. It is important to note that the intrinsic

OP^{WS-DTT} for SOA generated under all conditions in this study are in agreement with the isoprene-derived OA factor resolved from positive matrix factorization (PMF) analysis of ambient AMS data (Xu et al., 2015a; Xu et al., 2015b; Verma et al., 2015a). The isoprene-derived OA from ambient measurements is largely attributed to IEPOX uptake, but possibly contains some contribution from other isoprene oxidation pathways (Xu et al., 2015a; Xu et al., 2015b). The similarity between laboratory-generated and ambient isoprene SOA suggests that isoprene SOA may have low OP^{WS-DTT} regardless of reaction conditions. A previous laboratory chamber study by Kramer et al. (2016) also measured the DTT activity of isoprene SOA produced via different pathways, including SOA formed from direct photooxidation of isoprene. It was found that isoprene SOA formed under “high- NO_x ” conditions was more DTT active than that formed under “low- NO_x ” conditions. These results are in contrast with those obtained in this study, where the OP^{WS-DTT} of isoprene SOA was similar regardless of reaction condition. However, we caution that 1) the SOA measured in Kramer et al. (2016) was formed under different experimental conditions, and 2) they utilized a different method for measuring DTT consumption (i.e., different extraction solvent, different initial DTT concentration, different method for quantifying DTT activity), therefore the results from their study and ours may not be directly comparable. For instance, for isoprene photooxidation experiments, the “low- NO_x ” conditions in Kramer et al. (2016) corresponded to “5 ppm isoprene and 200 ppb NO ”, where the reaction regime was largely defined by the VOC/ NO_x ratio. It has been shown previously that SOA formed under the same VOC/ NO_x conditions can be drastically different and the use of this metric might not necessarily reflect the actual peroxy radical fate (Ng et al., 2007b; Kroll and Seinfeld, 2008; Wennberg, 2013). In our study, the “low-

NO_x” experimental condition is defined by the fate of peroxy radicals directly, i.e., no NO_x added, but with the presence of H₂O₂ to enhance the RO₂ + HO₂ reaction pathway, which is dominant in ambient environments when NO_x levels are low.

α-pinene, β-caryophyllene, and pentadecane produced low OP^{WS-DTT} across all conditions explored in this study (Figure 3-2). Specifically, the SOA formed under different reaction conditions do not appear to have significantly different OP^{WS-DTT}, even though different NO_x conditions have been shown to affect SOA loading and composition due to competing RO₂ chemistry (Chan et al., 2009; Eddingsaas et al., 2012; Loza et al., 2014; Ng et al., 2007a). For instance, under conditions that favor RO₂ + NO, organic nitrates are formed, whereas under conditions that favor RO₂ + HO₂, organic peroxides are the predominant products. In this study, the formation of organic nitrates is evident in the RO₂ + NO experiments with the relatively higher NO⁺:NO₂⁺ ratio in the AMS mass spectra. It is possible that the organic peroxides and organic nitrates formed from the oxidation of these precursors are both not highly redox active, such that the overall OP^{WS-DTT} is similar even though the products differ. Further studies are required to establish this.

Similarly, the OP^{WS-DTT} of SOA formed from *m*-xylene under conditions that favor different RO₂ fates were not significantly different. Since OP^{WS-DTT} is intended as a measure of redox activity, the reaction products’ ability to participate in electron transfer may explain this lack of difference (e.g., lack of conjugated systems and associated pi bonds with unbound electrons). Under both RO₂ + HO₂ and RO₂ + NO pathways, a large portion of *m*-xylene oxidation products do not retain the aromatic ring (Vivanco and Santiago, 2010; Jenkin et al., 2003). Therefore, these products may have similar OP^{WS-DTT} as reaction products of α-pinene, β-caryophyllene, and pentadecane, which also do not

contain an aromatic ring. Under humid conditions, aerosol formed from the oxidation of *m*-xylene were more DTT active than those formed under dry conditions. The AMS mass spectra for aerosol formed under humid conditions also differs notably for several characteristic fragments (Figure B-2), which may explain the difference observed in OP^{WS-DDT} . More specifically, m/z 44, which serves as an indication of oxidation (O:C ratio) (Ng et al., 2010), is very different for this experiment (dry signal: 0.098 vs. humid signal: 0.15). It is possible that the degree of oxidation may be an important factor for SOA formed from the same hydrocarbon, and systematic chamber studies investigating changes in O:C for SOA formed from a single hydrocarbon precursor would be valuable. Previous studies involving the effect of humidity on SOA composition also yield mixed results, with some finding significant changes in SOA composition and yields (Nguyen et al., 2011; Wong et al., 2015; Healy et al., 2009; Stirnweis et al., 2016) and others reporting little difference (Boyd et al., 2015; Edney et al., 2000; Cocker III et al., 2001). Humidity effects are therefore highly hydrocarbon-dependent. Further study into the specific oxidation mechanisms and products in the photooxidation of aromatic hydrocarbon under dry and humid conditions may be warranted to understand the difference in DTT activity.

For naphthalene, the OP^{WS-DDT} measured for SOA generated under dry, $RO_2 + HO_2$ dominant conditions is in agreement with that measured by McWhinney et al. (2013b), which generated naphthalene SOA under similar chamber conditions using the same $OH\bullet$ radical precursor. These values should be directly comparable as the same standard method described by Cho et al. (2005) was used to obtain the oxidative potentials in both McWhinney et al. (2013b) and this study. The OP^{WS-DDT} of naphthalene aerosol also appears to be strongly influenced by humidity and RO_2 fate (Figure 3-2), with higher

toxicities observed for aerosol formed under both humid and $\text{RO}_2 + \text{NO}$ dominant conditions. The effect of RO_2 fate may be explained by the different products known to form from $\text{RO}_2 + \text{HO}_2$ and $\text{RO}_2 + \text{NO}$ reaction pathways. Many of the same products, including naphthoquinones and all of the ring-opening derivatives of 2-formylcinnamaldehyde, are formed under both reaction conditions (Kautzman et al., 2010). Naphthoquinones are also known to be DTT active and have been shown to account for approximately 21% of the DTT activity observed for naphthalene SOA (Charrier and Anastasio, 2012; McWhinney et al., 2013b). In addition to these products, nitroaromatics including nitronaphthols and nitronaphthalenes are formed under $\text{RO}_2 + \text{NO}$ conditions (Kautzman et al., 2010). The nitrite group next to the aromatic ring in these products may further promote electron transfer between nitroaromatics and DTT, resulting in more DTT consumption and a higher $\text{OP}^{\text{WS-DTT}}$. This effect was not observed for *m*-xylene SOA due to the formation of predominantly ring-opening products (Vivanco and Santiago, 2010; Jenkin et al., 2003). The presence of an aromatic ring in SOA products may therefore be important for determining oxidative potentials and polyaromatic precursors may yield products of substantial toxicity. This is further supported by the observation that the AMS mass spectra for highly DTT active naphthalene SOA contains peaks at m/z 77 and m/z 91, which are indicative of aromatic phenyl and benzyl ions (Chhabra et al., 2010; McLafferty and Tureček, 1993). Additionally, peaks indicative of aromatic compounds greater than m/z 120 were observed with similar mass spectral features as those reported for aerosol generated from naphthalene oxidation by OH^\bullet radicals in previous studies (Riva et al., 2015). Aromatic species are also exclusive to HULIS (Sannigrahi et al., 2006), and ambient

data have shown that HULIS is a significant aerosol component contributing to OP^{WS-DTT} (Verma et al., 2015b; Verma et al., 2012; Dou et al., 2015; Lin and Yu, 2011).

Bulk aerosol elemental ratios (O:C, H:C, and N:C) were also determined for each SOA system as different types of aerosol are known to span a wide range of O:C (Chhabra et al., 2011; Lambe et al., 2011). All elemental ratios were stable during the filter collection period and could thus be represented by a single value. To visualize these differences in oxidation, the van Krevelen diagram was utilized (Figure 3-3), as changes in the slope of data points within the van Krevelen space can provide information on SOA functionalization (Heald et al., 2010; Van Krevelen, 1950; Ng et al., 2011). Starting from the precursor hydrocarbon, a slope of 0 indicates addition of alcohol groups, a slope of -1 indicates addition of carbonyl and alcohol groups on separate carbons or addition of carboxylic acids, and a slope of -2 indicates addition of ketones or aldehydes. Previous studies show that both laboratory-generated and ambient OA occupy a narrow van Krevelen space with a slope of ~ -1 – -0.5 (Heald et al., 2010; Ng et al., 2011). Ambient data included in Figure 3-3 are for different organic aerosol subtypes resolved from PMF analysis of AMS data collected in the southeastern U.S. (Verma et al., 2015a; Xu et al., 2015a; Xu et al., 2015b).

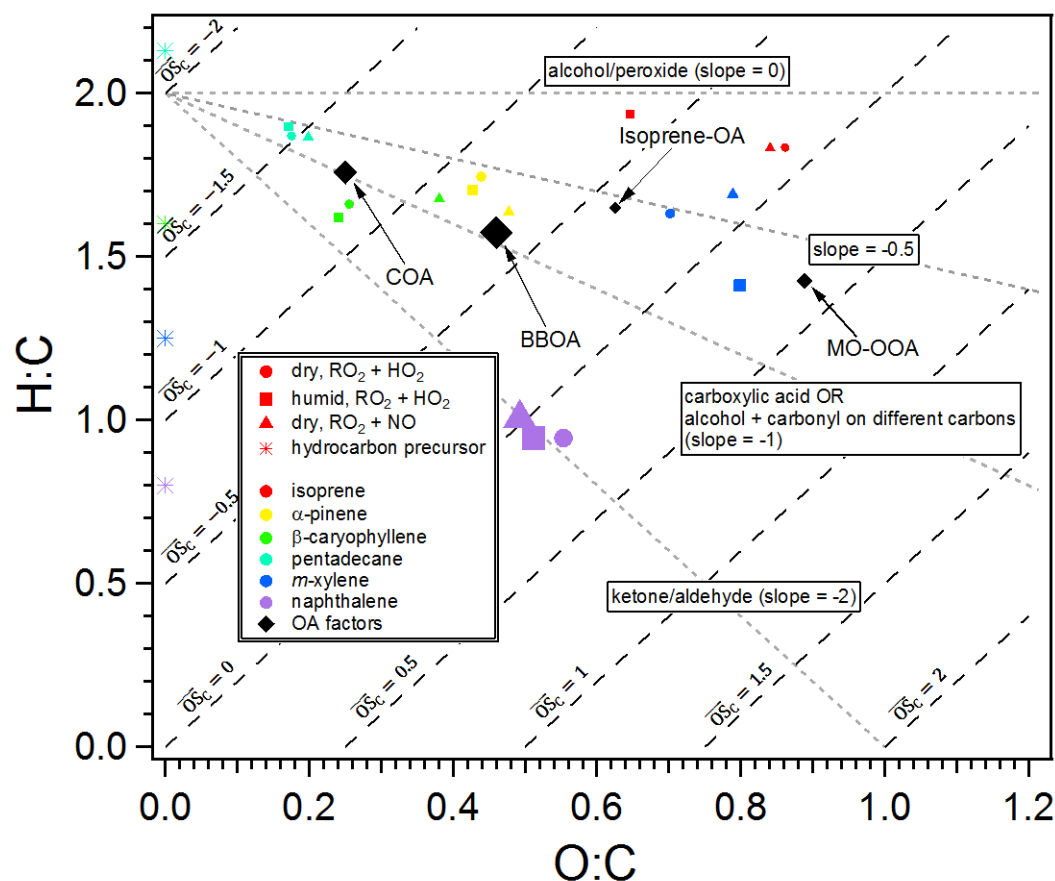


Figure 3-3. van Krevelen plot for various SOA systems. Data points are colored by SOA system (red: isoprene, yellow: α -pinene, green: β -caryophyllene, light blue: pentadecane, blue: *m*-xylene, and purple: naphthalene), shaped according to reaction conditions (circle: dry, RO₂ + HO₂; square: humid, RO₂ + HO₂; and triangle: dry, RO₂ + NO), and sized by intrinsic DTT activity. OA factors resolved from PMF analysis of ambient AMS data are shown as black markers, also sized by intrinsic DTT activity. Hydrocarbon precursors are shown as stars, colored by SOA system. Specifics on site locations and factor resolution methods are described elsewhere. COA: cooking OA, BBOA: biomass burning OA, Isoprene-OA: isoprene-derived OA, MO-OOA: more-oxidized oxygenated OA (Verma et al., 2015a; Xu et al., 2015a; Xu et al., 2015b).

The laboratory-generated aerosol span the range of H:C and O:C observed in the ambient. As seen in Figure 3-3 (data points sized by intrinsic OP^{WS-DTT}), while different reaction conditions produced aerosol of differing composition (i.e., different O:C and H:C), the intrinsic OP^{WS-DTT} does not appear to be affected by these differences. On the other

hand, the hydrocarbon precursor identity influences OP^{WS-DTT} substantially. It has been shown that ambient OA from different sources can become increasingly oxidized (increasing O:C ratio) with atmospheric aging (Jimenez et al., 2009; Ng et al., 2011). Based on the results shown in Figure 3-3, it appears that a higher O:C ratio did not correspond to a higher OP^{WS-DTT} . This is true for both the laboratory-generated SOA in this study and the different OA subtypes resolved from ambient data (Verma et al., 2015a; Xu et al., 2015a; Xu et al., 2015b). Nevertheless, the O:C ratios for individual systems (i.e. SOA formed from the same hydrocarbon precursor) may affect the intrinsic OP^{WS-DTT} . Indeed, for several SOA systems (β -caryophyllene, pentadecane, and *m*-xylene), SOA with higher O:C ratios also had a higher intrinsic OP^{WS-DTT} (Figure 3-2 and Figure 3-3). For SOA systems formed under $RO_2 + NO$ dominant conditions, N:C ratios were also determined to investigate if there is a link between N:C and intrinsic DTT activity (Figure B-3). Again, with the exception of naphthalene SOA, the intrinsic OP^{WS-DTT} does not appear to be affected by N:C ratio even though the systems explored span a wide range of N:C. This is consistent with that observed in the van Krevelen diagram and further emphasizes the importance of hydrocarbon identity in determining oxidative potentials.

3.3.3 Comparison to other types of PM

In order to evaluate how the oxidative potential of individual SOA systems compares to other sources and subtypes of PM, the intrinsic OP^{WS-DTT} from this study are compared to values reported in the literature (Figure 3-4). Comparatively, SOA formed from the photooxidation of isoprene, α -pinene, β -caryophyllene, pentadecane, and *m*-xylene were not very DTT active and produced low intrinsic OP^{WS-DTT} . The OP^{WS-DTT} of these aerosol systems were also within the range of various OA subtypes resolved from

ambient data. The method for determining intrinsic OP^{WS-DDT} for various OA subtypes is provided in Appendix B.

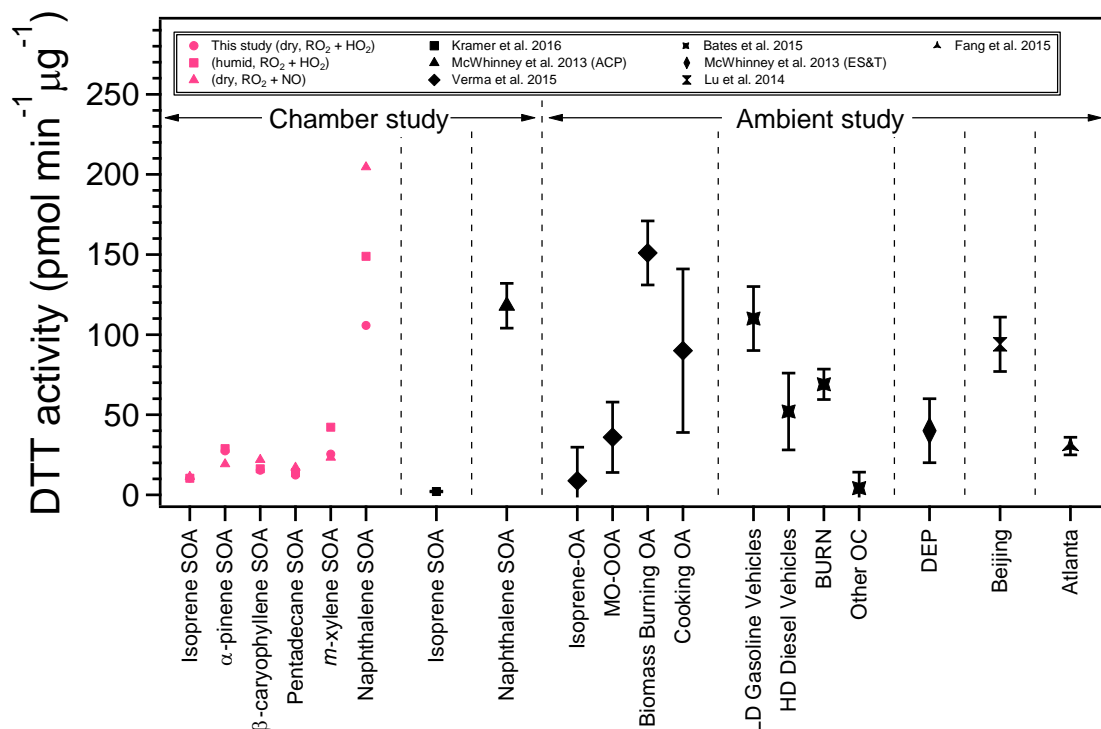


Figure 3-4. Intrinsic DTT activities for chamber SOA, various PM subtypes resolved from ambient data, and diesel exhaust particles. It should be noted that the DTT activity for isoprene SOA in Kramer et al. (2016) was determined using a different DTT method and may not be directly comparable. All other studies shown used the method outlined in Cho et al. (2005). DTT activities obtained in this study are shaped by reaction condition (circle: dry, RO₂ + HO₂; square: humid, RO₂ + HO₂; triangle: dry, RO₂ + NO). Specifics on site locations and factor resolution methods are described elsewhere. DTT activities for Beijing and Atlanta are averages obtained across multiple seasons. Isoprene-OA: isoprene-derived OA, MO-OOA: more-oxidized oxygenated OA, BBOA: biomass burning OA, COA: cooking OA, LDGV: light-duty gasoline vehicles, HDDV: heavy-duty diesel vehicles, BURN: biomass burning, DEP: diesel exhaust particles (Kramer et al., 2016; McWhinney et al., 2013b; Verma et al., 2015a; Bates et al., 2015; McWhinney et al., 2013a; Xu et al., 2015a; Xu et al., 2015b; Lu et al., 2014; Fang et al., 2015c).

As noted earlier, the OP^{WS-DDT} for isoprene SOA generated in this study is similar to the isoprene-derived OA factor from ambient data. The other ambient OA factors include a highly oxidized MO-OOA (more-oxidized oxygenated OA) factor resolved from PMF

analysis of ambient OA data, as well as an oxidized organic aerosol factor containing contributions from biogenic SOA (other OC) resolved using the chemical mass balance (CMB) method with ensemble-averaged source impact profiles (Bates et al., 2015; Xu et al., 2015a; Xu et al., 2015b; Verma et al., 2014). While sources of MO-OOA have not been identified, studies have shown that the aerosol mass spectra for various sources of OA approach that of MO-OOA as it ages (Ng et al., 2010) and it has been speculated that MO-OOA may contain aerosol from multiple aged sources (Xu et al., 2015b). Furthermore, MO-OOA has been shown to have widespread contributions across urban and rural sites, as well as different seasons (Xu et al., 2015a; Xu et al., 2015b). On the other hand, naphthalene SOA was highly DTT active with an OP^{WS-DTT} on the order of biomass burning OA [BBOA (Verma et al., 2015a), BURN (Bates et al., 2015)]. The BBOA and BURN factors were resolved using different source apportionment methods and as such, the range for comparison is large. Here, we focus on BBOA as Verma et al. (2015a) previously showed that BBOA had the highest intrinsic DTT activity among all OA subtypes resolved from PMF analysis of ambient AMS data collected in the southeastern U.S. (see Figure 3-4 for comparison). Because naphthalene aerosol formed under $RO_2 + NO$ dominant conditions may be even more redox active than BBOA and anthropogenic emissions are more abundant in urban environments with higher NO_x , this system warrants further systematic studies. It should however be noted that comparisons of intrinsic DTT activities between SOA from a pure VOC and an ambient source is difficult. BBOA is a source that contains many compounds, some of which may not be redox active. Thus, although it may contain highly DTT-active components with high intrinsic activities, the overall intrinsic activity will be much lower. As a result, a direct comparison with pure naphthalene SOA

on a per mass basis is tenuous. However, naphthalene SOA formed under urban conditions ($\text{RO}_2 + \text{NO}$) also produces nitroaromatics, which may induce DNA breaks and induce other mutagenic effects (Baird et al., 2005; Helmig et al., 1992). As such, aerosol formed from photooxidation of PAHs may be a particularly important OA source in terms of PM health effects.

Other common sources of PM are those related to traffic. Previous studies have determined that products of incomplete combustion include quinones capable of participating in redox reactions, including the oxidation of DTT (Kumagai et al., 2002; McWhinney et al., 2013a). The SOA systems investigated, including isoprene, α -pinene, β -caryophyllene, pentadecane, and *m*-xylene produced SOA that were less DTT active than diesel exhaust particles (DEP) collected from light-duty diesel vehicle (LDDV) engines operated under various conditions (McWhinney et al., 2013a) and resolved for heavy-duty diesel vehicles (HDDV) from ambient data (Bates et al., 2015). It should be noted that the DTT activity reported for DEP includes both water-soluble and water-insoluble fractions (total DTT activity), whereas the DTT activity measured for SOA is water-soluble. However, there should be very little contribution from water-insoluble species to SOA (McWhinney et al., 2013a). Conversely, the intrinsic $\text{OP}^{\text{WS-DTT}}$ of naphthalene SOA was on par with that of light-duty gasoline vehicles (LDGV) and higher than that of HDDV and DEP (Verma et al., 2014; Bates et al., 2015). Since naphthalene may also be emitted from gasoline and diesel combustion (Jia and Batterman, 2010), traffic-related controls may be extremely important to control these highly DTT active sources. Furthermore, since SOA often dominate over POA even in urban centers (Zhang et al., 2007; Ng et al., 2011), even

SOA that is only slightly DTT active may contribute significantly to PM-induced health effects.

3.4 Implications

The water-soluble oxidative potential, as measured by DTT consumption, was determined for SOA generated from six different hydrocarbon precursors under three conditions of varying humidity and RO₂ fate. Results from this study demonstrate that hydrocarbon precursor identity influenced intrinsic SOA oxidative potential substantially. The biogenic and anthropogenic precursors investigated yielded SOA with OP^{WS-DTT} ranging from 9 – 205 pmol min⁻¹ µg⁻¹, with isoprene SOA and naphthalene SOA having the lowest and highest intrinsic OP^{WS-DTT} respectively. In general, OP^{WS-DTT} for biogenic SOA were lower than those for anthropogenic SOA. Therefore, to evaluate overall oxidative potentials of ambient SOA, hydrocarbon precursor emissions and their corresponding SOA formation potential must be considered. Moreover, it may be possible to roughly estimate regional oxidative potentials using individual intrinsic OP^{WS-DTT} of different types of SOA in conjunction with VOC emissions and SOA loadings in models. For instance, DTT activities of aerosol collected in Beijing, China (77 – 111 pmol min⁻¹ µg⁻¹) (Lu et al., 2014), where anthropogenic emissions dominate, more closely resemble the OP^{WS-DTT} of naphthalene SOA, whereas ambient aerosol collected in the southeastern U.S. have DTT activities (25 – 36 pmol min⁻¹ µg⁻¹) (Fang et al., 2015c) that more closely resemble those of biogenic SOA. It may therefore be informative to investigate whether concentration addition can be applied to DTT consumption by exploring well-characterized PM mixtures.

Chamber reaction conditions, including relative humidity and specific RO₂ fate, influenced SOA elemental composition substantially and affected OP^{WS-DTT} in a hydrocarbon-specific manner, although hydrocarbon identity was by far the most influential in determining OP^{WS-DTT}. For several VOCs (isoprene, α -pinene, β -caryophyllene, and pentadecane), the reaction conditions had a negligible effect on OP^{WS-DTT}, which suggests that the organic peroxides and organic nitrates formed from the oxidation of these precursors may have similarly low redox activity. An investigation on the redox activity of individual known photooxidation products, including organic peroxides and organic nitrates, may elucidate further information on the lack of reaction condition effect. Similarly, nitroaromatics may explain the difference observed between naphthalene aerosol formed under different RO₂ reaction pathways as the nitrite group may promote electron transfer and result in a higher OP^{WS-DTT}. This effect was not observed for *m*-xylene SOA, due to the formation of predominantly ring-opening products. The loss of the aromatic ring may also explain the differences in intrinsic OP^{WS-DTT}. For instance, naphthalene SOA, which contains many aromatic ring-retaining products, is as redox active as BBOA, one of the most DTT active aerosol subtypes found in ambient studies. On the other hand, *m*-xylene SOA with predominantly aromatic ring-breaking products is much less redox active and the measured OP^{WS-DTT} is lower than that of traffic-related sources and several OA subtypes (BBOA and cooking OA, COA). This further supports earlier findings (Verma et al., 2015b) that the poly-aromatic ring structure may be an important consideration for understanding SOA redox activity, which may have implications for cellular redox imbalance (Tuet et al., 2016). Furthermore, nitroaromatics and polyaromatics may also have significant health effects beyond redox imbalance, including

various mutagenic effects (Baird et al., 2005; Helmig et al., 1992). As such, hydrocarbon precursors forming aromatic ring-retaining products may be the most important to consider in PM-induced health effects, in terms of oxidative potential. This is consistent with many studies using DTT to show oxidative potential associated with sources related to incomplete combustion (Bates et al., 2015; Verma et al., 2014; McWhinney et al., 2013b) and the identification of HULIS (Verma et al., 2015b; Dou et al., 2015; Lin and Yu, 2011), and more specifically, quinones as key components contributing to oxidative potential (Verma et al., 2014). Finally, redox-active metals are also emitted by traffic through mechanical processes, such as brake and tire wear (Charrier and Anastasio, 2012; Fang et al., 2015a). These species have not been considered in the chamber experiments explored in this study. Inclusion of redox-active metals in future SOA experiments may be valuable to further understand the roles of SOA and metal species in overall redox activity.

CHAPTER 4: INFLAMMATORY RESPONSES TO SECONDARY ORGANIC AEROSOL GENERATED FROM BIOGENIC AND ANTHROPOGENIC PRECURSORS

4.1 Background

Particulate matter (PM) exposure is a leading global risk factor for human health (Lim et al., 2012) with numerous studies reporting associations between elevated PM concentrations and increases in cardiopulmonary morbidity and mortality (Li et al., 2008; Pope III and Dockery, 2006; Brunekreef and Holgate, 2002; Dockery et al., 1993; Hoek et al., 2013; Anderson et al., 2011; Pope et al., 2002). A possible mechanism for PM-induced health effects has been suggested by toxicology studies, wherein PM-induced oxidant production, including reactive oxygen and nitrogen species (ROS/RNS), initiates inflammatory cascades thus resulting in oxidative stress and cellular damage (Li et al., 2003a; Tao et al., 2003; Castro and Freeman, 2001; Gurgueira et al., 2002; Wiseman and Halliwell, 1996; Hensley et al., 2000). Furthermore, prolonged stimulation of these inflammatory cascades may lead to chronic inflammation, for which there is a recognized link to cancer (Philip et al., 2004). Together, these findings suggest that a possible relationship exists between PM exposure and observed health effects.

Various assays have been developed to study PM-induced oxidant production, including cell-free chemical assays that measure the oxidative potential of PM samples (Kumagai et al., 2002; Cho et al., 2005; Fang et al., 2015c) as well as cellular assays that measure intracellular ROS/RNS produced as a result of PM exposure (Landreman et al., 2008; Tuet et al., 2016). Cell-free assays simulate biologically relevant redox reactions

using an antioxidant species (e.g. dithiothreitol, DTT; ascorbic acid, AA). The antioxidant is oxidized via electron transfer reactions catalyzed by redox-active species in the PM sample and its rate of decay serves as a measure of the concentration of redox-active species present (Fang et al., 2015c). On the other hand, cellular assays utilize a fluorescent probe (e.g. carboxy-H₂DCFDA) that reacts with ROS/RNS and the measured fluorescence is proportional to the concentration of ROS/RNS produced as a result of PM exposure (Landreman et al., 2008; Tuet et al., 2016). Both types of assays have been utilized extensively to characterize a variety of PM samples and identify sources that may be detrimental to health (Verma et al., 2015a; Saffari et al., 2015; Fang et al., 2015a; Bates et al., 2015; Li et al., 2003b; Tuet et al., 2016). In particular, numerous studies suggest that organic carbon constituents, especially humic-like substances (HULIS) and oxygenated polycyclic aromatic hydrocarbons (PAH), may contribute significantly to PM-induced oxidant production (Li et al., 2003b; Kleinman et al., 2005; Hamad et al., 2015; Verma et al., 2015b; Lin and Yu, 2011). Furthermore, recent measurements of ROS/RNS production and DTT activity using ambient samples collected in summer and winter around the greater Atlanta area showed that there is a significant correlation between summertime organic species and intracellular ROS/RNS production, suggesting a possible role for secondary organic aerosol (SOA) (Tuet et al., 2016). The same study also reported a significant correlation between ROS/RNS production and DTT activity for summer samples, while a relatively flat ROS/RNS response was observed for winter samples spanning a similar DTT activity range (Tuet et al., 2016). These results highlight a need to consider multiple endpoints as a simple correlation may not exist between different endpoints, especially cellular responses that may result from complicated response networks.

Despite these findings, there are still many gaps in knowledge regarding PM-induced health effects. The current work will focus on the relative toxicities of different SOA systems, as field studies have repeatedly shown that SOA often dominate over primary aerosol (e.g., PM emitted directly from combustion engines) even in urban environments (Zhang et al., 2007; Jimenez et al., 2009; Ng et al., 2010). Furthermore, in recent years, there have been an increasing number of studies on the health effects of SOA formed from the oxidation of emitted hydrocarbons, demonstrating their potential contribution to PM-induced health effects (McWhinney et al., 2013b; Rattanavaraha et al., 2011; Kramer et al., 2016; Lund et al., 2013; McDonald et al., 2010; McDonald et al., 2012; Baltensperger et al., 2008; Arashiro et al., 2016; Platt et al., 2014; Gallimore et al., 2017). However, the cellular exposure studies involving SOA focused on SOA formed from a single precursor and included different measures of response (e.g. ROS/RNS, inflammatory biomarkers, gene expression, etc.) (Arashiro et al., 2016; Lund et al., 2013; McDonald et al., 2010; McDonald et al., 2012; Baltensperger et al., 2008; Lin et al., 2017). As a result, there is a lack of understanding in terms of the relative toxicity of individual SOA systems. Recently, Tuet et al. (2017b) systematically investigated the DTT activities of SOA formed from different biogenic and anthropogenic precursors and demonstrated that intrinsic DTT activities were highly dependent on SOA precursor identity, with naphthalene SOA having the highest DTT activity. As a result, a systematic study on the cellular responses induced by these SOA systems may provide similar insights. Furthermore, cellular responses may complement these previously measured DTT activities to elucidate a more complete picture of the health effects of PM.

In the present study, alveolar macrophages were exposed to SOA generated under different formation conditions from various SOA precursors. Cellular responses induced by SOA exposure were measured, including intracellular ROS/RNS production and levels of tumor necrosis factor- α (TNF- α) and interleukin-6 (IL-6). Intracellular ROS/RNS production serves as a general indicator of oxidative stress, whereas TNF- α and IL-6 are pro-inflammatory cytokines indicative of the inflammatory response (Henkler et al., 2010; Kishimoto, 2003; Wang et al., 2003). TNF- α is a hallmark biomarker involved in triggering a number of cellular signaling cascades. More specifically, TNF- α is involved in the activation of NF κ B, which regulates the expression of a variety of genes involved in inflammation and cell death, and the activation of protein kinases, which regulate various signaling cascades (Witkamp and Monshouwer, 2000). IL-6 has both pro- and anti-inflammatory effects, and may directly inhibit TNF- α (Kamimura et al., 2004). Furthermore, both cytokines are produced at relatively high levels in MH-S cells, ensuring a high signal-to-noise ratio and thus reliable measurements (Matsunaga et al., 2001; Chen et al., 2007). Precursors were chosen to include major classes of biogenic and anthropogenic compounds known to produce SOA upon atmospheric oxidation (Table C-1). The selected biogenic precursors include: isoprene, the most abundant non-methane hydrocarbon (Guenther et al., 2006); α -pinene, a well-studied monoterpene with emissions on the order of global anthropogenic emissions (Guenther et al., 1993; Piccot et al., 1992); and β -caryophyllene, a representative sesquiterpene. Both monoterpenes and sesquiterpenes have been shown to contribute significantly to ambient aerosol (Eddingsaas et al., 2012; Hoffmann et al., 1997; Tasoglou and Pandis, 2015; Goldstein and Galbally, 2007). Similarly, the anthropogenic precursors include: pentadecane, a long-chain alkane;

m-xylene, a single-ring aromatic; and naphthalene, a poly-aromatic. These compounds are emitted as products of incomplete combustion (Robinson et al., 2007; Jia and Batterman, 2010; Bruns et al., 2016) and have considerable SOA yields (Chan et al., 2009; Ng et al., 2007b; Lambe et al., 2011). In addition to precursor identity, the effects of humidity (dry vs. humid) and NO_x levels (different predominant peroxy radical (RO₂) fates, RO₂ + HO₂ vs. RO₂ + NO) on SOA cellular inflammatory responses were investigated, as different formation conditions have been shown to affect aerosol chemical composition and mass loading, which could in turn result in a different cellular response (Chhabra et al., 2010; Chhabra et al., 2011; Eddingsaas et al., 2012; Ng et al., 2007b; Loza et al., 2014; Ng et al., 2007a; Chan et al., 2009; Boyd et al., 2015). Finally, correlations between bulk aerosol composition, specifically elemental ratios, and cellular inflammatory responses were investigated to determine whether there is a link between different inflammatory responses and aerosol composition.

4.2 Methods

4.2.1 Alveolar macrophage cell line

Exposures were conducted using immortalized murine alveolar macrophages (MH-S, ATCC[®]CRL-2019[™]) as they are the first line of defense against environmental insults (Oberdörster, 1993; Oberdörster et al., 1992). The particular cell line also retains many properties of primary alveolar macrophages, including phagocytosis as well as the production of ROS/RNS and cytokines (Sankaran and Herscowitz, 1995; Mbawuike and Herscowitz, 1989). MH-S cells were cultured in RPMI-1640 media supplemented with 10% fetal bovine serum (FBS, Quality Biological, Inc.), 1% penicillin-streptomycin, and

50 μM β -mercaptoethanol (BME) at 37°C and humid air containing 5% CO_2 . For exposure experiments, MH-S cells were seeded at a density of 2×10^4 cells well⁻¹ onto 96-well plates pre-treated with 10% FBS in phosphate buffered saline (PBS, Cellgro). For seeding and all assay procedures thereon, FBS-supplemented cell culture media without BME addition was used as BME is a reducing agent that may interfere with inflammatory measurements.

4.2.2 *Chamber experiments*

SOA formed from the photooxidation of biogenic and anthropogenic precursors were generated in the Georgia Tech Environmental Chamber (GTEC) facility. Details of the facility have been described elsewhere (Boyd et al., 2015). Briefly, the chamber facility consists of two 12 m³ Teflon chambers suspended within a 21 x 12 ft temperature-controlled enclosure. Black lights and natural sunlight fluorescent lamps surround the chambers, and multiple sampling ports allow for injection of reagents, as well as gas- and aerosol-phase measurements. Gas-phase O_3 , NO_2 , and NO_x concentrations were monitored using an O_3 analyzer (Teledyne T400), a cavity attenuated phase shift (CAPS) NO_2 monitor (Aerodyne), and a chemiluminescence NO_x monitor (Teledyne 200EU) respectively, while hydrocarbon decay was monitored using a gas chromatography-flame ionization detector (GC-FID, Agilent 7890A). Hydrocarbon decay was also used to estimate hydroxyl radical ($\text{OH}\cdot$) concentrations. For aerosol-phase measurements, a Scanning Mobility Particle Sizer (SMPS, TSI) was used to measure aerosol volume concentrations and distributions, while a High Resolution Time-of-Flight Aerosol Mass Spectrometer (HR-ToF-AMS, Aerodyne; henceforth referred to as the AMS) was used to determine bulk aerosol composition (DeCarlo et al., 2006). AMS data was analyzed using the data analysis toolkit SQUIRREL (v. 1.57) and PIKA (v. 1.16G). Elemental ratios, including O:C, H:C, and N:C, were

obtained using the method outlined by Canagaratna et al. (2015) and used to calculate the average carbon oxidation state ($\overline{\text{OS}}_c$) (Kroll et al., 2011). Temperature and relative humidity (RH) were also monitored using a hydro-thermometer (Vaisala HMP110).

Experiments were designed to probe the effects of humidity, RO_2 fate, and precursor identity on cellular inflammatory responses induced by different SOA formed under these conditions (Table 4-1). All chamber experiments were performed at $\sim 25^\circ\text{C}$ under dry ($\text{RH} < 5\%$) or humid ($\text{RH} \sim 45\%$) conditions. Chambers were flushed with pure air (generated from AADCO, 747-14) for ~ 24 hrs prior to each experiment. During this time, chambers were also humidified for humid experiments by means of a bubbler filled with deionized (DI) water. Seed aerosol was injected by atomizing a 15 mM $(\text{NH}_4)_2\text{SO}_4$ seed solution (Sigma Aldrich) to obtain a seed concentration of $\sim 20 \mu\text{g m}^{-3}$. It should be noted that experimental conditions deviate for experiment 7 (isoprene SOA under $\text{RO}_2 + \text{HO}_2$ dominant, “humid” conditions) due to low SOA mass yields. For this experiment, an acidic seed solution (8 mM MgSO_4 and 16 mM H_2SO_4) and a dry chamber were used to promote SOA formation via the isoprene epoxydiol (IEPOX) uptake pathway. This pathway has been shown to contribute significantly to ambient OA and has a higher SOA mass yield compared to the IEPOX + OH pathway (Surratt et al., 2010; Lin et al., 2012; Xu et al., 2015a).

Table 4-1. Experimental conditions for photooxidation SOA.

Experiment	SOA precursor	OH precursor	Relative humidity (%)	[HC] ₀ (ppb)
1	isoprene	H ₂ O ₂	<5%	97
2	α -pinene	H ₂ O ₂	<5%	191
3	β -caryophyllene	H ₂ O ₂	<5%	36
4	pentadecane	H ₂ O ₂	<5%	106
5	<i>m</i> -xylene	H ₂ O ₂	<5%	450
6	naphthalene	H ₂ O ₂	<5%	178
7	isoprene	H ₂ O ₂	<5% ^a	97
8	α -pinene	H ₂ O ₂	40%	334
9	β -caryophyllene	H ₂ O ₂	42%	63
10	pentadecane	H ₂ O ₂	45%	106
11	<i>m</i> -xylene	H ₂ O ₂	45%	450
12	naphthalene	H ₂ O ₂	44%	431
13	isoprene	HONO	<5%	970
14	α -pinene	HONO	<5%	174
15	β -caryophyllene	HONO	<5%	21
16	pentadecane	HONO	<5%	74
17	<i>m</i> -xylene	HONO	<5%	431
18	naphthalene	HONO	<5%	145

^a Acidic seed (8 mM MgSO₄ and 16 mM H₂SO₄) was used instead of 8 mM (NH₄)₂SO₄

SOA precursor was then introduced by injecting a known amount of hydrocarbon solution [isoprene, 99%; α -pinene, \geq 99%; β -caryophyllene, $>$ 98.5%; pentadecane, \geq 99%; *m*-xylene, \geq 99%; naphthalene, 99% (Sigma Aldrich)] into a glass injection bulb and passing pure air over the solution until it fully evaporated. For pentadecane and β -caryophyllene, the glass bulb was also heated gently during hydrocarbon injection to ensure full evaporation (Tasoglou and Pandis, 2015). Naphthalene was injected by passing pure

air over solid naphthalene flakes as described in previous studies (Chan et al., 2009). OH precursor was then introduced via injection of hydrogen peroxide (H_2O_2) for $\text{RO}_2 + \text{HO}_2$ experiments or nitrous acid (HONO) for $\text{RO}_2 + \text{NO}$ experiments. For H_2O_2 , a 50% aqueous solution (Sigma Aldrich) was injected using the same method described for hydrocarbon injection to achieve an H_2O_2 concentration of 3 ppm. This amount yielded OH concentrations on the order of $10^6 \text{ molec cm}^{-3}$. For HONO injections, HONO was first prepared by adding 10 mL of 1% wt aqueous NaNO_2 (VWR International) dropwise into 20 mL of 10% wt H_2SO_4 (VWR International) in a glass bulb. Zero air was then passed over the solution to introduce HONO into the chamber (Chan et al., 2009; Kroll et al., 2005). Photolysis of HONO yielded OH concentrations on the order of $10^7 \text{ molec cm}^{-3}$. NO and NO_2 were also formed as byproducts of HONO synthesis. Once all the H_2O_2 evaporated ($\text{RO}_2 + \text{HO}_2$ experiments) or NO_x concentrations stabilized ($\text{RO}_2 + \text{NO}$ experiments), the UV lights were turned on to initiate photooxidation.

4.2.3 Aerosol collection and extraction

Aerosol samples were collected onto 47 mm TeflonTM filters (0.45 μm pore size, Pall Laboratory). The total mass collected onto each filter was determined by integrating the SMPS time-dependent volume concentration over the filter collection period and multiplying by the total volume of air collected. SMPS volume concentrations were converted to mass concentrations by assuming a density of 1 g cm^{-3} to facilitate comparison between studies. To account for potential H_2O_2 or HONO uptake, background filters were also collected. These filters were collected when only seed particles and OH precursor (H_2O_2 or HONO) were injected into the chamber under otherwise identical experimental conditions. All collected samples were placed in sterile petri dishes, sealed with Parafilm

M[®], and stored at -20 °C until extraction and analysis (Fang et al., 2015c). Collected particles were extracted following the procedure outlined in Fang et al. (2015a) with modifications for cellular exposure. Briefly, filter samples were submerged in cell culture media (RPMI-1640) and sonicated for two 30 min intervals (1 hr total) using an Ultrasonic Cleanser (VWR International). In between sonication intervals, the water was replaced to reduce bath temperature. After the final sonication interval, sample extracts were filtered using 0.45 µm PTFE syringe filters (Fisherbrand™) to remove any insoluble material and supplemented with 10% FBS (Fang et al., 2015c).

4.2.4 Intracellular ROS/RNS measurement

ROS/RNS were detected using the assay optimized in Tuet et al. (2016). Briefly, the assay consists of five major steps: (1) pre-treatment of 96-well plates to ensure a uniform cell density, (2) seeding of cells onto pre-treated wells at 2×10^4 cells well⁻¹, (3) incubation with ROS/RNS probe (carboxy-H₂DCFDA, Molecular Probes C-400) diluted to a final concentration of 10 µM, (4) exposure of probe-treated cells to samples and controls for 24 hrs, and (5) detection of ROS/RNS using a microplate reader (BioTek Synergy H4, ex/em: 485/525 nm). Positive controls included bacterial cell wall component lipopolysaccharide (LPS, 1 µg mL⁻¹), H₂O₂ (100 µM), and reference filter extract (10 filter punches mL⁻¹, 1 per filter sample, from various ambient filters collected at the Georgia Tech site, while negative controls included blank filter extract (2 punches mL⁻¹) and control cells (probe-treated cells exposed to media only, no stimulants).

A previous study on the ROS/RNS produced induced by exposure to ambient PM samples found that ROS/RNS production was highly dose-dependent and could therefore

not be represented by measurements taken at a single dose (Tuet et al., 2016). Here, we utilize the dose-response curve approach described in Tuet et al. (2016). For each aerosol sample, ROS/RNS production was measured over ten dilutions and expressed as a fold increase in fluorescence over control cells. A representative dose-response curve is shown in Figure 4-1. For comparisons to other inflammatory endpoints and chemical composition, ROS/RNS production was represented using the area under the dose-response curve (AUC), as AUC has been shown to be the most robust metric for comparing PM samples (Tuet et al., 2016).

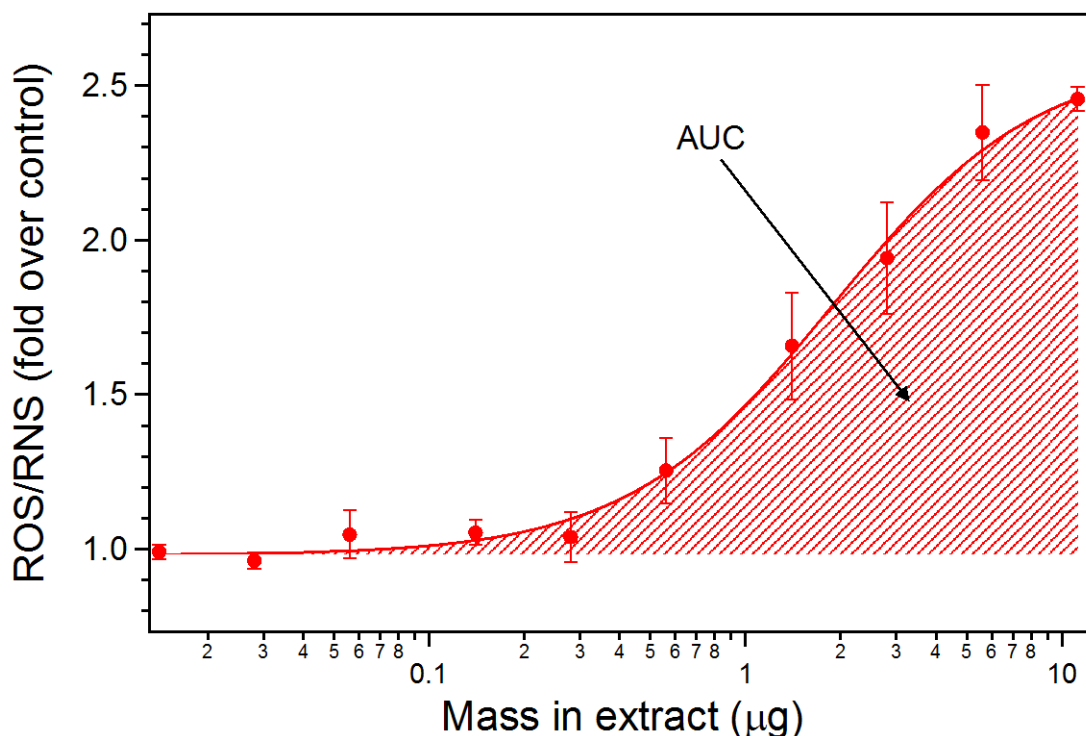


Figure 4-1. Representative dose-response curve of ROS/RNS produced as a result of filter exposure (naphthalene SOA formed under dry, RO₂ + NO dominant conditions). ROS/RNS is expressed as a fold increase over control cells, defined as probe-treated cells incubated with stimulant-free media. Dose is expressed as mass in extract (μg). Data shown are means ± standard error of triplicate exposure experiments. The Hill equation was used to fit the dose-response curve and the area under the dose-response curve (AUC) is shown.

4.2.5 Cytokine measurement

Secreted levels of TNF- α and IL-6 were measured post-exposure (24 hrs) using enzyme-linked immunosorbent assay (ELISA) kits following manufacturer's specifications (ThermoFisher). This time point was chosen to enable comparison with ROS/RNS levels (also measured at 24 hrs, optimized in Tuet et al. (2016)) and to ensure a high signal for both cytokines. Previous literature have shown that TNF- α and IL-6 production peak around 4 and 24 hrs, respectively (Haddad, 2001). However, while TNF- α production peaks earlier, the signal at 24 hrs is well above the detection limit of the assay, and previous studies have utilized this time point to measure both cytokines (Haddad, 2001; Matsunaga et al., 2001). Nonetheless, it should be noted that these measurements represent a single time point in the cellular response. All measurements were carried out using undiluted cell culture supernatant. For each aerosol sample, TNF- α and IL-6 were measured over seven dilutions and represented as a fold increase over control. Similarly, the AUC was used to represent each endpoint for comparison purposes.

4.2.6 Cellular metabolic activity

The MTT (3-(4,5-dimethylthiazol-2-yl)-2,5-diphenyltetrazolium bromide) assay (Biotium) was used to assess cellular metabolic activity. Briefly, supernatants containing sample extracts were removed after the exposure period and replaced with media containing MTT. Cells were then returned to the incubator for 4 hrs, during which the tetrazolium dye was reduced by cellular NAD(P)H-dependent oxidoreductases to produce an insoluble purple salt (formazan). Dimethyl sulfoxide was then used to solubilize the salt

and the absorbance at 570 nm was determined using a microplate reader (BioTek Synergy H4).

4.2.7 Statistical analysis

Linear regressions between bulk aerosol composition and cellular inflammatory responses were evaluated using Pearson's correlation coefficient, and the significance of each correlation coefficient was determined using multiple imputation, which calculated the total variance associated with the slope of each regression. Details of this method are described in Pan and Shimizu (2009). Briefly, response parameters (i.e. AUCs for each endpoint) were assumed to follow a normal distribution. Ten "estimates" were obtained for each response using the average and standard deviation determined from the dose-response curve fit. These estimates were then plotted against bulk aerosol composition (e.g. O:C, H:C, and N:C) to obtain ten fits, and the slopes and variances generated from these fits were used to calculate the between and within variance. Finally, a Student's *t*-test was used to calculate and evaluate the associated *p*-values using a 95% confidence interval.

4.3 Results and Discussion

4.3.1 Effect of SOA precursor and formation condition on inflammatory response

To investigate whether SOA formed from different precursors elicited different inflammatory responses, levels of ROS/RNS, TNF- α , and IL-6 were measured after exposing alveolar macrophages to SOA generated from six VOCs generated under three formation conditions (Table 4-1). The AUC per mass of SOA (μ g) in the extract for ROS/RNS, TNF- α and IL-6 are shown in Figure 4-2, shaped by SOA formation condition.

It should be noted that all responses were normalized to probe-treated control cells to account for differences between endogenous levels of ROS/RNS produced in cells (Henkler et al., 2010). Uncertainties associated with AUC were determined by averaging the AUCs obtained by fitting dose-response data with each point removed systematically, following the methodology described in Tuet et al. (2016). ROS/RNS production was also measured for background filters and found to be within the uncertainty of control cells, indicating that there was no evidence for significant H₂O₂ or HONO uptake onto seed particles (Figure C-1). Furthermore, exposure to filter extract did not result in decreases in metabolic activity as measured by the MTT assay for all SOA systems investigated (Figure C-2). Since results from MTT may represent the number of viable cells present, changes in inflammatory endpoints did not likely result from changes in the number of cells exposed (i.e. decreases in response cannot be attributed to cell death).

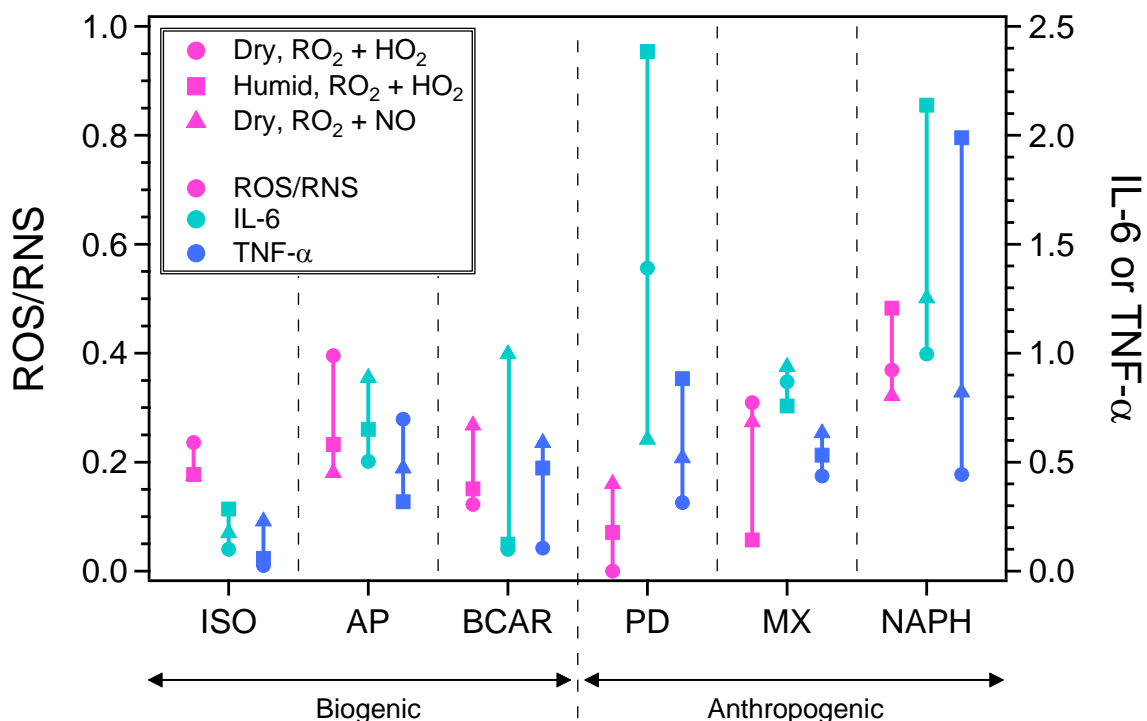


Figure 4-2. Area under the dose-response curve for various inflammatory responses induced as a result of SOA exposure: ROS/RNS, IL-6, and TNF- α . SOA were generated from various precursors (ISO: isoprene, AP: α -pinene, BCAR: β -caryophyllene, PD: pentadecane, MX: *m*-xylene, and NAPH: naphthalene) under various conditions (circles: dry, RO₂ + HO₂; squares: humid, RO₂ + HO₂; and triangles: dry, RO₂ + NO). Lines connecting the same inflammatory response for SOA generated from the same precursor under different formation conditions are also shown.

For all inflammatory responses measured (levels of ROS/RNS, TNF- α , and IL-6), SOA precursor identity and formation condition influenced the level of response, as demonstrated by the range of values obtained from different SOA precursors and different formation conditions (Figure 4-2). Despite having a clear effect, no obvious trends were observed for each variable (precursor or formation condition) on individual responses. This is in contrast to that observed for the oxidative potential as measured by DTT (OP^{WS-DTT}) for these samples, where only precursor identity influenced OP^{WS-DTT} substantially (Tuet et al., 2017b). However, this may not be surprising as DTT is a chemical assay, which only

accounts for the potential of species to participate in redox reactions (Cho et al., 2005), whereas cellular assays account for many complicated cellular events involved in intricate positive and negative feedback loops. Due to the considerably different classes of compounds chosen as SOA precursors, aerosol compositional changes between different precursors were generally larger than those between different formation conditions of the same precursor (see Figure 4-3a) (Tuet et al., 2017b). DTT may only be sensitive to larger differences arising from different precursors, whereas cellular assays could also be sensitive to differences between different formation conditions and chemical composition of the same precursor. Moreover, while Tuet et al. (2017b) showed that the intrinsic OP^{WS-DTT} spanned a wide range, with isoprene and naphthalene SOA generating the lowest and highest OP^{WS-DTT} , these bounds were less clear for cellular responses. While isoprene and naphthalene SOA still generated the lowest and highest inflammatory responses in general, a few exceptions exist (e.g. ROS/RNS levels induced by pentadecane SOA formed under dry, $RO_2 + HO_2$ dominant conditions, Figure 4-2).

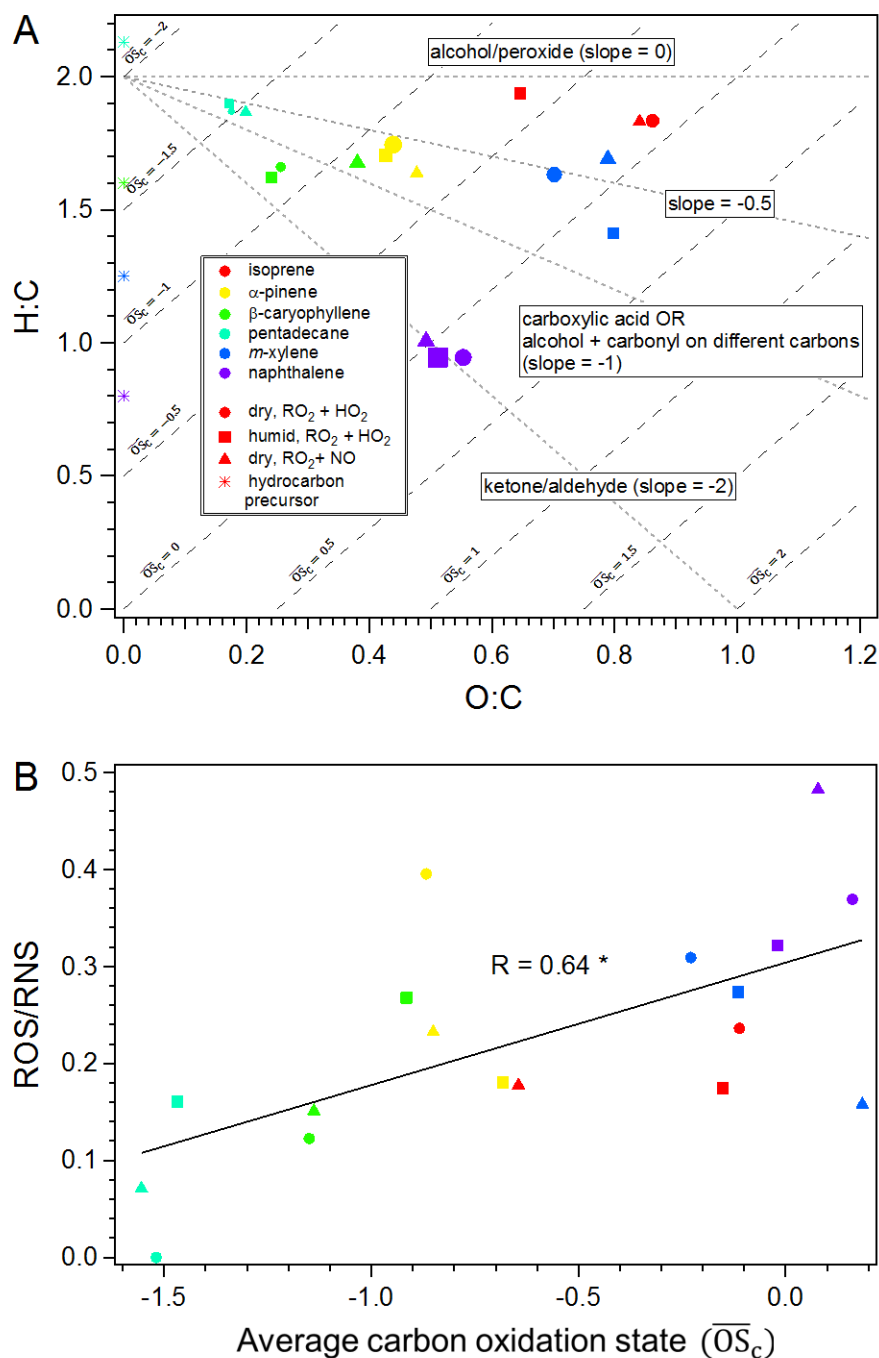


Figure 4-3. van Krevelen plot for various SOA systems sized by ROS/RNS levels (panel A) and correlation between ROS/RNS levels and average carbon oxidation state (panel B). Data points are colored by SOA system (red: isoprene, yellow: α -pinene, green: β -caryophyllene, light blue: pentadecane, blue: *m*-xylene, and purple: naphthalene), shaped according to formation conditions (circle: dry, $\text{RO}_2 + \text{HO}_2$; square: humid, $\text{RO}_2 + \text{HO}_2$; and triangle: dry, $\text{RO}_2 + \text{NO}$). SOA precursors are shown as stars, colored by SOA system. * indicates significance, $p < 0.05$.

Though no apparent trends in individual inflammatory responses were observed as a function of SOA precursor identity or formation condition, several patterns among all three inflammatory responses were observed for SOA precursors whose products share similar chemical structures (i.e., similar carbon chain length and functionalities). Exposure to isoprene SOA induced the lowest levels of TNF- α and IL-6 among the aerosol systems studied (Figure 4-2). Furthermore, isoprene SOA generated from different pathways (i.e. photooxidation under different RO₂ fates and reactive uptake of IEPOX) (Surratt et al., 2010; Xu et al., 2014; Chan et al., 2010) produced similar responses for each inflammatory endpoint. These results suggest that different isoprene SOA products (Surratt et al., 2010; Xu et al., 2014; Chan et al., 2010) may induce similarly low inflammatory responses and are consistent with the intrinsic OP^{WS-DTT} obtained for these SOA samples, where isoprene SOA generated the lowest OP^{WS-DTT} of all SOA systems studied and the OP^{WS-DTT} was similar for all SOA formation conditions explored (Tuet et al., 2017b). This finding is in contrast to a previous study by Lin et al. (2016), where methacrylic acid epoxide (MAE)-derived SOA was found to be substantially more potent than IEPOX-derived SOA. However, while exposure to MAE-derived SOA induced the upregulation of a larger number of oxidative stress response genes than IEPOX-derived SOA, the fold change of several genes reported in Lin et al. (2016) are actually similar (e.g., *ALOX12*, *NQO1*). Several of these genes directly affect the production of inflammatory cytokines measured in this study. For instance, studies have observed that arachidonate 12-lipoxygenase (*ALOX12*) products induce the production of both TNF- α and IL-6 in macrophages (Wen et al., 2007). As such, a similar response level regardless of SOA formation condition may be observed depending on the biological endpoints measured. Thus, it is possible that the

inflammatory cytokines measured in this study are involved in pathways concerning those genes, resulting in a similar response level regardless of SOA formation condition.

Similarly, exposure to SOA generated from the photooxidation of α -pinene and *m*-xylene resulted in similar inflammatory responses for all three formation conditions (Figure 4-2). These cellular assay results are consistent with results from the DTT assay where the OP^{WS-DTT} was not significantly different between SOA formed under different formation conditions (Tuet et al., 2017b). Response levels induced by these two SOA systems are also similar across all three inflammatory measurements investigated (Figure 4-2). This suggests that products from both precursors may induce similar cellular pathways resulting in the production of similar levels of inflammatory markers. Indeed, there are several similarities between products formed from the photooxidation of α -pinene and *m*-xylene. For instance, a large portion of α -pinene and *m*-xylene oxidation products under both $RO_2 + HO_2$ and $RO_2 + NO$ pathways are ring-breaking products with a similar carbon chain length (Eddingsaas et al., 2012; Vivanco and Santiago, 2010; Jenkin et al., 2003). As a result of this similarity, products from both SOA systems may interact with the same cellular targets and induce similar cellular pathways, resulting in a similar response regardless of precursor identity and formation condition. These observations further imply that the chemical structures (e.g., carbon chain lengths and functionalities) of oxidation products may be important regardless of PM source/precursor.

A different pattern was observed for β -caryophyllene and pentadecane SOA, where the IL-6 response spanned a much larger range than ROS/RNS and $TNF-\alpha$ (Figure 4-2). This is in contrast to the trends observed for the OP^{WS-DTT} for β -caryophyllene and pentadecane SOA, where OP^{WS-DTT} was similar regardless of formation condition (Tuet et

al., 2017b). This suggests that there are differences between organic peroxides and organic nitrates formed from certain precursors that influence cellular responses, but are not captured by redox potential measurements. Less is known about the effects of humidity on SOA formation and chemical composition for all SOA systems investigated, as most laboratory chamber studies in literature have been conducted under dry conditions. Specifically here, very high levels of IL-6 were observed post-exposure to pentadecane SOA formed under humid conditions. Prior studies reported opposing findings with some showing a significant effect of water on aerosol formation and chemical composition (Nguyen et al., 2011; Wong et al., 2015; Healy et al., 2009; Stirnweis et al., 2016), while others found little influence (Edney et al., 2000; Boyd et al., 2015; Cocker III et al., 2001). It is clear that humidity effects are highly hydrocarbon-dependent and further studies into the specific products formed under humid conditions are required to understand how these differences in chemical composition may translate to different cellular endpoints. Nonetheless, the known products formed from the photooxidation of these hydrocarbons may provide some insight into the inflammatory responses observed. While there are no prior studies involving pentadecane oxidation products, it is expected that the oxidation products will be similar to those reported in the oxidation of dodecane (i.e. same functionalities with a longer carbon chain) (Loza et al., 2014). It is therefore likely that pentadecane oxidation products resemble long chain fatty acids and could potentially insert into the cell membrane (Loza et al., 2014), as previous studies have shown that fatty acids can feasibly insert into the cell membrane bilayer (Khmelinskaia et al., 2014; Cerezo et al., 2011). This insertion could potentially affect membrane fluidity, which is known to affect cell function substantially although the specific effect depends strongly on the particular

modification and cell type of interest (Baritaki et al., 2007; Spector and Yorek, 1985). In some cases, these alterations lead to the induction of apoptosis, which involves pathways leading to the production of TNF- α (Baritaki et al., 2007; Wang et al., 2003). TNF- α can then induce the production of IL-6, which once produced can also inhibit the production of TNF- α in a feedback loop (Kishimoto, 2003; Wang et al., 2003). These cellular events are consistent with the observed inflammatory response induced by pentadecane SOA exposure, where there is a high IL-6 response and a lower TNF- α response. The low ROS/RNS response observed is also in line with these cellular events, as IL-6 exhibits anti-inflammatory functions, which can neutralize ROS/RNS production. These responses are less pronounced for β -caryophyllene aerosol, which may be due to the shorter carbon chain observed in known products (Chan et al., 2011). While β -caryophyllene and pentadecane are both C15 precursors, β -caryophyllene is a bicyclic compound and many SOA products retain the 4-membered ring, resulting in a shorter carbon backbone (Chan et al., 2011). As a result, fewer products may insert into the cell membrane, leading to a lesser response compared to pentadecane SOA exposure. These observations, particularly those for pentadecane SOA, suggest that aerosol from meat cooking may have health implications, as fatty acids comprise a majority of these aerosol (Mohr et al., 2009; Rogge et al., 1991).

Naphthalene exhibits a different, more distinct pattern compared to the rest of the SOA systems investigated, with a large range observed for both TNF- α and IL-6 under different formation conditions (Figure 4-2). Higher levels of ROS/RNS were also observed as a result of exposure to naphthalene aerosol irrespective of SOA formation condition. Similarly, the OP^{WS-DTT} of naphthalene SOA previously measured by Tuet et al. (2017b) was an outlier among all SOA systems investigated, as the measured OP^{WS-DTT} was at least

twice that of the next highest SOA system. These observations are consistent with the formation of specific SOA products such as naphthoquinones, which are known to induce redox-cycling in cells and are formed under both $\text{RO}_2 + \text{HO}_2$ and $\text{RO}_2 + \text{NO}$ pathways (Henkler et al., 2010; Kautzman et al., 2010). Consequently, aerosol generated from naphthalene may induce higher levels of inflammatory responses than other SOA due to this process (Henkler et al., 2010; Lorentzen et al., 1979). However, as shown by the high levels of IL-6, exposure to naphthalene SOA may also induce anti-inflammatory pathways not captured by $\text{OP}^{\text{WS- DTT}}$ measurements. Moreover, a clear increasing trend is apparent for $\text{TNF-}\alpha$ and IL-6 produced upon naphthalene SOA exposure, with a higher level of both cytokines observed for aerosol formed under $\text{RO}_2 + \text{NO}$ dominant and humid conditions. Previously, the effect of different RO_2 fates on SOA $\text{OP}^{\text{WS- DTT}}$ was attributed to the different products known to form under both pathways (Tuet et al., 2017b). The same explanation applies for cellular measurements as SOA products that promote electron transfer reactions with antioxidants can result in redox imbalance as measured by $\text{OP}^{\text{WS- DTT}}$ and the induction of related cellular pathways such as ROS/RNS and cytokine production (Tuet et al., 2017b). Finally, naphthalene SOA induced cellular responses outside of those observed for other aerosol systems, with higher levels of all inflammatory markers than other SOA systems. As shown previously for $\text{OP}^{\text{WS- DTT}}$, naphthalene may be an outlier due to aromatic ring-containing products, which may then induce different cellular pathways compared to other aerosol systems investigated, the products of which do not contain aromatic rings. Additionally, many known aerosol products formed from the photooxidation of naphthalene have functionalities that resemble those of dinitrophenol, which is known to decouple phosphorylation from electron transfer (Terada,

1990). It is therefore possible that the aromatic functionality present in the majority of naphthalene SOA products results in the involvement of very different cellular pathways, leading to outlier inflammatory endpoint responses. Various products of naphthalene oxidation such as nitroaromatics and polyaromatics are known to have mutagenic properties and may induce the formation of DNA adducts (Baird et al., 2005; Helmig et al., 1992). As such, it is possible that these products may induce health effects via other pathways as well and naphthalene SOA exposure may have effects beyond redox imbalance and oxidative stress.

Bulk aerosol elemental ratios (O:C, H:C, and N:C) were determined for each SOA system investigated. Different types of organic aerosol are known to span a wide range of O:C, which may be utilized as an indication of oxidation, and the van Krevelen diagram was used to visualize whether changes in O:C and H:C ratios corresponded to changes in levels of inflammatory response (Figure 4-3a and Figure C-3) (Chhabra et al., 2011; Lambe et al., 2011; Ng et al., 2010). Changes in the slope within the van Krevelen space provide information on SOA functionalization (Heald et al., 2010; Van Krevelen, 1950; Ng et al., 2011). Beginning from the precursor hydrocarbon, a slope of 0 indicates alcohol group additions, a slope of -1 indicates carbonyl and alcohol additions on separate carbons or carboxylic acid additions, and a slope of -2 indicates ketone or aldehyde additions.

As seen in Figure 4-3a, the laboratory-generated aerosol span a large range of O:C and H:C ratios. Both SOA formation condition and precursor identity influenced elemental ratios, however, precursor identity generally had a larger effect as evident by the clusters observed for different SOA precursors. Despite these differences in chemical composition, there were no obvious trends between O:C or H:C and any inflammatory endpoint

measured. This is similar to that observed for chemical oxidative potential as measured by DTT, where a higher O:C did not correspond to a higher oxidative potential for both laboratory-generated and ambient aerosol (Tuet et al., 2017b). This is likely due to the different formation conditions used to generate SOA, which may not be directly comparable. Nevertheless, a significant correlation ($p < 0.05$) was observed between ROS/RNS and \overline{OS}_c (Figure 4-3b). This positive correlation is not surprising, as a higher average oxidation state would likely correspond to a better oxidizing agent. Future studies should evaluate the effect of the degree of oxidation for SOA formed from the same SOA precursor under the same formation condition to investigate whether atmospheric aging of aerosol (which typically leads to increases in the degree of oxidation) affects inflammatory responses. Finally, the N:C ratio was also determined for SOA systems formed under conditions that favor the $RO_2 + NO$ pathway (Figure C-4) and were found to span a large range. Similarly, there was no obvious trend between N:C ratios and the inflammatory endpoints measured.

4.3.2 *Relationship between inflammatory responses*

To visualize whether there exists a relationship between inflammatory markers measured, levels of TNF- α and IL-6 are shown in Figure 4-4, sized by ROS/RNS. With the exception of naphthalene SOA, the inflammatory cytokine responses for all aerosol systems investigated follow an exponential curve (Figure 4-4, shown in black) where there appears to be a plateau for TNF- α levels. Along this curve, ROS/RNS levels also appear to increase with increasing inflammatory cytokine levels to a certain point, after which ROS/RNS levels decrease. These observations are in line with the interconnected effects of both cytokines. While both TNF- α and IL-6 have pro-inflammatory effects that may

lead to the increase of ROS/RNS production, the individual pathways are also involved in many complicated stimulation and inhibition loops and there is extensive cross-talk between both pathways. For instance, TNF- α induces the production of glucocorticoids, which in turn inhibits both TNF- α and IL-6 production (Wang et al., 2003). IL-6 also directly inhibits the production of TNF- α and other cytokines induced as a result of TNF- α (e.g. IL-1) and stimulates pathways that lead to the production of glucocorticoids (Kishimoto, 2003). As a result, increases in IL-6 may be accompanied by decreases in TNF- α , resulting in the observed plateau. Furthermore, ROS/RNS levels may represent a fine balance between anti-inflammatory and pro-inflammatory effects. Both cytokines are involved in the acute phase reaction and can affect ROS/RNS levels via pro-inflammatory pathways. IL-6 also exhibits some anti-inflammatory functions and may thus lower ROS/RNS levels as well. These interconnected pathways could account for the observed parabolic pattern for ROS/RNS production. Exposure to naphthalene SOA resulted in responses outside of those observed for other aerosol systems, likely due to the formation of aromatic ring-retaining products as discussed in the previous section.

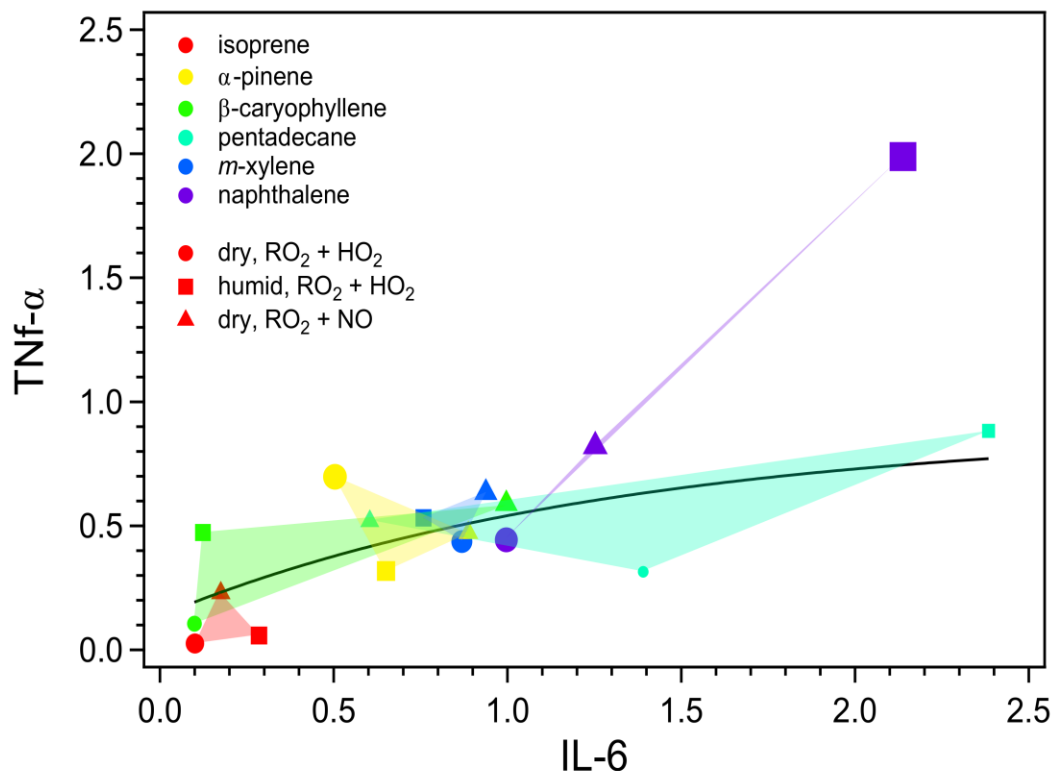


Figure 4-4. Area under the dose-response curve per mass of SOA for various inflammatory responses induced as a result of SOA exposure. Data points are sized according to ROS/RNS level. SOA were generated from various SOA precursors (red: isoprene, yellow: α -pinene, green: β -caryophyllene, light blue: pentadecane, blue: *m*-xylene, and purple: naphthalene) under various conditions (circles: dry, $\text{RO}_2 + \text{HO}_2$; squares: humid, $\text{RO}_2 + \text{HO}_2$; and triangles: dry, $\text{RO}_2 + \text{NO}$). A fitted curve excluding naphthalene data is shown as a guide. Shaded regions for each system, colored by SOA precursor, are also shown to show the extent of clustering and provide a visualization for the different patterns observed.

4.3.3 Comparison with ambient data

To evaluate how the oxidative potential and ROS/RNS production of the SOA systems investigated compare in the context of ambient samples, the measurements obtained in this study were plotted with those obtained in our previous study involving ambient samples collected around the greater Atlanta area (Figure 4-5) (Tuet et al., 2016). These ambient samples were analyzed using the same methods for determining oxidative

potential (DTT assay (Cho et al., 2005; Fang et al., 2015c)) and ROS/RNS production (cellular carboxy-H₂DCFDA assay (Tuet et al., 2016)). Furthermore, the same extraction protocol (water-soluble extract) was followed in both studies (Tuet et al., 2016). Results from both studies are therefore directly comparable. Previously, a significant correlation between ROS/RNS production and oxidative potential as measured by DTT was observed for summer ambient samples. In the same study, correlations between ROS/RNS production and organic species were also observed for summer ambient samples, and it was suggested that these correlations may reflect contributions from photochemically produced SOA (Tuet et al., 2016).

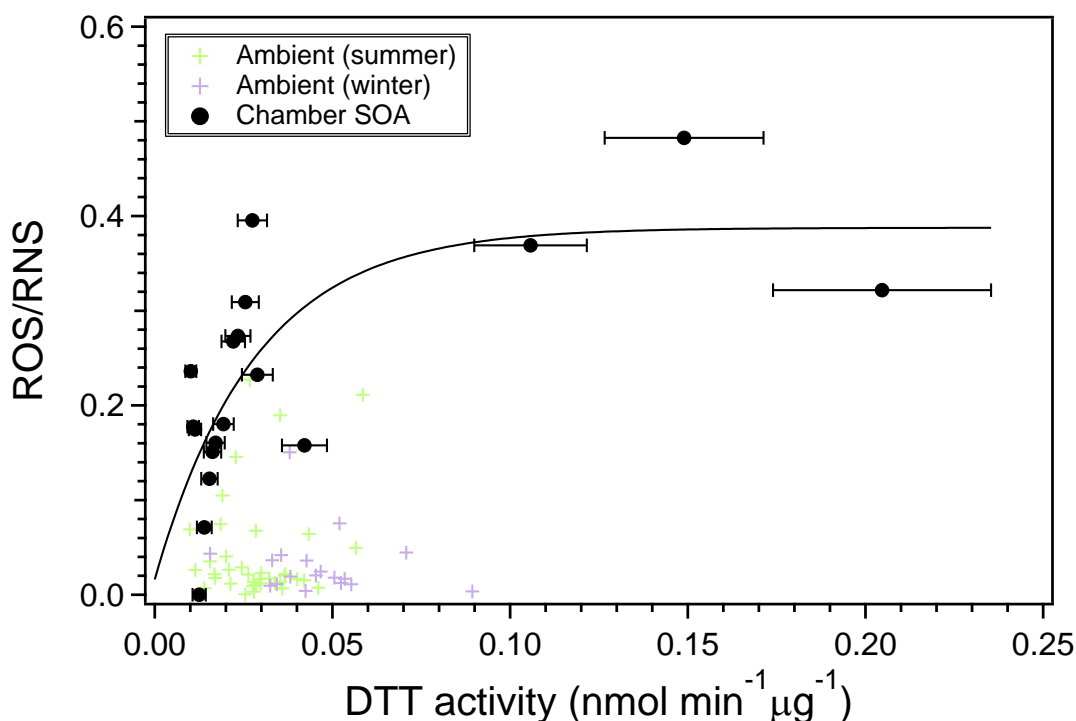


Figure 4-5. ROS/RNS production and intrinsic DTT activities for chamber SOA and ambient samples collected around the greater Atlanta area. All samples were analyzed using the method outlined in Cho et al. (2005) and Tuet et al. (2016). Ambient samples are colored by season as determined by solstice and equinox dates between June 2012 and October 2013 (Tuet et al., 2016). A fitted curve for laboratory-generated samples is shown as a guide.

Figure 4-5 shows that laboratory-generated SOA oxidative potential is comparable to that observed in ambient samples, with the exception of naphthalene SOA, which produced higher DTT activities due to its aromatic ring retaining products (Tuet et al., 2017b; Kautzman et al., 2010). Laboratory-generated SOA also induced similar or higher levels of ROS/RNS compared to ambient samples. There are many possible explanations for the observed higher response for some SOA samples. For instance, individual, single precursor SOA systems were considered in this study, whereas ambient aerosol contains SOA from multiple precursors as well as other species that are not considered in this study (e.g. metals). Interactions between SOA from different precursors is likely to occur and may result in different response levels. Complex interactions between SOA and other species present in the ambient (e.g. metals or other organic species) are also likely involved (Tuet et al., 2016). Previous studies have also suggested the possibility of metal-organic complexes. For instance, Verma et al. (2012) showed that certain metals were retained on a C-18 column, which is utilized to remove hydrophobic components, suggesting that these metals were likely complexed and removed in the process. Further chamber studies involving photochemically generated SOA and metals may elucidate these interactions. Furthermore, there are likely species present in the ambient that do not contribute to ROS/RNS production. That is, while certain species contribute to the mass of PM, there is little to no ROS/RNS production associated with these species. Ambient samples where these species comprise a significant fraction will have a low per mass ROS/RNS production level. Finally, only three SOA formation conditions were investigated in this study. There are multiple other possible oxidation mechanisms that lead to the formation of SOA in the ambient, which were not accounted for in this study. Nonetheless, despite the low

ROS/RNS levels observed post SOA exposure, there is an association between ROS/RNS production and DTT activity (Figure 4-5). These results suggest that our previous findings based on ambient filter samples may be extended to SOA samples. That is, while the relationship between ROS/RNS production and DTT activity is complex, DTT may serve as a useful screening tool as samples with low DTT activities are likely to produce low levels of ROS/RNS (Tuet et al., 2016).

4.4 Implications

Levels of ROS/RNS, TNF- α , and IL-6 were measured after exposing cells to the water-soluble extract of SOA generated from the photooxidation of six SOA precursors under various formation conditions. Although previous epidemiological and ambient studies have found correlations between metals and various measures of health effects (Verma et al., 2010; Pardo et al., 2015; Burnett et al., 2001; Huang et al., 2003; Akhtar et al., 2010; Charrier and Anastasio, 2012), the measured levels of TNF- α , IL-6, and ROS/RNS obtained in this study demonstrate that organic aerosol alone can induce a cellular response. This was previously observed for the oxidative potential as measured by DTT activity as well, where the same laboratory-generated organic aerosol samples catalyzed redox reactions and resulted in measureable DTT decay in the absence of metal species (Tuet et al., 2017b).

Results from this study also show that SOA precursor identity and formation condition influenced response levels, with naphthalene SOA producing the highest cellular responses of the SOA systems investigated. As discussed previously, the aromatic functionality present in many naphthalene photooxidation products may be an important

consideration for health effects. It may therefore be worthwhile to investigate other anthropogenic aromatic ring-containing precursors as well and to closely study the cellular effects of naphthalene SOA products given its high response. Several patterns were also noted for SOA systems whose products shared similar functionalities and chemical structures. For instance, photooxidation productions from pentadecane and β -caryophyllene share similarities with long chain fatty acids and may participate in membrane insertions, whereas many known products of naphthalene photooxidation are mutagens capable of inducing cellular pathways beyond those that affect cellular redox balance (Baird et al., 2005; Helmig et al., 1992). Given these observations, it may be possible to roughly predict responses based on known SOA products as SOA systems whose products share similar functionalities and carbon chain length are likely to induce similar cellular pathways and produce similar levels of various inflammatory endpoints. Exposure studies involving individual classes of SOA products may elucidate further details as to whether these types of predictions would be plausible. Moreover, such studies could be used to determine whether the hypothesized cellular pathways are indeed involved and whether certain cellular functions are indeed affected by specific products (e.g. membrane insertion by pentadecane photooxidation products and oxidative phosphorylation decoupling by naphthalene photooxidation products).

Mixture effects may be another important consideration as ambient PM contains SOA formed from multiple SOA precursors. As a result, precursor emissions and their corresponding SOA formation potential must be considered to fully assess PM health effects. Furthermore, it may be worthwhile to investigate various prediction models for multi-component mixtures to bridge the gap between laboratory studies and real ambient

exposures. For instance, concentration addition may not apply as ambient aerosol is formed in the presence of multiple precursors and the SOA produced may induce response levels completely different from those observed for single precursor SOA systems that comprise the mixture. Interactions between organic components and metal species have also been suggested in previous studies (Verma et al., 2012; Tuet et al., 2016) and may influence responses significantly. While these interactions were not considered in the current study, there may be evidence to support the plausibility of mixture effects as ambient PM samples produced lower levels of ROS/RNS than that of any single SOA system investigated. Laboratory chambers can serve as an ideal platform to investigate mixture effects, as experiments can be conducted under well-controlled conditions where the aerosol chemical composition and health endpoints can be determined.

Additionally, this study confirms that while there is not one simple correlation between oxidative potential and cellular responses for different PM samples, the DTT assay may serve as a useful screening tool as a low DTT activity will likely correspond to a low cellular response. Furthermore, while ROS/RNS may serve as a general indicator of oxidative stress, there may be instances where a low level of ROS/RNS does not necessary indicate a lack of cellular response. In the current study, ROS/RNS levels were associated with levels of inflammatory cytokines for the majority of SOA systems investigated. However, aerosol formed from the photooxidation of pentadecane induced low levels of ROS/RNS production and relatively high levels of both cytokines (i.e. higher than expected given the ROS/RNS level measured). These results suggest that at least one additional measure (e.g. inflammatory cytokines) may be required to fully interpret ROS/RNS measurements. Finally, several limitations must be considered before generalizing results

from this study to *in vivo* exposures. For instance, only one cell type was explored in this study, whereas an organism consists of multiple tissues comprised of multiple cell types. Interactions between different cell types and tissue systems were not considered in this study. Furthermore, the doses investigated may not fully represent real world exposures due to differences in exposure routes and potential recovery from doses due to clearance. Nevertheless, this study provides perspective on the relative toxicities of different SOA systems which future studies can build upon.

CHAPTER 5: OXIDANT PRODUCTION INDUCED BY NAPHTHALENE SECONDARY ORGANIC AEROSOL: EFFECT OF REDOX-ACTIVE METALS AND PHOTOCHEMICAL AGING

5.1 Background

Air pollution exposure ranks among the top ten global human health risks (Lim et al., 2012) with multiple epidemiological studies reporting associations between various cardiopulmonary health effects, elevated particulate matter (PM) concentrations (Li et al., 2008; Pope III and Dockery, 2006; Brunekreef and Holgate, 2002; Dockery et al., 1993; Hoek et al., 2013; Anderson et al., 2011; Pope et al., 2002; Lim et al., 2012), and particle oxidative potential (OP) (Bates et al., 2015; Fang et al., 2016; Yang et al., 2016; Weichenthal et al., 2016). Toxicological studies suggest PM-induced oxidant production as a possible mechanism linking PM exposure and observed health effects (Li et al., 2003a; Tao et al., 2003; Castro and Freeman, 2001; Gurgueira et al., 2002). Multiple chemical and cellular assays have been developed and utilized to measure PM-induced oxidant production. For instance, cell-free chemical assays that utilize an antioxidant to simulate biologically relevant redox reactions and ultimately measure the redox potential of PM (Kumagai et al., 2002; Cho et al., 2005) and cellular assays that employ a probe capable of reacting with reactive oxygen and nitrogen species (ROS/RNS) produced as a result of PM exposure (Landreman et al., 2008; Tuet et al., 2016) have been developed. Both types of assay have been used in prior studies to elucidate chemical species associated with oxidant production (Fang et al., 2015c; Bates et al., 2015; Fang et al., 2015a; Verma et al., 2015a; Verma et al., 2014; Li et al., 2003b; Kleinman et al., 2005; Hamad et al., 2015; Verma et al., 2015b; Verma et al., 2012; Dou et al., 2015; Lin and Yu, 2011; Tuet et al., 2016).

Despite these efforts, the specific constituents responsible for the overall health effects induced by PM exposure remain unclear as ambient mixtures are complex.

Organic aerosol constitute a significant portion of ambient PM (Kanakidou et al., 2005; Jimenez et al., 2009), and multiple field studies have repeatedly shown that secondary organic aerosol (SOA, formed from the oxidation of volatile organic compounds in the atmosphere) often dominate over aerosol of primary origin (e.g., aerosol emitted directly from combustion engines), even in urban centers (Zhang et al., 2007; Jimenez et al., 2009; Ng et al., 2010). While there have been several recent studies regarding the health effects of SOA (McWhinney et al., 2013b; Rattanavaraha et al., 2011; Kramer et al., 2016; Lund et al., 2013; McDonald et al., 2010; McDonald et al., 2012; Baltensperger et al., 2008; Arashiro et al., 2016; Platt et al., 2014; Tuet et al., 2017b), there are still important gaps in knowledge that have not been addressed. For instance, organic aerosol have a lifetime of approximately one week (Seinfeld and Pandis, 2016); continued photochemical aging can alter the chemical and physical properties of aerosol, which may have implications on resulting health effects. These potential effects have not been fully explored as the majority of current studies have focused on freshly formed SOA (McWhinney et al., 2013b; Lin et al., 2017; Lin et al., 2016; Tuet et al., 2017a; Tuet et al., 2017b). In addition, the presence of redox-active metals on SOA health effects have not been considered even though laboratory studies have shown that the presence of metal-containing seeds influences SOA formation and chemical composition (Chu et al., 2014; Chu et al., 2012; Chu et al., 2017; Daumit et al., 2016), and these metals are readily emitted via various processes (e.g., traffic, mechanical processes, combustion) (Charrier and Anastasio, 2012; Fang et al., 2015a). Furthermore, redox-active metals such as iron may participate in redox cycling, as well as

Fenton-like reactions (Frei, 1994; Chevion, 1988). These reactions produce radicals capable of enhancing the degree of oxidation of organic aerosol when internally mixed with organic aerosol, resulting in stronger oxidizing agents that may induce more ROS/RNS production upon cellular exposure (Tuet et al., 2017a). Depending on the source, iron may exist in either coarse or fine mode, with a majority in the coarse mode and a small fraction in the fine mode (Fang et al., 2017a; Allen et al., 2001; Espinosa et al., 2001). As such, there exists some overlap between the size distributions of iron and submicron organic aerosol, which is sufficient for iron to serve as a catalyst in Fenton-like reactions in some fraction of the organic aerosol.

In the present study, naphthalene photooxidation SOA were generated in the presence of metal-containing (iron (II) sulfate, FS) and inorganic (ammonium sulfate, AS) seed. For both seed types, a series of laboratory chamber experiments with different initial naphthalene concentrations was conducted to produce aerosol of various degrees of oxidation. Multiple samples were also collected from a single experiment to obtain aerosol of different photochemical age. Oxidant production was measured using chemical and cellular assays (i.e., water-soluble OP as determined by dithiothreitol (DTT) consumption (Fang et al., 2015c) and intracellular ROS/RNS production as detected using carboxy-H₂DCFDA (Tuet et al., 2016)). Tuet et al. (2017a; 2017b) recently investigated the water-soluble oxidative potential and cellular ROS/RNS production for SOA formed from common biogenic and anthropogenic precursors. Here, we choose to focus on naphthalene SOA as it was shown to have the highest response among different SOA systems previously studied in Tuet et al. (2017a; 2017b).

5.2 Methods

5.2.1 Naphthalene aerosol generation

Naphthalene photooxidation SOA (naphthalene + hydroxyl ($\text{OH}\bullet$) radical) was generated under humid conditions in the presence of NO in the Georgia Tech Environmental Chamber (GTEC) facility. Briefly, the facility consists of two 12 m^3 TeflonTM chambers suspended inside a temperature-controlled enclosure surrounded by black lights (Sylvania 24922) and natural sunlight fluorescent lamps (Sylvania 24477) (Boyd et al., 2015). Each chamber is equipped with multiple sampling ports for reagent introduction and various gas- and aerosol-phase measurements. NO_2 , NO_x , and O_3 were monitored using a cavity-attenuated phase shift (CAPS) NO_2 monitor (Aerodyne), a chemiluminescence NO_x monitor (Teledyne 200EU), and an O_3 analyzer (Teledyne T400), respectively. Hydrocarbon concentration was monitored using a gas chromatography flame ionization detector (GC-FID, Agilent 7890A) and hydroxyl radical concentration was calculated from the hydrocarbon decay. Aerosol volume concentrations and size distributions as well as bulk aerosol compositions were measured using a scanning mobility particle sizer (SMPS, TSI) and a high resolution time-of-flight aerosol mass spectrometer (HR-ToF-AMS, Aerodyne; henceforth referred to as the AMS), respectively (DeCarlo et al., 2006). AMS data were analyzed using data analysis toolkits SQUIRREL (v. 1.57) and PIKA (v. 1.16), while elemental ratios (O:C, H:C, and N:C) were determined using the method outlined in Canagaratna et al. (2015). O:C and H:C ratios were then used to calculate the average carbon oxidation state ($\overline{\text{OS}}_c$) (Kroll et al., 2011). Finally, temperature and relative humidity (RH) were monitored using a hydro-thermometer (Vaisala HMP110).

Experimental conditions, given in Table 5-1, were designed to probe the effects of metal seed and aerosol chemical composition on OP and intracellular ROS/RNS production. All experiments were performed at $\sim 25\text{ }^{\circ}\text{C}$ under humid conditions ($\text{RH} \sim 50\%$). Prior to each experiment, chambers were flushed with pure air and humidified using a bubbler filled with deionized (DI) water. Once the desired humidity was reached, seed aerosol was injected by atomizing seed solution (15 mM $(\text{NH}_4)_2\text{SO}_4$ for ammonium sulfate (AS) experiments and 15 mM FeSO_4 for iron sulfate (FS) experiments (Sigma Aldrich)) until the seed concentration inside the chamber was approximately $30\text{ }\mu\text{g m}^{-3}$. Naphthalene was then injected by passing pure air at 5 L min^{-1} over solid naphthalene flakes (99%, Sigma Aldrich) (Chan et al., 2009). NO (500 ppm, Matheson) and OH precursor (H_2O_2 , 50% aqueous solution, Sigma Aldrich) were injected afterwards to attain an initial NO concentration of 300 ppb and an H_2O_2 concentration of 3 ppm, which yielded OH concentrations on the order of $10^6 - 10^7\text{ molec cm}^{-3}$. Once all reagent concentrations stabilized, UV lights were switched on to initiate photooxidation.

Table 5-1. Experimental conditions for naphthalene SOA.

Experiment	Hydrocarbon	Seed	Relative humidity (%)	[HC] ₀ (ppb)	[NO] ₀ (ppb)	[SOA] ^c (μg m ⁻³)
1	naphthalene	AS ^a	51%	32	315	11.7
2	naphthalene	FS ^b	50%	32	303	7.28
3	naphthalene	AS ^a	49%	92	368	66.7
4	naphthalene	FS ^b	48%	84	214	24.0
5 ^d	naphthalene	AS ^a	54%	186	344	187
6	naphthalene	FS ^b	52%	182	321	149
7	naphthalene	AS ^a	53%	342	320	348
8	naphthalene	FS ^b	51%	331	295	369

^a Ammonium sulfate seed (15 mM (NH₄)₂SO₄); ^b Iron sulfate seed (15 mM FeSO₄);

^c Average SOA concentration in the chamber during filter collection; ^d Experiment was repeated and multiple filters were collected over the course of the experiment to investigate the effects of photochemical aging

5.2.2 Aerosol collection and extraction

Aerosol samples were collected at peak growth onto 47 mm TeflonTM filters (0.45 μm pore size, Pall Laboratory) for 1.6 hrs at a flow rate of 29 L min⁻¹. The total mass collected on each filter was determined by integrating time-dependent SMPS volume concentrations over the filter collection period and multiplying the integrated value by the total volume of air collected. A density of 1 g cm⁻³ was assumed to facilitate comparison between studies, as SOA density varies with precursor identity and formation condition (Ng et al., 2007a; Ng et al., 2007b; Chan et al., 2009; Tasoglou and Pandis, 2015; Bahreini et al., 2005; Ng et al., 2006). Background filters only containing seed (AS or FS), OH precursor (H₂O₂), and NO at experimental conditions were also collected to account for potential H₂O₂ uptake onto seed particles since this may affect oxidative potential and

ROS/RNS measurements. After collection, filters were placed in sterile petri dishes, sealed with Parafilm M[®], and stored at -20 °C until extraction and analysis (Fang et al., 2015c).

Collected filter samples were extracted following the procedure outlined in Fang et al. (2015a) with modifications for cellular exposure described in Tuet et al. (2016). Briefly, filters were submerged in extraction media (DI water for OP and cell culture media (RPMI-1640) for ROS/RNS) and sonicated for two 30 min intervals using an Ultrasonic Cleanser (VWR International). Post-sonication, sample extracts were filtered using a 0.45 µm polytetrafluoroethylene (PTFE) syringe filter (Fisherbrand[™]) to remove insoluble material (Fang et al., 2015c) and extracts for cellular exposure were supplemented with 10% fetal bovine serum (FBS).

5.2.3 *Oxidative potential*

The intrinsic water soluble oxidative potential as measured by DTT (OP) of naphthalene aerosol, method blanks, and positive controls (9,10-phenanthraquinone) were determined using a semi-automated DTT system, described in detail in Fang et al. (2015c). Briefly, the method consisted of three major steps: (1) oxidation of DTT by redox-active species in the extract, (2) reaction of remaining DTT with 5,5-dithio-bis-(2-nitrobenzoic acid) (DTNB) to form 2-nitro-5-mercaptobenzoic acid (TNB), and (3) measurement of TNB at 412 nm.

5.2.4 *Intracellular ROS/RNS measurement*

Murine alveolar macrophages (MH-S, ATCC[®]CRL-2019[™]) were cultured in RPMI-1640 media supplemented with 10% FBS, 1% penicillin-streptomycin, and 50 µM

β -mercaptoethanol (BME) at 37 °C and 5% CO₂. ROS/RNS were detected using the assay described in Tuet et al. (2016). The assay consisted of five steps: pre-treatment of 96-well plates with 10% FBS in phosphate buffered saline (PBS), (2) seeding of cells at 2×10^4 cells well⁻¹, (3) incubation of cells with ROS/RNS probe (10 μ M, carboxy-H₂DCFDA, Molecular Probes C-400), (4) exposure of cells to samples and controls for 24 hrs, and (5) detection of ROS/RNS using a microplate reader (BioTek Synergy H4, ex: 485 nm, em: 525 nm). Positive controls included bacterial cell wall component, lipopolysaccharide (LPS, 1 μ g mL⁻¹), H₂O₂ (100 μ M), and reference filter extract (10 filter punches mL⁻¹, 1 per filter sample, from various ambient filters collected at the Georgia Tech site (Tuet et al., 2016); negative controls included blank filter extract and control cells (probe-treated cells exposed to media only, no stimulants).

For each filter sample, intracellular ROS/RNS production was measured over ten doses to fully capture dose-response relationships (Figure D-1). At each dose, ROS/RNS levels were normalized to basal ROS/RNS production (Henkler et al., 2010) (i.e. ROS/RNS produced from probe-treated control cells) and corrected for changes in relative cellular metabolic activity (Zhang et al., 2016) (measured using MTT, 3-(4,5-dimethylthiazol-2-yl)-2,5-diphenyltetrazolium bromide, assay) (Biotium) prior to fitting dose-response curves. Area under the dose-response curve (AUC) was then used to represent ROS/RNS for comparison to chemical oxidative potential as AUC is the most robust metric for comparing different PM samples (Tuet et al., 2016).

5.2.5 *Cellular metabolic activity*

MTT was used to assess cellular metabolic activity post-exposure. Sample extracts were removed after the exposure period (24 hrs), replaced with media containing MTT, and returned to the incubator for 4 hrs. Dimethyl sulfoxide was then added to solubilize the insoluble purple salt formed from the reduction of the tetrazolium dye and the absorbance at 570 nm was measured using a microplate reader (BioTek Synergy H4).

5.3 **Results and Discussion**

5.3.1 *Laboratory-generated aerosol*

Experiments were conducted in the Georgia Tech Environmental Chamber (GTEC) facility. Typical time series for NO, NO₂, O₃, gas-phase naphthalene concentrations, and aerosol mass concentrations are shown in Figure D-2 for the two seed particles investigated. In both cases, NO decreased due to reaction with peroxy radicals (RO₂), which are important radical intermediates formed from hydrocarbon oxidation, and whose fates affect the oxidation products and SOA formation (Kroll and Seinfeld, 2008; Orlando and Tyndall, 2012). Aerosol growth was observed shortly following the initiation of photooxidation (i.e., turning on the lights). Most of the hydrocarbon was consumed in two hours and peak aerosol mass was reached. In general, FS seeded experiments (Figure D-2b) yielded less aerosol mass compared to AS seeded experiments (Figure D-2a). Previous studies exploring the effect of iron sulfate seed on aerosol formation (e.g., α -pinene and toluene photooxidation SOA in the presence and absence of iron sulfate seed) have also reported on the decreasing effect of iron sulfate seed on SOA yield, that is less aerosol mass was formed in the presence of iron sulfate seed (Chu et al., 2012; Chu et al., 2014).

Aerosol chemical composition was monitored using a high resolution time-of-flight aerosol mass spectrometer (HR-ToF-AMS, Aerodyne; henceforth referred to as the AMS) for all chamber experiments. The average, normalized AMS mass spectra (Figure D-3) are consistent with those reported in previous studies (Chhabra et al., 2010; Riva et al., 2015). A fragmentation pattern characterized by distinct ions at m/z 77, 91, 105, 119, 133, 147, and 160, was observed, which is likely representative of phenylalkyl fragments (McLafferty and Tureček, 1993). Differences in AMS mass spectra between aerosol formed in the presence of AS and FS seed were observed as well (Figure D-4 and Figure D-5). Elemental ratios (O:C, H:C, and N:C) of SOA were also determined using the AMS, and average aerosol carbon oxidation states ($\overline{OS}_c = 2 \text{ O:C} - \text{H:C}$) (Kroll et al., 2011) of SOA were calculated. O:C ratios and \overline{OS}_c were higher for all FS seeded SOA compared to AS seeded SOA (Table D-1). This is consistent with previous laboratory studies, where the presence of iron sulfate seed resulted in the generation of more oxidized aerosol (higher O:C and \overline{OS}_c) due to Fenton-type reactions (Daumit et al., 2016). Additionally, for both AS and FS seeded SOA, \overline{OS}_c followed a decreasing trend with the mass of organic aerosol formed (ΔM_o), which is consistent with semi-volatile partitioning (Odum et al., 1996; Donahue et al., 2006) (Figure D-6). Specifically, more SOA was formed in experiments with a higher initial naphthalene concentration. With a higher aerosol mass loading, more volatile species (with a lower O:C and \overline{OS}_c) will also partition into the particle phase, thus lowering the overall \overline{OS}_c of the aerosol.

5.3.2 *Effect of iron seed on cellular ROS/RNS production*

To investigate whether the presence of metal-containing seed particles affected SOA toxicity, chemical and cellular oxidant production was measured for naphthalene SOA formed in the presence of iron-containing seed vs. inorganic seed (denoted $OP_{\text{seed} + \text{SOA}}$ or $ROS/RNS_{\text{seed} + \text{SOA}}$, where seed = FS or AS, where applicable). ROS/RNS production, expressed as the area under the dose-response curve (AUC) per mass of SOA (μg) in the filter extract, is shown in Figure 5-1, colored by seed type. AUC was used as previous drug and aerosol studies have shown that it is the most robust dose-response metric, whose informativeness does not rely on the presence of a baseline or maximum response (Tuet et al., 2016; Huang and Pang, 2012). It should be noted that for all experiments, FS seeded SOA exposure resulted in higher ROS/RNS levels compared to AS seeded SOA. This observed difference can potentially be attributed to both the seed itself (FS vs. AS) and organic aerosol formed in the presence of difference seeds.

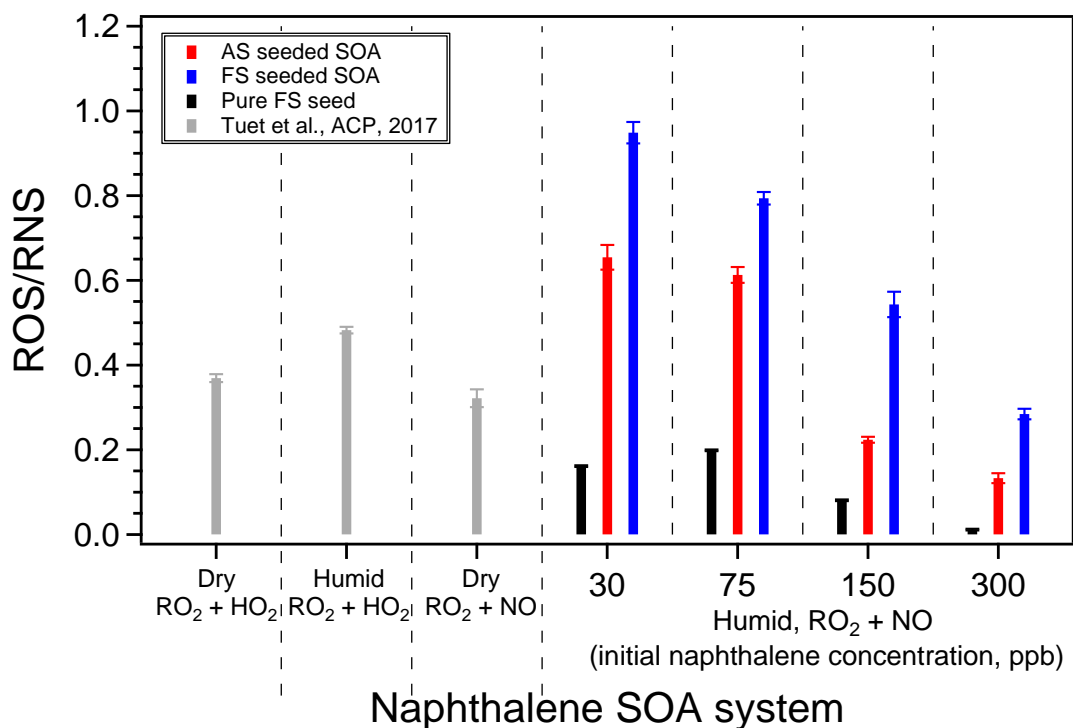


Figure 5-1. ROS/RNS produced as a result of naphthalene SOA exposure and corresponding ROS/RNS response from pure iron sulfate seed. ROS/RNS are expressed as the area under the dose-response curve (AUC). SOA were generated from the photooxidation of naphthalene in the presence of different seed particles (ammonium sulfate or iron sulfate), OH^\bullet radical precursor (H_2O_2), and NO. Data from previous studies, where SOA were generated in the presence of ammonium sulfate seed, were included for comparison. Initial hydrocarbon concentrations for other experiments are as follows: dry, $\text{RO}_2 + \text{HO}_2$ (178 ppb); humid, $\text{RO}_2 + \text{HO}_2$ (431 ppb); and dry, $\text{RO}_2 + \text{NO}$ (146 ppb) (Tuet et al., 2017b).

The seed effect was explored by exposing cells to pure iron sulfate seed. Exposure to both aerosolized (injected into the chamber, collected onto a filter, and extracted into media; see methods section and SI for details on filter collection and extraction) and aqueous (seed solution diluted in media) iron sulfate resulted in ROS/RNS levels that fall along the same dose-response curve (Figure D-7). This suggests that the aerosolization, collection, and extraction process does not alter the iron sulfate in a way which changes its ROS/RNS inducing ability. We then use this dose-response curve to estimate the ROS/RNS

response attributable to the presence of iron sulfate alone ($\text{ROS/RNS}_{\text{FS}}$) in SOA experiments. For each FS seeded SOA experiment, the seed mass collected onto the filter was approximated by fitting a double exponential (Nah et al., 2017) to the seed concentration time series (in the absence of chemical reactions, prior to aerosol formation) and integrating the fitted function over the filter collection period (Figure D-8). The corresponding $\text{ROS/RNS}_{\text{FS}}$ response as a result of exposure to this seed mass was then calculated using the iron sulfate dose-response curve (Figure D-7). These calculations were only performed for FS seeded SOA as exposure to ammonium sulfate seed has previously been shown to induce negligible ROS/RNS response at similar seed mass concentrations (Tuet et al., 2017a). The $\text{ROS/RNS}_{\text{FS}}$ response based on the determined iron sulfate seed mass accounted for about 2 – 12 % of the measured $\text{ROS/RNS}_{\text{FS} + \text{SOA}}$ response. It should be noted that these estimated contributions are only simple approximations to provide perspective as concentration addition may not apply for cellular responses. Nevertheless, these results are interesting as pure iron sulfate seed induced relatively low ROS/RNS production compared to that induced by the collected samples (i.e., $\text{ROS/RNS}_{\text{FS}} \ll \text{ROS/RNS}_{\text{FS} + \text{SOA}}$). This suggests that the measured $\text{ROS/RNS}_{\text{FS} + \text{SOA}}$ response may be predominantly attributed to organic components. These results confirm the importance of organic species to aerosol health effects, and previous studies on ROS/RNS produced as a result of aerosol exposure have also found significant correlations between the concentration of water soluble organic carbon (WSOC) and ROS/RNS response (Hamad et al., 2015; Saffari et al., 2013; Zhang et al., 2008; Daher et al., 2012).

The degree of oxidation is a parameter of interest for organic aerosol, as atmospheric photochemical aging occurs over an aerosol's lifetime, yielding more oxidized

species and aerosol with a higher \overline{OS}_c (Kroll et al., 2011). The observed difference in ROS/RNS levels between AS and FS seeded SOA is likely an effect of the degree of oxidation, where the presence of iron serves to increase the oxidation of species via Fenton-like reactions (Table D-1) (Frei, 1994; Chevion, 1988). In fact, a positive exponentially decreasing trend was observed between ROS/RNS levels and \overline{OS}_c of aerosol for all experiments (Figure 5-2). These results are consistent with our previous study on the ROS/RNS levels of SOA generated from various precursors, where a significant positive correlation was observed between ROS/RNS and \overline{OS}_c (Tuet et al., 2017a). Results from this study therefore further support the idea that more oxidized products are likely better oxidizing agents which can induce higher levels of ROS/RNS. In addition, the observed trend suggests that different seed types do not affect the ROS/RNS response as both AS and FS seeded SOA fall on the same ROS/RNS vs \overline{OS}_c curve.

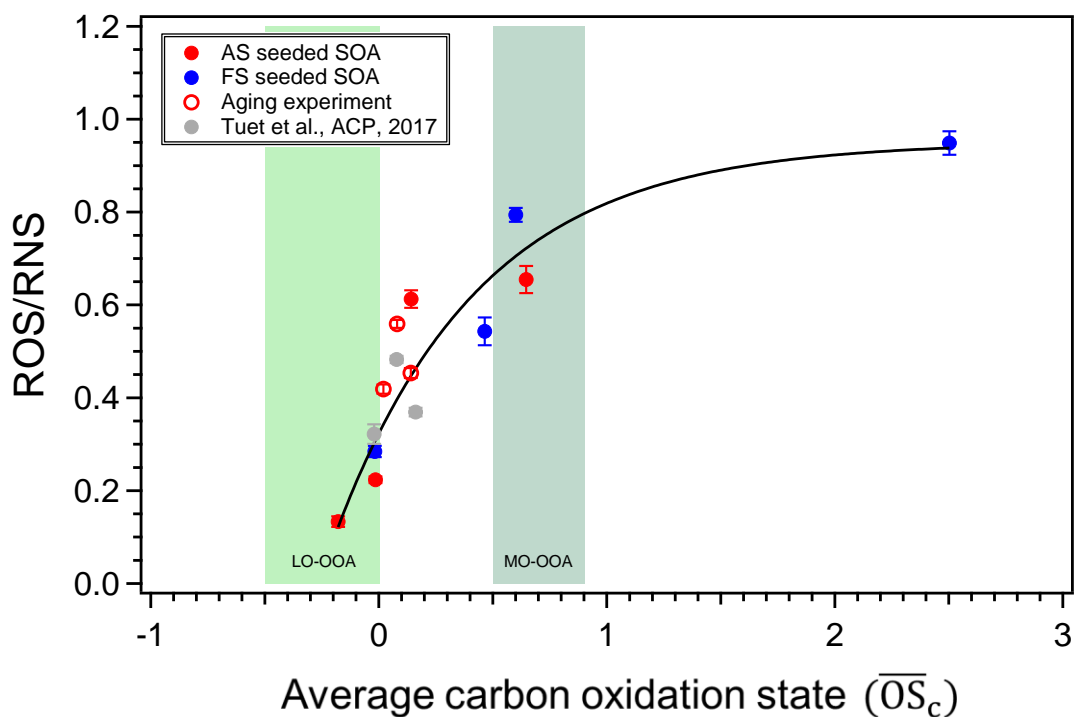


Figure 5-2. Exponential trend between ROS/RNS levels and average carbon oxidation state (\overline{OS}_c) for naphthalene photooxidation SOA generated in the presence of different seed particles (ammonium sulfate or iron sulfate), OH^\bullet radical precursor (H_2O_2), and NO. ROS/RNS production are expressed as the area under the dose-response curve (AUC). Error bars were determined using the methodology outlined in Tuet et al. (2016). Data from previous studies were included for comparison (Tuet et al., 2017b). \overline{OS}_c ranges for less oxidized oxygenated organic aerosol (LO-OOA) and more oxidized OOA (MO-OOA) are shaded for context (Kroll et al., 2011).

It is also interesting to note that the ROS/RNS levels for filter samples collected over the course of a single experiment (Expt. 5) roughly follow the time series for aromatic phenyl and benzyl ions measured by the AMS (m/z 77 and 91, respectively, Figure 5-3). Previous studies comparing cellular inflammatory responses from naphthalene and *m*-xylene SOA have suggested that aromatic-retaining products may have significant health implications (Tuet et al., 2017a; Tuet et al., 2017b). While results from this study are not sufficient to conclude causation, these observations along with findings from previous studies on the importance of humic-like substances (HULIS) (Dou et al., 2015; Lin and

Yu, 2011; Verma et al., 2015b) should inspire future studies to focus on assessing the health implications of aromatic SOA and determine whether the presence of aromaticity directly induces adverse outcomes.

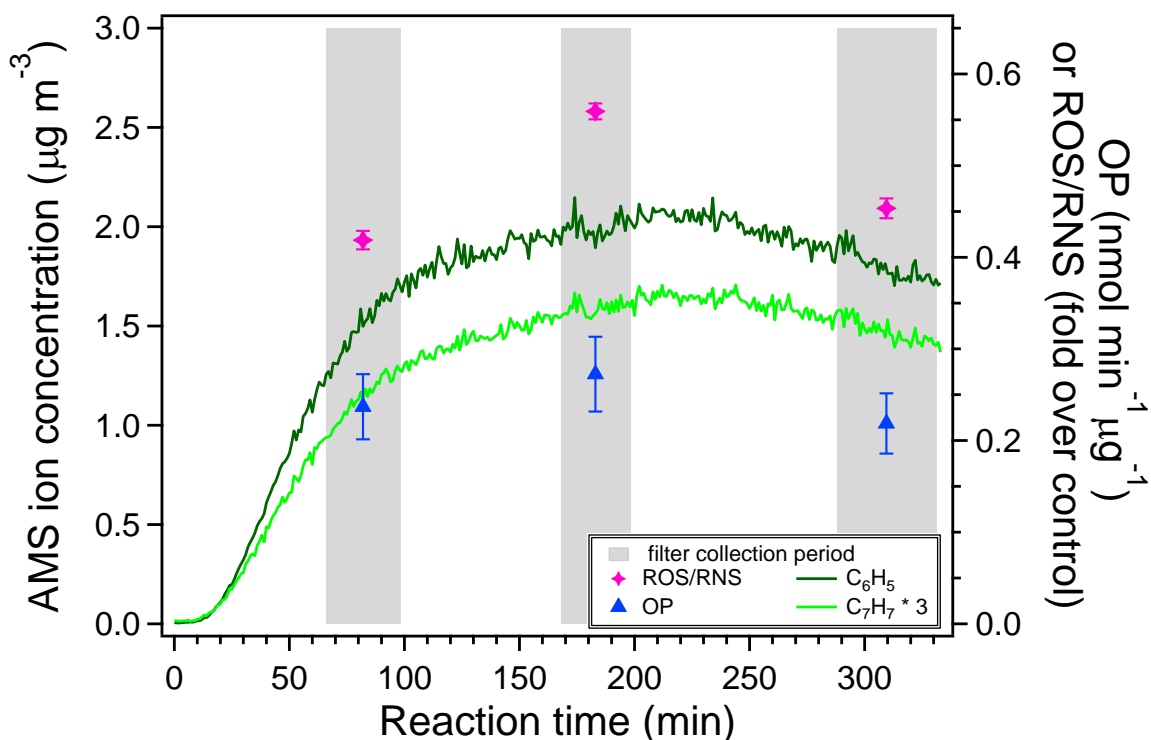


Figure 5-3. Intrinsic OP and ROS/RNS levels for naphthalene photooxidation SOA collected over the course of a single experiment (Expt. 5). Time series for AMS m/z 77 and 91, which are likely phenyl and benzyl ions, are also shown. SOA was generated in a humid chamber in the presence of ammonium sulfate, OH^\bullet radical precursor (H_2O_2), and NO . Error bars represent a 15% coefficient of variation for OP (Fang et al., 2015c). ROS/RNS levels are expressed as the area under the dose-response curve (AUC) with error bars calculated following the methodology described in Tuet et al. (2016).

The ROS/RNS levels induced by naphthalene SOA generated under different formation conditions (e.g., RH, peroxy radical fate, OH^\bullet source) have been measured in our previous study (Tuet et al., 2017a) and are also shown in Figure 5-1 for comparison. In both the previous and this study, the same cellular assay and analysis method was utilized. However, comparing ROS/RNS levels directly between these two studies may not be

applicable as there are several differences between SOA formation condition (e.g., different initial naphthalene concentrations, different relative humidities, and different OH radical precursors) (Tuet et al., 2017a). It is interesting to note that the exponential relationship between ROS/RNS and \overline{OS}_c holds for all naphthalene SOA generated under different formation conditions (Figure 5-2).

5.3.3 *Effect of iron seed on OP*

Intrinsic OP values (per μg) for naphthalene SOA ($OP_{\text{seed} + \text{SOA}}$) and pure iron sulfate seed (OP_{FS}) are shown in Figure 5-4, colored by seed type. For each FS seeded SOA experiment, the contribution of seed alone to the overall $OP_{\text{FS} + \text{SOA}}$ level is relatively low ($< 20\%$), which parallels that observed for the ROS/RNS response. It should be noted that DTT does not respond significantly to iron, and the low OP_{FS} is consistent with previous studies, where a low DTT reactivity by iron was observed (Charrier and Anastasio, 2012). Previous studies have shown that AS alone is not redox active, that is OP_{AS} is equivalent to the response of a blank filter within experimental error (Tuet et al., 2017b). It is therefore also interesting to note that $OP_{\text{FS} + \text{SOA}}$ is not always higher than $OP_{\text{AS} + \text{SOA}}$, suggesting that the presence of iron seed does not always induce an additive effect. Further studies should explore various effect models for OP to investigate additivity.

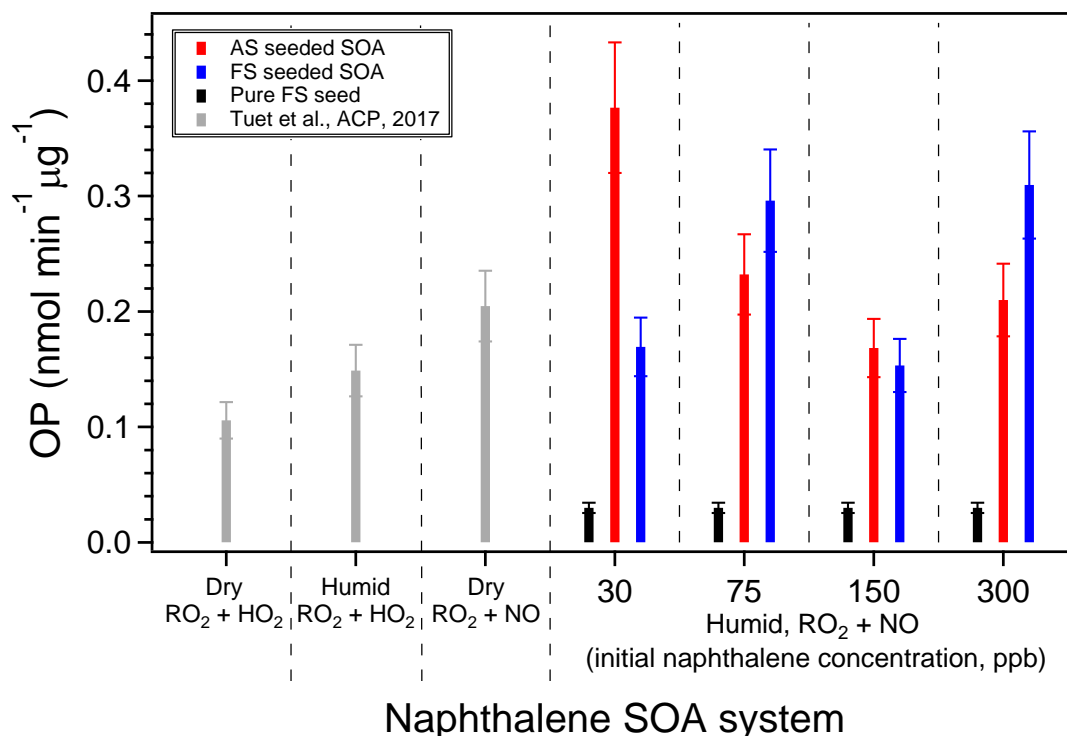


Figure 5-4. Intrinsic OP for SOA generated from the photooxidation of naphthalene under various conditions and pure iron sulfate seed. SOA from this study was generated in a humid chamber in the presence of different seed particles (ammonium sulfate or iron sulfate), OH• radical precursor (H₂O₂), and NO. Data from previous studies, where SOA were generated in the presence of ammonium sulfate seed, were included for comparison. Initial hydrocarbon concentrations for other experiments are as follows: dry, RO₂ + HO₂ (178 ppb); humid, RO₂ + HO₂ (431 ppb); and dry, RO₂ + NO (146 ppb) (Tuet et al., 2017b).

Overall, there are no apparent trends for the OP values obtained for SOA generated using different initial naphthalene concentrations (hence different organic aerosol mass loadings and \overline{OS}_c) or in the presence of different seed types. Furthermore, there was no observable relationship between OP and \overline{OS}_c (Figure D-9). While these results are in contrast to trends observed for ROS/RNS levels, they are consistent with previous studies on the DTT activities of different SOA systems and various ambient PM subtypes (Verma et al., 2015a; Xu et al., 2015a; Xu et al., 2015b; Tuet et al., 2017b). Tuet et al. (2017b) previously measured the intrinsic OP of different SOA systems (including naphthalene

SOA) and found that while different SOA precursors and formation conditions produced SOA of differing \overline{OS}_c , there was no apparent relation between OP and \overline{OS}_c . The study also showed that for both laboratory-generated SOA and different organic aerosol subtypes (Verma et al., 2015a; Xu et al., 2015a; Xu et al., 2015b) resolved from ambient data, a higher \overline{OS}_c did not correspond to a higher OP. It should be noted that these results may be complicated by mixture effects and/or dependent on the PM subtype, as previous studies have found that oxidation of quinones, diesel exhaust, or freshly emitted trash-burning aerosol enhances their redox activity (Li et al., 2009; Verma et al., 2015b; Vreeland et al., 2016). Nevertheless, results from this study may further highlight the differences between chemical and cellular assays. More specifically, it was suggested in a previous study by Tuet et al. that chemical assays, such as DTT, may only be sensitive to larger differences (i.e., different SOA precursors rather than different SOA formation conditions), while cellular assays are sensitive to differences arising from different SOA formation conditions as well as SOA precursor (Tuet et al., 2017a). The lack of correlation between OP and \overline{OS}_c in this study may therefore be a result of that all SOA in this study were generated from the same precursor (i.e., naphthalene) under the same formation condition (same RH and OH source). The specific oxidants (exogenous vs. endogenous) measured by each assay may be another potential explanation for the differences observed. DTT is primarily a measure of endogenous oxidant production as it is sensitive to redox-active species capable of interacting with anti-oxidants and less sensitive to the oxidants themselves (exogenous oxidants, e.g., H_2O_2). The cellular ROS/RNS assay also predominantly measures post-exposure endogenous oxidant production since extracellular ROS/RNS probe is removed after the probe incubation time (Tuet et al., 2016). However, while the cellular assay may

not directly measure exogenous oxidants, these species can interact with cells and induce pathways that may produce ROS/RNS. Therefore, the cellular assay may contain contributions from both endogenous and exogenous oxidants, while the DTT assay is largely a measure of only endogenous oxidants.

5.3.4 Relationship between photochemical aging of aerosol and toxicity

As the laboratory experiment progressed, OH exposure of aerosol and \overline{OS}_c increased as a result of increased photochemical aging. To investigate whether the effects of photochemical aging are comparable to those observed for SOA of different \overline{OS}_c (a proxy for aging), multiple filter samples were collected over the course of a single experiment (Table 5-1, repeat of Expt. 5). It should be noted that this aging experiment is an exact repeat of the previous experiment (Expt. 5), with the exception of a longer experimental time and multiple filter sample collections to explore changes in \overline{OS}_c associated with photochemical aging. The ROS/RNS levels and OP for these samples are shown in Figure 5-3. The OP for these three samples are the same within uncertainty, consistent with the hypothesis that the DTT assay may only be sensitive to larger differences (such as hydrocarbon precursor identity). On the other hand, the ROS/RNS response followed the same trend as that of \overline{OS}_c . The ROS/RNS response induced by these samples and the \overline{OS}_c calculated for each collection period are also shown in Figure 5-2 (opened markers) for comparison. These values fall within the exponential trend observed between ROS/RNS and \overline{OS}_c for SOA generated from different initial hydrocarbon concentrations. This suggests that the proxy for aging (\overline{OS}_c) investigated in this study may

be used to understand the potential health implications of aged particles for SOA from a single pure compound.

These observations have significant implications for future health studies as atmospheric aging leads to increases in aerosol oxidation (Jimenez et al., 2009; Ng et al., 2011), which may affect cellular responses. This is important as aerosols have an atmospheric lifetime of about a week, over which these aging processes can occur. If the observed relationship between cellular ROS/RNS response and \overline{OS}_c holds for other SOA systems, as well as ambient mixtures, these results may lead to ROS/RNS predictions based on more accessible bulk aerosol properties that are readily measured by the AMS. These approximations would not require the additional processing (e.g., filter collection and extraction) that actual ROS/RNS measurements entail. As an example, the \overline{OS}_c ranges for various organic aerosol subtypes resolved from ambient data world-wide, specifically less-oxidized oxygenated organic aerosol (LO-OOA) and more-oxidized OOA (MO-OOA), have been measured previously and are shaded in Figure 5-2 to provide context (Kroll et al., 2011; Xu et al., 2015a; Xu et al., 2015b). ROS/RNS levels measured in this study span the shaded regions, and the observed exponential trend suggests that exposure to MO-OOA would likely induce more ROS/RNS production compared to LO-OOA. This may have important implications as studies have shown that ambient organic aerosol from different sources converge towards MO-OOA as they age (Ng et al., 2010; Jimenez et al., 2009), and MO-OOA has widespread contributions to organic aerosol in both rural and urban locations across different seasons (Xu et al., 2015a; Xu et al., 2015b; Jimenez et al., 2009; Ng et al., 2010). Additional studies are required to establish whether the ROS/RNS and \overline{OS}_c relationship holds for different aerosol systems as previous studies have shown that

SOA generated from different precursors induce different cellular inflammatory responses (Tuet et al., 2017a).

5.4 Implications

The intracellular ROS/RNS production and water-soluble OP were measured for naphthalene photooxidation SOA formed under humid conditions in the presence of metal-containing and inorganic seed. Experiments were conducted using different initial hydrocarbon concentrations to generate aerosol of differing mass loadings and degrees of oxidation. Multiple filters were also collected from a single experiment to obtain aerosol of different photochemical age. Cellular assay results show that exposure to FS seeded aerosol resulted in higher levels of ROS/RNS production compared to AS seeded aerosol. Furthermore, the ROS/RNS response may be largely attributed to the organic components rather than the metals portion. This has important implications for future studies as organic aerosol constitute a large fraction of ambient fine PM (Kanakidou et al., 2005; Jimenez et al., 2009). However, it should be noted that possible synergistic and/or antagonistic metal-organic interactions were not explored and only one metal species and VOC were investigated in this study. Further studies are necessary to determine how metals and organics interact with each other and in the context of biologically-relevant species (e.g. proteins, sugars, and lipids present in the alveolar fluid). These interactions between co-exposed species may increase or decrease the overall cellular response (Barbosa Jr., 2017; Wildemann et al., 2015; Zhou et al., 2016), and a thorough understanding of these dynamics are necessary to evaluate the health implications of ambient aerosol. Results from this study also highlight the differences between chemical and cellular assays. There were no obvious trends between OP values and aerosol bulk composition measured by the AMS,

suggesting that the DTT assay may only be sensitive to large differences, such as that arising from different SOA precursors. The lack of correlation between OP and \overline{OS}_c is consistent with previous DTT studies, where a higher \overline{OS}_c did not correspond to a higher OP (Verma et al., 2015a; Xu et al., 2015a; Xu et al., 2015b).

An exponential trend was also observed between ROS/RNS levels and \overline{OS}_c for all naphthalene photooxidation SOA, including those formed in the presence of different seed particles (AS and FS), those formed under different formation conditions (dry vs. humid, $RO_2 + HO_2$ vs. $RO_2 + NO$), and those collected at different times over the course of a single experiment (different degrees of photochemical aging). There are several important implications arising from this trend. For one, the trend implies that there is negligible seed effect with respect to ROS/RNS produced as a result of SOA exposure. The aerosol formed in all experiments fall on the same ROS/RNS vs. \overline{OS}_c curve regardless of whether AS or FS seed was used. Hence, the observed difference between AS and FS seeded SOA (where all FS seeded SOA induced more ROS/RNS production) is likely an effect of differences in the degree of aerosol oxidation resulting from increased free radical production via Fenton-like reactions. The aerosol collected at multiple time points over the course of a single experiment (prolonged aging experiment) yield results that fall along this curve as well, which suggests that results obtained using \overline{OS}_c (a proxy for aging) may be generalized for photochemical atmospheric aging for this parent VOC and specific metal. Further studies are still required to establish whether the observed relationship between ROS/RNS and \overline{OS}_c holds for other aerosol systems, as only naphthalene photooxidation SOA was investigated in this study. Ambient aerosol are complex mixtures formed from multiple precursors and containing a variety of metallic species. These mixtures have not been

considered in this study, and results may be different due to synergistic and antagonistic mixture effects that have yet to be explored. However, if measures of bulk aerosol oxidation state (i.e., \overline{OS}_c) are validated with more aerosol systems to be used as a proxy for cellular ROS/RNS produced upon aerosol exposure, then the ability to perform more bulk aerosol measurements may lead to ROS/RNS predictions in the absence of cellular measurements.

CHAPTER 6: SUMMARY AND FUTURE WORK

6.1 Summary of major findings

Results from this dissertation addressed several important gaps in aerosol toxicity literature. A cell-based ROS/RNS assay was developed to investigate whether results from chemical assays commonly used to assess aerosol oxidative potential were representative of cellular responses induced by aerosol exposure. Cellular measurements demonstrated that ROS/RNS production was highly dose-dependent and non-linear with respect to PM dose. While no simple correlation was observed between ROS/RNS levels and chemical oxidative potential, chemical assays may serve as useful screening tools to narrow down sample sizes for cell-based analyses. Correlations between cellular ROS/RNS levels and concentrations of PM constituents were also evaluated to elucidate potential indicators of aerosol toxicity. While correlation may not necessarily equate to causation, these correlations provide possible directions for further studies. In this case, significant correlations were observed between organic species and ROS/RNS production for summer samples, highlighting a need to better understand the contribution of organic aerosol, particularly photochemically-driven SOA, to aerosol-induced health effects.

To provide perspective on the relative toxicities of different SOA systems, chemical oxidative potentials and cellular inflammatory responses were measured for SOA formed from various biogenic and anthropogenic precursors under different formation conditions. These results represent the first study to explore the toxicity of a wide variety of SOA systems using both cellular and acellular assays. Precursor identity influenced chemical oxidative potentials significantly, with isoprene and naphthalene SOA having the lowest

and highest oxidative potentials, respectively. Both precursor identity and formation condition influenced inflammatory responses induced by SOA exposure, and several response patterns were identified for SOA precursors whose photooxidation products share similar carbon chain length and functionalities. These results can raise awareness on the relative toxicity of aerosol constituents, provide guidance to aid policy making in air pollution management, and offer recommendations for emission control strategies (e.g., tighter controls for the emission of products of incomplete combustion may be proposed due to the toxicity of naphthalene SOA). Finally, the presence of iron sulfate seed was found to increase the aerosol average carbon oxidation state and result in higher ROS/RNS production. These findings suggest that aerosol may become more toxic over time as a result of atmospheric aging. Overall, findings from this dissertation have improved understanding on aerosol (particularly SOA) toxicity and the perspectives gained from these findings provide a foundation on which future studies can build upon.

6.2 Suggestions for future work

While this work addressed some important gaps and significantly improved our understanding of aerosol toxicity, there are a number of limitations that warrant further studies. For instance, only one cell type was investigated in our exposure experiments, whereas an organism consists of multiple tissues and the lungs alone consist of multiple cell types. Interactions between tissue systems and different cell types may produce very different results and would be important to consider to extrapolate results from this dissertation to *in vivo* exposures. The doses investigated in this dissertation may also not entirely represent real-world exposures due to different exposure routes and potential recovery effects due to clearance. Additionally, resuspension extracts (used in this study)

differ from real-world exposures. A recent study explored the health effects of isoprene SOA and found similar cellular responses for both filter resuspension extracts and direct air-liquid deposition, which more closely represent real-world aerosol exposures (Arashiro et al., 2016). These results may be a positive indication for the extrapolation of *in vitro* results, although further investigations using different aerosol systems and cell types are warranted to confirm these conclusions.

On another point regarding the relevance of exposure doses, all measurements in this dissertation were performed using water-soluble extracts (either in water or cell culture medium). Inclusion of water-insoluble material may induce different cellular response, as previous studies have shown that insoluble particles have substantial oxidative potential which may translate into cellular responses (Fang et al., 2017b; McWhinney et al., 2013a; Yang et al., 2014; Verma et al., 2012). A comparison study on the cellular effects of different fractions (e.g., water-soluble, water-insoluble, total) may provide interesting insights on the constituents responsible for adverse health outcomes and guide future studies.

Another important question arising from this dissertation is the use of ROS/RNS measurements as a general indicator of oxidative stress. Cellular inflammatory responses induced as a result of exposure to laboratory-generated aerosol in our studies demonstrate that a low ROS/RNS response may not necessary indicate a lack of cellular response. While ROS/RNS levels were generally associated with inflammatory cytokine production, there were aerosol systems where a low ROS/RNS response was accompanied by levels of cytokine production that were higher than expected given the ROS/RNS level detected. These findings suggest that a single cellular measurement may not be adequate in terms of

understanding aerosol toxicity and that additional measures, such as inflammatory cytokine production, may be required to fully interpret cellular ROS/RNS responses. Furthermore, the endpoints measured in this dissertation only represent a small portion of the many possible cellular endpoints that may be affected by aerosol exposure. Ultimately, there is a need to develop a high-throughput device or method to measure multiple cellular endpoints for multiple aerosol samples. With a large enough dataset, subtle connections may become apparent and cellular mechanisms may be elucidated.

Finally, results from this study demonstrate that aerosol species cannot be treated as individual components in a mixture. That is, complex interactions may occur between aerosol species such that the overall response cannot be approximated by a simple linear combination of individual effects. While mixture effects were not explored in this dissertation, their importance is apparent given the results obtained from both ambient and laboratory-generated aerosol cellular exposures. For instance, while few metal species were correlated with ROS/RNS response for ambient samples, exposure to individual metals induced measureable ROS/RNS production. Recent studies have also begun to explore the different synergistic and antagonistic interactions that occur between aerosol components (Xiong et al., 2017; Yu et al., 2018; Wang et al., 2017) and the results support the occurrence of these complex interactions.

Beyond the field of aerosol toxicology, results from this dissertation may inspire future directions for epidemiological studies and policy making. The perspective gained on the relative toxicity of different aerosol constituents can offer potential directions for air pollution control policy, which may involve new model inputs and simulations based on findings from this dissertation. Furthermore, the cellular assay developed to measure

ROS/RNS as a result of PM exposure can be extended to assess other environmental toxins. For instance, it may be possible to apply the cell-based assay to wastewater treatment evaluations. The assay may also be effectively adapted to investigate pharmaceuticals, especially those related to inflammation. These additional applications of the optimized cellular assay are worth further exploration.

APPENDIX A: SUPPLEMENT FOR CHAPTER 2

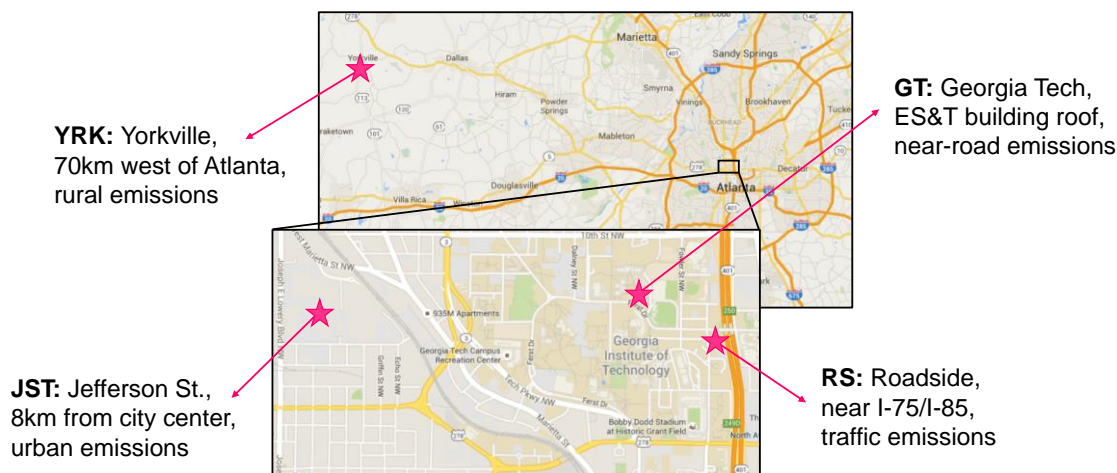


Figure A-1. Ambient sampling sites for the Southeastern Center for Air Pollution and Epidemiology (SCAPE) study. Sites include: JST (located on Jefferson Street, representative of urban Atlanta), RS (located near Interstate Highways I-75/I-85, representative of traffic emissions), GT (located on the roof of the Ford Environmental Science and Technology building at Georgia Tech, representative of near-road emissions), and YRK (located in Yorkville, representative of rural background).

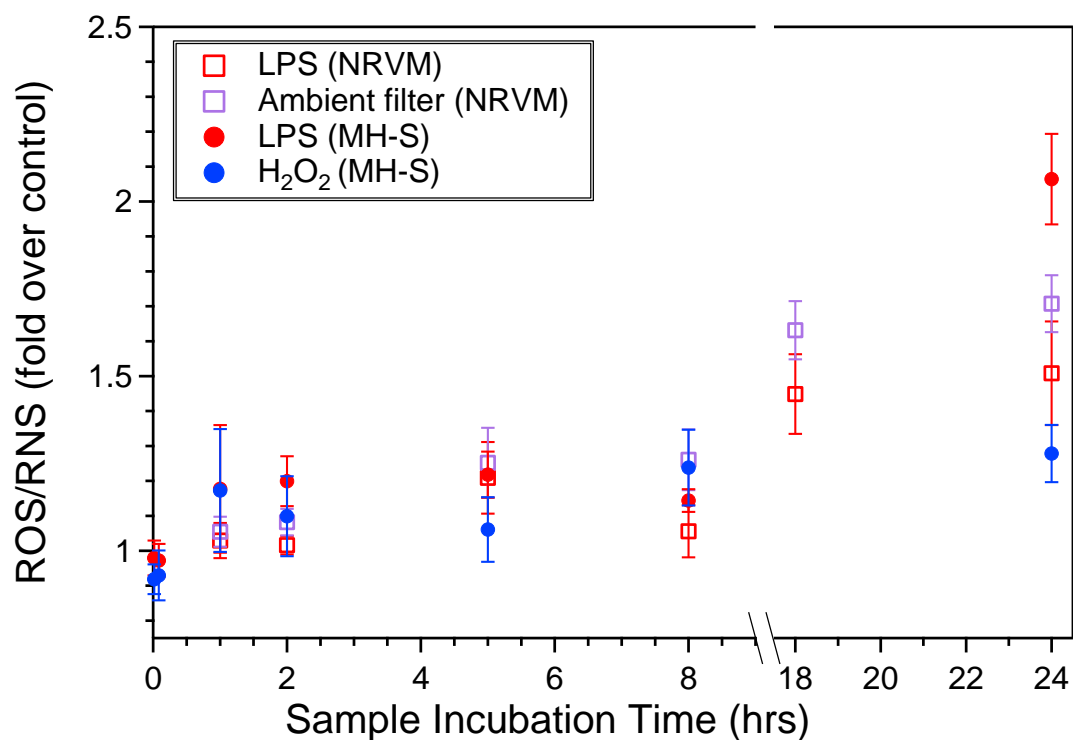


Figure A-2. ROS/RNS production as a result of treatment with positive controls over various sample incubation times. Data shown are means \pm SE of experiments performed in triplicate. ROS/RNS production is expressed as fold increase over probe-treated cells incubated with stimulant-free media (control cells). At 24 hrs, the normalized positive response is highest for both cell types.

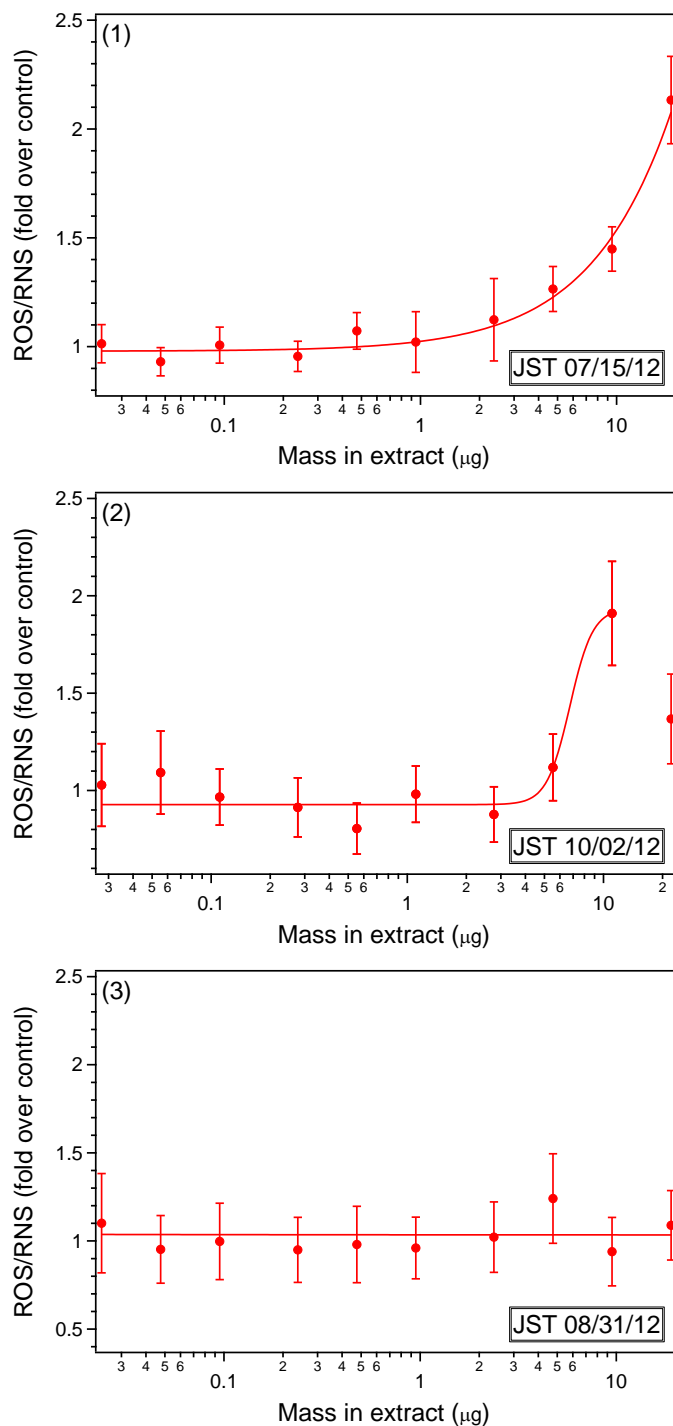


Figure A-3. Dose-response behaviors observed in this study: (1) maximum response not attained, (2) decreased response at higher doses, and (3) no response above baseline at all doses. Data shown are means \pm SE of experiments performed in triplicate. ROS/RNS production is expressed as fold increase over probe-treated cells incubated with stimulant-free media (control cells).

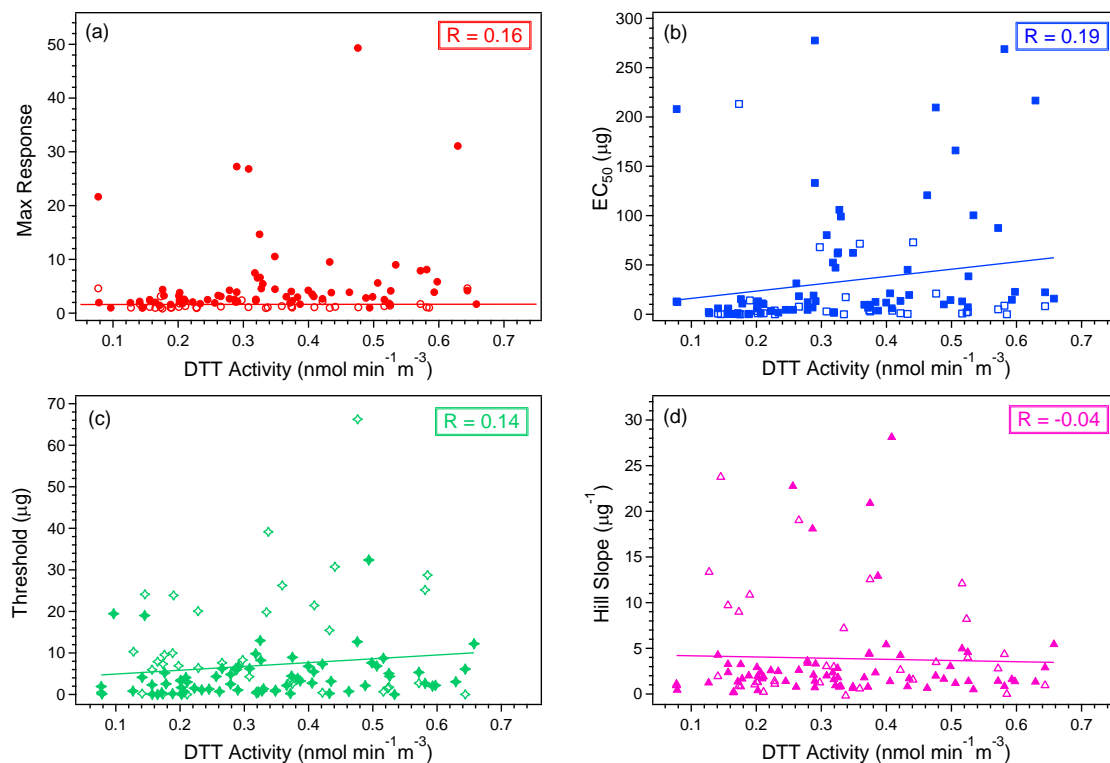


Figure A-4. Dose-response parameters for ambient filters spanning a wide range of extrinsic DTT activity. Each data point represents a single dose-response obtained from 10 dilutions (1x to 0.00125x) performed in triplicate. Solid markers represent MH-S data; open markers represent NRV data. Linear regressions and corresponding Pearson's coefficients are given for each parameter. $n = 104$ ambient filters; * indicates significance, $p < 0.05$.

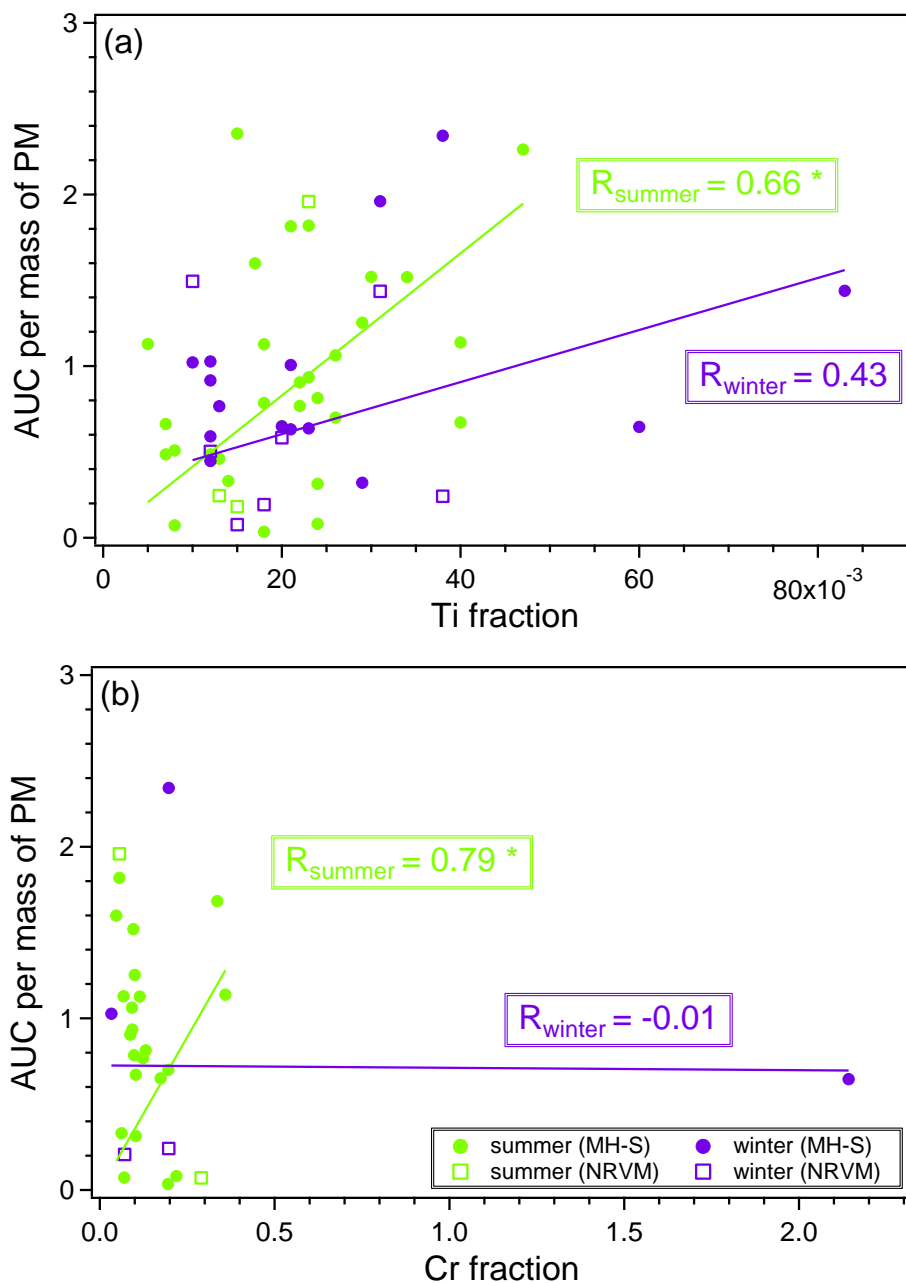


Figure A-5. AUC per mass of PM for ambient samples containing various fractions of (a) titanium (Ti) and (b) chromium (Cr). Each data point represents a single ambient filter for which a dose-response was obtained (10 dilutions performed in triplicate) and fitted to the Hill equation. Data points are colored by season with cut-off dates determined by solstice and equinox dates. Linear regressions and Pearson's correlation coefficients are shown for summer and winter filter samples. $n = 104$ ambient filters (10 spring, 47 summer, 15 autumn, and 32 winter); * indicates significance, $p < 0.05$.

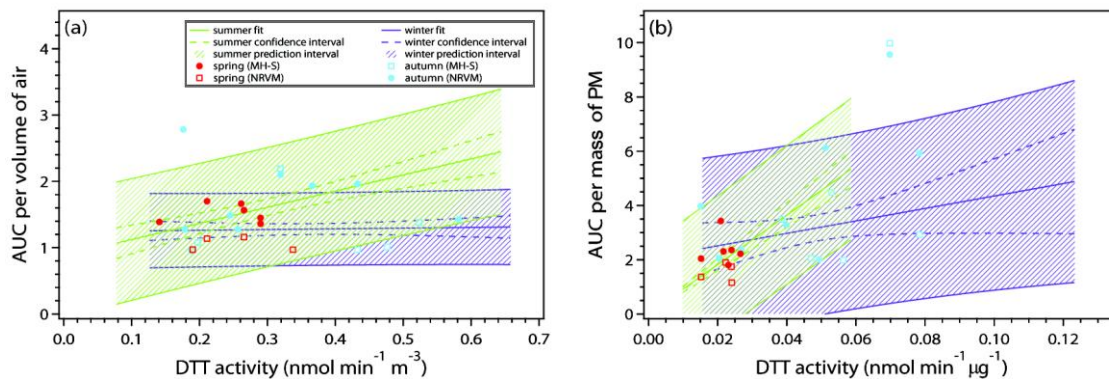


Figure A-6. AUCs for spring and autumn filter samples spanning a range of (a) extrinsic and (b) intrinsic DTT activity. Each data point represents a single ambient filter for which a dose-response was obtained (10 dilutions performed in triplicate) and fitted to the Hill equation. Linear regressions with corresponding confidence (dashed) and prediction (shaded) intervals are shown for summer and winter filter samples. $n = 104$ ambient filters (10 spring, 47 summer, 15 autumn, and 32 winter).

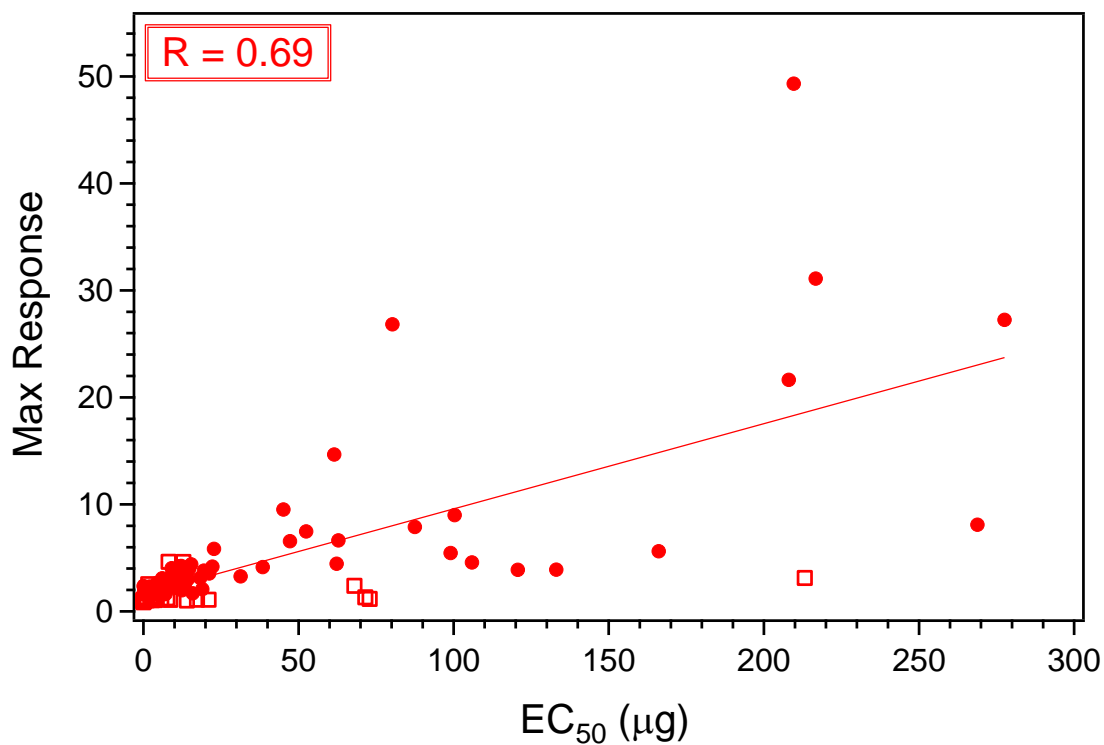


Figure A-7. Maximum ROS/RNS production and corresponding EC₅₀ for ambient filters investigated. Each data point represents a single dose-response obtained from 10 dilutions (1x to 0.00125x) performed in triplicate. Solid markers represent MH-S data; open markers represent NRVM data. A simple linear regression and corresponding Pearson's coefficient are given. $n = 104$ ambient filters; * indicates significance, $p < 0.05$.

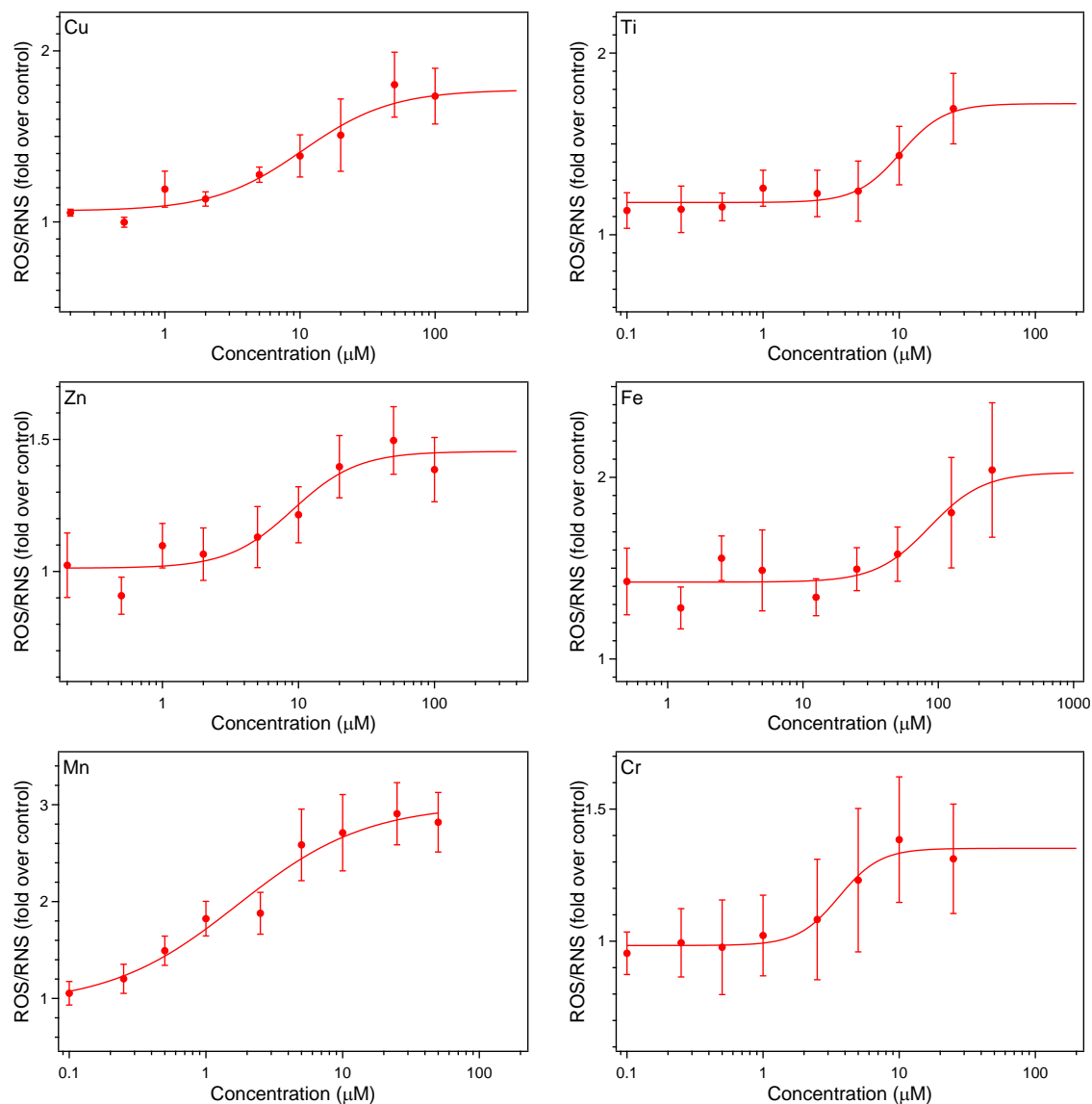


Figure A-8. ROS/RNS production as a result of exposure to 6 pure metal salt solutions and corresponding dose-response curves. Concentrations span the water soluble metal concentrations observed in ambient samples. ROS/RNS production is expressed as fold increase over control, probe-treated cells not exposed to stimulant. Data shown are means \pm SE of triplicate experiments.

Table A-1. Pearson's correlation coefficients for overall linear regressions between dose-response parameters and PM components. Dose-response parameters were obtained from Hill Equation fits and include max response, EC₅₀, Hill slope, threshold, and AUC per volume of air sampled. PM components include water-soluble metals, water-soluble organic carbon (WSOC), and brown carbon (BrC). Metals were also grouped by metal sources: Brake/Tire Wear (BTW: Ti, Cu, Zn, Ba), Biomass Burning (BB: K, As, Br, Pb), Secondary Formation (SF: S, Fe, Se), and Mineral Dust (MD: Ca, Mn, Sr). $n = 104$ ambient filters; * indicates significance, $p < 0.05$.

PM component	Max response	EC ₅₀	Hill slope	Threshold	AUC _{air}
WSOC	0.18	0.09	-0.11	-0.05	0.39
BrC	0.09	0.26	-0.05	0.12	-0.03
Ti	-0.02	-0.12	0.05	-0.11	0.38
Cu	-0.04	-0.11	0.19	-0.10	0.21
Zn	0.05	0.02	0.02	-0.01	0.23
Ba	-0.07	-0.09	0.14	-0.13	0.17
BTW	0.01	-0.05	0.14	-0.06	0.26
K	0.13	0.20	-0.05	0.12	0.15
As	0.02	0.12	0.11	0.12	-0.02
Br	0.09	0.12	-0.09	0.04	0.25
Pb	0.09	0.13	-0.08	0.13	0.15
BB	0.14	0.22	-0.03	0.13	0.13
S	0.24	0.12	-0.01	-0.01	0.28
Fe	0.11	-0.02	0.04	-0.13	0.43
Se	0.20	0.20	0.02	0.14	0.22
SF	0.23	0.10	-0.03	-0.04	0.35
Ca	0.20	-0.01	-0.10	-0.15	0.15
Mn	0.23	0.09	-0.12	-0.16	0.38
Sr	0.10	-0.03	0.28	-0.11	0.16
MD	0.20	-0.02	-0.10	-0.13	0.22
Cr	-0.04	-0.05	-0.11	-0.11	-0.09
V	0.12	0.06	-0.23	-0.09	0.18
Total metals	0.24	0.09	-0.04	-0.05	0.36
PM _{2.5}	0.29	0.20	-0.05	0.01	0.30

Table A-2. Pearson's correlation coefficients for overall linear regressions between dose-response parameters and PM component fractions. Dose-response parameters include max response, EC₅₀, Hill slope, threshold, and AUC per mass of PM. PM components include water-soluble metals, water-soluble organic carbon (WSOC), and metals grouped by source: Brake/Tire Wear (BTW: Ti, Cu, Zn, Ba), Biomass Burning (BB: K, As, Br, Pb), Secondary Formation (SF: S, Fe, Se), and Mineral Dust (MD: Ca, Mn, Sr). $n = 104$ ambient filters; * indicates significance, $p < 0.05$.

PM component (fraction)	Max response	EC ₅₀	Hill slope	Threshold	AUC _{mass}
WSOC	-0.01	-0.05	-0.07	-0.07	0.15
Ti	-0.13	-0.21	0.17	-0.12	0.42
Cu	-0.08	-0.17	0.29	-0.10	0.11
Zn	-0.10	-0.17	0.07	-0.05	0.37
Ba	-0.13	-0.17	0.20	-0.16	0.31
BTW	-0.01	-0.04	0.19	-0.004	-0.0003
K	-0.05	0.04	0.06	0.12	0.21
As	-0.06	0.01	0.19	0.09	0.03
Br	-0.10	-0.07	-0.08	0.02	0.11
Pb	-0.08	-0.03	-0.05	0.15	-0.04
BB	0.03	0.18	0.11	0.20	-0.19
S	-0.03	-0.12	-0.03	-0.10	0.16
Fe	-0.03	-0.15	0.08	-0.18	0.19
Se	0.03	0.08	0.08	0.25	-0.32
SF	-0.04	0.04	-0.03	0.03	-0.16
Ca	-0.04	-0.19	-0.08	-0.15	0.45
Mn	-0.02	-0.05	-0.10	-0.20	0.55*
Sr	-0.03	-0.10	0.35	-0.11	0.16
MD	0.03	-0.14	-0.06	-0.14	0.29
Cr	-0.12	-0.12	-0.14	-0.11	0.10
V	-0.08	-0.07	-0.17	-0.11	0.28

Table A-3. Comparison between assays parameters used in previous studies and this study. Parameters include: ROS/RNS probe, cell density, ROS/RNS probe concentration, sample incubation time, signal normalization scheme, and analysis approach. All parameters were optimized for measuring ROS/RNS production as a result of PM exposure in this study.

Parameter	This study	Previous studies
ROS/RNS probe	carboxy-H ₂ DCFDA	DCFH-DA
Cell density	2x10 ⁴ cells well ⁻¹	1x10 ⁵ cells well ⁻¹
Probe concentration	10μM	45μM
Sample incubation time	24hrs	2.5hrs
Signal normalization	Control cells (probe-treated cells incubated with media)	Positive control (zymosan)
Analysis	Dose-response curve and associated parameters	Single measurement or linear slope using few dilutions

Table A-4. Root-mean-squared error (RMSE) between observed and fitted area under the curve (AUC) for summer and winter filter samples. Fits are based on a simple linear regression between AUC and the predictor of interest, which include: dithiothreitol (DTT) activity, water-soluble organic carbon (WSOC) concentration, brown carbon (BrC) concentration, and iron (Fe) concentration. $n = 104$ ambient filters (10 spring, 47 summer, 15 autumn, and 32 winter).

Predictor	RMSE _{summer}	RMSE _{winter}
DTT	0.4506	0.2517
WSOC	0.4352	0.2544
BrC	0.4553	0.2513
Fe	0.4408	0.2388

APPENDIX B: SUPPLEMENT FOR CHAPTER 3

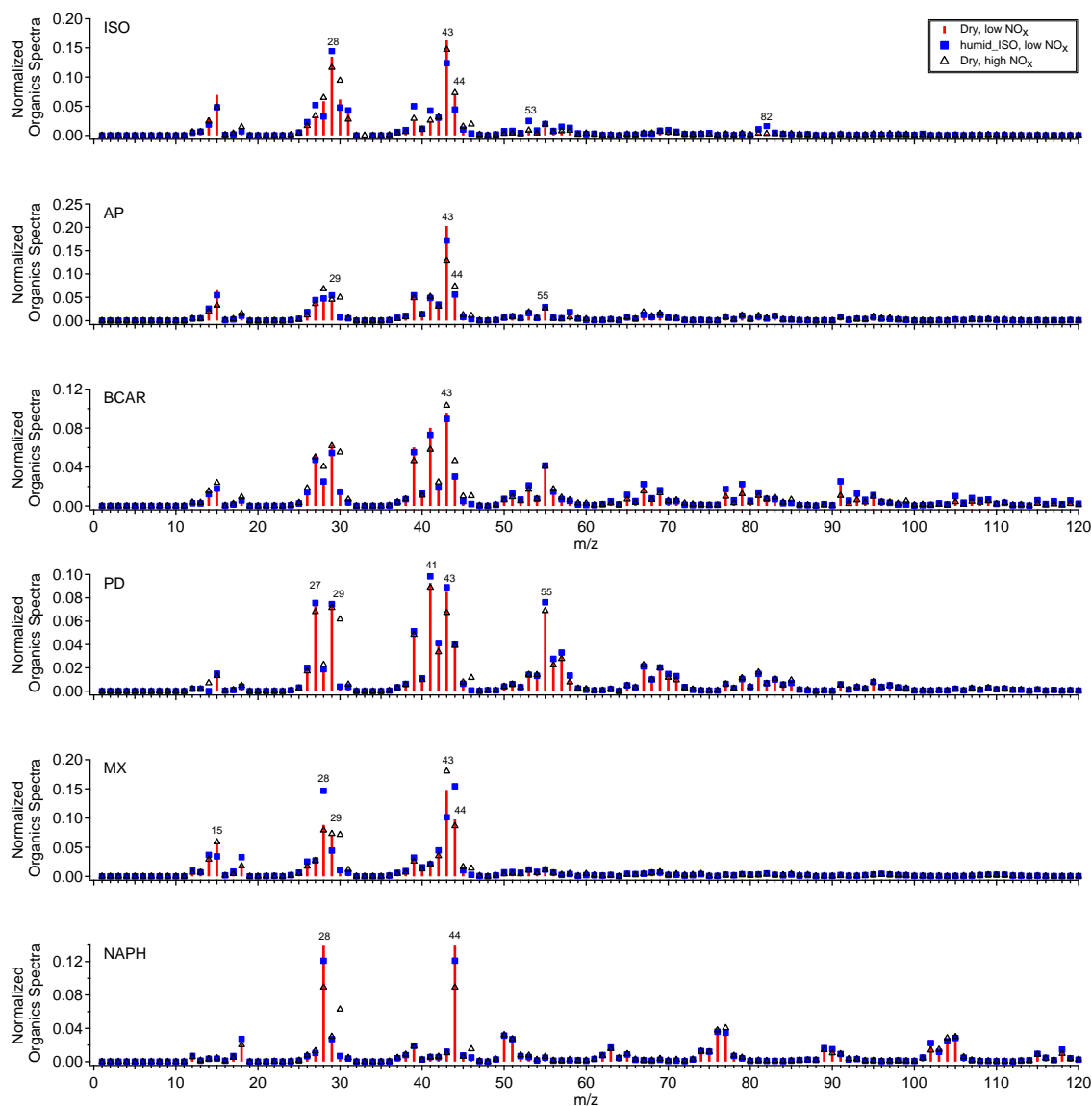
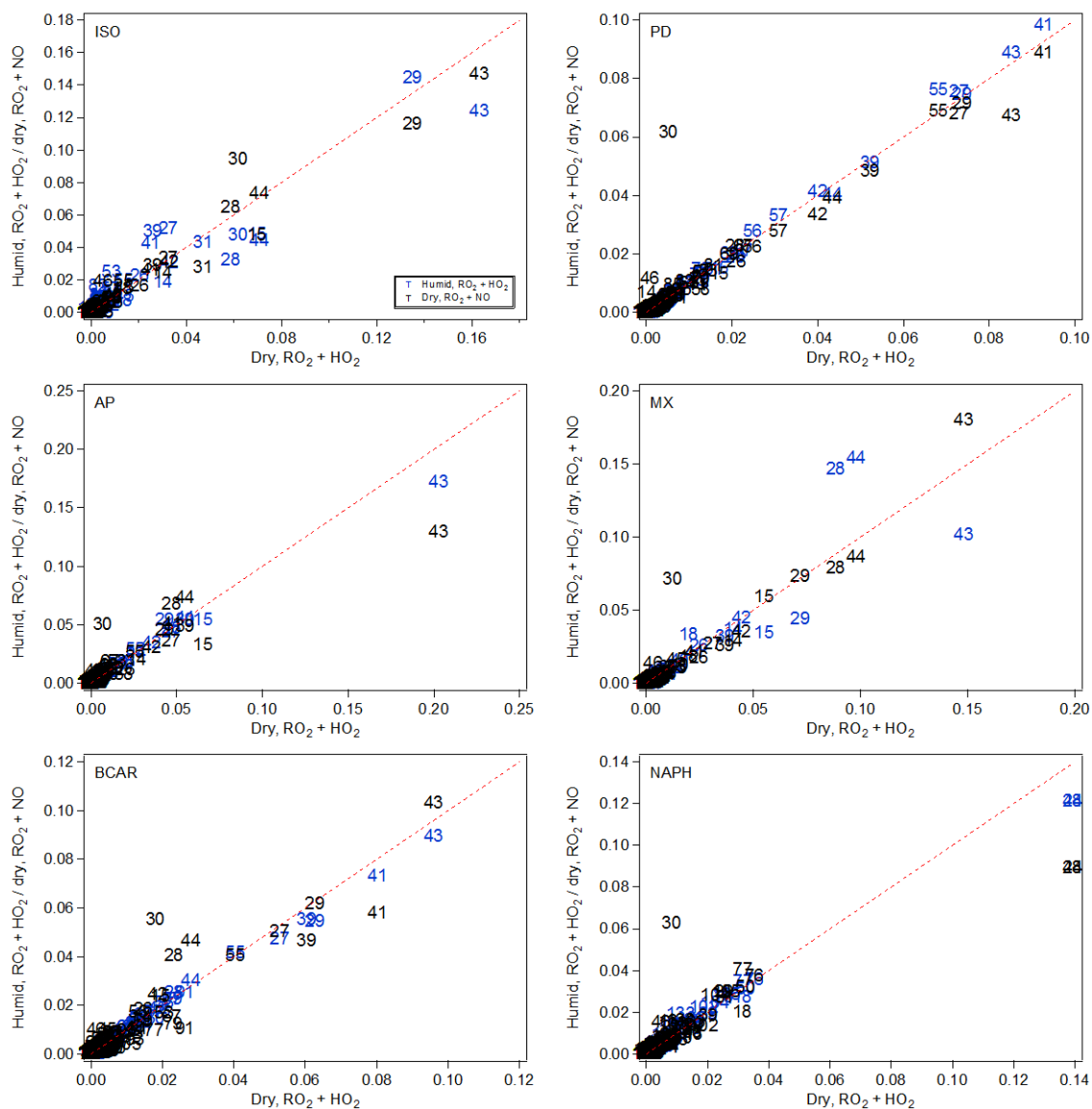


Figure B-1. Aerosol mass spectra of SOA formed from the photooxidation of various hydrocarbon precursors (ISO: isoprene, AP: α -pinene, BCAR: β -caryophyllene, PD: pentadecane, MX: m-xylene, and NAPH: naphthalene) under various conditions (red bars: dry, $\text{RO}_2 + \text{HO}_2$; blue squares: humid, $\text{RO}_2 + \text{HO}_2$; and black triangles: dry, $\text{RO}_2 + \text{NO}$). Characteristic fragments for each system are labeled.



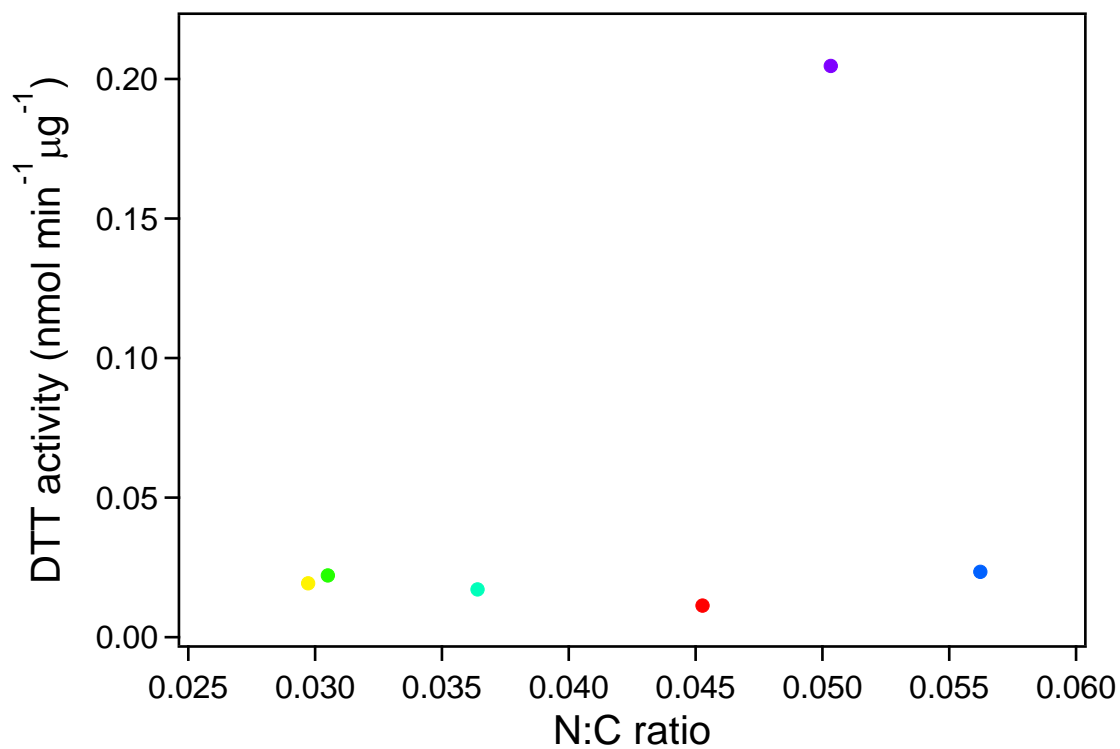
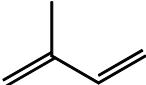
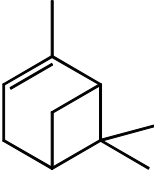
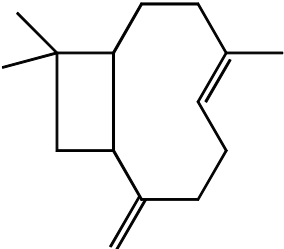

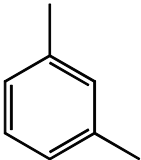
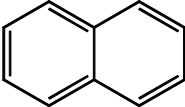


Figure B-3. Intrinsic DTT activities (per μg) for various SOA systems spanning a wide range of N:C. Data points are colored by SOA system (red: isoprene, yellow: α -pinene, green: β -caryophyllene, light blue: pentadecane, blue: *m*-xylene, and purple: naphthalene).

Method for determining intrinsic OP^{WS-DTT} for various OA subtypes:

Verma et al. (2015a) used multiple regression analysis to estimate the OP^{WS-DTT} of different OA subtypes (Verma et al., 2015a; Xu et al., 2015a; Xu et al., 2015b). PMF analysis on AMS data collected in the southeastern U.S. resolved multiple OA factors, which represent different OA subtypes. The coefficients associated with each OA subtype from the multiple linear regression represented an estimation of the intrinsic DTT activity of that type of OA. These results are also included in Fig. 4 for comparison and discussed more below. The different aerosol subtypes with at least some contributions to DTT activity as determined by the multiple regression include isoprene-derived OA (Isoprene-OA), biomass burning OA (BBOA), more-oxidized oxygenated OA (MO-OOA), and cooking OA (COA) (Xu et al., 2015b; Verma et al., 2015a).

Table B-1. Hydrocarbon precursor structure and reaction rate constants.

Compound	Structure	k_{OH+HC} (cm ³ /molec*s)
Isoprene		1.01×10^{-10}
α -pinene		5.37×10^{-11}
β -caryophyllene		2.00×10^{-10}
Pentadecane		2.07×10^{-11}
m-xylene		2.31×10^{-11}
Naphthalene		2.44×10^{-11}

APPENDIX C: SUPPLEMENT FOR CHAPTER 4

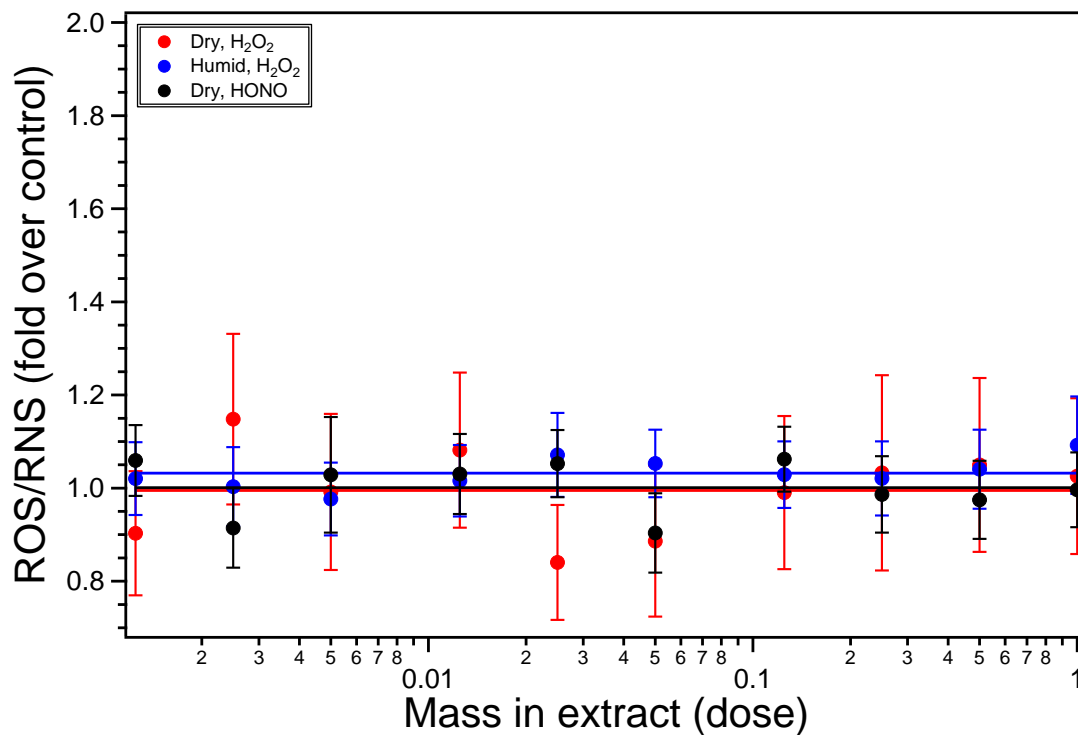


Figure C-1. ROS/RNS produced as a result of exposure to background filters (OH precursor and seed only). ROS/RNS is expressed as a fold increase over probe-treated control cells incubated with stimulant-free media. Data shown are means \pm standard error of triplicate exposure experiments.

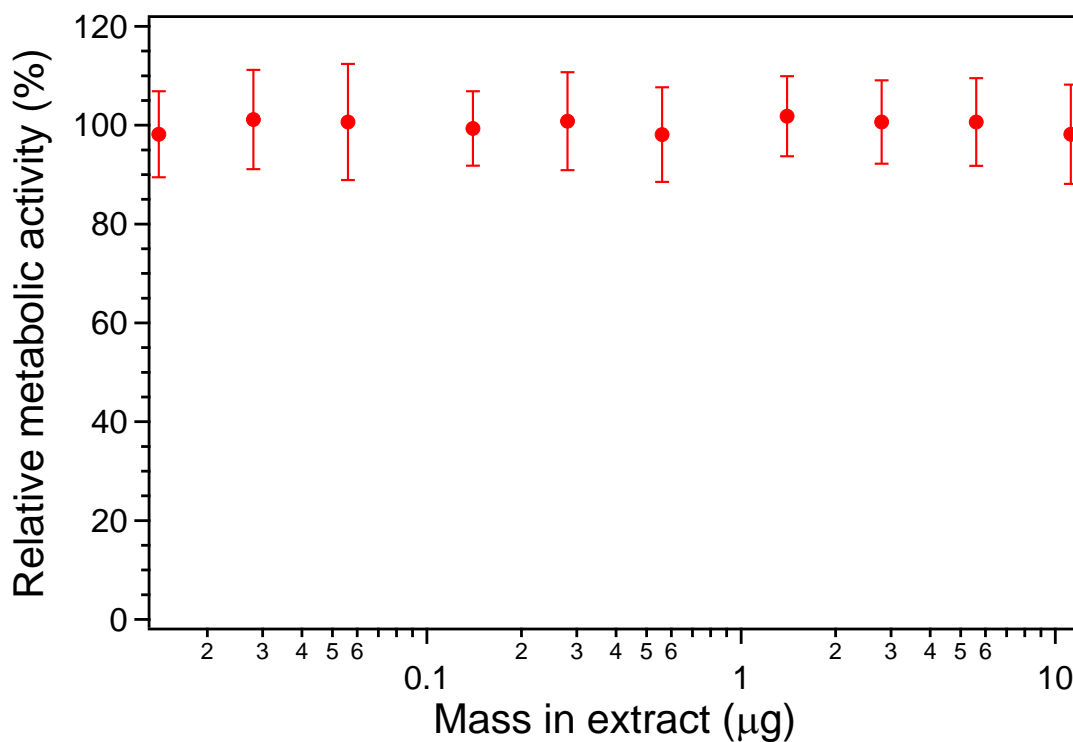


Figure C-2. Post filter exposure cellular metabolic activity as measured by the MTT assay (filter: naphthalene SOA formed under dry, $\text{RO}_2 + \text{NO}$ dominant conditions). Cellular metabolic activity is normalized to cells exposed to stimulant-free media. Data shown are means \pm standard error of triplicate exposure experiments. All filter exposures produced similar results.

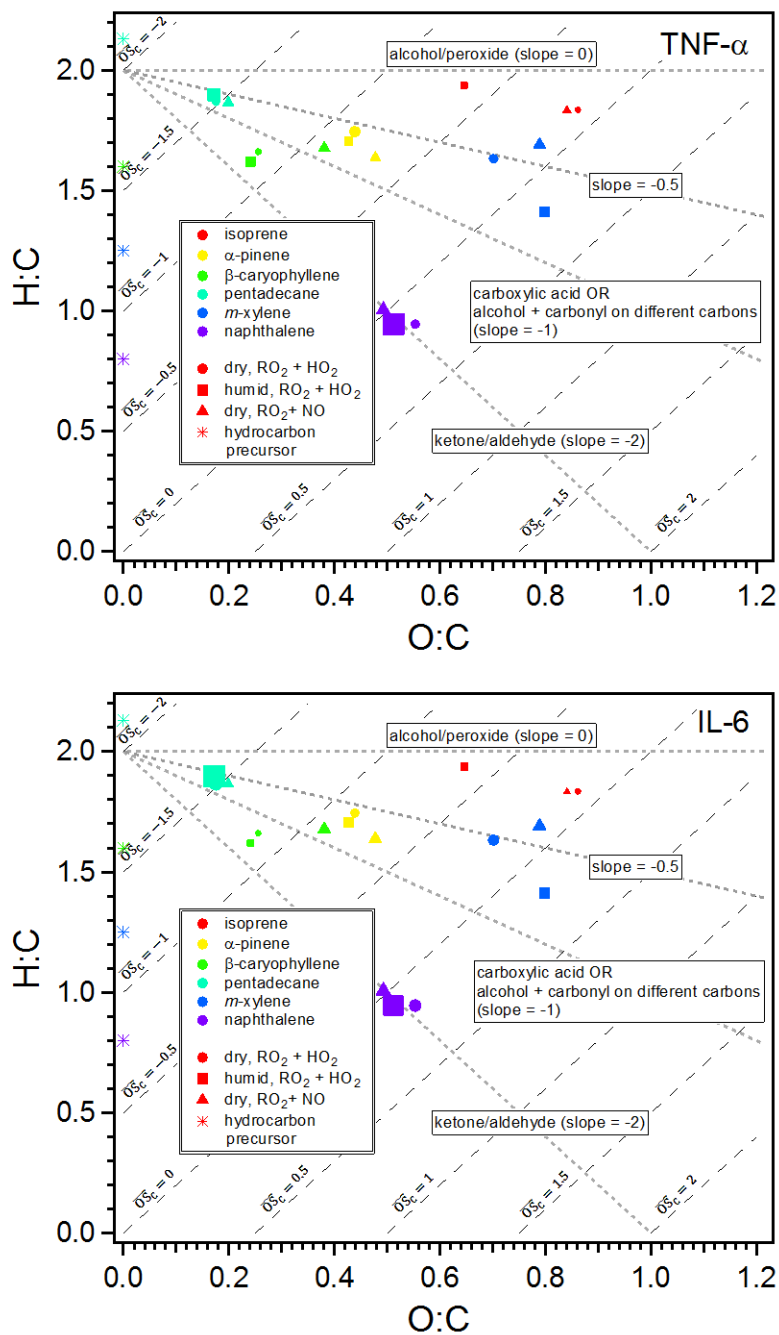


Figure C-3. van Krevelen plot for various SOA systems. Data points are colored by SOA system (red: isoprene, yellow: α-pinene, green: β-caryophyllene, light blue: pentadecane, blue: m-xylene, and purple: naphthalene), shaped according to formation conditions (circle: dry, RO₂ + HO₂; square: humid, RO₂ + HO₂; and triangle: dry, RO₂ + NO), and sized by TNF-α and IL-6 levels. SOA precursors are shown as stars, colored by SOA system.

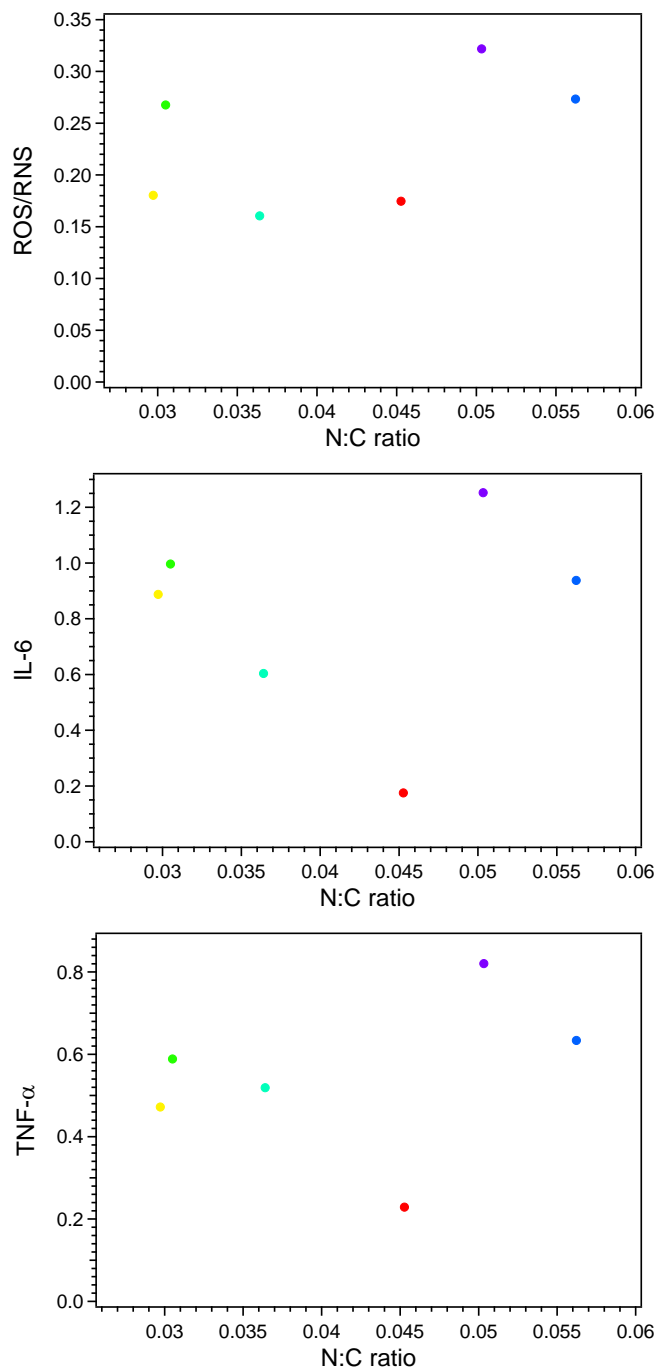
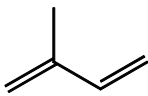
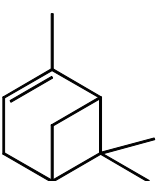
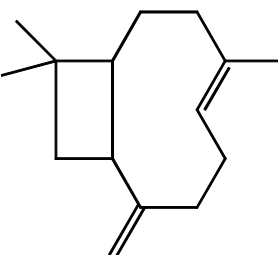
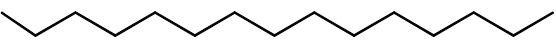
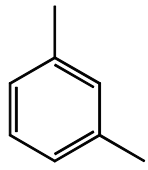
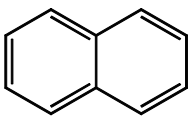


Figure C-4. ROS/RNS, TNF- α , and IL-6 (represented as AUC per μg) for various SOA systems spanning a wide range of N:C ratios. Data points are colored by SOA system (red: isoprene, yellow: α -pinene, green: β -caryophyllene, light blue: pentadecane, blue: *m*-xylene, and purple: naphthalene).

Table C-1. SOA precursor structures.

Compound	Structure
Isoprene	 <chem>CC(=C)C=C</chem>
α -pinene	 <chem>CC1=C(C)CC2=C1C=CC2</chem>
β -caryophyllene	 <chem>CC1=C(C)CCC2=C1C=CC3=C2C=CC3</chem>
Pentadecane	 <chem>CCCCCCCCCCCCCCC</chem>
m-xylene	 <chem>CC1=CC=C(C)C=C1</chem>
Naphthalene	 <chem>c1ccc2ccccc2c1</chem>

APPENDIX D: SUPPLEMENT FOR CHAPTER 5

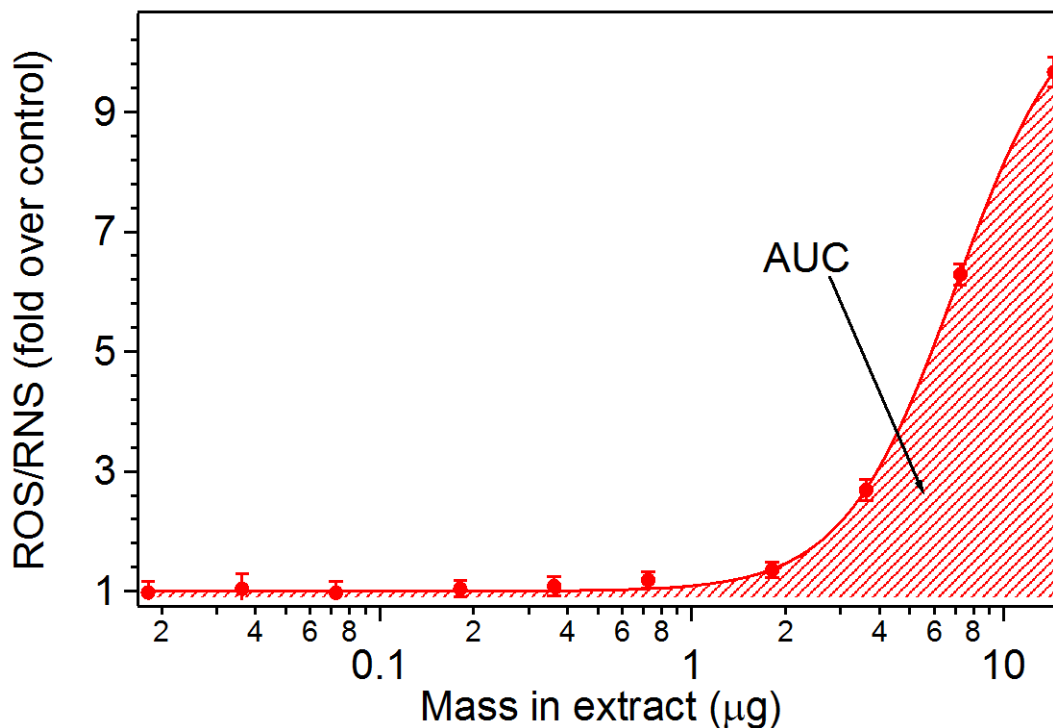


Figure D-1. Representative dose-response curve of ROS/RNS produced as a result of filter exposure (Expt. 7). ROS/RNS is expressed as a fold increase over control (probe-treated cells incubated with stimulant-free media); dose is expressed as mass in the filter extract (μg). Data shown are means \pm standard error of experiments performed in triplicate. The dose-response curve was fitted using the Hill equation and the area under the curve (AUC) is shown.

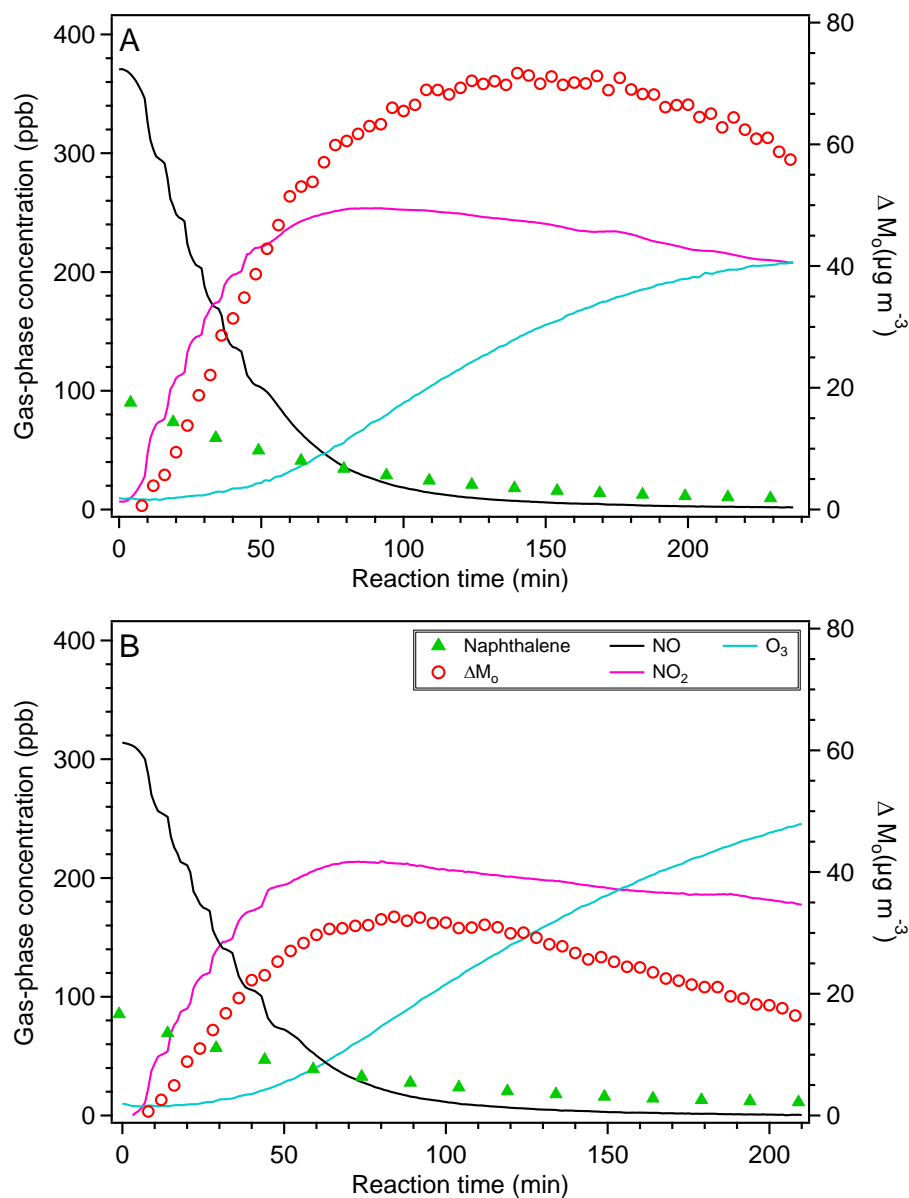


Figure D-2. Typical reaction profile for a chamber experiment under humid conditions in the presence of NO using A) ammonium sulfate seed particles (Expt. 3) and B) iron sulfate seed particles (Expt. 4). Naphthalene and NO concentrations were monitored using a GC-FID and chemiluminescence NO_x monitor, respectively. Aerosol mass concentrations were determined using SMPS volume concentration and assuming an aerosol density of 1 g cm⁻³. It should be noted that aerosol mass concentrations have not been corrected for particle wall loss.

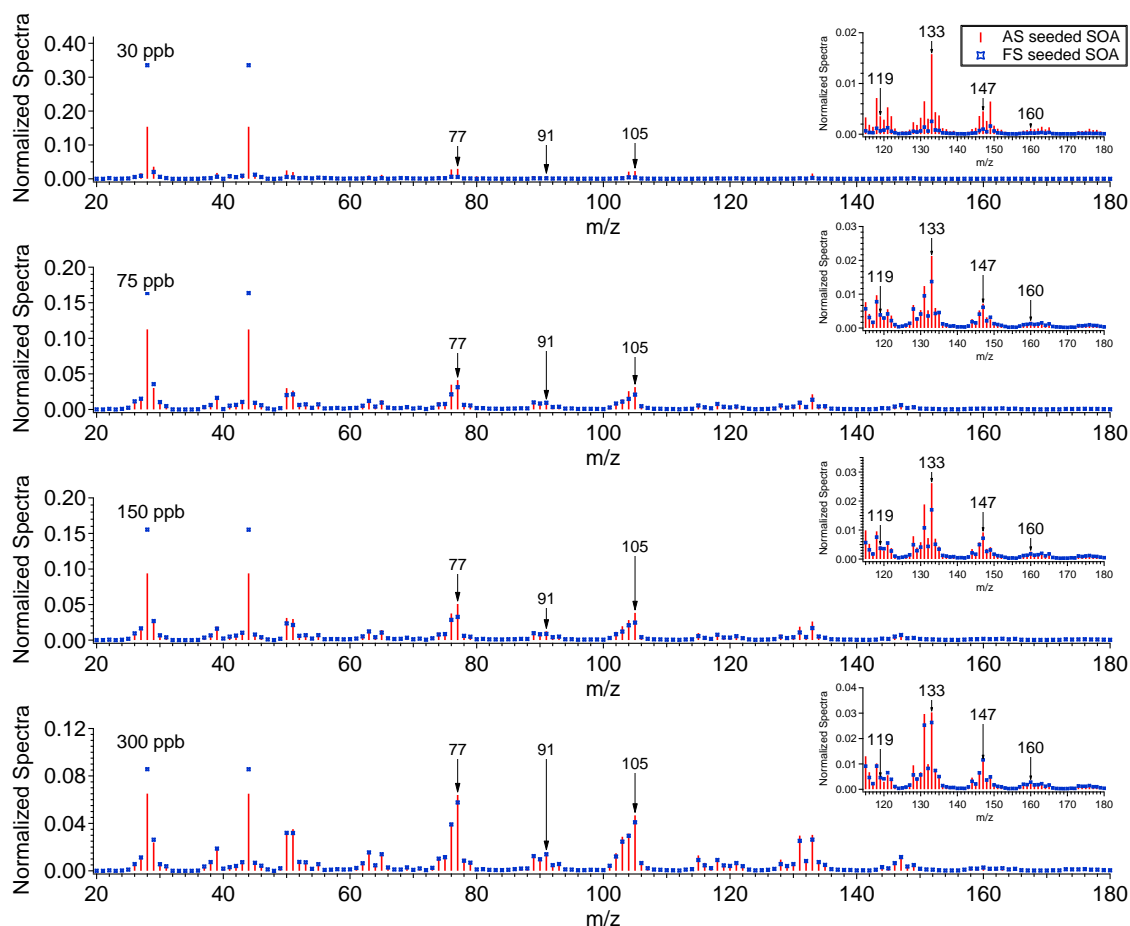


Figure D-3. Aerosol mass spectra of SOA formed from the photooxidation of naphthalene under humid conditions in the presence of NO using various seed (red bars: ammonium sulfate; blue markers: iron sulfate). Each row represents a different initial naphthalene concentration (30, 75, 150, and 300 ppb). Characteristics fragments are labeled. Ions greater than m/z 120 are shown in the inset of each mass spectrum.

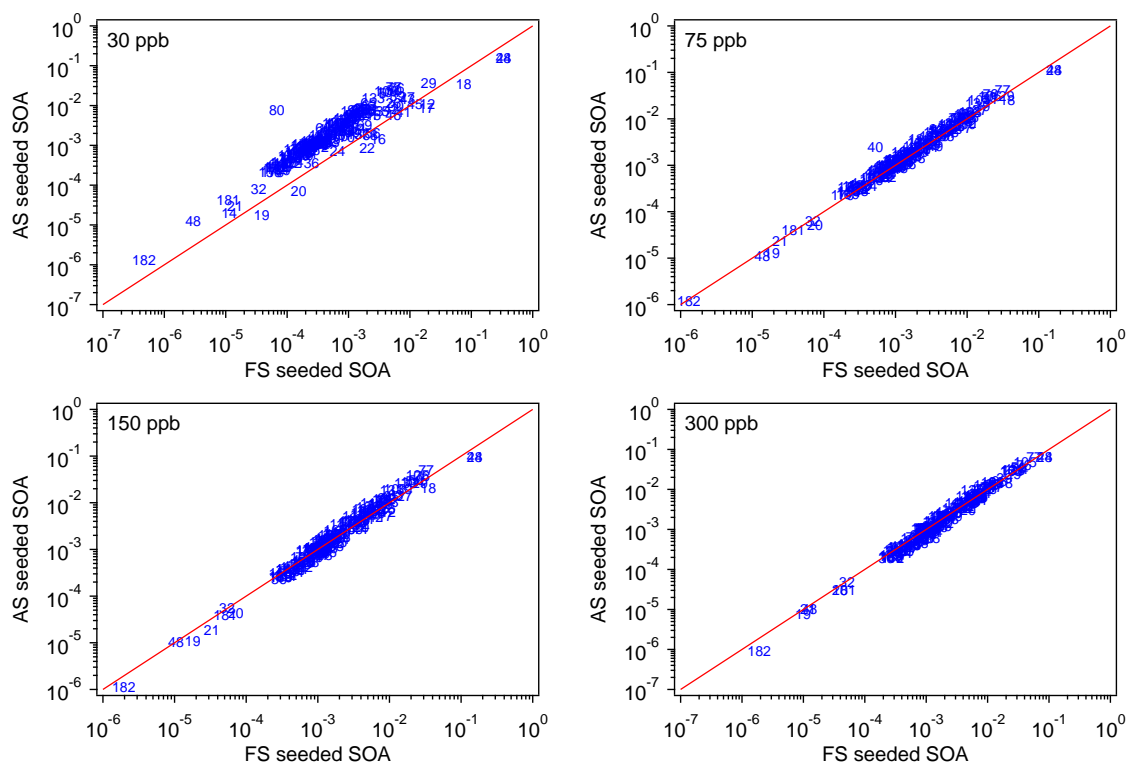


Figure D-4. Comparison between mass spectra of SOA formed from the photooxidation of naphthalene under humid conditions in the presence of NO using various seeds. A 1:1 line is shown for reference.

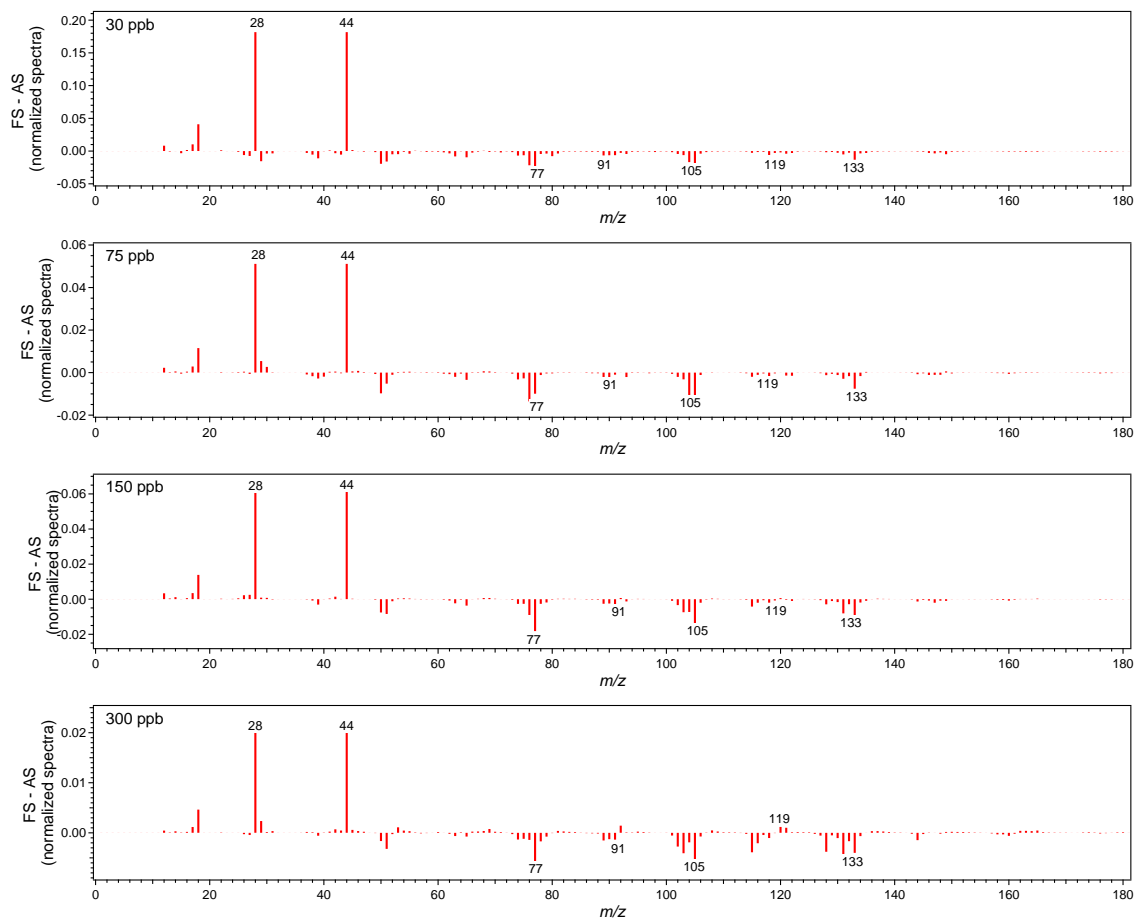


Figure D-5. Difference (FS seeded SOA – AS seeded SOA) between normalized mass spectra of SOA formed from the photooxidation of naphthalene under humid conditions in the presence of NO using various seeds.

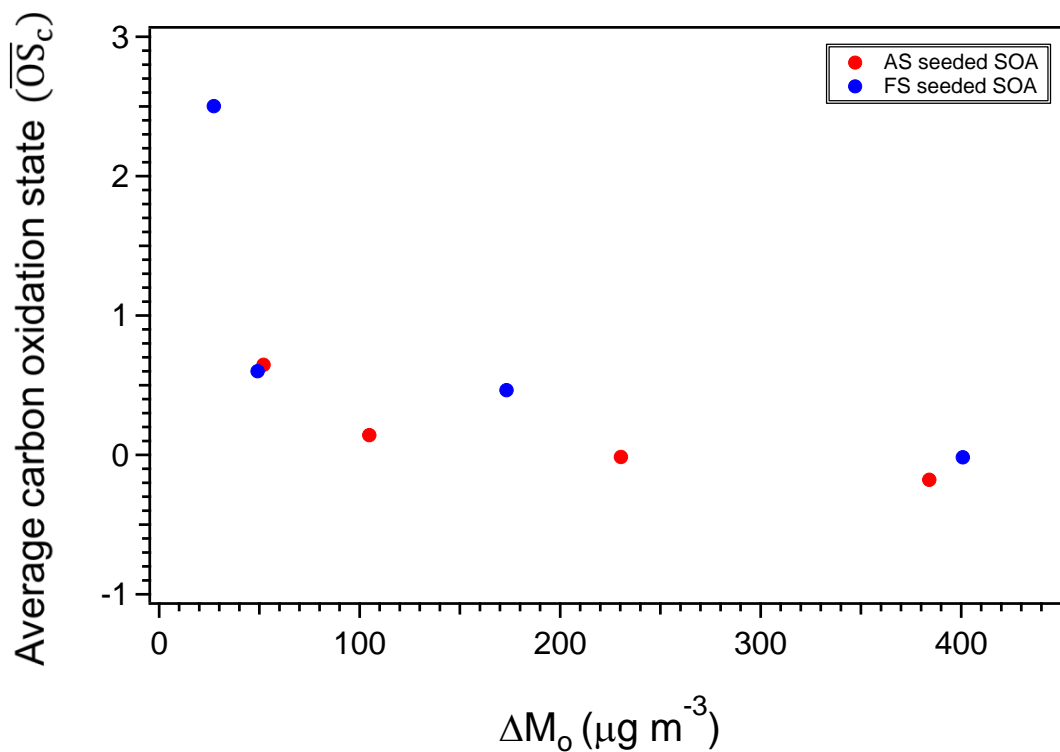


Figure D-6. Average carbon oxidation state (\overline{OS}_c) for naphthalene SOA spanning a range of organic mass loading (ΔM_o). SOA from this study was generated in a humid chamber in the presence of different seed particles (ammonium sulfate or iron sulfate), OH radical precursor (H_2O_2), and NO.

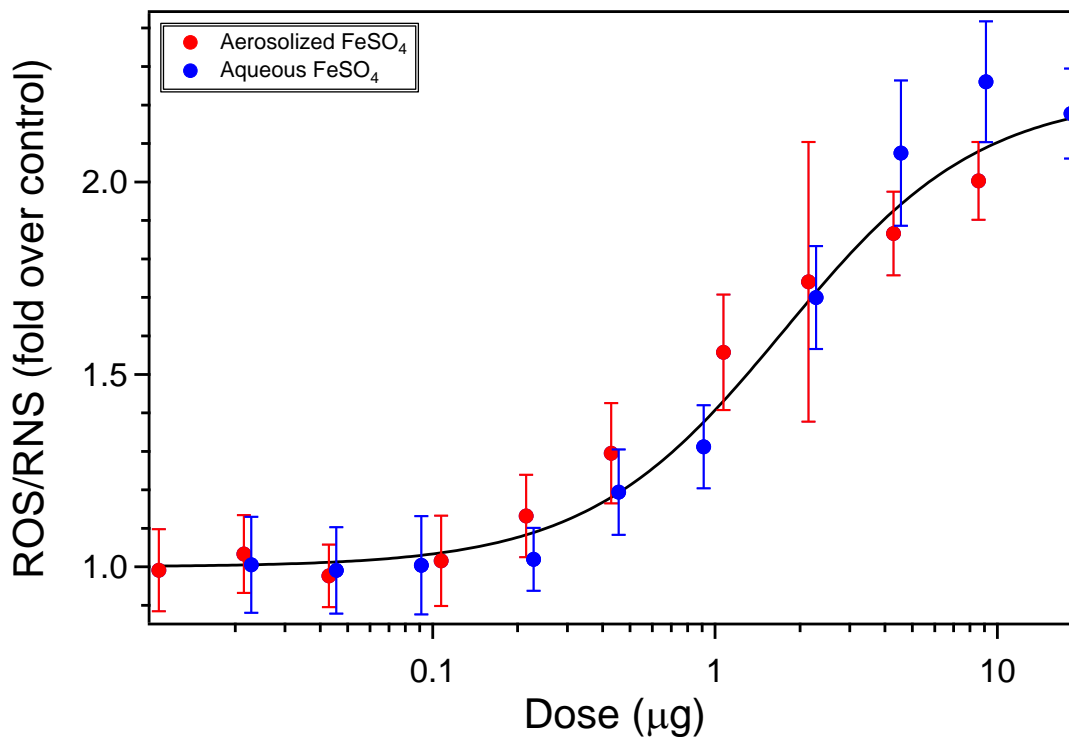


Figure D-7. ROS/RNS produced as a result of exposure to FeSO₄ (red: aerosolized into the chamber at experimental concentration, collected onto a filter, and extracted into media; blue: aqueous seed solution diluted in media). ROS/RNS is expressed as a fold increase over probe-treated control cells incubated with stimulant-free media. Data shown are means \pm standard error of triplicate exposure experiments.

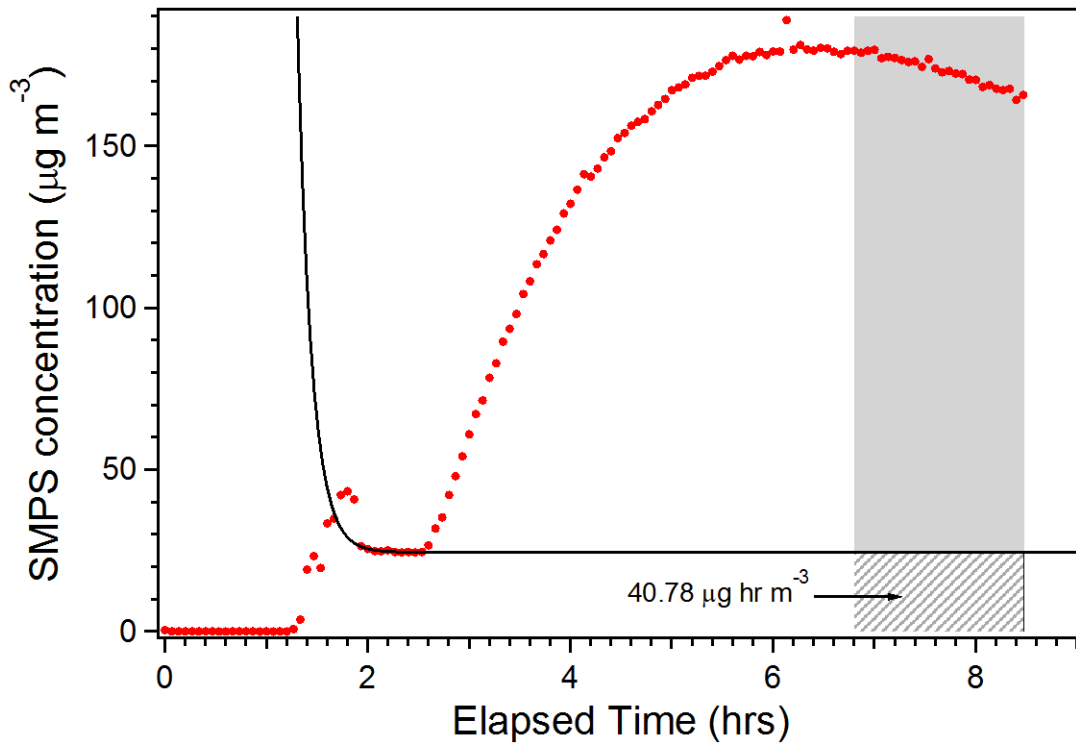


Figure D-8. Method for estimating the mass of seed collected onto each filter (Expt. 6). A double exponential was used to characterize seed particle wall loss (using seed concentrations obtained from the SMPS as a function of time). The fitted seed concentration as a function of time was then integrated over the filter collection period (shown as the shaded region). To obtain the total mass of seed collected, the integral ($40.78 \mu\text{g m}^{-3}$) was multiplied by the volumetric flow rate ($1.72 \text{ m}^3 \text{ hr}^{-1}$, for an estimated total seed mass of $70.14 \mu\text{g}$ on the filter for this experiment).

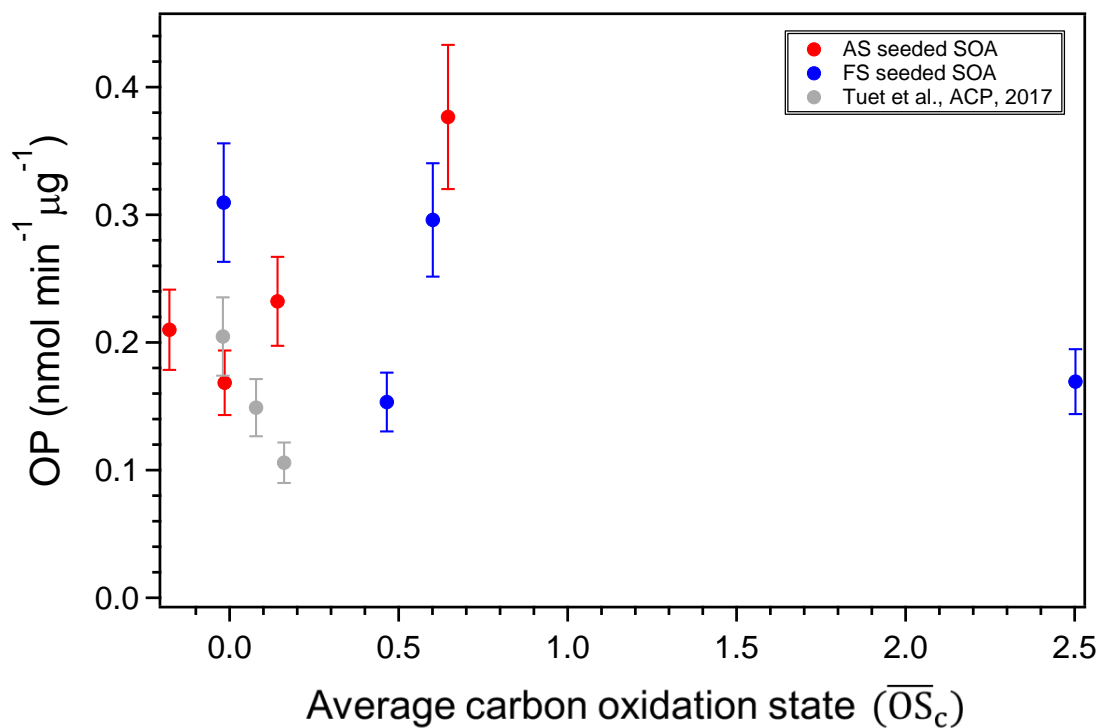


Figure D-9. Intrinsic OP for naphthalene SOA spanning a range of average carbon oxidation states (\overline{OS}_c). SOA from this study was generated in a humid chamber in the presence of different seed particles (ammonium sulfate or iron sulfate), OH radical precursor (H_2O_2), and NO. Error bars represent a 15% coefficient of variation (Fang et al., 2015c). Data from previous studies were included for comparison (Tuet et al., 2017b).

Table D-1. Elemental ratios (O:C, H:C, N:C) as determined by AMS.

Experiment	Hydrocarbon	Seed	[HC] ₀ (ppb)	O:C	H:C	N:C	\overline{OS}_c
1	naphthalene	AS ^a	32	0.78	0.99	0.015	0.58
2	naphthalene	FS ^b	32	1.59	0.77	0.012	2.4
3	naphthalene	AS ^a	92	0.56	0.98	0.012	0.13
4	naphthalene	FS ^b	84	0.78	0.98	0.014	0.58
5	naphthalene	AS ^a	186	0.48	0.98	0.010	-0.015
6	naphthalene	FS ^b	182	0.70	0.94	0.014	0.46
7	naphthalene	AS ^a	342	0.40	0.98	0.0091	-0.18
8	naphthalene	FS ^b	331	0.47	0.97	0.0093	-0.020

REFERENCES

- Akhtar, U. S., McWhinney, R. D., Rastogi, N., Abbatt, J. P. D., Evans, G. J., and Scott, J. A.: Cytotoxic and proinflammatory effects of ambient and source-related particulate matter (PM) in relation to the production of reactive oxygen species (ROS) and cytokine adsorption by particles, *Inhal. Toxicol.*, 22, 37-47, 2010.
- Allen, A. G., Nemitz, E., Shi, J. P., Harrison, R. M., and Greenwood, J. C.: Size distributions of trace metals in atmospheric aerosols in the United Kingdom, *Atmos. Environ.*, 35, 4581-4591, 10.1016/S1352-2310(01)00190-X, 2001.
- Anderson, J. O., Thundiyil, J. G., and Stolbach, A.: Clearing the Air: A Review of the Effects of Particulate Matter Air Pollution on Human Health, *Journal of Medical Toxicology*, 8, 166-175, 10.1007/s13181-011-0203-1, 2011.
- Antinolo, M., Willis, M. D., Zhou, S., and Abbatt, J. P. D.: Connecting the oxidation of soot to its redox cycling abilities, *Nat Commun*, 6, 10.1038/ncomms7812, 2015.
- Arashiro, M., Lin, Y. H., Sexton, K. G., Zhang, Z., Jaspers, I., Fry, R. C., Vizuite, W. G., Gold, A., and Surratt, J. D.: In Vitro Exposure to Isoprene-Derived Secondary Organic Aerosol by Direct Deposition and its Effects on COX-2 and IL-8 Gene Expression, *Atmos. Chem. Phys. Discuss.*, 2016, 1-29, 10.5194/acp-2016-371, 2016.
- Bahreini, R., Keywood, M. D., Ng, N. L., Varutbangkul, V., Gao, S., Flagan, R. C., Seinfeld, J. H., Worsnop, D. R., and Jimenez, J. L.: Measurements of Secondary Organic Aerosol from Oxidation of Cycloalkenes, Terpenes, and m-Xylene Using an Aerodyne Aerosol Mass Spectrometer, *Environmental Science & Technology*, 39, 5674-5688, 10.1021/es048061a, 2005.
- Bai, Y., Suzuki, A. K., and Sagai, M.: The cytotoxic effects of diesel exhaust particles on human pulmonary artery endothelial cells in vitro: role of active oxygen species, *Free Radical Biology and Medicine*, 30, 555-562, [http://dx.doi.org/10.1016/S0891-5849\(00\)00499-8](http://dx.doi.org/10.1016/S0891-5849(00)00499-8), 2001.
- Baird, W. M., Hooven, L. A., and Mahadevan, B.: Carcinogenic polycyclic aromatic hydrocarbon-DNA adducts and mechanism of action, *Environmental and Molecular Mutagenesis*, 45, 106-114, 10.1002/em.20095, 2005.
- Baltensperger, U., Dommen, J., Alfarra, R., Duplissy, J., Gaeggeler, K., Metzger, A., Facchini, M. C., Decesari, S., Finessi, E., Reinnig, C., Schott, M., Warnke, J., Hoffmann, T., Klatzer, B., Puxbaum, H., Geiser, M., Savi, M., Lang, D., Kalberer, M., and Geiser, T.: Combined determination of the chemical composition and of health effects of secondary organic aerosols: The POLYSOA project, *J. Aerosol Med. Pulm. Drug Deliv.*, 21, 145-154, 10.1089/jamp.2007.0655, 2008.

Barbosa Jr., F.: Toxicology of metals and metalloids: Promising issues for future studies in environmental health and toxicology, *Journal of Toxicology and Environmental Health, Part A*, 80, 137-144, 10.1080/15287394.2016.1259475, 2017.

Baritaki, S., Apostolakis, S., Kanellou, P., Dimanche-Boitrel, M. T., Spandidos, D. A., and Bonavida, B.: Reversal of Tumor Resistance to Apoptotic Stimuli by Alteration of Membrane Fluidity: Therapeutic Implications, in: *Advances in Cancer Research*, Academic Press, 149-190, 2007.

Bates, J. T., Weber, R. J., Abrams, J., Verma, V., Fang, T., Klein, M., Strickland, M. J., Sarnat, S. E., Chang, H. H., Mulholland, J. A., Tolbert, P. E., and Russell, A. G.: Reactive Oxygen Species Generation Linked to Sources of Atmospheric Particulate Matter and Cardiorespiratory Effects, *Environmental Science & Technology*, 49, 13605-13612, 10.1021/acs.est.5b02967, 2015.

Beam, A., and Motsinger-Reif, A.: Beyond IC(50)s: Towards Robust Statistical Methods for in vitro Association Studies, *Journal of pharmacogenomics & pharmacoproteomics*, 5, 1000121, 10.4172/2153-0645.1000121, 2014.

Becker, S., Dailey, L. A., Soukup, J. M., Grambow, S. C., Devlin, R. B., and Huang, Y. C. T.: Seasonal variations in air pollution particle-induced inflammatory mediator release and oxidative stress, *Environmental Health Perspectives*, 113, 1032-1038, 2005.

Bellavia, A., Urch, B., Speck, M., Brook, R. D., Scott, J. A., Albeti, B., Behbod, B., North, M., Valeri, L., Bertazzi, P. A., Silverman, F., Gold, D., and A. Baccarelli, A.: DNA Hypomethylation, Ambient Particulate Matter, and Increased Blood Pressure: Findings From Controlled Human Exposure Experiments, *Journal of the American Heart Association*, 2, 10.1161/jaha.113.000212, 2013.

Bermudez, E., Mangum, J. B., Wong, B. A., Asgharian, B., Hext, P. M., Warheit, D. B., and Everitt, J. I.: Pulmonary responses of mice, rats, and hamsters to subchronic inhalation of ultrafine titanium dioxide particles, *Toxicol. Sci.*, 77, 347-357, 10.1093/toxsci/kfh019, 2004.

Boyd, C. M., Sanchez, J., Xu, L., Eugene, A. J., Nah, T., Tuet, W. Y., Guzman, M. I., and Ng, N. L.: Secondary organic aerosol formation from the β -pinene+NO₃ system: effect of humidity and peroxy radical fate, *Atmos. Chem. Phys.*, 15, 7497-7522, 10.5194/acp-15-7497-2015, 2015.

Brunekreef, B., and Holgate, S. T.: Air pollution and health, *Lancet*, 360, 1233-1242, 2002.

Bruns, E. A., Perraud, V., Zelenyuk, A., Ezell, M. J., Johnson, S. N., Yu, Y., Imre, D., Finlayson-Pitts, B. J., and Alexander, M. L.: Comparison of FTIR and Particle Mass Spectrometry for the Measurement of Particulate Organic Nitrates, *Environmental Science & Technology*, 44, 1056-1061, 10.1021/es9029864, 2010.

Bruns, E. A., El Haddad, I., Slowik, J. G., Kilic, D., Klein, F., Baltensperger, U., and Prévôt, A. S. H.: Identification of significant precursor gases of secondary organic aerosols from residential wood combustion, *Scientific Reports*, 6, 27881, 10.1038/srep27881, 2016.

Burnett, R., Brook, J., Dann, T., Delocla, C., Philips, O., Cakmak, S., Vincent, R., Goldberg, M., and Krewski, D.: Association between particulate-and gas-phase components of urban air pollution and daily mortality in eight Canadian cities, 2001.

Calderón-Garcidueñas, L., Solt, A. C., Henríquez-Roldán, C., Torres-Jardón, R., Nuse, B., Herritt, L., Villarreal-Calderón, R., Osnaya, N., Stone, I., García, R., Brooks, D. M., González-Maciel, A., Reynoso-Robles, R., Delgado-Chávez, R., and Reed, W.: Long-term Air Pollution Exposure Is Associated with Neuroinflammation, an Altered Innate Immune Response, Disruption of the Blood-Brain Barrier, Ultrafine Particulate Deposition, and Accumulation of Amyloid β -42 and α -Synuclein in Children and Young Adults, *Toxicologic Pathology*, 36, 289-310, 10.1177/0192623307313011, 2008.

Canagaratna, M. R., Jimenez, J. L., Kroll, J. H., Chen, Q., Kessler, S. H., Massoli, P., Hildebrandt Ruiz, L., Fortner, E., Williams, L. R., Wilson, K. R., Surratt, J. D., Donahue, N. M., Jayne, J. T., and Worsnop, D. R.: Elemental ratio measurements of organic compounds using aerosol mass spectrometry: characterization, improved calibration, and implications, *Atmos. Chem. Phys.*, 15, 253-272, 10.5194/acp-15-253-2015, 2015.

Castro, L., and Freeman, B. A.: Reactive oxygen species in human health and disease, *Nutrition*, 17, 161-165, 2001.

Cerezo, J., Zúñiga, J., Bastida, A., Requena, A., and Cerón-Carrasco, J. P.: Atomistic Molecular Dynamics Simulations of the Interactions of Oleic and 2-Hydroxyoleic Acids with Phosphatidylcholine Bilayers, *The Journal of Physical Chemistry B*, 115, 11727-11738, 10.1021/jp203498x, 2011.

Chan, A. W. H., Kautzman, K. E., Chhabra, P. S., Surratt, J. D., Chan, M. N., Crounse, J. D., Kurten, A., Wennberg, P. O., Flagan, R. C., and Seinfeld, J. H.: Secondary organic aerosol formation from photooxidation of naphthalene and alkylnaphthalenes: implications for oxidation of intermediate volatility organic compounds (IVOCs), *Atmos. Chem. Phys.*, 9, 3049-3060, 2009.

Chan, A. W. H., Chan, M. N., Surratt, J. D., Chhabra, P. S., Loza, C. L., Crounse, J. D., Yee, L. D., Flagan, R. C., Wennberg, P. O., and Seinfeld, J. H.: Role of aldehyde chemistry and NO_x concentrations in secondary organic aerosol formation, *Atmos. Chem. Phys.*, 10, 7169-7188, 10.5194/acp-10-7169-2010, 2010.

Chan, M. N., Surratt, J. D., Chan, A. W. H., Schilling, K., Offenberg, J. H., Lewandowski, M., Edney, E. O., Kleindienst, T. E., Jaoui, M., Edgerton, E. S., Tanner, R. L., Shaw, S. L., Zheng, M., Knipping, E. M., and Seinfeld, J. H.: Influence of aerosol acidity on the chemical composition of secondary organic aerosol from β -caryophyllene, *Atmos. Chem. Phys.*, 11, 1735-1751, 10.5194/acp-11-1735-2011, 2011.

Charrier, J. G., and Anastasio, C.: On dithiothreitol (DTT) as a measure of oxidative potential for ambient particles: evidence for the importance of soluble transition metals, *Atmos. Chem. Phys.*, 12, 9321-9333, 10.5194/acp-12-9321-2012, 2012.

Charrier, J. G., Richards-Henderson, N. K., Bein, K. J., McFall, A. S., Wexler, A. S., and Anastasio, C.: Oxidant production from source-oriented particulate matter – Part 1: Oxidative potential using the dithiothreitol (DTT) assay, *Atmos. Chem. Phys.*, 15, 2327-2340, 10.5194/acp-15-2327-2015, 2015.

Chen, C. Y., Peng, W. H., Tsai, K. D., and Hsu, S. L.: Luteolin suppresses inflammation-associated gene expression by blocking NF-kappa B and AP-1 activation pathway in mouse alveolar macrophages, *Life Sci.*, 81, 1602-1614, 10.1016/j.lfs.2007.09.028, 2007.

Chen, X. P., Zhong, Z. F., Xu, Z. T., Chen, L. D., and Wang, Y. T.: 2',7'-Dichlorodihydrofluorescein as a fluorescent probe for reactive oxygen species measurement: Forty years of application and controversy, *Free Radic. Res.*, 44, 587-604, 10.3109/10715761003709802, 2010.

Chevion, M.: A site-specific mechanism for free radical induced biological damage: the essential role of redox-active transition metals, *Free Radical Biology and Medicine*, 5, 27-37, 1988.

Chhabra, P. S., Flagan, R. C., and Seinfeld, J. H.: Elemental analysis of chamber organic aerosol using an aerodyne high-resolution aerosol mass spectrometer, *Atmos. Chem. Phys.*, 10, 4111-4131, 10.5194/acp-10-4111-2010, 2010.

Chhabra, P. S., Ng, N. L., Canagaratna, M. R., Corrigan, A. L., Russell, L. M., Worsnop, D. R., Flagan, R. C., and Seinfeld, J. H.: Elemental composition and oxidation of chamber organic aerosol, *Atmos. Chem. Phys.*, 11, 8827-8845, 10.5194/acp-11-8827-2011, 2011.

Chiang, S. S., Ulziijargal, E., Chien, R. C., and Mau, J. L.: Antioxidant and Anti-Inflammatory Properties of Solid-State Fermented Products from a Medicinal Mushroom, *Taiwanofungus salmoneus* (Higher Basidiomycetes) from Taiwan, *International journal of medicinal mushrooms*, 17, 2015.

Cho, A. K., Sioutas, C., Miguel, A. H., Kumagai, Y., Schmitz, D. A., Singh, M., Eiguen-Fernandez, A., and Froines, J. R.: Redox activity of airborne particulate matter at different sites in the Los Angeles Basin, *Environmental Research*, 99, 40-47, 10.1016/j.envres.2005.01.003, 2005.

Chu, B., Hao, J., Takekawa, H., Li, J., Wang, K., and Jiang, J.: The remarkable effect of FeSO₄ seed aerosols on secondary organic aerosol formation from photooxidation of α -pinene/NO_x and toluene/NO_x, *Atmos. Environ.*, 55, 26-34, 10.1016/j.atmosenv.2012.03.006, 2012.

Chu, B., Liu, Y., Li, J., Takekawa, H., Liggio, J., Li, S. M., Jiang, J., Hao, J., and He, H.: Decreasing effect and mechanism of FeSO₄ seed particles on secondary organic aerosol in

α -pinene photooxidation, *Environmental Pollution*, 193, 88-93, 10.1016/j.envpol.2014.06.018, 2014.

Chu, B., Liggiio, J., Liu, Y., He, H., Takekawa, H., Li, S.-M., and Hao, J.: Influence of metal-mediated aerosol-phase oxidation on secondary organic aerosol formation from the ozonolysis and OH-oxidation of α -pinene, *Scientific Reports*, 7, 40311, 10.1038/srep40311, 2017.

Cocker III, D. R., Mader, B. T., Kalberer, M., Flagan, R. C., and Seinfeld, J. H.: The effect of water on gas-particle partitioning of secondary organic aerosol: II. m-xylene and 1,3,5-trimethylbenzene photooxidation systems, *Atmos. Environ.*, 35, 6073-6085, [http://dx.doi.org/10.1016/S1352-2310\(01\)00405-8](http://dx.doi.org/10.1016/S1352-2310(01)00405-8), 2001.

Conny, J. M., and Slater, J. F.: Black carbon and organic carbon in aerosol particles from crown fires in the Canadian boreal forest, *Journal of Geophysical Research: Atmospheres*, 107, AAC 4-1-AAC 4-12, 10.1029/2001JD001528, 2002.

Conroy, L. E., and Park, K. C.: Electrical properties of the Group IV disulfides, titanium disulfide, zirconium disulfide, hafnium disulfide and tin disulfide, *Inorganic Chemistry*, 7, 459-463, 10.1021/ic50061a015, 1968.

Daher, N., Ruprecht, A., Invernizzi, G., De Marco, C., Miller-Schulze, J., Heo, J. B., Shafer, M. M., Shelton, B. R., Schauer, J. J., and Sioutas, C.: Characterization, sources and redox activity of fine and coarse particulate matter in Milan, Italy, *Atmos. Environ.*, 49, 130-141, 10.1016/j.atmosenv.2011.12.011, 2012.

Daher, N., Saliba, N. A., Shihadeh, A. L., Jaafar, M., Baalbaki, R., Shafer, M. M., Schauer, J. J., and Sioutas, C.: Oxidative potential and chemical speciation of size-resolved particulate matter (PM) at near-freeway and urban background sites in the greater Beirut area, *Sci. Total Environ.*, 470, 417-426, 10.1016/j.scitotenv.2013.09.104, 2014.

Daumit, K. E., Carrasquillo, A. J., Sugrue, R. A., and Kroll, J. H.: Effects of Condensed-Phase Oxidants on Secondary Organic Aerosol Formation, *The Journal of Physical Chemistry A*, 120, 1386-1394, 10.1021/acs.jpca.5b06160, 2016.

DeCarlo, P. F., Kimmel, J. R., Trimborn, A., Northway, M. J., Jayne, J. T., Aiken, A. C., Gonin, M., Fuhrer, K., Horvath, T., Docherty, K. S., Worsnop, D. R., and Jimenez, J. L.: Field-Deployable, High-Resolution, Time-of-Flight Aerosol Mass Spectrometer, *Analytical Chemistry*, 78, 8281-8289, 10.1021/ac061249n, 2006.

Dockery, D. W., Pope, C. A., Xu, X., Spengler, J. D., Ware, J. H., Fay, M. E., Ferris, B. G., and Speizer, F. E.: An Association between Air Pollution and Mortality in Six U.S. Cities, *New England Journal of Medicine*, 329, 1753-1759, 10.1056/NEJM199312093292401, 1993.

Donahue, N. M., Robinson, A. L., Stanier, C. O., and Pandis, S. N.: Coupled Partitioning, Dilution, and Chemical Aging of Semivolatile Organics, *Environmental Science & Technology*, 40, 2635-2643, 10.1021/es052297c, 2006.

Dou, J., Lin, P., Kuang, B. Y., and Yu, J. Z.: Reactive Oxygen Species Production Mediated by Humic-like Substances in Atmospheric Aerosols: Enhancement Effects by Pyridine, Imidazole, and Their Derivatives, *Environmental Science & Technology*, 49, 6457-6465, 10.1021/es5059378, 2015.

Eddingsaas, N. C., Loza, C. L., Yee, L. D., Chan, M., Schilling, K. A., Chhabra, P. S., Seinfeld, J. H., and Wennberg, P. O.: α -pinene photooxidation under controlled chemical conditions – Part 2: SOA yield and composition in low- and high-NOx environments, *Atmos. Chem. Phys.*, 12, 7413-7427, 10.5194/acp-12-7413-2012, 2012.

Edney, E. O., Driscoll, D. J., Speer, R. E., Weathers, W. S., Kleindienst, T. E., Li, W., and Smith, D. F.: Impact of aerosol liquid water on secondary organic aerosol yields of irradiated toluene/propylene/NOx/(NH₄)₂SO₄/air mixtures, *Atmos. Environ.*, 34, 3907-3919, [http://dx.doi.org/10.1016/S1352-2310\(00\)00174-6](http://dx.doi.org/10.1016/S1352-2310(00)00174-6), 2000.

Espinosa, A. J. F., Ternero Rodríguez, M., Barragán de la Rosa, F. J., and Jiménez Sánchez, J. C.: Size distribution of metals in urban aerosols in Seville (Spain), *Atmos. Environ.*, 35, 2595-2601, 10.1016/S1352-2310(00)00403-9, 2001.

Fallahi-Sichani, M., Honarnejad, S., Heiser, L. M., Gray, J. W., and Sorger, P. K.: Metrics other than potency reveal systematic variation in responses to cancer drugs, *Nature chemical biology*, 9, 708-714, 10.1038/nchembio.1337, 2013.

Fang, T., Guo, H., Verma, V., Peltier, R. E., and Weber, R. J.: PM_{2.5} water-soluble elements in the southeastern United States: automated analytical method development, spatiotemporal distributions, source apportionment, and implications for health studies, *Atmos. Chem. Phys.*, 15, 11667-11682, 10.5194/acp-15-11667-2015, 2015a.

Fang, T., Verma, V., Bates, J., Abrams, J., Klein, M., Strickland, M., Sarnat, S., Chang, H., Mulholland, J., and Tolbert, P.: Oxidative potential of ambient water-soluble PM_{2.5} measured by Dithiothreitol (DTT) and Ascorbic Acid (AA) assays in the southeastern United States: contrasts in sources and health associations, *Atmospheric Chemistry and Physics Discussions*, 15, 30609-30644, 2015b.

Fang, T., Verma, V., Guo, H., King, L. E., Edgerton, E. S., and Weber, R. J.: A semi-automated system for quantifying the oxidative potential of ambient particles in aqueous extracts using the dithiothreitol (DTT) assay: results from the Southeastern Center for Air Pollution and Epidemiology (SCAPE), *Atmos. Meas. Tech.*, 8, 471-482, 10.5194/amt-8-471-2015, 2015c.

Fang, T., Verma, V., Bates, J. T., Abrams, J., Klein, M., Strickland, M. J., Sarnat, S. E., Chang, H. H., Mulholland, J. A., Tolbert, P. E., Russell, A. G., and Weber, R. J.: Oxidative potential of ambient water-soluble PM_{2.5} in the southeastern United States: contrasts in sources and health associations between ascorbic acid (AA) and dithiothreitol (DTT) assays, *Atmos. Chem. Phys.*, 16, 3865-3879, 10.5194/acp-16-3865-2016, 2016.

Fang, T., Guo, H., Zeng, L., Verma, V., Nenes, A., and Weber, R. J.: Highly Acidic Ambient Particles, Soluble Metals, and Oxidative Potential: A Link between Sulfate and

Aerosol Toxicity, Environmental Science & Technology, 51, 2611-2620, 10.1021/acs.est.6b06151, 2017a.

Fang, T., Zeng, L., Gao, D., Verma, V., Stefaniak, A. B., and Weber, R. J.: Ambient Size Distributions and Lung Deposition of Aerosol Dithiothreitol-Measured Oxidative Potential: Contrast between Soluble and Insoluble Particles, Environmental Science & Technology, 51, 6802-6811, 10.1021/acs.est.7b01536, 2017b.

Farmer, D. K., Matsunaga, A., Docherty, K. S., Surratt, J. D., Seinfeld, J. H., Ziemann, P. J., and Jimenez, J. L.: Response of an aerosol mass spectrometer to organonitrates and organosulfates and implications for atmospheric chemistry, Proceedings of the National Academy of Sciences, 107, 6670-6675, 10.1073/pnas.0912340107, 2010.

Frei, B.: Reactive oxygen species and antioxidant vitamins: Mechanisms of action, The American Journal of Medicine, 97, S5-S13, 10.1016/0002-9343(94)90292-5, 1994.

Fry, J. L., Kiendler-Scharr, A., Rollins, A. W., Wooldridge, P. J., Brown, S. S., Fuchs, H., Dubé, W., Mensah, A., dal Maso, M., Tillmann, R., Dorn, H. P., Brauers, T., and Cohen, R. C.: Organic nitrate and secondary organic aerosol yield from NO₃ oxidation of β -pinene evaluated using a gas-phase kinetics/aerosol partitioning model, Atmos. Chem. Phys., 9, 1431-1449, 10.5194/acp-9-1431-2009, 2009.

Fubini, B., and Hubbard, A.: Reactive oxygen species (ROS) and reactive nitrogen species (RNS) generation by silica in inflammation and fibrosis, Free Radical Biology and Medicine, 34, 1507-1516, [http://dx.doi.org/10.1016/S0891-5849\(03\)00149-7](http://dx.doi.org/10.1016/S0891-5849(03)00149-7), 2003.

Gakidou, E., Afshin, A., Abajobir, A. A., Abate, K. H., Abbafati, C., Abbas, K. M., Abd-Allah, F., Abdulle, A. M., Abera, S. F., Aboyans, V., Abu-Raddad, L. J., Abu-Rmeileh, N. M. E., Abyu, G. Y., Adedeji, I. A., Adetokunboh, O., Afarideh, M., Agrawal, A., Agrawal, S., Ahmadieh, H., Ahmed, M. B., Aichour, M. T. E., Aichour, A. N., Aichour, I., Akinyemi, R. O., Akseer, N., Alahdab, F., Al-Aly, Z., Alam, K., Alam, N., Alam, T., Alasfoor, D., Alene, K. A., Ali, K., Alizadeh-Navaei, R., Alkerwi, A. a., Alla, F., Allebeck, P., Al-Raddadi, R., Alsharif, U., Altirkawi, K. A., Alvis-Guzman, N., Amare, A. T., Amini, E., Ammar, W., Amoako, Y. A., Ansari, H., Antó, J. M., Antonio, C. A. T., Anwari, P., Arian, N., Ärnlöv, J., Artaman, A., Aryal, K. K., Asayesh, H., Asgedom, S. W., Atey, T. M., Avila-Burgos, L., Avokpaho, E. F. G. A., Awasthi, A., Azzopardi, P., Bacha, U., Badawi, A., Balakrishnan, K., Ballew, S. H., Barac, A., Barber, R. M., Barker-Collo, S. L., Barnighausen, T., Barquera, S., Barregard, L., Barrero, L. H., Batis, C., Battle, K. E., Baumgarner, B. R., Baune, B. T., Beardsley, J., Bedi, N., Beghi, E., Bell, M. L., Bennett, D. A., Bennett, J. R., Bensenor, I. M., Berhane, A., Berhe, D. F., Bernabé, E., Betsu, B. D., Beuran, M., Beyene, A. S., Bhansali, A., Bhutta, Z. A., Bicer, B. K., Bikbov, B., Birungi, C., Biryukov, S., Blosser, C. D., Boneya, D. J., Bou-Orm, I. R., Brauer, M., Breitborde, N. J. K., Brenner, H., Brugha, T. S., Bulto, L. N. B., Butt, Z. A., Cahuana-Hurtado, L., Cárdenas, R., Carrero, J. J., Castañeda-Orjuela, C. A., Catalá-López, F., Cercy, K., Chang, H.-Y., Charlson, F. J., Chimed-Ochir, O., Chisumpa, V. H., Chitheer, A. A., Christensen, H., Christopher, D. J., Cirillo, M., Cohen, A. J., Comfort, H., Cooper, C., Coresh, J., Cornaby, L., Cortesi, P. A., Criqui, M. H., Crump, J. A., Dandona, L., Dandona, R., das

Neves, J., Davey, G., Davitoiu, D. V., Davletov, K., de Courten, B., Defo, B. K., Degenhardt, L., Deiparine, S., Dellavalle, R. P., Deribe, K., Deshpande, A., Dharmaratne, S. D., Ding, E. L., Djalalinia, S., Do, H. P., Dokova, K., Doku, D. T., Donkelaar, A. v., Dorsey, E. R., Driscoll, T. R., Dubey, M., Duncan, B. B., Duncan, S., Ebrahimi, H., El-Khatib, Z. Z., Enayati, A., Endries, A. Y., Ermakov, S. P., Erskine, H. E., Eshrati, B., Eskandarieh, S., Esteghamati, A., Estep, K., Faraon, E. J. A., Farinha, C. S. e. S., Faro, A., Farzadfar, F., Fay, K., Feigin, V. L., Fereshtehnejad, S.-M., Fernandes, J. C., Ferrari, A. J., Feyissa, T. R., Filip, I., Fischer, F., Fitzmaurice, C., Flaxman, A. D., Foigt, N., Foreman, K. J., Frostad, J. J., Fullman, N., Fürst, T., Furtado, J. M., Ganji, M., Garcia-Basteiro, A. L., Gebrehiwot, T. T., Geleijnse, J. M., Geleto, A., Gemechu, B. L., Gesesew, H. A., Gething, P. W., Ghajar, A., Gibney, K. B., Gill, P. S., Gillum, R. F., Giref, A. Z., Gishu, M. D., Giussani, G., Godwin, W. W., Gona, P. N., Goodridge, A., Gopalani, S. V., Goryakin, Y., Goulart, A. C., Graetz, N., Gughani, H. C., Guo, J., Gupta, R., Gupta, T., Gupta, V., Gutiérrez, R. A., Hachinski, V., Hafezi-Nejad, N., Hailu, G. B., Hamadeh, R. R., Hamidi, S., Hammami, M., Handal, A. J., Hankey, G. J., Hanson, S. W., Harb, H. L., Hareri, H. A., Hassanvand, M. S., Havmoeller, R., Hawley, C., Hay, S. I., Hedayati, M. T., Hendrie, D., Heredia-Pi, I. B., Hernandez, J. C. M., Hoek, H. W., Horita, N., Hosgood, H. D., Hostiuc, S., Hoy, D. G., Hsairi, M., Hu, G., Huang, J. J., Huang, H., Ibrahim, N. M., Iburg, K. M., Ikeda, C., Inoue, M., Irvine, C. M. S., Jackson, M. D., Jacobsen, K. H., Jahanmehr, N., Jakovljevic, M. B., Jauregui, A., Javanbakht, M., Jeemon, P., Johansson, L. R. K., Johnson, C. O., Jonas, J. B., Jürisson, M., Kabir, Z., Kadel, R., Kahsay, A., Kamal, R., Karch, A., Karema, C. K., Kasaeian, A., Kassebaum, N. J., Kastor, A., Katikireddi, S. V., Kawakami, N., Keiyoro, P. N., Kelbore, S. G., Kemmer, L., Kengne, A. P., Kesavachandran, C. N., Khader, Y. S., Khalil, I. A., Khan, E. A., Khang, Y.-H., Khosravi, A., Khubchandani, J., Kiadaliri, A. A., Kieling, C., Kim, J. Y., Kim, Y. J., Kim, D., Kimokoti, R. W., Kinfu, Y., Kisa, A., Kissimova-Skarbek, K. A., Kivimaki, M., Knibbs, L. D., Knudsen, A. K., Kopec, J. A., Kosen, S., Koul, P. A., Koyanagi, A., Kravchenko, M., Krohn, K. J., Kromhout, H., Kumar, G. A., Kutz, M., Kyu, H. H., Lal, D. K., Lalloo, R., Lallukka, T., Lan, Q., Lansingh, V. C., Larsson, A., Lee, P. H., Lee, A., Leigh, J., Leung, J., Levi, M., Levy, T. S., Li, Y., Li, Y., Liang, X., Liben, M. L., Linn, S., Liu, P., Lodha, R., Logroscino, G., Looker, K. J., Lopez, A. D., Lorkowski, S., Lotufo, P. A., Lozano, R., Lunevicius, R., Macarayan, E. R. K., Magdy Abd El Razek, H., Magdy Abd El Razek, M., Majdan, M., Majdzadeh, R., Majeed, A., Malekzadeh, R., Malhotra, R., Malta, D. C., Mamun, A. A., Manguerra, H., Mantovani, L. G., Mapoma, C. C., Martin, R. V., Martinez-Raga, J., Martins-Melo, F. R., Mathur, M. R., Matsushita, K., Matzopoulos, R., Mazidi, M., McAlinden, C., McGrath, J. J., Mehata, S., Mehndiratta, M. M., Meier, T., Melaku, Y. A., Memiah, P., Memish, Z. A., Mendoza, W., Mengesha, M. M., Mensah, G. A., Mensink, G. B. M., Mereta, S. T., Meretoja, T. J., Meretoja, A., Mezgebe, H. B., Micha, R., Millear, A., Miller, T. R., Minnig, S., Mirarefin, M., Mirrakhimov, E. M., Misganaw, A., Mishra, S. R., Mohammad, K. A., Mohammed, K. E., Mohammed, S., Mohan, M. B. V., Mokdad, A. H., Monasta, L., Montico, M., Moradi-Lakeh, M., Moraga, P., Morawska, L., Morrison, S. D., Mountjoy-Venning, C., Mueller, U. O., Mullany, E. C., Muller, K., Murthy, G. V. S., Musa, K. I., Naghavi, M., Naheed, A., Nangia, V., Natarajan, G., Negoi, R. I., Negoi, I., Nguyen, C. T., Nguyen, Q. L., Nguyen, T. H., Nguyen, G., Nguyen, M., Nichols, E., Ningrum, D. N. A., Nomura, M., Nong, V. M., Norheim, O. F., Norrving, B., Noubiap, J. J. N., Obermeyer, C. M., Ogbo, F. A., Oh, I.-H., Oladimeji, O., Olagunju, A.

T., Olagunju, T. O., Olivares, P. R., Olsen, H. E., Olusanya, B. O., Olusanya, J. O., Opio, J. N., Oren, E., Ortiz, A., Ota, E., Owolabi, M. O., Pa, M., Pacella, R. E., Pana, A., Panda, B. K., Panda-Jonas, S., Pandian, J. D., Papachristou, C., Park, E.-K., Parry, C. D., Patten, S. B., Patton, G. C., Pereira, D. M., Perico, N., Pesudovs, K., Petzold, M., Phillips, M. R., Pillay, J. D., Piradov, M. A., Pishgar, F., Plass, D., Pletcher, M. A., Polinder, S., Popova, S., Poulton, R. G., Pourmalek, F., Prasad, N., Purcell, C., Qorbani, M., Radfar, A., Rafay, A., Rahimi-Movaghar, A., Rahimi-Movaghar, V., Rahman, M. H. U., Rahman, M. A., Rahman, M., Rai, R. K., Rajsic, S., Ram, U., Rawaf, S., Rehm, C. D., Rehm, J., Reiner, R. C., Reitsma, M. B., Remuzzi, G., Renzaho, A. M. N., Resnikoff, S., Reynales-Shigematsu, L. M., Rezaei, S., Ribeiro, A. L., Rivera, J. A., Roba, K. T., Rojas-Rueda, D., Roman, Y., Room, R., Roshandel, G., Roth, G. A., Rothenbacher, D., Rubagotti, E., Rushton, L., Sadat, N., Safdarian, M., Safi, S., Safiri, S., Sahathevan, R., Salama, J., Salomon, J. A., Samy, A. M., Sanabria, J. R., Sanchez-Niño, M. D., Sánchez-Pimienta, T. G., Santomauro, D., Santos, I. S., Santric Milicevic, M. M., Sartorius, B., Satpathy, M., Sawhney, M., Saxena, S., Schmidt, M. I., Schneider, I. J. C., Schutte, A. E., Schwebel, D. C., Schwendicke, F., Seedat, S., Sepanlou, S. G., Serdar, B., Servan-Mori, E. E., Shaddick, G., Shaheen, A., Shahraz, S., Shaikh, M. A., Shamsipour, M., Shamsizadeh, M., Shariful Islam, S. M., Sharma, J., Sharma, R., She, J., Shen, J., Shi, P., Shibuya, K., Shields, C., Shiferaw, M. S., Shigematsu, M., Shin, M.-J., Shiri, R., Shirkoochi, R., Shishani, K., Shoman, H., Shrima, M. G., Sigfusdottir, I. D., Silva, D. A. S., Silva, J. P., Silveira, D. G. A., Singh, J. A., Singh, V., Sinha, D. N., Skiadaresi, E., Slepak, E. L., Smith, D. L., Smith, M., Sobaih, B. H. A., Sobngwi, E., Soneji, S., Sorensen, R. J. D., Sposato, L. A., Sreeramareddy, C. T., Srinivasan, V., Steel, N., Stein, D. J., Steiner, C., Steinke, S., Stokes, M. A., Strub, B., Subart, M., Sufiyan, M. B., Suliankatchi, R. A., Sur, P. J., Swaminathan, S., Sykes, B. L., Szoek, C. E. I., Tabarés-Seisdedos, R., Tadakamadla, S. K., Takahashi, K., Takala, J. S., Tandon, N., Tanner, M., Tarekegn, Y. L., Tavakkoli, M., Tegegne, T. K., Tehrani-Banihashemi, A., Terkawi, A. S., Tessaema, B., Thakur, J. S., Thamsuwan, O., Thankappan, K. R., Theis, A. M., Thomas, M. L., Thomson, A. J., Thrift, A. G., Tillmann, T., Tobe-Gai, R., Tobollik, M., Tollanes, M. C., Tonelli, M., Topor-Madry, R., Torre, A., Tortajada, M., Touvier, M., Tran, B. X., Truelsen, T., Tuem, K. B., Tuzcu, E. M., Tyrovolas, S., Ukwaja, K. N., Uneke, C. J., Updike, R., Uthman, O. A., van Boven, J. F. M., Varughese, S., Vasankari, T., Veerman, L. J., Venkateswaran, V., Venketasubramanian, N., Violante, F. S., Vladimirov, S. K., Vlassov, V. V., Vollset, S. E., Vos, T., Wadilo, F., Wakayo, T., Wallin, M. T., Wang, Y.-P., Weichenthal, S., Weiderpass, E., Weintraub, R. G., Weiss, D. J., Werdecker, A., Westerman, R., Whiteford, H. A., Wiysonge, C. S., Woldeyes, B. G., Wolfe, C. D. A., Woodbrook, R., Workicho, A., Xavier, D., Xu, G., Yadgir, S., Yakob, B., Yan, L. L., Yaseri, M., Yimam, H. H., Yip, P., Yonemoto, N., Yoon, S.-J., Yotebieng, M., Younis, M. Z., Zaidi, Z., Zaki, M. E. S., Zavala-Arciniega, L., Zhang, X., Zimsen, S. R. M., Zipkin, B., Zodpey, S., Lim, S. S., and Murray, C. J. L.: Global, regional, and national comparative risk assessment of 84 behavioural, environmental and occupational, and metabolic risks or clusters of risks, 1990–2016: a systematic analysis for the Global Burden of Disease Study 2016, *The Lancet*, 390, 1345–1422, 10.1016/S0140-6736(17)32366-8, 2017.

Gali, N. K., Yang, F., Jiang, S. Y., Chan, K. L., Sun, L., Ho, K.-f., and Ning, Z.: Spatial and seasonal heterogeneity of atmospheric particles induced reactive oxygen species in

urban areas and the role of water-soluble metals, *Environmental Pollution*, 198, 86-96, 2015.

Gallimore, P. J., Mahon, B. M., Wragg, F. P. H., Fuller, S. J., Giorio, C., Kourtchev, I., and Kalberer, M.: Multiphase composition changes and reactive oxygen species formation during limonene oxidation in the new Cambridge Atmospheric Simulation Chamber (CASC), *Atmos. Chem. Phys. Discuss.*, 2017, 1-30, 10.5194/acp-2017-186, 2017.

Goldstein, A. H., and Galbally, I. E.: Known and Unexplored Organic Constituents in the Earth's Atmosphere, *Environmental Science & Technology*, 41, 1514-1521, 10.1021/es072476p, 2007.

Goutelle, S., Maurin, M., Rougier, F., Barbaut, X., Bourguignon, L., Ducher, M., and Maire, P.: The Hill equation: a review of its capabilities in pharmacological modelling, *Fundamental & Clinical Pharmacology*, 22, 633-648, 10.1111/j.1472-8206.2008.00633.x, 2008.

Grosberg, A., Nesmith, A. P., Goss, J. A., Brigham, M. D., McCain, M. L., and Parker, K. K.: Muscle on a chip: In vitro contractility assays for smooth and striated muscle, *Journal of Pharmacological and Toxicological Methods*, 65, 126-135, <http://dx.doi.org/10.1016/j.vascn.2012.04.001>, 2012.

Guenther, A., Karl, T., Harley, P., Wiedinmyer, C., Palmer, P. I., and Geron, C.: Estimates of global terrestrial isoprene emissions using MEGAN (Model of Emissions of Gases and Aerosols from Nature), *Atmos. Chem. Phys.*, 6, 3181-3210, 10.5194/acp-6-3181-2006, 2006.

Guenther, A. B., Zimmerman, P. R., Harley, P. C., Monson, R. K., and Fall, R.: Isoprene and monoterpene emission rate variability: Model evaluations and sensitivity analyses, *Journal of Geophysical Research: Atmospheres*, 98, 12609-12617, 10.1029/93JD00527, 1993.

Gurgueira, S. A., Lawrence, J., Coull, B., Murthy, G. G. K., and Gonzalez-Flecha, B.: Rapid increases in the steady-state concentration of reactive oxygen species in the lungs and heart after particulate air pollution inhalation, *Environmental Health Perspectives*, 110, 749-755, 2002.

Haddad, J. J.: L-buthionine-(S,R)-sulfoximine, an irreversible inhibitor of gamma-glutamylcysteine synthetase, augments LPS-mediated pro-inflammatory cytokine biosynthesis: evidence for the implication of an I kappa B-alpha/NF-kappa B insensitive pathway, *Eur. Cytokine Netw.*, 12, 614-624, 2001.

Haibe-Kains, B., El-Hachem, N., Birkbak, N. J., Jin, A. C., Beck, A. H., and Aerts, H. J. W. L.: Inconsistency in large pharmacogenomic studies, *Nature*, 504, 10.1038/nature12831, 2013.

Halliwell, B., and Gutteridge, J. M.: Oxygen toxicity, oxygen radicals, transition metals and disease, *Biochem. J.*, 219, 1-14, 1984.

Hallquist, M., Wenger, J. C., Baltensperger, U., Rudich, Y., Simpson, D., Claeys, M., Dommen, J., Donahue, N. M., George, C., Goldstein, A. H., Hamilton, J. F., Herrmann, H., Hoffmann, T., Iinuma, Y., Jang, M., Jenkin, M. E., Jimenez, J. L., Kiendler-Scharr, A., Maenhaut, W., McFiggans, G., Mentel, T. F., Monod, A., Prévôt, A. S. H., Seinfeld, J. H., Surratt, J. D., Szmigielski, R., and Wildt, J.: The formation, properties and impact of secondary organic aerosol: current and emerging issues, *Atmos. Chem. Phys.*, 9, 5155-5236, 10.5194/acp-9-5155-2009, 2009.

Hamad, S. H., Shafer, M. M., Kadhim, A. K. H., Al-Omran, S. M., and Schauer, J. J.: Seasonal trends in the composition and ROS activity of fine particulate matter in Baghdad, Iraq, *Atmos. Environ.*, 100, 102-110, 10.1016/j.atmosenv.2014.10.043, 2015.

Hardin, B. J., Campbell, K. S., Smith, J. D., Arbogast, S., Smith, J., Moylan, J. S., and Reid, M. B.: TNF- α acts via TNFR1 and muscle-derived oxidants to depress myofibrillar force in murine skeletal muscle, *Journal of Applied Physiology*, 104, 694-699, 2008.

Heald, C. L., Kroll, J. H., Jimenez, J. L., Docherty, K. S., DeCarlo, P. F., Aiken, A. C., Chen, Q., Martin, S. T., Farmer, D. K., and Artaxo, P.: A simplified description of the evolution of organic aerosol composition in the atmosphere, *Geophysical Research Letters*, 37, n/a-n/a, 10.1029/2010GL042737, 2010.

Healy, R. M., Temime, B., Kuprovskyte, K., and Wenger, J. C.: Effect of Relative Humidity on Gas/Particle Partitioning and Aerosol Mass Yield in the Photooxidation of p-Xylene, *Environmental Science & Technology*, 43, 1884-1889, 10.1021/es802404z, 2009.

Hecobian, A., Zhang, X., Zheng, M., Frank, N., Edgerton, E. S., and Weber, R. J.: Water-Soluble Organic Aerosol material and the light-absorption characteristics of aqueous extracts measured over the Southeastern United States, *Atmos. Chem. Phys.*, 10, 5965-5977, 10.5194/acp-10-5965-2010, 2010.

Helmig, D., Arey, J., Harger, W. P., Atkinson, R., and Lopez-Cancio, J.: Formation of mutagenic nitrodibenzopyranones and their occurrence in ambient air, *Environmental Science & Technology*, 26, 622-624, 10.1021/es00027a028, 1992.

Henkler, F., Brinkmann, J., and Luch, A.: The Role of Oxidative Stress in Carcinogenesis Induced by Metals and Xenobiotics, *Cancers*, 2, 376, 2010.

Hensley, K., Robinson, K. A., Gabbita, S. P., Salsman, S., and Floyd, R. A.: Reactive oxygen species, cell signaling, and cell injury, *Free Radical Biology and Medicine*, 28, 1456-1462, [http://dx.doi.org/10.1016/S0891-5849\(00\)00252-5](http://dx.doi.org/10.1016/S0891-5849(00)00252-5), 2000.

Hill, A. V.: The possible effects of the aggregation of the molecules of haemoglobin on its dissociation curves, *J Physiol (Lond)*, 40, 4-7, 1910.

Hoek, G., Krishnan, R. M., Beelen, R., Peters, A., Ostro, B., Brunekreef, B., and Kaufman, J. D.: Long-term air pollution exposure and cardio-respiratory mortality: a review, *Environ Health*, 12, 43, 2013.

Hoffmann, T., Odum, J., Bowman, F., Collins, D., Klockow, D., Flagan, R., and Seinfeld, J.: Formation of Organic Aerosols from the Oxidation of Biogenic Hydrocarbons, *Journal of Atmospheric Chemistry*, 26, 189-222, 10.1023/A:1005734301837, 1997.

Horcajada, P., Chalati, T., Serre, C., Gillet, B., Sebrie, C., Baati, T., Eubank, J. F., Heurtaux, D., Clayette, P., Kreuz, C., Chang, J.-S., Hwang, Y. K., Marsaud, V., Bories, P.-N., Cynober, L., Gil, S., Ferey, G., Couvreur, P., and Gref, R.: Porous metal-organic-framework nanoscale carriers as a potential platform for drug delivery and imaging, *Nat Mater*, 9, 172-178, <http://www.nature.com/nmat/journal/v9/n2/abs/nmat2608.html#supplementary-information>, 2010.

Hu, S., Polidori, A., Arhami, M., Shafer, M. M., Schauer, J. J., Cho, A., and Sioutas, C.: Redox activity and chemical speciation of size fractionated PM in the communities of the Los Angeles-Long Beach harbor, *Atmos. Chem. Phys.*, 8, 6439-6451, 2008.

Huang, S., and Pang, L.: Comparing statistical methods for quantifying drug sensitivity based on in vitro dose-response assays, *Assay Drug Dev Technol*, 10, 88-96, 10.1089/adt.2011.0388, 2012.

Huang, Y. C. T., Ghio, A. J., Stonehuerner, J., McGee, J., Carter, J. D., Grambow, S. C., and Devlin, R. B.: The role of soluble components in ambient fine particles-induced changes in human lungs and blood, *Inhal. Toxicol.*, 15, 327-342, 2003.

Janssen, N. A. H., Yang, A., Strak, M., Steenhof, M., Hellack, B., Gerlofs-Nijland, M. E., Kuhlbusch, T., Kelly, F., Harrison, R., Brunekreef, B., Hoek, G., and Cassee, F.: Oxidative potential of particulate matter collected at sites with different source characteristics, *Sci. Total Environ.*, 472, 572-581, <http://dx.doi.org/10.1016/j.scitotenv.2013.11.099>, 2014.

Jenkin, M. E., Saunders, S. M., Wagner, V., and Pilling, M. J.: Protocol for the development of the Master Chemical Mechanism, MCM v3 (Part B): tropospheric degradation of aromatic volatile organic compounds, *Atmos. Chem. Phys.*, 3, 181-193, 10.5194/acp-3-181-2003, 2003.

Jia, C., and Batterman, S.: A Critical Review of Naphthalene Sources and Exposures Relevant to Indoor and Outdoor Air, *International Journal of Environmental Research and Public Health*, 7, 2903-2939, 10.3390/ijerph7072903, 2010.

Jimenez, J. L., Canagaratna, M. R., Donahue, N. M., Prevot, A. S. H., Zhang, Q., Kroll, J. H., DeCarlo, P. F., Allan, J. D., Coe, H., Ng, N. L., Aiken, A. C., Docherty, K. S., Ulbrich, I. M., Grieshop, A. P., Robinson, A. L., Duplissy, J., Smith, J. D., Wilson, K. R., Lanz, V. A., Hueglin, C., Sun, Y. L., Tian, J., Laaksonen, A., Raatikainen, T., Rautiainen, J., Vaattovaara, P., Ehn, M., Kulmala, M., Tomlinson, J. M., Collins, D. R., Cubison, M. J., Dunlea, J., Huffman, J. A., Onasch, T. B., Alfarra, M. R., Williams, P. I., Bower, K., Kondo, Y., Schneider, J., Drewnick, F., Borrmann, S., Weimer, S., Demerjian, K., Salcedo, D., Cottrell, L., Griffin, R., Takami, A., Miyoshi, T., Hatakeyama, S., Shimono, A., Sun, J. Y., Zhang, Y. M., Dzepina, K., Kimmel, J. R., Sueper, D., Jayne, J. T., Herndon, S. C., Trimborn, A. M., Williams, L. R., Wood, E. C., Middlebrook, A. M., Kolb, C. E.,

Baltensperger, U., and Worsnop, D. R.: Evolution of Organic Aerosols in the Atmosphere, *Science*, 326, 1525-1529, 10.1126/science.1180353, 2009.

Kamimura, D., Ishihara, K., and Hirano, T.: IL-6 signal transduction and its physiological roles: the signal orchestration model, in: *Reviews of Physiology, Biochemistry and Pharmacology*, Springer Berlin Heidelberg, Berlin, Heidelberg, 1-38, 2004.

Kanakidou, M., Seinfeld, J. H., Pandis, S. N., Barnes, I., Dentener, F. J., Facchini, M. C., Van Dingenen, R., Ervens, B., Nenes, A., Nielsen, C. J., Swietlicki, E., Putaud, J. P., Balkanski, Y., Fuzzi, S., Horth, J., Moortgat, G. K., Winterhalter, R., Myhre, C. E. L., Tsigaridis, K., Vignati, E., Stephanou, E. G., and Wilson, J.: Organic aerosol and global climate modelling: a review, *Atmos. Chem. Phys.*, 5, 1053-1123, 2005.

Kautzman, K. E., Surratt, J. D., Chan, M. N., Chan, A. W. H., Hersey, S. P., Chhabra, P. S., Dalleska, N. F., Wennberg, P. O., Flagan, R. C., and Seinfeld, J. H.: Chemical Composition of Gas- and Aerosol-Phase Products from the Photooxidation of Naphthalene, *The Journal of Physical Chemistry A*, 114, 913-934, 10.1021/jp908530s, 2010.

Khmelinskaia, A., Ibarguren, M., de Almeida, R. F. M., López, D. J., Paixão, V. A., Ahyauch, H., Goñi, F. M., and Escribá, P. V.: Changes in Membrane Organization upon Spontaneous Insertion of 2-Hydroxylated Unsaturated Fatty Acids in the Lipid Bilayer, *Langmuir*, 30, 2117-2128, 10.1021/la403977f, 2014.

Kishimoto, T.: Interleukin-6, *The cytokine handbook*, 4, 281-304, 2003.

Kleinman, M. T., Hamade, A., Meacher, D., Oldham, M., Sioutas, C., Chakrabarti, B., Stram, D., Froines, J. R., and Cho, A. K.: Inhalation of concentrated ambient particulate matter near a heavily trafficked road stimulates antigen-induced airway responses in mice, *Journal of the Air & Waste Management Association*, 55, 1277-1288, 2005.

Knaapen, A. M., Albrecht, C., Becker, A., Höhr, D., Winzer, A., Haenen, G. R., Borm, P. J. A., and Schins, R. P. F.: DNA damage in lung epithelial cells isolated from rats exposed to quartz: role of surface reactivity and neutrophilic inflammation, *Carcinogenesis*, 23, 1111-1120, 10.1093/carcin/23.7.1111, 2002.

Koike, E., and Kobayashi, T.: Chemical and biological oxidative effects of carbon black nanoparticles, *Chemosphere*, 65, 946-951, 10.1016/j.chemosphere.2006.03.078, 2006.

Kramer, A. J., Rattanavaraha, W., Zhang, Z., Gold, A., Surratt, J. D., and Lin, Y.-H.: Assessing the oxidative potential of isoprene-derived epoxides and secondary organic aerosol, *Atmos. Environ.*, 130, 211-218, 10.1016/j.atmosenv.2015.10.018, 2016.

Kroll, J. H., Ng, N. L., Murphy, S. M., Flagan, R. C., and Seinfeld, J. H.: Secondary organic aerosol formation from isoprene photooxidation under high-NO_x conditions, *Geophysical Research Letters*, 32, n/a-n/a, 10.1029/2005GL023637, 2005.

Kroll, J. H., and Seinfeld, J. H.: Chemistry of secondary organic aerosol: Formation and evolution of low-volatility organics in the atmosphere, *Atmos. Environ.*, 42, 3593-3624, 10.1016/j.atmosenv.2008.01.003, 2008.

Kroll, J. H., Donahue, N. M., Jimenez, J. L., Kessler, S. H., Canagaratna, M. R., Wilson, K. R., Altieri, K. E., Mazzoleni, L. R., Wozniak, A. S., Bluhm, H., Mysak, E. R., Smith, J. D., Kolb, C. E., and Worsnop, D. R.: Carbon oxidation state as a metric for describing the chemistry of atmospheric organic aerosol, *Nat Chem*, 3, 133-139, 2011.

Kumagai, Y., Koide, S., Taguchi, K., Endo, A., Nakai, Y., Yoshikawa, T., and Shimojo, N.: Oxidation of proximal protein sulfhydryls by phenanthraquinone, a component of diesel exhaust particles, *Chemical Research in Toxicology*, 15, 483-489, 10.1021/tx0100993, 2002.

Lambe, A. T., Onasch, T. B., Massoli, P., Croasdale, D. R., Wright, J. P., Ahern, A. T., Williams, L. R., Worsnop, D. R., Brune, W. H., and Davidovits, P.: Laboratory studies of the chemical composition and cloud condensation nuclei (CCN) activity of secondary organic aerosol (SOA) and oxidized primary organic aerosol (OPOA), *Atmos. Chem. Phys.*, 11, 8913-8928, 10.5194/acp-11-8913-2011, 2011.

Landreman, A. P., Shafer, M. M., Hemming, J. C., Hannigan, M. P., and Schauer, J. J.: A macrophage-based method for the assessment of the reactive oxygen species (ROS) activity of atmospheric particulate matter (PM) and application to routine (daily-24 h) aerosol monitoring studies, *Aerosol Sci. Technol.*, 42, 946-957, 10.1080/02786820802363819, 2008.

Landrigan, P. J., Fuller, R., Acosta, N. J. R., Adeyi, O., Arnold, R., Basu, N., Baldé, A. B., Bertollini, R., Bose-O'Reilly, S., Boufford, J. I., Breyse, P. N., Chiles, T., Mahidol, C., Coll-Seck, A. M., Cropper, M. L., Fobil, J., Fuster, V., Greenstone, M., Haines, A., Hanrahan, D., Hunter, D., Khare, M., Krupnick, A., Lanphear, B., Lohani, B., Martin, K., Mathiasen, K. V., McTeer, M. A., Murray, C. J. L., Ndahimananjara, J. D., Perera, F., Potočník, J., Preker, A. S., Ramesh, J., Rockström, J., Salinas, C., Samson, L. D., Sandilya, K., Sly, P. D., Smith, K. R., Steiner, A., Stewart, R. B., Suk, W. A., van Schayck, O. C. P., Yadama, G. N., Yumkella, K., and Zhong, M.: The Lancet Commission on pollution and health, *The Lancet*, 10.1016/S0140-6736(17)32345-0, 2017.

Li, N., Hao, M. Q., Phalen, R. F., Hinds, W. C., and Nel, A. E.: Particulate air pollutants and asthma - A paradigm for the role of oxidative stress in PM-induced adverse health effects, *Clinical Immunology*, 109, 250-265, 10.1016/j.clim.2003.08.006, 2003a.

Li, N., Sioutas, C., Cho, A., Schmitz, D., Misra, C., Sempf, J., Wang, M. Y., Oberley, T., Froines, J., and Nel, A.: Ultrafine particulate pollutants induce oxidative stress and mitochondrial damage, *Environmental Health Perspectives*, 111, 455-460, 10.1289/ehp.6000, 2003b.

Li, N., Xia, T., and Nel, A. E.: The role of oxidative stress in ambient particulate matter-induced lung diseases and its implications in the toxicity of engineered nanoparticles, *Free*

Radical Biology and Medicine, 44, 1689-1699, 10.1016/j.freeradbiomed.2008.01.028, 2008.

Li, Q., Wyatt, A., and Kamens, R. M.: Oxidant generation and toxicity enhancement of aged-diesel exhaust, *Atmos. Environ.*, 43, 1037-1042, 10.1016/j.atmosenv.2008.11.018, 2009.

Lim, S. S., Vos, T., Flaxman, A. D., Danaei, G., Shibuya, K., Adair-Rohani, H., AlMazroa, M. A., Amann, M., Anderson, H. R., Andrews, K. G., Aryee, M., Atkinson, C., Bacchus, L. J., Bahalim, A. N., Balakrishnan, K., Balmes, J., Barker-Collo, S., Baxter, A., Bell, M. L., Blore, J. D., Blyth, F., Bonner, C., Borges, G., Bourne, R., Boussinesq, M., Brauer, M., Brooks, P., Bruce, N. G., Brunekreef, B., Bryan-Hancock, C., Bucello, C., Buchbinder, R., Bull, F., Burnett, R. T., Byers, T. E., Calabria, B., Carapetis, J., Carnahan, E., Chafe, Z., Charlson, F., Chen, H., Chen, J. S., Cheng, A. T.-A., Child, J. C., Cohen, A., Colson, K. E., Cowie, B. C., Darby, S., Darling, S., Davis, A., Degenhardt, L., Dentener, F., Des Jarlais, D. C., Devries, K., Dherani, M., Ding, E. L., Dorsey, E. R., Driscoll, T., Edmond, K., Ali, S. E., Engell, R. E., Erwin, P. J., Fahimi, S., Falder, G., Farzadfar, F., Ferrari, A., Finucane, M. M., Flaxman, S., Fowkes, F. G. R., Freedman, G., Freeman, M. K., Gakidou, E., Ghosh, S., Giovannucci, E., Gmel, G., Graham, K., Grainger, R., Grant, B., Gunnell, D., Gutierrez, H. R., Hall, W., Hoek, H. W., Hogan, A., Hosgood, H. D., III, Hoy, D., Hu, H., Hubbell, B. J., Hutchings, S. J., Ibeanusi, S. E., Jacklyn, G. L., Jasrasaria, R., Jonas, J. B., Kan, H., Kanis, J. A., Kassebaum, N., Kawakami, N., Khang, Y.-H., Khatibzadeh, S., Khoo, J.-P., Kok, C., Laden, F., Lalloo, R., Lan, Q., Lathlean, T., Leasher, J. L., Leigh, J., Li, Y., Lin, J. K., Lipshultz, S. E., London, S., Lozano, R., Lu, Y., Mak, J., Malekzadeh, R., Mallinger, L., Marcenes, W., March, L., Marks, R., Martin, R., McGale, P., McGrath, J., Mehta, S., Memish, Z. A., Mensah, G. A., Merriman, T. R., Micha, R., Michaud, C., Mishra, V., Hanafiah, K. M., Mokdad, A. A., Morawska, L., Mozaffarian, D., Murphy, T., Naghavi, M., Neal, B., Nelson, P. K., Nolla, J. M., Norman, R., Olives, C., Omer, S. B., Orchard, J., Osborne, R., Ostro, B., Page, A., Pandey, K. D., Parry, C. D. H., Passmore, E., Patra, J., Pearce, N., Pelizzari, P. M., Petzold, M., Phillips, M. R., Pope, D., Pope, C. A., III, Powles, J., Rao, M., Razavi, H., Rehfuss, E. A., Rehm, J. T., Ritz, B., Rivara, F. P., Roberts, T., Robinson, C., Rodriguez-Portales, J. A., Romieu, I., Room, R., Rosenfeld, L. C., Roy, A., Rushton, L., Salomon, J. A., Sampson, U., Sanchez-Riera, L., Sanman, E., Sapkota, A., Seedat, S., Shi, P., Shield, K., Shivakoti, R., Singh, G. M., Sleet, D. A., Smith, E., Smith, K. R., Stapelberg, N. J. C., Steenland, K., Stöckl, H., Stovner, L. J., Straif, K., Straney, L., Thurston, G. D., Tran, J. H., Van Dingenen, R., van Donkelaar, A., Veerman, J. L., Vijayakumar, L., Weintraub, R., Weissman, M. M., White, R. A., Whiteford, H., Wiersma, S. T., Wilkinson, J. D., Williams, H. C., Williams, W., Wilson, N., Woolf, A. D., Yip, P., Zielinski, J. M., Lopez, A. D., Murray, C. J. L., and Ezzati, M.: A comparative risk assessment of burden of disease and injury attributable to 67 risk factors and risk factor clusters in 21 regions, 1990–2010: a systematic analysis for the Global Burden of Disease Study 2010, *The Lancet*, 380, 2224-2260, 10.1016/S0140-6736(12)61766-8, 2012.

Lin, P., and Yu, J. Z.: Generation of Reactive Oxygen Species Mediated by Humic-like Substances in Atmospheric Aerosols, *Environmental Science & Technology*, 45, 10362-10368, 10.1021/es2028229, 2011.

Lin, Y.-H., Arashiro, M., Clapp, P. W., Cui, T., Sexton, K. G., Vizuete, W., Gold, A., Jaspers, I., Fry, R. C., and Surratt, J. D.: Gene Expression Profiling in Human Lung Cells Exposed to Isoprene-Derived Secondary Organic Aerosol, *Environmental Science & Technology*, 10.1021/acs.est.7b01967, 2017.

Lin, Y. H., Zhang, Z., Docherty, K. S., Zhang, H., Budisulistiorini, S. H., Rubitschun, C. L., Shaw, S. L., Knipping, E. M., Edgerton, E. S., Kleindienst, T. E., Gold, A., and Surratt, J. D.: Isoprene Epoxydiols as Precursors to Secondary Organic Aerosol Formation: Acid-Catalyzed Reactive Uptake Studies with Authentic Compounds, *Environmental science & technology*, 46, 250-258, 10.1021/es202554c, 2012.

Lin, Y. H., Arashiro, M., Martin, E., Chen, Y., Zhang, Z., Sexton, K. G., Gold, A., Jaspers, I., Fry, R. C., and Surratt, J. D.: Isoprene-Derived Secondary Organic Aerosol Induces the Expression of Oxidative Stress Response Genes in Human Lung Cells, *Environmental Science & Technology Letters*, 3, 250-254, 10.1021/acs.estlett.6b00151, 2016.

Loomis, D., Grosse, Y., Lauby-Secretan, B., Ghissassi, F. E., Bouvard, V., Benbrahim-Tallaa, L., Guha, N., Baan, R., Mattock, H., and Straif, K.: The carcinogenicity of outdoor air pollution, *The Lancet Oncology*, 14, 1262-1263, 10.1016/S1470-2045(13)70487-X, 2013.

Lorentzen, R. J., Lesko, S. A., McDonald, K., and Ts'o, P. O. P.: <div xmlns="http://www.w3.org/1999/xhtml">Toxicity of Metabolic Benzo(a)pyrenediones to Cultured Cells and the Dependence upon Molecular Oxygen</div>, *Cancer Research*, 39, 3194-3198, 1979.

Loza, C. L., Craven, J. S., Yee, L. D., Coggon, M. M., Schwantes, R. H., Shiraiwa, M., Zhang, X., Schilling, K. A., Ng, N. L., Canagaratna, M. R., Ziemann, P. J., Flagan, R. C., and Seinfeld, J. H.: Secondary organic aerosol yields of 12-carbon alkanes, *Atmos. Chem. Phys.*, 14, 1423-1439, 10.5194/acp-14-1423-2014, 2014.

Lu, Y., Su, S., Jin, W., Wang, B., Li, N., Shen, H., Li, W., Huang, Y., Chen, H., Zhang, Y., Chen, Y., Lin, N., Wang, X., and Tao, S.: Characteristics and cellular effects of ambient particulate matter from Beijing, *Environmental Pollution*, 191, 63-69, <http://dx.doi.org/10.1016/j.envpol.2014.04.008>, 2014.

Lund, A. K., Doyle-Eisele, M., Lin, Y. H., Arashiro, M., Surratt, J. D., Holmes, T., Schilling, K. A., Seinfeld, J. H., Rohr, A. C., Knipping, E. M., and McDonald, J. D.: The effects of alpha-pinene versus toluene-derived secondary organic aerosol exposure on the expression of markers associated with vascular disease, *Inhal. Toxicol.*, 25, 309-324, 10.3109/08958378.2013.782080, 2013.

Matsukawa, Y., Lee, V. H. L., Crandall, E. D., and Kim, K.-J.: Size-Dependent Dextran Transport across Rat Alveolar Epithelial Cell Monolayers, *Journal of Pharmaceutical Sciences*, 86, 305-309, <http://dx.doi.org/10.1021/js960352x>, 1997.

Matsunaga, K., Klein, T. W., Friedman, H., and Yamamoto, Y.: Involvement of Nicotinic Acetylcholine Receptors in Suppression of Antimicrobial Activity and Cytokine

Responses of Alveolar Macrophages to *Legionella pneumophila* Infection by Nicotine, *The Journal of Immunology*, 167, 6518-6524, 10.4049/jimmunol.167.11.6518, 2001.

Mbawuike, I. N., and Herscowitz, H. B.: MH-S, a murine alveolar macrophage cell line: morphological, cytochemical, and functional characteristics, *Journal of Leukocyte Biology*, 46, 119-127, 1989.

McDonald, J. D., Doyle-Eisele, M., Campen, M. J., Seagrave, J., Holmes, T., Lund, A., Surratt, J. D., Seinfeld, J. H., Rohr, A. C., and Knipping, E. M.: Cardiopulmonary response to inhalation of biogenic secondary organic aerosol, *Inhal. Toxicol.*, 22, 253-265, 10.3109/08958370903148114, 2010.

McDonald, J. D., Doyle-Eisele, M., Kracko, D., Lund, A., Surratt, J. D., Hersey, S. P., Seinfeld, J. H., Rohr, A. C., and Knipping, E. M.: Cardiopulmonary response to inhalation of secondary organic aerosol derived from gas-phase oxidation of toluene, *Inhal. Toxicol.*, 24, 689-697, 10.3109/08958378.2012.712164, 2012.

McLafferty, F. W., and Tureček, F.: Interpretation of mass spectra, University science books, 1993.

McWhinney, R. D., Badali, K., Liggio, J., Li, S.-M., and Abbatt, J. P. D.: Filterable Redox Cycling Activity: A Comparison between Diesel Exhaust Particles and Secondary Organic Aerosol Constituents, *Environmental Science & Technology*, 47, 3362-3369, 10.1021/es304676x, 2013a.

McWhinney, R. D., Zhou, S., and Abbatt, J. P. D.: Naphthalene SOA: redox activity and naphthoquinone gas-particle partitioning, *Atmos. Chem. Phys.*, 13, 9731-9744, 10.5194/acp-13-9731-2013, 2013b.

Mohr, C., Huffman, J. A., Cubison, M. J., Aiken, A. C., Docherty, K. S., Kimmel, J. R., Ulbrich, I. M., Hannigan, M., and Jimenez, J. L.: Characterization of Primary Organic Aerosol Emissions from Meat Cooking, Trash Burning, and Motor Vehicles with High-Resolution Aerosol Mass Spectrometry and Comparison with Ambient and Chamber Observations, *Environmental Science & Technology*, 43, 2443-2449, 10.1021/es8011518, 2009.

Møller, P., Jacobsen, N. R., Folkmann, J. K., Danielsen, P. H., Mikkelsen, L., Hemmingsen, J. G., Vesterdal, L. K., Forchhammer, L., Wallin, H., and Loft, S.: Role of oxidative damage in toxicity of particulates, *Free Radic. Res.*, 44, 1-46, 10.3109/10715760903300691, 2009.

Murphy, Michael P.: How mitochondria produce reactive oxygen species, *Biochem. J.*, 417, 1-13, 10.1042/bj20081386, 2009.

Murray, J. I., Whitfield, M. L., Trinklein, N. D., Myers, R. M., Brown, P. O., and Botstein, D.: Diverse and Specific Gene Expression Responses to Stresses in Cultured Human Cells, *Molecular Biology of the Cell*, 15, 2361-2374, 10.1091/mbc.E03-11-0799, 2004.

Nah, T., McVay, R. C., Pierce, J. R., Seinfeld, J. H., and Ng, N. L.: Constraining uncertainties in particle-wall deposition correction during SOA formation in chamber experiments, *Atmos. Chem. Phys.*, 17, 2297-2310, 10.5194/acp-17-2297-2017, 2017.

Ng, N. L., Kroll, J. H., Keywood, M. D., Bahreini, R., Varutbangkul, V., Flagan, R. C., Seinfeld, J. H., Lee, A., and Goldstein, A. H.: Contribution of First- versus Second-Generation Products to Secondary Organic Aerosols Formed in the Oxidation of Biogenic Hydrocarbons, *Environmental Science & Technology*, 40, 2283-2297, 10.1021/es052269u, 2006.

Ng, N. L., Chhabra, P. S., Chan, A. W. H., Surratt, J. D., Kroll, J. H., Kwan, A. J., McCabe, D. C., Wennberg, P. O., Sorooshian, A., Murphy, S. M., Dalleska, N. F., Flagan, R. C., and Seinfeld, J. H.: Effect of NO_x level on secondary organic aerosol (SOA) formation from the photooxidation of terpenes, *Atmos. Chem. Phys.*, 7, 5159-5174, 10.5194/acp-7-5159-2007, 2007a.

Ng, N. L., Kroll, J. H., Chan, A. W. H., Chhabra, P. S., Flagan, R. C., and Seinfeld, J. H.: Secondary organic aerosol formation from m-xylene, toluene, and benzene, *Atmos. Chem. Phys.*, 7, 3909-3922, 10.5194/acp-7-3909-2007, 2007b.

Ng, N. L., Canagaratna, M. R., Zhang, Q., Jimenez, J. L., Tian, J., Ulbrich, I. M., Kroll, J. H., Docherty, K. S., Chhabra, P. S., Bahreini, R., Murphy, S. M., Seinfeld, J. H., Hildebrandt, L., Donahue, N. M., DeCarlo, P. F., Lanz, V. A., Prévôt, A. S. H., Dinar, E., Rudich, Y., and Worsnop, D. R.: Organic aerosol components observed in Northern Hemispheric datasets from Aerosol Mass Spectrometry, *Atmos. Chem. Phys.*, 10, 4625-4641, 10.5194/acp-10-4625-2010, 2010.

Ng, N. L., Canagaratna, M. R., Jimenez, J. L., Chhabra, P. S., Seinfeld, J. H., and Worsnop, D. R.: Changes in organic aerosol composition with aging inferred from aerosol mass spectra, *Atmos. Chem. Phys.*, 11, 6465-6474, 10.5194/acp-11-6465-2011, 2011.

Nguyen, T. B., Roach, P. J., Laskin, J., Laskin, A., and Nizkorodov, S. A.: Effect of humidity on the composition of isoprene photooxidation secondary organic aerosol, *Atmos. Chem. Phys.*, 11, 6931-6944, 10.5194/acp-11-6931-2011, 2011.

Oberdörster, G., Ferin, J., Gelein, R., Soderholm, S. C., and Finkelstein, J.: Role of the alveolar macrophage in lung injury: studies with ultrafine particles, *Environmental Health Perspectives*, 97, 193-199, 1992.

Oberdörster, G.: Lung Dosimetry: Pulmonary Clearance of Inhaled Particles, *Aerosol Sci. Technol.*, 18, 279-289, 10.1080/02786829308959605, 1993.

Odum, J. R., Hoffmann, T., Bowman, F., Collins, D., Flagan, R. C., and Seinfeld, J. H.: Gas/Particle Partitioning and Secondary Organic Aerosol Yields, *Environmental Science & Technology*, 30, 2580-2585, 10.1021/es950943+, 1996.

Orlando, J. J., and Tyndall, G. S.: Laboratory studies of organic peroxy radical chemistry: an overview with emphasis on recent issues of atmospheric significance, *Chemical Society Reviews*, 41, 6294-6317, 10.1039/C2CS35166H, 2012.

Pan, Q., and Shimizu, I.: Imputation Variance Estimation by Multiple Imputation Method for the National Hospital Discharge Survey, 2009.

Pardo, M., Shafer, M. M., Rudich, A., Schauer, J. J., and Rudich, Y.: Single Exposure to near Roadway Particulate Matter Leads to Confined Inflammatory and Defense Responses: Possible Role of Metals, *Environmental Science & Technology*, 49, 8777-8785, 10.1021/acs.est.5b01449, 2015.

Philip, M., Rowley, D. A., and Schreiber, H.: Inflammation as a tumor promoter in cancer induction, *Seminars in Cancer Biology*, 14, 433-439, <http://dx.doi.org/10.1016/j.semcancer.2004.06.006>, 2004.

Piccot, S. D., Watson, J. J., and Jones, J. W.: A global inventory of volatile organic compound emissions from anthropogenic sources, *Journal of Geophysical Research: Atmospheres*, 97, 9897-9912, 10.1029/92JD00682, 1992.

Platt, S. M., Haddad, I. E., Pieber, S. M., Huang, R. J., Zardini, A. A., Clairotte, M., Suarez-Bertoa, R., Barmet, P., Pfaffenberger, L., Wolf, R., Slowik, J. G., Fuller, S. J., Kalberer, M., Chirico, R., Dommen, J., Astorga, C., Zimmermann, R., Marchand, N., Hellebust, S., Temime-Roussel, B., Baltensperger, U., and Prévôt, A. S. H.: Two-stroke scooters are a dominant source of air pollution in many cities, *Nature Communications*, 5, 3749, 10.1038/ncomms4749, 2014.

Pope, C. A., Burnett, R. T., Thun, M. J., Calle, E. E., Krewski, D., Ito, K., and Thurston, G. D.: Lung cancer, cardiopulmonary mortality, and long-term exposure to fine particulate air pollution, *Jama-Journal of the American Medical Association*, 287, 1132-1141, 10.1001/jama.287.9.1132, 2002.

Pope III, C. A., and Dockery, D. W.: Health effects of fine particulate air pollution: Lines that connect, *Journal of the Air and Waste Management Association*, 56, 709-742, 2006.

Rattanaavaraha, W., Rosen, E., Zhang, H., Li, Q., Pantong, K., and Kamens, R. M.: The reactive oxidant potential of different types of aged atmospheric particles: An outdoor chamber study, *Atmos. Environ.*, 45, 3848-3855, 10.1016/j.atmosenv.2011.04.002, 2011.

Riva, M., Robinson, E. S., Perraudin, E., Donahue, N. M., and Villenave, E.: Photochemical Aging of Secondary Organic Aerosols Generated from the Photooxidation of Polycyclic Aromatic Hydrocarbons in the Gas-Phase, *Environmental Science & Technology*, 49, 5407-5416, 10.1021/acs.est.5b00442, 2015.

Robinson, A. L., Donahue, N. M., Shrivastava, M. K., Weitkamp, E. A., Sage, A. M., Grieshop, A. P., Lane, T. E., Pierce, J. R., and Pandis, S. N.: Rethinking Organic Aerosols: Semivolatile Emissions and Photochemical Aging, *Science*, 315, 1259-1262, 10.1126/science.1133061, 2007.

Rogge, W. F., Hildemann, L. M., Mazurek, M. A., Cass, G. R., and Simoneit, B. R. T.: Sources of fine organic aerosol. 1. Charbroilers and meat cooking operations, *Environmental Science & Technology*, 25, 1112-1125, 10.1021/es00018a015, 1991.

Rue, E. L., and Bruland, K. W.: COMPLEXATION OF IRON(III) BY NATURAL ORGANIC-LIGANDS IN THE CENTRAL NORTH PACIFIC AS DETERMINED BY A NEW COMPETITIVE LIGAND EQUILIBRATION ADSORPTIVE CATHODIC STRIPPING VOLTAMMETRIC METHOD, *Marine Chemistry*, 50, 117-138, 10.1016/0304-4203(95)00031-1, 1995.

Saffari, A., Daher, N., Shafer, M. M., Schauer, J. J., and Sioutas, C.: Seasonal and spatial variation in reactive oxygen species activity of quasi-ultrafine particles (PM_{0.25}) in the Los Angeles metropolitan area and its association with chemical composition, *Atmos. Environ.*, 79, 566-575, 10.1016/j.atmosenv.2013.07.058, 2013.

Saffari, A., Daher, N., Shafer, M. M., Schauer, J. J., and Sioutas, C.: Global perspective on the oxidative potential of airborne particulate matter: A synthesis of research findings, *Environmental science & technology*, 48, 7576-7583, 2014a.

Saffari, A., Daher, N., Shafer, M. M., Schauer, J. J., and Sioutas, C.: Seasonal and spatial variation in dithiothreitol (DTT) activity of quasi-ultrafine particles in the Los Angeles Basin and its association with chemical species, *J. Environ. Sci. Health Part A-Toxic/Hazard. Subst. Environ. Eng.*, 49, 441-451, 10.1080/10934529.2014.854677, 2014b.

Saffari, A., Hasheminassab, S., Wang, D., Shafer, M. M., Schauer, J. J., and Sioutas, C.: Impact of primary and secondary organic sources on the oxidative potential of quasi-ultrafine particles (PM_{0.25}) at three contrasting locations in the Los Angeles Basin, *Atmos. Environ.*, 120, 286-296, <http://dx.doi.org/10.1016/j.atmosenv.2015.09.022>, 2015.

Sankaran, K., and Herscowitz, H. B.: Phenotypic and functional heterogeneity of the murine alveolar macrophage-derived cell line MH-S, *Journal of Leukocyte Biology*, 57, 562-568, 1995.

Sannigrahi, P., Sullivan, A. P., Weber, R. J., and Ingall, E. D.: Characterization of Water-Soluble Organic Carbon in Urban Atmospheric Aerosols Using Solid-State ¹³C NMR Spectroscopy, *Environmental Science & Technology*, 40, 666-672, 10.1021/es051150i, 2006.

Sarkar, B.: Metal-protein interactions in transport, accumulation, and excretion of metals, *Biological Trace Element Research*, 21, 137-144, 10.1007/bf02917246, 1989.

Sato, K., Takami, A., Iozaki, T., Hikida, T., Shimono, A., and Imamura, T.: Mass spectrometric study of secondary organic aerosol formed from the photo-oxidation of aromatic hydrocarbons, *Atmos. Environ.*, 44, 1080-1087, <http://dx.doi.org/10.1016/j.atmosenv.2009.12.013>, 2010.

Seinfeld, J. H., and Pandis, S. N.: *Atmospheric chemistry and physics: from air pollution to climate change*, John Wiley & Sons, 2016.

Sheng-Hann, W., Chia-Wei, L., Arthur, C., and Pei-Kuen, W.: Size-dependent endocytosis of gold nanoparticles studied by three-dimensional mapping of plasmonic scattering images, *Journal of Nanobiotechnology*, 8, 33-45, 10.1186/1477-3155-8-33, 2010.

Spector, A. A., and Yorek, M. A.: Membrane lipid composition and cellular function, *Journal of Lipid Research*, 26, 1015-1035, 1985.

Stirnweis, L., Marcolli, C., Dommen, J., Barmet, P., Frege, C., Platt, S. M., Bruns, E. A., Krapf, M., Slowik, J. G., Wolf, R., Prévôt, A. S. H., El-Haddad, I., and Baltensperger, U.: α -Pinene secondary organic aerosol yields increase at higher relative humidity and low NO_x conditions, *Atmos. Chem. Phys. Discuss.*, 2016, 1-41, 10.5194/acp-2016-717, 2016.

Sullivan, A. P., and Weber, R. J.: Chemical characterization of the ambient organic aerosol soluble in water: 1. Isolation of hydrophobic and hydrophilic fractions with a XAD-8 resin, *Journal of Geophysical Research: Atmospheres*, 111, n/a-n/a, 10.1029/2005JD006485, 2006.

Sung, S. Y., Kubo, H., Shigemura, K., Arnold, R. S., Logani, S., Wang, R., Konaka, H., Nakagawa, M., Mousses, S., Amin, M., Anderson, C., Johnstone, P., Petros, J. A., Marshall, F. F., Zhau, H. E., and Chung, L. W. K.: Oxidative Stress Induces ADAM9 Protein Expression in Human Prostate Cancer Cells, *Cancer Research*, 66, 9519-9526, 10.1158/0008-5472.can-05-4375, 2006.

Surratt, J. D., Chan, A. W. H., Eddingsaas, N. C., Chan, M., Loza, C. L., Kwan, A. J., Hersey, S. P., Flagan, R. C., Wennberg, P. O., and Seinfeld, J. H.: Reactive intermediates revealed in secondary organic aerosol formation from isoprene, *Proceedings of the National Academy of Sciences*, 107, 6640-6645, 10.1073/pnas.0911114107, 2010.

Sutton, H. C., and Winterbourn, C. C.: On the participation of higher oxidation states of iron and copper in fenton reactions, *Free Radical Biology and Medicine*, 6, 53-60, [http://dx.doi.org/10.1016/0891-5849\(89\)90160-3](http://dx.doi.org/10.1016/0891-5849(89)90160-3), 1989.

Tang, D., Shi, Y., Kang, R., Li, T., Xiao, W., Wang, H., and Xiao, X.: Hydrogen peroxide stimulates macrophages and monocytes to actively release HMGB1, *Journal of Leukocyte Biology*, 81, 741-747, 10.1189/jlb.0806540, 2007.

Tao, F., Gonzalez-Flecha, B., and Kobzik, L.: Reactive oxygen species in pulmonary inflammation by ambient particulates, *Free Radical Biology and Medicine*, 35, 327-340, 10.1016/S0891-5849(03)00280-6, 2003.

Tasoglou, A., and Pandis, S. N.: Formation and chemical aging of secondary organic aerosol during the β -caryophyllene oxidation, *Atmos. Chem. Phys.*, 15, 6035-6046, 10.5194/acp-15-6035-2015, 2015.

Terada, H.: Uncouplers of oxidative phosphorylation, *Environmental Health Perspectives*, 87, 213-218, 1990.

Thierse, H.-J., Moulon, C., Allespach, Y., Zimmermann, B., Doetze, A., Kuppig, S., Wild, D., Herberg, F., and Weltzien, H. U.: Metal-Protein Complex-Mediated Transport and Delivery of Ni²⁺ to TCR/MHC Contact Sites in Nickel-Specific Human T Cell Activation, *The Journal of Immunology*, 172, 1926-1934, 10.4049/jimmunol.172.3.1926, 2004.

Tinoco, A. D., and Valentine, A. M.: Ti(IV) Binds to Human Serum Transferrin More Tightly Than Does Fe(III), *Journal of the American Chemical Society*, 127, 11218-11219, 10.1021/ja052768v, 2005.

Tuet, W. Y., Fok, S., Verma, V., Tagle Rodriguez, M. S., Grosberg, A., Champion, J. A., and Ng, N. L.: Dose-dependent intracellular reactive oxygen and nitrogen species (ROS/RNS) production from particulate matter exposure: comparison to oxidative potential and chemical composition, *Atmos. Environ.*, 144, 335-344, 10.1016/j.atmosenv.2016.09.005, 2016.

Tuet, W. Y., Chen, Y., Fok, S., Champion, J. A., and Ng, N. L.: Inflammatory responses to secondary organic aerosols (SOA) generated from biogenic and anthropogenic precursors, *Atmos. Chem. Phys.*, 17, 11423-11440, 10.5194/acp-17-11423-2017, 2017a.

Tuet, W. Y., Chen, Y., Xu, L., Fok, S., Gao, D., Weber, R. J., and Ng, N. L.: Chemical oxidative potential of secondary organic aerosol (SOA) generated from the photooxidation of biogenic and anthropogenic volatile organic compounds, *Atmos. Chem. Phys.*, 17, 839-853, 10.5194/acp-17-839-2017, 2017b.

Turner, J., Hernandez, M., Snawder, J. E., Handorean, A., and McCabe, K. M.: A Toxicology Suite Adapted for Comparing Parallel Toxicity Responses of Model Human Lung Cells to Diesel Exhaust Particles and Their Extracts, *Aerosol Sci. Technol.*, 49, 599-610, 10.1080/02786826.2015.1053559, 2015.

Uchida, Y., Ohba, K.-i., Yoshioka, T., Irie, K., Muraki, T., and Maru, Y.: Cellular Carbonyl Stress Enhances the Expression of Plasminogen Activator Inhibitor-1 in Rat White Adipocytes via Reactive Oxygen Species-dependent Pathway, *J. Biol. Chem.*, 279, 4075-4083, 10.1074/jbc.M304222200, 2004.

Van Krevelen, D.: Graphical-statistical method for the study of structure and reaction processes of coal, *Fuel*, 29, 269-284, 1950.

Verma, V., Ning, Z., Cho, A. K., Schauer, J. J., Shafer, M. M., and Sioutas, C.: Redox activity of urban quasi-ultrafine particles from primary and secondary sources, *Atmos. Environ.*, 43, 6360-6368, 10.1016/j.atmosenv.2009.09.019, 2009.

Verma, V., Shafer, M. M., Schauer, J. J., and Sioutas, C.: Contribution of transition metals in the reactive oxygen species activity of PM emissions from retrofitted heavy-duty vehicles, *Atmos. Environ.*, 44, 5165-5173, 10.1016/j.atmosenv.2010.08.052, 2010.

Verma, V., Rico-Martinez, R., Kotra, N., King, L., Liu, J. M., Snell, T. W., and Weber, R. J.: Contribution of Water-Soluble and Insoluble Components and Their Hydrophobic/Hydrophilic Subfractions to the Reactive Oxygen Species-Generating

Potential of Fine Ambient Aerosols, *Environmental Science & Technology*, 46, 11384-11392, 10.1021/es302484r, 2012.

Verma, V., Fang, T., Guo, H., King, L., Bates, J. T., Peltier, R. E., Edgerton, E., Russell, A. G., and Weber, R. J.: Reactive oxygen species associated with water-soluble PM 2.5 in the southeastern United States: spatiotemporal trends and source apportionment, *Atmos. Chem. Phys.*, 14, 12915-12930, 2014.

Verma, V., Fang, T., Xu, L., Peltier, R. E., Russell, A. G., Ng, N. L., and Weber, R. J.: Organic Aerosols Associated with the Generation of Reactive Oxygen Species (ROS) by Water-Soluble PM2.5, *Environmental Science & Technology*, 49, 4646-4656, 10.1021/es505577w, 2015a.

Verma, V., Wang, Y., El-Afifi, R., Fang, T., Rowland, J., Russell, A. G., and Weber, R. J.: Fractionating ambient humic-like substances (HULIS) for their reactive oxygen species activity – Assessing the importance of quinones and atmospheric aging, *Atmos. Environ.*, 120, 351-359, 10.1016/j.atmosenv.2015.09.010, 2015b.

Visentin, M., Pagnoni, A., Sarti, E., and Pietrogrande, M. C.: Urban PM2.5 oxidative potential: Importance of chemical species and comparison of two spectrophotometric cell-free assays, *Environmental Pollution*, 219, 72-79, <http://dx.doi.org/10.1016/j.envpol.2016.09.047>, 2016.

Vivanco, M. G., and Santiago, M.: Secondary Organic Aerosol Formation from the Oxidation of a Mixture of Organic Gases in a Chamber, *Air Quality*, Ashok Kumar (Ed.), InTech, DOI: 10.5772/9761. Available from: <http://www.intechopen.com/books/air-quality/secondary-organic-aerosols-experiments-in-an-outdoor-chamber->, 2010.

Vreeland, H., Schauer, J. J., Russell, A. G., Marshall, J. D., Fushimi, A., Jain, G., Sethuraman, K., Verma, V., Tripathi, S. N., and Bergin, M. H.: Chemical characterization and toxicity of particulate matter emissions from roadside trash combustion in urban India, *Atmos. Environ.*, 147, 22-30, 10.1016/j.atmosenv.2016.09.041, 2016.

Wang, D., Pakbin, P., Shafer, M. M., Antkiewicz, D., Schauer, J. J., and Sioutas, C.: Macrophage reactive oxygen species activity of water-soluble and water-insoluble fractions of ambient coarse, PM2.5 and ultrafine particulate matter (PM) in Los Angeles, *Atmos. Environ.*, 77, 301-310, <http://dx.doi.org/10.1016/j.atmosenv.2013.05.031>, 2013.

Wang, H., Czura, C., and Tracey, K.: Tumor necrosis factor, *The cytokine handbook*, 4, 837-860, 2003.

Wang, S., Ye, J., Soong, R., Wu, B., Yu, L., Simpson, A., and Chan, A. W. H.: Relationship between Chemical Composition and Oxidative Potential of Secondary Organic Aerosol from Polycyclic Aromatic Hydrocarbons, *Atmos. Chem. Phys. Discuss.*, 2017, 1-53, 10.5194/acp-2017-1012, 2017.

Weichenthal, S. A., Lavigne, E., Evans, G. J., Godri Pollitt, K. J., and Burnett, R. T.: Fine Particulate Matter and Emergency Room Visits for Respiratory Illness. *Effect Modification*

by Oxidative Potential, American Journal of Respiratory and Critical Care Medicine, 194, 577-586, 10.1164/rccm.201512-2434OC, 2016.

Wen, Y., Gu, J., Chakrabarti, S. K., Aylor, K., Marshall, J., Takahashi, Y., Yoshimoto, T., and Nadler, J. L.: The Role of 12/15-Lipoxygenase in the Expression of Interleukin-6 and Tumor Necrosis Factor- α in Macrophages, Endocrinology, 148, 1313-1322, 10.1210/en.2006-0665, 2007.

Wennberg, P.: Let's abandon the "high NO_x" and "low NO_x" terminology, IGAC news, 50, 3-4, 2013.

Wildemann, T. M., Weber, L. P., and Siciliano, S. D.: Combined exposure to lead, inorganic mercury and methylmercury shows deviation from additivity for cardiovascular toxicity in rats, J. Appl. Toxicol., 35, 918-926, 10.1002/jat.3092, 2015.

Wiseman, H., and Halliwell, B.: Damage to DNA by reactive oxygen and nitrogen species: role in inflammatory disease and progression to cancer, Biochem. J., 313, 17-29, 1996.

Witkamp, R., and Monshouwer, M.: Signal transduction in inflammatory processes, current and future therapeutic targets: A mini review, Veterinary Quarterly, 22, 11-16, 10.1080/01652176.2000.9695016, 2000.

Wong, J. P. S., Lee, A. K. Y., and Abbatt, J. P. D.: Impacts of Sulfate Seed Acidity and Water Content on Isoprene Secondary Organic Aerosol Formation, Environmental Science & Technology, 49, 13215-13221, 10.1021/acs.est.5b02686, 2015.

Xiong, Q., Yu, H., Wang, R., Wei, J., and Verma, V.: Rethinking Dithiothreitol-Based Particulate Matter Oxidative Potential: Measuring Dithiothreitol Consumption versus Reactive Oxygen Species Generation, Environmental Science & Technology, 51, 6507-6514, 10.1021/acs.est.7b01272, 2017.

Xu, L., Kollman, M. S., Song, C., Shilling, J. E., and Ng, N. L.: Effects of NO_x on the Volatility of Secondary Organic Aerosol from Isoprene Photooxidation, Environmental Science & Technology, 48, 2253-2262, 10.1021/es404842g, 2014.

Xu, L., Guo, H., Boyd, C. M., Klein, M., Bougiatioti, A., Cerully, K. M., Hite, J. R., Isaacman-VanWertz, G., Kreisberg, N. M., Knote, C., Olson, K., Koss, A., Goldstein, A. H., Hering, S. V., de Gouw, J., Baumann, K., Lee, S.-H., Nenes, A., Weber, R. J., and Ng, N. L.: Effects of anthropogenic emissions on aerosol formation from isoprene and monoterpenes in the southeastern United States, Proceedings of the National Academy of Sciences, 112, 37-42, 10.1073/pnas.1417609112, 2015a.

Xu, L., Suresh, S., Guo, H., Weber, R. J., and Ng, N. L.: Aerosol characterization over the southeastern United States using high-resolution aerosol mass spectrometry: spatial and seasonal variation of aerosol composition and sources with a focus on organic nitrates, Atmos. Chem. Phys., 15, 7307-7336, 10.5194/acp-15-7307-2015, 2015b.

Yang, A., Jedynska, A., Hellack, B., Kooter, I., Hoek, G., Brunekreef, B., Kuhlbusch, T. A. J., Cassee, F. R., and Janssen, N. A. H.: Measurement of the oxidative potential of PM_{2.5} and its constituents: The effect of extraction solvent and filter type, *Atmos. Environ.*, 83, 35-42, <http://dx.doi.org/10.1016/j.atmosenv.2013.10.049>, 2014.

Yang, A., Janssen, N. A. H., Brunekreef, B., Cassee, F. R., Hoek, G., and Gehring, U.: Children's respiratory health and oxidative potential of PM_{2.5}: the PIAMA birth cohort study, *Occupational and Environmental Medicine*, 10.1136/oemed-2015-103175, 2016.

Yoo, E., Crall, B. M., Balakrishna, R., Malladi, S. S., Fox, L. M., Hermanson, A. R., and David, S. A.: Structure–activity relationships in Toll-like receptor 7 agonistic 1 H-imidazo [4, 5-c] pyridines, *Organic & biomolecular chemistry*, 11, 6526-6545, 2013.

Yu, H., Wei, J., Cheng, Y., Subedi, K., and Verma, V.: Synergistic and Antagonistic Interactions among the Particulate Matter Components in Generating Reactive Oxygen Species Based on the Dithiothreitol Assay, *Environmental Science & Technology*, 10.1021/acs.est.7b04261, 2018.

Zhang, J., Stanley, R. A., Adaim, A., Melton, L. D., and Skinner, M. A.: Free radical scavenging and cytoprotective activities of phenolic antioxidants, *Molecular nutrition & food research*, 50, 996-1005, 2006.

Zhang, J., Doshi, U., Suzuki, A., Chang, C.-W., Borlak, J., Li, A. P., and Tong, W.: Evaluation of multiple mechanism-based toxicity endpoints in primary cultured human hepatocytes for the identification of drugs with clinical hepatotoxicity: Results from 152 marketed drugs with known liver injury profiles, *Chemico-Biological Interactions*, 10.1016/j.cbi.2015.11.008, 2016.

Zhang, Q., Jimenez, J. L., Canagaratna, M. R., Allan, J. D., Coe, H., Ulbrich, I., Alfarra, M. R., Takami, A., Middlebrook, A. M., Sun, Y. L., Dzepina, K., Dunlea, E., Docherty, K., DeCarlo, P. F., Salcedo, D., Onasch, T., Jayne, J. T., Miyoshi, T., Shimo, A., Hatakeyama, S., Takegawa, N., Kondo, Y., Schneider, J., Drewnick, F., Borrmann, S., Weimer, S., Demerjian, K., Williams, P., Bower, K., Bahreini, R., Cottrell, L., Griffin, R. J., Rautiainen, J., Sun, J. Y., Zhang, Y. M., and Worsnop, D. R.: Ubiquity and dominance of oxygenated species in organic aerosols in anthropogenically-influenced Northern Hemisphere midlatitudes, *Geophysical Research Letters*, 34, L13801, 10.1029/2007GL029979, 2007.

Zhang, Y., Schauer, J. J., Shafer, M. M., Hannigan, M. P., and Dutton, S. J.: Source Apportionment of in Vitro Reactive Oxygen Species Bioassay Activity from Atmospheric Particulate Matter, *Environmental Science & Technology*, 42, 7502-7509, 10.1021/es800126y, 2008.

Zhou, F., Feng, C., and Fan, G.: Combined exposure of low dose lead, cadmium, arsenic, and mercury in mice, *Chemosphere*, 165, 564-565, 10.1016/j.chemosphere.2016.08.132, 2016.